THE UNIVERSITY OF HULL

Foaming and Anti-foaming of Nonionic Surfactant Solutions

Being a Thesis Submitted for the Degree of
Doctor of Philosophy

in the University of Hull

by

Matthew David Haynes M.Chem. (Hons) MRSC

June 2004

To Mum and Dad

ACKNOWLEDGEMENTS

I would like to thank my supervisors Prof. Bernie Binks and Prof. Paul Fletcher of the Surfactant and Colloid Group at the University of Hull for all of their help, guidance and ideas, throughout the duration of this project.

I would also like to thank Dr. Ian Callaghan and LFE-GTC, The Netherlands, for the provision of a 3 Year Studentship to fund this work.

I would like to thank all of my friends and various members of the Department of Chemistry for making my time at Hull so enjoyable.

Special thanks are due to my parents for all of their support and encouragement throughout my 7 years of study at the University of Hull.

Finally I would like to thank my partner Laura for her patience, understanding and support over the past 3 years, especially during the writing-up stage of this thesis.

ABSTRACT

Foam is important for many processes such as enhanced oil recovery and fire-fighting. Although a large volume of foam is desirable for these particular applications, for other applications it needs to be suppressed, for example, in washing machines. In order to suppress foam formation, an anti-foam agent is added to the foaming solution. An anti-foam agent may take the form of oil, solid particles (generally of the micron (μm) size range), or a combination of both. This thesis is concerned with understanding the foaming and anti-foaming of nonionic surfactants of the polyoxyethylene glycol ether type of general structure $H\text{-}(CH_2)_n(O\text{-}CH_2\text{-}CH_2)_m\text{-}OH$ (abbreviated to C_nE_m).

In the first results chapter, the foaming of the homologous series of C_nE_m surfactants is investigated in the absence of any additives (i.e. anti-foam agents). The foamability of the surfactant is determined by measuring the volume of foam generated by bubbling nitrogen gas, through the surfactant solution as a function of surfactant concentration. It is found that the surfactant concentration corresponding to the transition from non-foaming to foaming behaviour, $C(1/2)$, is less than the critical micelle concentration cmc for short tailed surfactants (low n) and greater than the cmc for long tailed surfactants (higher n). This is explained in terms of two requirements which must both be fulfilled before a surfactant can stabilise foam. Firstly, the rate of adsorption of the surfactant must be sufficiently fast to stabilise a foam bubble as it is being formed and secondly, the level of surfactant adsorption must be sufficiently high relative to the adsorption isotherm such that there is sufficient surfactant surrounding the bubble for it to be stable.

Chapter 4 examines a new mechanism for the way in which oil may affect the stability of aqueous foam. It is known that alkane vapours can co-adsorb with surfactant at the air-water surface to form mixed alkane/surfactant monolayers. The effects of alkane vapours on the foamability and foam stability for foams stabilised by C_nE_m surfactants of different head and tail chain lengths has been systematically investigated. The addition of alkane vapours within the gas stream during foam

formation increases $C(1/2)$ to concentrations in excess of the cmc, i.e. oil vapours inhibit foamability. In addition to the effects on foamability, oil vapours also accelerate the decay rates of foams (i.e. reduce the foam stability).

Chapter 5 looks at the effects that nanometre (nm)-silica particles of different hydrophobicities have on aqueous foams stabilised by $C_{12}E_5$. In the past, most studies have focussed on solid particles in the μm size range. It is found that the nonionic surfactant can adsorb onto the surface of the silica particles, lowering the equilibrium surfactant concentration. This adsorption is the highest for the most hydrophobic silica particles. Reducing the equilibrium surfactant concentration lowers the foamability of the system. Whilst the foamability is decreased, the foam stability is increased however. This is explained in terms of the silica particles blocking the drainage channels in the foam by networking together in solution and thus slowing liquid drainage from the foam.

Finally in chapter 6, the effects that oil and nm-sized silica particles have when used in combination on foam stabilised by $C_{12}E_5$ are investigated. Here it is found that a synergistic anti-foam action is observed for some systems i.e. the oil and particles are more effective when used together than individually. When silica particles of an intermediate hydrophobicity are used, there is a sharp increase in the foamability and foam stability for many of the systems. These differences in foaming behaviour are explained in terms of the hydrophobicity of the overall entity which is formed when surfactant, oil and nm-sized silica particles of different initial hydrophobicities are shaken together to produce foam.

PUBLICATIONS AND PRESENTATIONS

The work contained within this thesis has given rise to the following publications and presentations:

Presentations

1. Oral presentation entitled: "*Foaming and Antifoaming of Nonionic Surfactants*"
   Eurofoam2002 Conference (UMIST), 9 July 2002.

2. Oral presentation entitled: "*Foaming and Antifoaming of Nonionic Surfactants*"
   Departmental Research Colloquium (University of Hull), 18 June 2003.

3. Oral presentation entitled: "*Antifoam Action of Oil Vapours*"
   European Student Colloid Conference, (University of Bristol), 17 July 2003.

4. Oral presentation entitled: "*Controlling the Foaming of Nonionic Surfactants*"
   Unilever Research Technology Forum (Vlaardingen, The Netherlands), 21 November 2003.

Publications

1. B. P. Binks, P. D. I. Fletcher and M. D. Haynes, "Antifoam Action of Oil Vapours", *Colloids and Surfaces A*, (2003), **216**, 1-8.

CONTENTS

Chapter 1

CHAPTER 1

Introduction

1.1 Introduction and industrial relevance

Foams are useful in many contexts including, for example, fire-fighting applications. A controlled level of foam formation is desirable in many consumer products such as in beer and detergents for washing-up. In other processes, such as the production of paper and the operation of machine dishwashers and laundries, foam is often an unwanted consequence and must be suppressed.[1] This thesis is concerned with understanding the foaming properties of aqueous nonionic surfactant solutions together with mechanisms for their control.

1.2 Surfactant structure and behaviour

Foam stabilisation generally relies on the presence of molecules called surfactants. In this section, the structure and properties of surfactants will be described.

Surfactants (or SURFace ACTive AgeNTS) are molecules which can accumulate (adsorb) at the gas-water or oil-water interface forming a so-called surfactant monolayer. Surfactant molecules can adsorb at interfaces due to the amphiphilic nature of their molecular structure. Surfactants comprise a hydrophobic tail group (typically, a straight or branched hydrocarbon chain) and a hydrophilic headgroup (typically either an ionic group or a poly(ethylene oxide) chain). Figure 1.1 depicts a typical surfactant molecule and shows the two distinct parts of its structure.

The apolar chain of the surfactant molecule is insoluble in water whereas strong attractive interactions exist between the polar headgroup and water. The surfactant molecules therefore adsorb at the interface such that the apolar tails are out of the water (i.e. in gas or oil) and the polar headgroups are in contact with the water. This

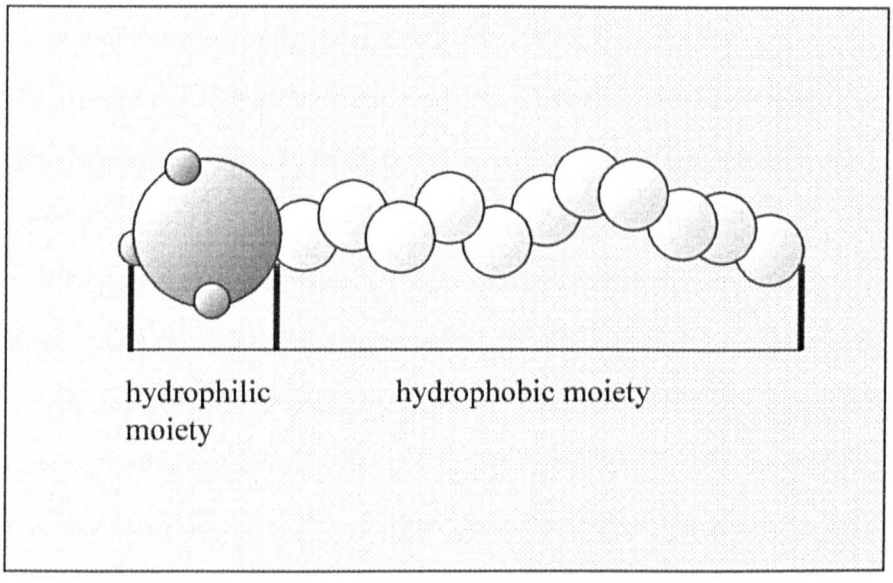

Figure 1.1 Schematic diagram of a typical single-tailed surfactant molecule. The hydrophobic moiety favours oil (or air) and the hydrophilic group favours water.

configuration minimises the unfavourable interaction of the apolar chain group with the water. The adsorption of surfactant at the air-water interface causes a decrease in the solution's surface tension. As the surfactant concentration is increased, the surface tension becomes progressively lower until a specific surfactant concentration is reached at which stage the surface tension remains at an approximately constant value regardless of further increases in surfactant concentration. At this surfactant concentration, termed the critical micelle concentration (cmc) surfactant molecules self assemble in solution to form micelles. Further increase in surfactant concentration above the cmc results in the formation of additional micelles. Figure 1.2 is a summary of this process and Figure 1.3 shows the structure of a typical spherical micelle.

1.3 Formation and structure of foams

Foam is a dispersion of gas in a continuous liquid phase. It is thermodynamically-unstable which means that energy must be supplied to form foam and there is a driving force leading to foam breakdown and minimisation of the liquid-vapour surface area. Pure liquids do not foam. In order for a foam system to be kinetically-stable, a surface active agent (surfactant) is required to provide an energy barrier to breakdown.

Foam is produced by introducing gas into a surfactant solution using one of three methods. Firstly, gas bubbles can be introduced by chemical reactions or the release of dissolved gas by changes in pressure or temperature. Pressure change induced release of CO_2 is the process that occurs when a fizzy drink container is opened. Secondly, foam is produced when a surfactant solution containing gas is vigorously shaken in a stoppered container. In the third method, known as "gas sparging", gas is directly added to the liquid phase as fine bubbles blown through a sinter underneath the foaming solution. In the work described in this thesis, foam is produced by shaking surfactant in a stoppered cylinder and by gas sparging methods. The initial volume of foam produced by any of the methods described above reflects the *foamability* of the foaming solution.

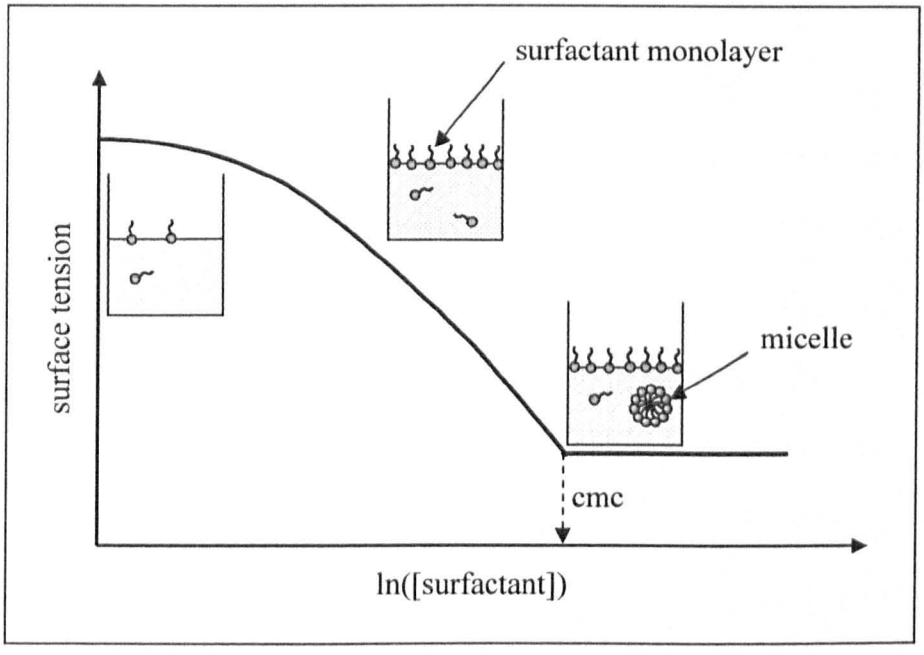

Figure 1.2 Surface tension as a function of ln([surfactant] plot for a typical surfactant. The dashed vertical line denotes the cmc of surfactant. At this point, further increases in surfactant concentration result in approximately constant surface tensions.

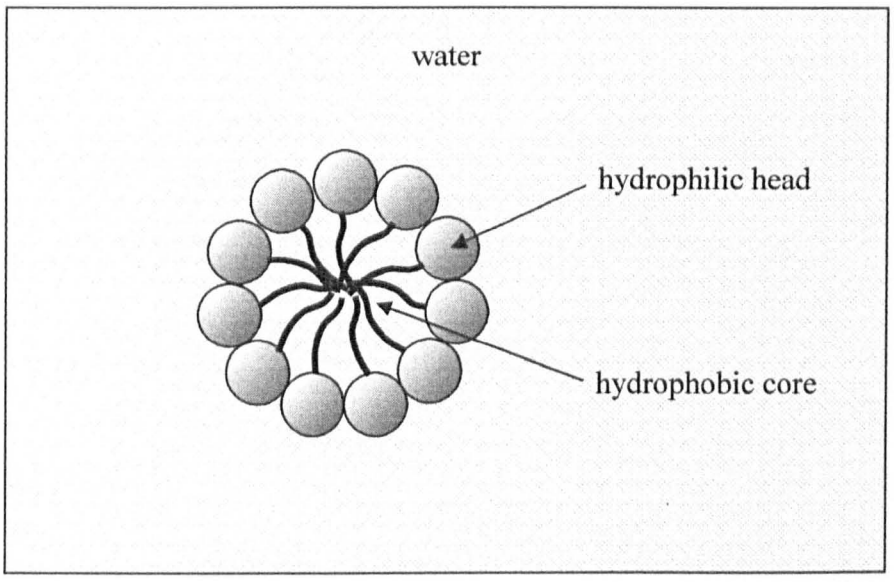

Figure 1.3 Schematic representation of a cross-section of a spherical micelle.

Isolated bubbles in a liquid are nearly perfect spheres, but are slightly distorted by gravity. Because of their buoyancy, they rise rapidly in the liquid and close-pack at a volume fraction of approximately 0.7. The exact volume fraction depends on the polydispersity of the bubbles. In this state, called "kugelschaum", the gas bubbles are separated by relatively thick liquid films as shown in Figure 1.4. Continued drainage of the liquid from the kugelschaum causes the liquid films to thin resulting in bubble deformation to polyhedral shapes. This state of the foam is called "polyederschaum". As shown in Figures 1.5 and 1.6, the bubbles are separated by thin lamellae which meet at Plateau borders. The angle between a pair of lamellae is always 120°. Within the polyederschaum state, the initial thickness of the lamellae is typically of the order of 10 μm. As described later, continued liquid drainage can cause the lamellae to thin down to thicknesses of a few nm.

1.4 Foam breakdown

In the absence of any additives, there are three coupled mechanisms leading to foam collapse, these are briefly summarised in the following sections 1.4.1 – 1.4.3.[2] It should be noted here that *foam stability* is a measure of the foam breakdown, and that this is a different aspect to foaming than foamability (defined in the previous section). For example, a surfactant solution could have a high foamability (produce a large volume of foam upon shaking for example) but have a low foam stability i.e. the (large) foam volume falls to 0 quickly. An example of this type of foaming is when champagne is poured into a glass.

1.4.1 Film thinning

In kugelschaum and freshly formed foams, the liquid films are relatively thick and drain primarily by gravity. Following gravity drainage to form a polyederschaum, the film deformation aids liquid flow from the films into the Plateau borders by capillary suction, as shown in Figure 1.6. Due to the curved surfaces in the region of the Plateau border, a pressure gradient $P(c) < P(b) = P(a)$ is formed because the internal

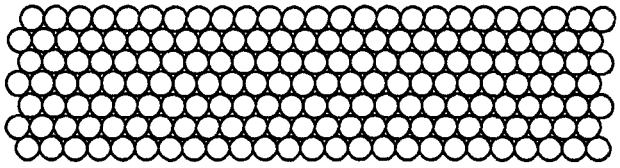

Figure 1.4 "Kugelschaum" foam state. The bubbles are close packed spheres before liquid drainage and subsequent foam thinning occurs.

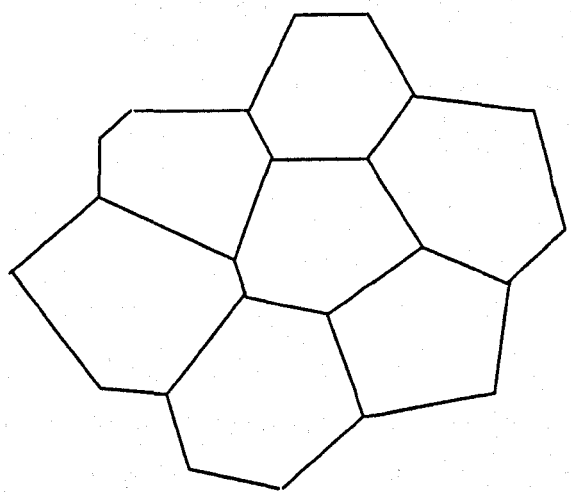

Figure 1.5 The Lamellae meet at plateau borders. The angle between pairs of lamellae is 120°.

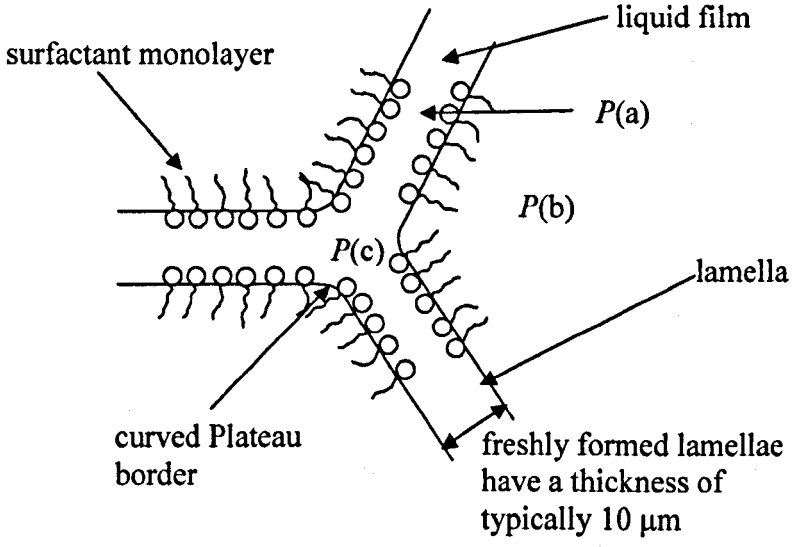

Figure 1.6 Plateau border region of a foam. Due to a differential Laplace pressure caused by the curved surfaces, liquid is forced from the films into the Plateau borders. P(a), P(b) and P(c) refer to the pressures in a Plateau border, a foam bubble and the node between three Plateau borders respectively.

(Laplace) pressure of a bubble is inversely proportional to the bubble radius (r) according to:

$$\Delta P = 2\gamma / r \qquad [1.1]$$

This pressure difference causes liquid to flow from the films into the borders. Gravity drainage then proceeds, primarily through the network of Plateau borders. For the exposed surfaces of the foam (e.g. at the top of the foam column), evaporation of water can also contribute to film thinning.

1.4.2 Bubble coalescence

Bubble coalescence is the irreversible fusion of two or more bubbles and may occur when the foam lamellae reach a critically low thickness. Stability to bubble coalescence is improved by factors which reduce the rate of film drainage (e.g. increasing the viscosity of the foaming liquid or the surface viscosity of the adsorbed surfactant monolayers), increasing the colloidal repulsive forces between the lamellae surfaces (e.g. by using charged surfactants) or by increasing the film elasticity (see later).

1.4.3 Bubble disproportionation

Bubble disproportionation is the process whereby large bubbles grow at the expense of smaller bubbles due to gas transport between bubbles. The pressure difference (ΔP) responsible for disproportionation arises because of the inverse relationship between Laplace pressure and bubble radius according to equation [1.1]. The pressure inside the smaller bubbles is greater than that in larger bubbles and causes transfer of gas from small to large bubbles. The rate of this gas transfer depends on the solubility of the gas in the liquid film. For example, N_2 is less soluble that CO_2 in water by a factor of 56, and hence bubble disproportionation is faster for CO_2 foams than those containing N_2. The rate also depends on the thickness of the film and thus the rate of disproportionation is strongly coupled to the rate of film drainage. At this

point it is noteworthy to state that bubble disproportionation is the only mechanism linked to the breakdown of spherical bubble foams before drainage occurs followed by subsequent lamellae formation.

1.4.4 The role of disjoining pressure in film stability

As noted above, the film thickness in a freshly formed polyederschaum is typically of the order of 10 μm. Film thinning due to gravity and capillary suction leads to film thicknesses comparable with the wavelength of visible light (in the order of hundreds of nm) which show characteristic optical interference colours. When the lamellae thickness becomes less than half the wavelength of the light (around 100 nm or so), the films appear black in reflected light because of destructive optical interference. Such films are known as "common black films". When the liquid has almost drained completely from the lamellae a "Newton black film" is formed and this has a thickness of a few nm.

When the films thin to below approximately 100 nm, colloidal forces become the important determinants in dictating the overall film stability. A quantity termed disjoining pressure (Π) will now be defined to explain these forces of interaction. Π is defined as the repulsive force per unit area between the film surfaces. If Π has a positive value, the surfaces are repulsive and act to thicken and stabilise the films. If Π has a negative value the films become thinner and less stable. The overall Π is a summation of three main components $\Pi = \Pi_{vdw} + \Pi_{el} + \Pi_{sr}$. Firstly, dispersion (van der Waals) forces (Π_{vdw}) have a range of around 10 nm and are always attractive (Π is negative) for foam films. Secondly, repulsive electrostatic forces (Π_{el} is positive) across foam films arise from the surface charges of the surfactant monolayers. The range of the electrostatic forces is long for low electrolyte concentrations and short for high electrolyte concentrations. Thirdly, short range forces (Π_{sr}) arising from steric, hydration and film undulation interactions operate over distances of a few nm and are repulsive forces (Π is positive).

If Π is plotted as a function of film thickness (h), the resulting plot is an isotherm illustrating that, in some cases, a barrier to film thinning and rupture can be present.

These barriers prevent thinning and rupture if Π is larger than the capillary suction pressure. If there is no barrier the film will rupture. If only a short-range barrier is present a Newton black film will be created and if there is a long range barrier at play a common black film will form as shown in Figure 1.7. Foam films can still rupture in the presence of these barriers due to external perturbations such as mechanical shock or evaporation of liquid from the film.

The three horizontal lines on Figure 1.7 correspond to three different values of capillary suction pressure (P_{cap}). The pressure, P_{cap} acts to thin the film through liquid suction from the lamellae into the Plateau borders as described above. At capillary suction pressure 1, the repulsive force arising from Π is balanced by P_{cap} at a value of film thickness corresponding to the formation of a common black film. At capillary suction pressure 2, the repulsive force arising from Π is balanced by P_{cap} at a value of film thickness corresponding to the formation of a Newton black film. Capillary suction pressure 3 corresponds to a value of P_{cap} which is too large to be balanced by Π at any film thickness. This results in film thinning and subsequent rupture.

1.4.5 The role of film elasticity

Film elasticity is defined as the differential change in surface tension with relative change in the natural logarithm of surface area.[3] Film elasticity depends on the time scale of the area expansion relative to the adsorption rate of the surfactant and hence the rate at which surfactant can be replenished to restore the equilibrium surface tension. This effect is pronounced in foam because of the slow adsorption of surfactant (arising from relatively low levels of surfactant within the foam) available to replenish the depleted surfactant in the film and restore the equilibrium surface tension within the required time scale.

An inherent mechanism of foam stability constantly operating within a foam film is the Gibbs-Marangoni effect. If a film is subjected to local stretching as a result of some external disturbance, the increase in surface area will be accompanied by a decrease in the surface excess concentration of the surfactant adsorbed at the surface resulting in a local increase in surface tension gradient (Gibbs effect). If this gradient

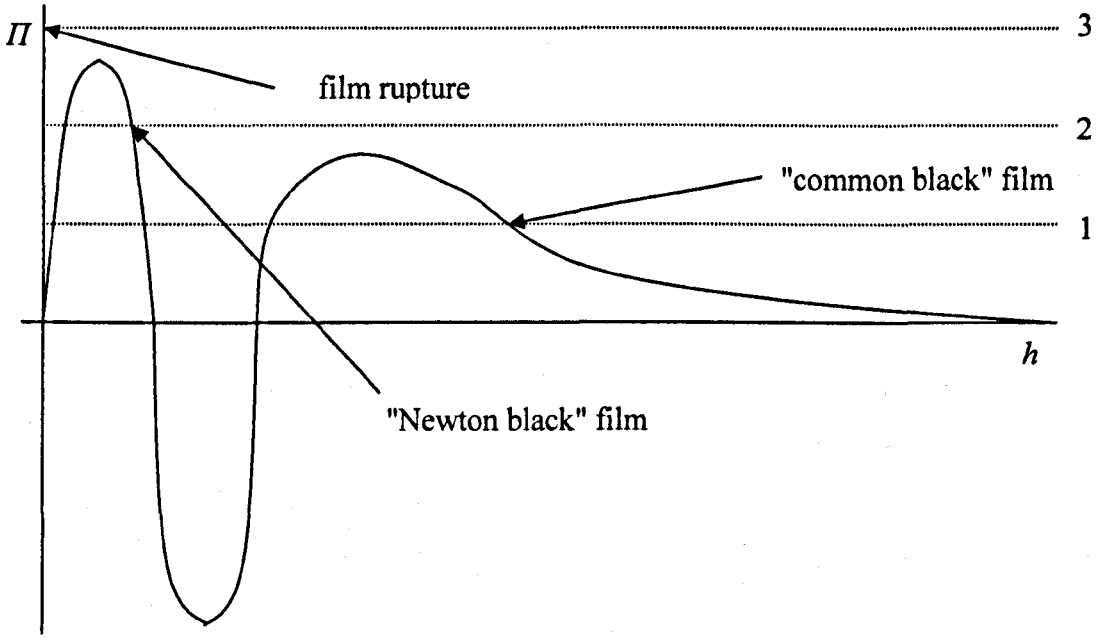

Figure 1.7 Disjoining pressure isotherm. Disjoining pressure (Π) is expressed as a function of film thickness (h). The horizontal lines (1, 2 and 3) refer to different capillary suction pressures (P_{cap}).

is sufficiently large, the surfactant molecules will move along the surface so that the surface tension is restored to its equilibrium value (Marangoni effect). As the surfactant molecules move along the surface, they drag with them underlying liquid which acts to thicken the film and helps to prevent film rupture. Hence, high film elasticity acts to stabilise the foam.[4]

1.5 Nonionic surfactants as foam-stabilisers

A nonionic surfactant is a surfactant in which the polar group does not carry a charge. Examples of such molecules include polyoxyethylene glycol ethers and sugar-based surfactants such as alkylglucosides. The study described in this thesis focuses on a homologous series of pure nonionic surfactants of general structure $H\text{-}(CH_2)_n\text{-}(O\text{-}CH_2\text{-}CH_2)_m\text{-}OH$ abbreviated to C_nE_m. In discussing the relevant literature it is necessary to distinguish between pure nonionic surfactants and commercial grade surfactants containing a distribution of E chain lengths. The latter type will be denoted by C_nE_m (range) where m refers to the average E chain length in the distribution.

1.5.1 Effect of nonionic surfactant molecular structure on foaming properties

Shinoda et al.[5] compared the foamability and foam stability of octanol, octyl glycerol ether and octyl glucoside stabilised foams to see what effect the hydrophilic moiety of a surfactant molecule had on these parameters. They found that foamability and foam stability increased to a maximum value with the size of the hydrophilic group before decreasing. The foam stability of octyl glucoside was found to be 100 times greater than that of octyl glycol ether. The conclusion of this study is that foamability and foam stability depend on the hydrophilic-lyophilic balance (HLB) of the molecule. HLB is an empirical scale which categorises surfactants in terms of their tendencies to be mostly oil-soluble or mostly water soluble.[6]

In a separate study, Schick and Beyer[7] studied the effect of ethylene oxide chain length on foamability and foam stability for pure nonionic surfactants prepared from

five different hydrophobes. They found that the foamability and foam stability passed through maxima at a particular mole ratio of ethylene oxide and hydrophobic group. When this ratio is such that it gives rise to a maximum in foamability and foam stability, it is termed the critical hydrophilic-hydrophobic balance (CHHB). They suggest that the CHHB corresponds to a condition of maximum resistance to film rupture, which depends on the cohesive forces in the adsorbed film of surfactant molecules. The cohesive forces are the summation of van der Waals forces between the hydrophobic groups and of inter- or intramolecular hydrogen bonding forces between the ether oxygens of the hydrated ethylene oxide coils. The size of the ethylene oxide coils increases with increasing numbers of ethylene oxide units. This acts to reduce van der Waals forces between hydrophobes but increases the hydrogen-bonding forces. The summation of these two forces is thought to result in a maximum foam stabilisation effect at an intermediate ethylene oxide ratio.[8]

1.5.2 Relationship between surfactant adsorption and stability of nonionic stabilised foam films and foams

It can be shown that high foam stability is connected to the formation of black films which are formed above a well-defined surfactant concentration.[9] This concentration, associated with changes in the adsorbed layer of surfactant, is a characteristic of the surfactant and is denoted by (C_{bl}). The kinetics describing the growth of black films have been studied. It was found that for foam stabilised by a nonionic surfactant, there is a linear increase in the decay constants of the foam with the rate of growth of black films. The conclusion of this study is that, although stable foams can be formed above C_{bl}, the ultimate foam stability above C_{bl} is dependant on both the total area of black film and on the rate at which the black spots expand.

Foam lifetime (τ) (i.e. stability) was measured as a function of the surfactant concentration. The surfactant concentration at which the foam becomes very stable (denoted as C_s) was measured for a series of nonionic surfactants with varying hydrophilic chain length.[9] For a series of homologous polyoxyethylene adducts (either polyoxyethylene octylphenols or polyoxyethylene dodecyl alcohols), the C_{bl} values for single films coincide with the C_s values measured in foams, the C_{bl} values

decrease with increasing hydrophilic chain length[9] and C_{bl} values are typically 1 - 2 orders of magnitude less than the corresponding cmc values. With increasing hydrophilic chain length, C_{bl} values decrease and the corresponding cmc values increase. The overall conclusion of these studies is that foam stability is not related to bulk properties of the surfactants, such as micelle formation, but is dependant on surfactant adsorption in relation to the thin film properties.

1.5.3 Effects of temperature and the cloud points of aqueous nonionic surfactant solutions on foaming properties

Micellar solutions of nonionic surfactants in water tend to phase separate at a well-defined temperature to give a micelle-rich phase in equilibrium with a micelle-poor phase. Increasing the temperature above that corresponding to the phase boundary causes clouding of the solution and hence the temperature is referred to as the cloud point (Cp.). It depends on the concentration of the nonionic surfactant in the bulk aqueous phase. The phase separation occurring at the cloud point is driven by the tendency of the micelles to aggregate (and form a concentrated phase) at high temperatures which is thought to be caused by the decreased hydration of nonionic headgroups at increased temperature.[10]

If Cp. temperature is plotted as a function of surfactant concentration, a phase diagram is obtained with a curve separating the one- and two- phase regions. The curve can either exhibit a maximum or a minimum and this is characteristic of the homologous series of surfactant used. A tie-line can be drawn across the curve parallel to the concentration axis corresponding to a given Cp. temperature. The two points at which this line bisects the curve correspond to the compositions (expressed in surfactant concentrations) of the upper phase (normally micelle poor phase) and the lower phase (normally the micelle rich phase). For surfactants of the polyoxyethylene glycol ether type used in the study detailed in this thesis, the phase diagrams exhibit a minimum in the phase boundary curves.[11] This minimum in the curve corresponds to the minimum Cp. temperature and is termed the lowest critical temperature (LCT). By definition, LCT corresponds to a single concentration (i.e. the turning point of the

curve at the minimum) where compositions in the upper and lower phases are the same.

At temperatures above the Cp., foaming is dramatically reduced (often by a factor of 10).[12] The surfactant-rich phase plays the role of an anti-foam. It has been shown that the mechanism of this anti-foam action involves the bridging of the foam films made with the dilute phase by tiny drops of the surfactant-rich phase which merge into the air-water surfaces of the foam films.[13]

The Cp. of nonionic surfactants is strongly sensitive to impurities. Schubert et al.[14] have used the (known) phase behaviour of ternary systems of water, oil, and nonionic surfactants to simultaneously extract water- and oil-soluble impurities. The three phase extraction described in their work is shown to yield reproducible Cp. temperatures of binary water + nonionic surfactant mixtures. This means that in principle, the purity of a nonionic surfactant can be evaluated by comparing its measured Cp. with a reliable literature value. This method relies on the fact that further repeated purification steps do not change the Cp of the surfactant solution.

Having surveyed the literature, there appear to be significant discrepancies in reported Cp. temperatures for the same surfactants. For example, in the compilation by N. M. van Os et al., "Physico-chemical properties of selected anionic, cationic and nonionic surfactants"[15], values of Cp. for the nonionic surfactant $C_{12}E_5$ at 1 wt. % vary between 25 and 31.5 °C. It must therefore be ensured that any Cp. taken from the literature is from a reliable source.

1.6 Oil anti-foams

In order to control the stability of foams, an anti-foam is employed. An anti-foam is any substance that acts to reduce either foamability or foam stability.[3] Anti-foams are typically emulsion formulations such as hydrocarbons or silcone oils in water. Hydrophobic solid particles of μm size dispersed in another liquid can also exhibit anti-foam effects. Complex anti-foam formulations sometimes contain both dispersed hydrophobic particles and oil-in-water emulsions. In liquid anti-foams, the oil drop is

initially present as an emulsion droplet in the foaming solution. In order for oil droplets to act as anti-foam agents, an oil droplet must enter at least one of the thin film surfaces. Whether or not an oil drop enters a thin film surface depends on the tensions of the air-water (γ_{aw}), oil-water (γ_{ow}) and oil-air (γ_{oa}) surfaces. These conditions are summarised by the value of the entry coefficient for oil into the air-water surface from dispersion in the water (E_{oil}), defined as follows:

$$E_{oil} = \gamma_{aw} + \gamma_{ow} - \gamma_{oa} \qquad [1.2]$$

The oil drop will enter the surface if E_{oil} is positive, although entry can be slow if there is resistance from thin film forces. Microscopic observations show that the entering coefficients cannot consistently predict the configuration of the oil at the air-water surface because it is difficult to measure equilibrium values accurately and consequently, cannot predict the effect of oil on foam stability. The reason for this inconsistency is that the classical entry coefficient treatment of the oil drop does not take into account the formation of a pseudoemulsion film which is formed between an air-water surface and the surface of an oil drop which is approaching it (Figure 1.8).[16] The pseudoemulsion film creates an energy barrier which must be overcome before drop entry can take place.

Once the oil drop has entered the film surface, it can potentially spread on the thin film surface to form a continuous oil film. Oils which do not completely spread form discrete lenses on the surface. The thermodynamic tendency to spread is related to the magnitudes of the three tensions in the system. These are related by the spreading coefficient (S_{oil}), defined as follows:

$$S_{oil} = \gamma_{aw} - \gamma_{ow} - \gamma_{ao} \qquad [1.3]$$

When $S_{oil} = 0$, the oil will spread. The addition of the spreading oil to the surface will cause the measured tension to fall from that of the aqueous solution to that of the composite film including both the surfactant monolayer and the oil film. Small quantities of added oil will yield thin films (less than a few nm) for which the strength of interaction between the oil-water and air-oil interfaces may be sufficient to cause the measured tension to be significantly different to the sum of the bulk phase

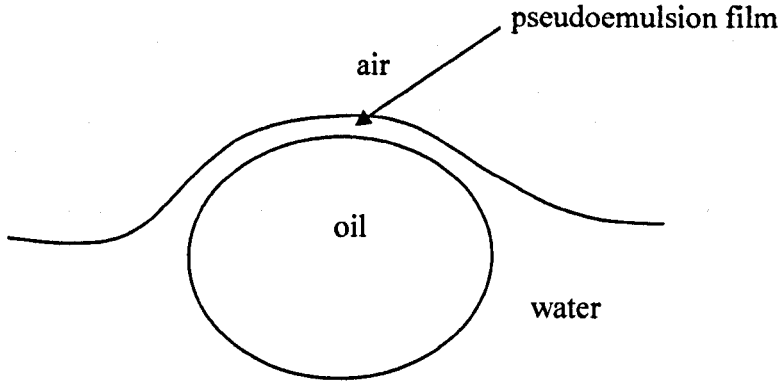

Figure 1.8 Thin film of the continuous phase separating an oil drop from an air-water surface as postulated by Fineman et al.[12] The pdeudoemulsion film can act as a barrier to entry of the oil drop to the surface.

tensions ($\gamma_{ao} + \gamma_{ow}$). The addition of more oil will cause the film to thicken and the measured composite film tension to approach the sum ($\gamma_{ao} + \gamma_{ow}$). Film excess tensions arising from colloidal interactions across thin aqueous films have been found to be of the order of 0.01 mN m^{-1} for films with a thickness of a few nm.

For cases where the oil does not spread macroscopically ($S_{oil} < 0$), a surfactant/oil mixed monolayer can form at equilibrium and coexist with macroscopic oil lenses.[17] In this situation the mixed film can either consist of a monolayer of oil solubilised within the surfactant chain region or can thicken to give a multilayer oil film. For many surfactant monolayers at the air-water surface, mixed hydrocarbon monolayers are found for non-spreading alkanes where typically the chain length is greater than 11.[18] Mixed surfactant/oil monolayers are described in more detail later.

Providing the oil drop enters an air-water surface by satisfying the criteria detailed above, there are three proposed film rupture mechanisms which can potentially operate.

1.6.1 The spreading-fluid entrainment mechanism

If $E_{oil} > 0$ and $S_{oil} > 0$ (S_{oil} can only be positive in non-equilibrium conditions), oil drops will emerge into the air-water surface (Figure 1.9, picture 1) and spread as a duplex film. The duplex film will drag out the original underlying liquid in the foam film by a Marangoni-type-mechanism (Figure 1.9, picture 2). Rupture may occur if a sufficiently low foam film thickness is reached (Figure 1.9, picture 3).[6]

1.6.2 The bridging-dewetting mechanism

This mechanism, proposed by Garrett[6], relies on the oil drop entering the air-water surface but not spreading. As the film drains under the forces of gravity and by capillary suction, the second surface of the film can come in contact with the oil drop. This forms a bridge between the two surfaces of the film. There are two possibilities

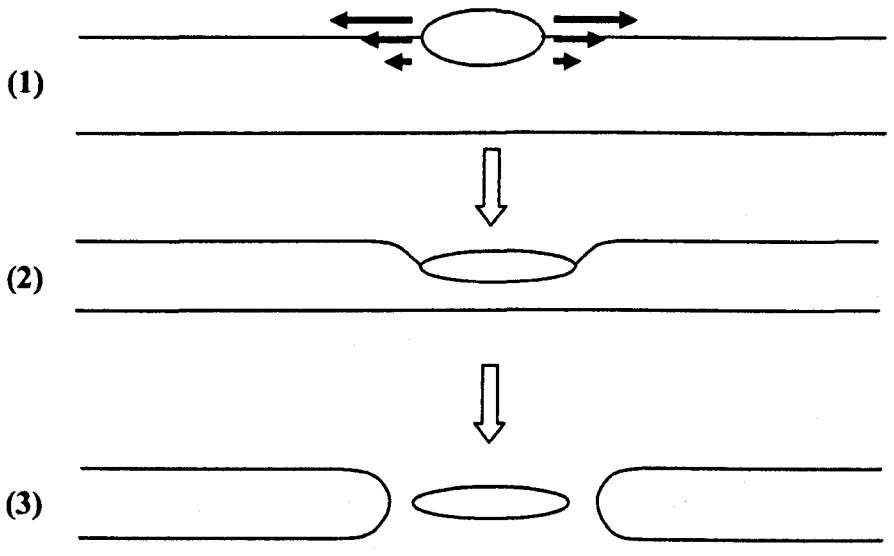

Figure 1.9 The spreading-fluid entrainment mechanism. Depending on the value of the entering and spreading coefficients, an oil drop can enter an air-water surface and spread as a duplex film causing film thinning and subsequent rupture.

for what can happen next dictated by the bridging coefficient for an oil lens in an oil film (B_{oil}) defines as follows:

$$B_{oil} = \gamma_{ow}^2 + \gamma_{aw}^2 - \gamma_{ao}^2 \qquad [1.4]$$

If the bridge is hydrophobic ($B_{oil} > 0$) the contact angle between the bridge and the film is greater than 90° (Figure 1.10).[19] The Laplace pressure forces aqueous liquid away from the oil bridge causing thinning and rupture. In the case of the hydrophilic bridge, (formed when $B_{oil} < 0$) where the contact angle is less than 90°, the Laplace pressure tends to draw water in the film towards the edge and acts to slow film drainage and stabilise the thin liquid film.

1.6.3 The bridging-stretching mechanism

This mechanism was proposed by Denkov et al.[20,21], and is a variation of the bridging-dewetting mechanism proposed by Garrett (section 1.6.2). Providing drop entry can take place a stable or unstable oil bridge can form (according to B_{oil}) in exactly the same way as explained above (Figure 1.11, picture 3). This bridge then stretches due to uncompensated capillary pressure at the oil-water and oil-air interfaces (Figure 1.11, picture 4). Finally the oil bridge ruptures in its thinnest central region and breaks the film (Figure 1.11, picture 5).

1.7 Microemulsions as anti-foams

A microemulsion is a thermodynamically stable dispersion of either oil in water or water in oil and contains droplets or domains of oil and/or water in the size range 2 - 100 nm. Unpublished results have shown that microemulsions can act as anti-foams.[22] Initially, the microemulsion is present in the foaming solution before gas is sparged through it. The mechanism of anti-foam action cannot be that of bridging-dewetting (explained above) because the oil droplets are too small to bridge the two surfaces of the foam film. One possibility for the mechanism of action is that the vapour phase becomes saturated with oil during foam formation resulting in a mixed

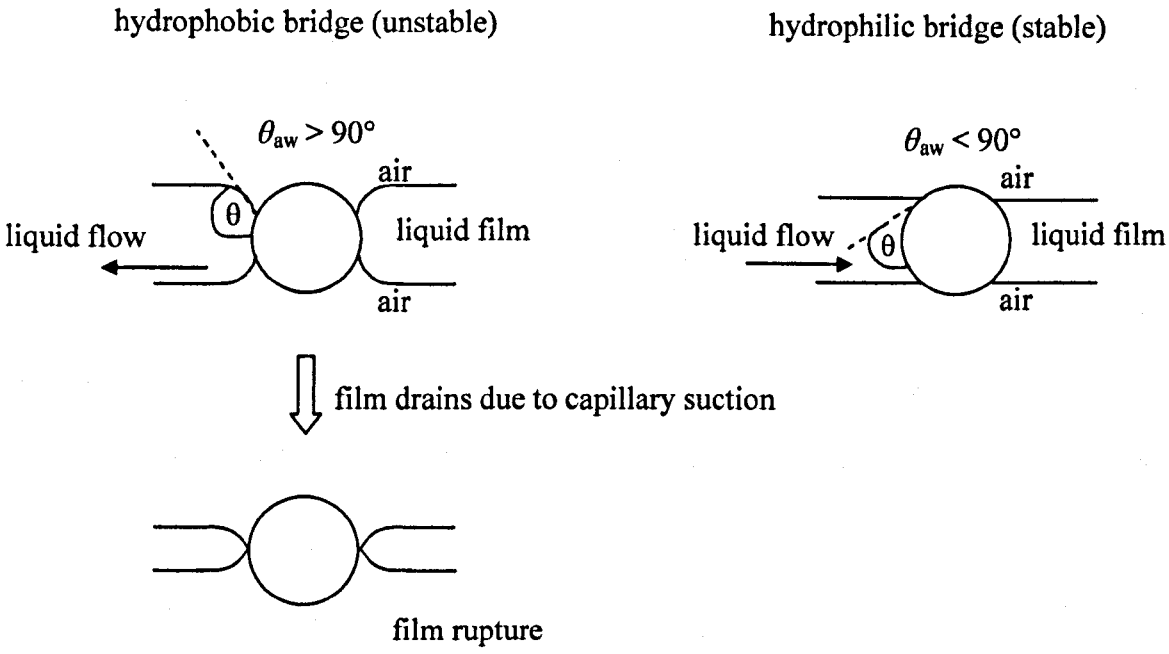

Figure 1.10 "Bridging-dewetting" mechanism of liquid oil droplet anti-foam action.

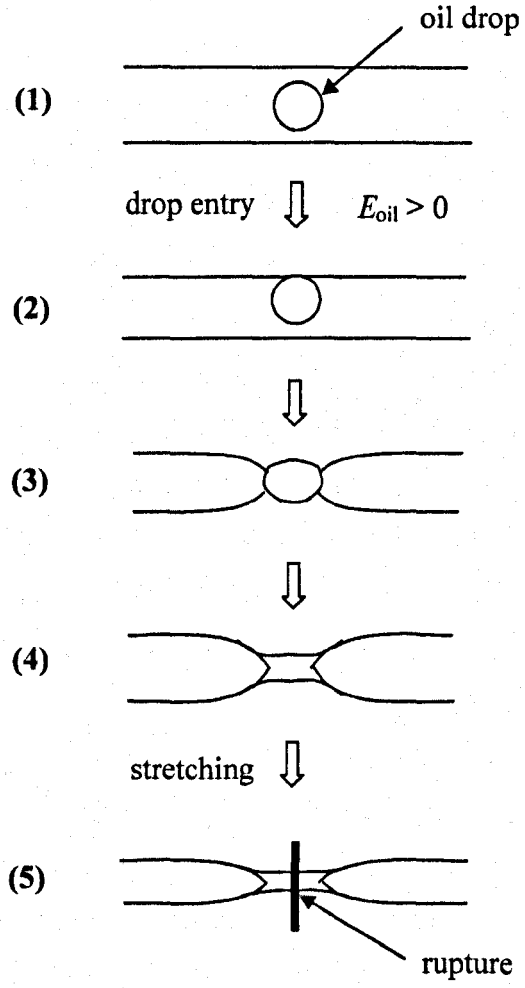

Figure 1.11 "Bridging-stretching" mechanism of liquid oil droplet anti-foam action.

surfactant/oil monolayer being formed. This possibility is investigated in detail in this work.

1.7.1 Mixed surfactant/oil adsorbed films at the air-water surface

Alkanes can adsorb into the tail group region of an adsorbed surfactant monolayer from either a liquid lens or the vapour phase, resulting in a surfactant/oil mixed monolayer. Such adsorption will occur in foam films in the presence of oil anti-foam agents but has not been considered explicitly in foam studies previously.

Alkane adsorption has been investigated for a variety of different surfactants including nonionic surfactants such as alkyl polyoxyethylene glycol ethers (C_nE_m) and ionic surfactants such as tri methyl ammonium bromide (DoTAB)[23], cetyl trimethyl ammonium bromides (CTAB), sodium diethylhexylsulphosuccinate (AOT)[24] and sodium dodecyl sulfate (SDS).[25] These studies have shown that alkane adsorption depends on a variety of different parameters, briefly summarised below.

1. Oil activity. The activity of the adsorbing oil (a_{oil}) is equal to the relative partial pressure of the oil vapour (P/P_0) where P is the partial pressure of the vapour and P_0 is the vapour pressure in equilibrium with the pure liquid at the same temperature. One way to vary the value of a_{oil} is by adding non-adsorbing diluent oil (such as squalane) to the alkane. As a_{oil} is increased, the surface concentration of the oil (Γ_{oil}) increases. For example, at a_{oil} = 0.2, 0.6 and 1 for decane on aqueous solutions of the nonionic surfactant $C_{12}E_5$ (6.4 mM), the surface concentrations of decane are 0.2, 0.9 and 2.6 molecules nm^{-2} respectively.[17]

2. Surfactant and oil type. Smaller length alkanes adsorb into the monolayer more than longer length alkanes, and adsorption becomes progressively more favoured with increasing alkane content of the mixed surfactant/oil film.[17] For example, at a mole fraction activity of 1, addition of octane and decane onto aqueous $C_{12}E_5$ (6.4 mM) results in Γ_{oil} values of 4.5 and 2.6 molecules nm^{-2}

respectively. Oil adsorption into the monolayer increases with increasing surfactant tail length[24] and increasing headgroup size (Figure 1.12). A $C_{12}E_5$ monolayer has a higher capacity for oil (dodecane) than that of a comparable hydrocarbon chain length cationic surfactant such as $C_{12}TAB$.[25] The separation centres of the surfactant chain and dodecane distributions is only 3 Å in the $C_{12}E_5$ system in comparison with 6.5 Å for $C_{12}TAB$. This is attributed to a favourable interaction between the dodecane and ethylene glycol chain.

3. Surfactant concentration. For systems at or above the cmc, Γ_{oil} remains constant with respect to bulk surfactant concentration.[24]

   As surfactant monolayers are progressively diluted (i.e. by dilution of the bulk surfactant concentration below the cmc), the alkane adsorption is found to rise initially but then to fall rapidly when the surface concentration of the surfactant (Γ_{surf}) is reduced to approximately half that at the cmc.

4. Temperature. The effect of temperature on the adsorption of dodecane onto nonionic surfactant ($C_{12}E_5$) and ionic surfactant (DoTAB) monolayers has been studied.[23] It was found that for the nonionic surfactant, dodecane adsorption decreases with increasing temperature at low surface concentration of the oil whereas it increases at high surface concentrations. With the ionic surfactant DoTAB, the temperature effect showed a similar crossover in behaviour but the changes in adsorption are opposite in direction to those seen for the nonionic surfactant.

Based on adsorption and neuatron reflection measurements for several oil/surfactant systems, it is found that oil adsorption occurs primarily by the filling of the empty volume between the surfactant chains with little effect on the packing density of the surfactant chains.[18] The solubilisation of alkanes in surfactant monolayers generally decreases the value of Γ_{surf} by a maximum of about 10 %.[24]

Chapter 4 discusses effects of oil adsorption on both foamability and foam stability.

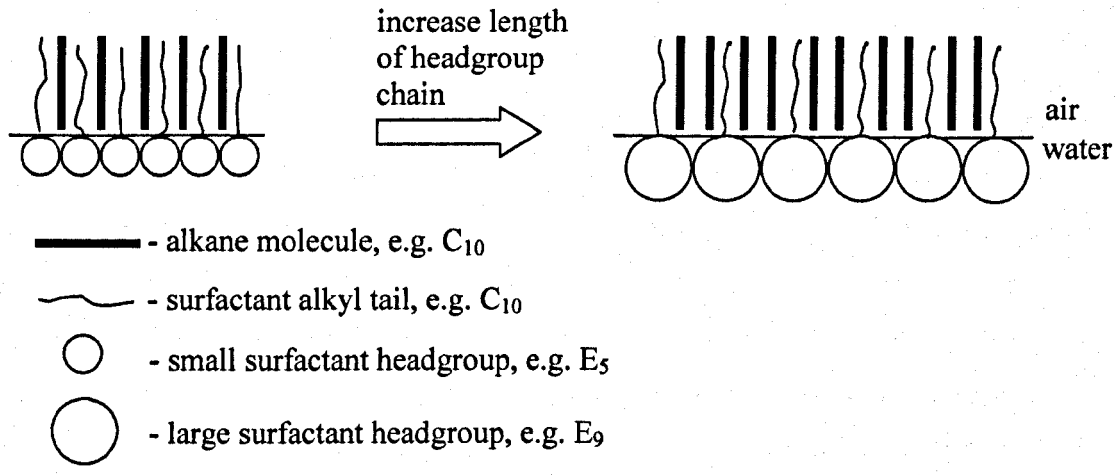

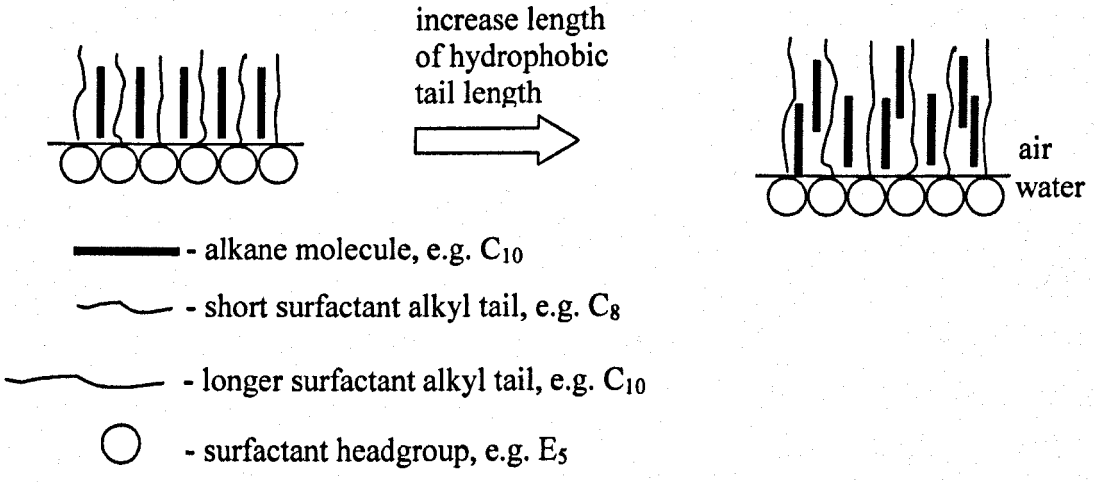

Figure 1.12 Increased oil adsorption in surfactant monolayers, $\Gamma_{oil,max}$ at the air-water interface due to (i) headgroup chain length increase (upper diagram) and (ii) hydrophobic tail length increase (lower diagram).

1.8 Solid particles as foam control agents

1.8.1 Classification of solid particles

Solid particles are often classified according to their average size, their aspect ratio, and their hydrophobicity. All of these aspects are important when considering the possible anti-foam action of solid particles. Of particular interest in this section is the particle's hydrophobicity. Hydrophobic particles prefer to be in contact with oil (or air) than water, whereas hydrophilic particles favour contact with water. A convenient way of describing the hydrophobicity of a particular particle type is by stating its contact angle θ_{aw} (measured through the aqueous phase). Figure 1.13 shows how contact angles (measured through the aqueous phase) control the particle positions in the interface.

Another way of classifying solid particles is by the % of residual hydrophilic groups (e.g. silanol, Si-OH on silica) remaining on the particle surfaces after they have been treated with a suitable agent to render them hydrophobic. Here, the contact angles are not known, but particles with 100 % SiOH on their surfaces would correspond to the most hydrophilic particles and particles with 0 % SiOH on their surfaces would correspond to the most hydrophobic particles. Also, as an example, a particle with 36.0 % SiOH on its surface would be more hydrophilic than one with 31.0 % SiOH on its surface but both would have an intermediate hydrophobicity. This method of classifying solid particles requires a high level of accuracy to be associated with the analytical determination of residual % SiOH groups (or other hydrophilic groups) on particle surfaces. See section 2.1.4 for a more detailed explanation of this.

1.8.2 Mode of action of solid particles

As discussed above (section 1.8.1), solid particles can exhibit a finite contact angle at, for example an air-water interface. Early research suggested that the adverse effect that particles had on aqueous froths could be attributable to the low wettability (high contact angle measured through the aqueous phase) of these particles.[26-28] More recently, Garrett found that finely divided polytetrafluoroethylene (PTFE) functioned

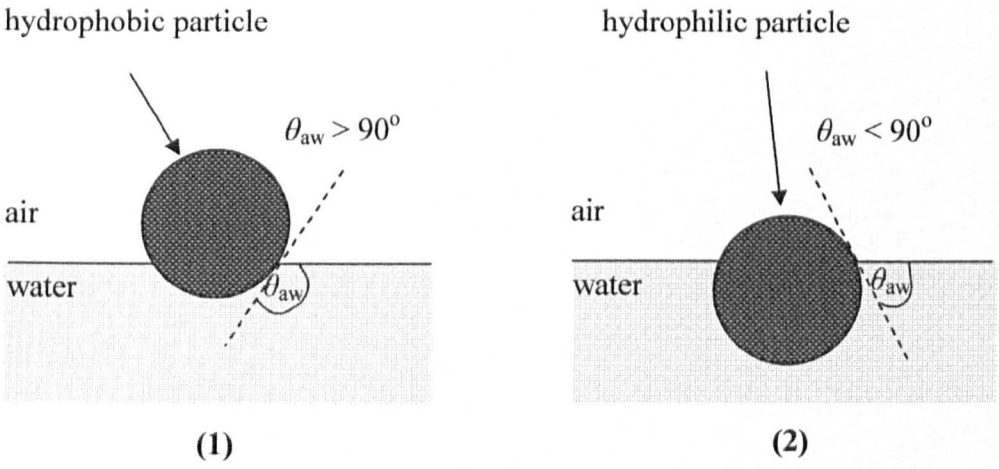

Figure 1.13 Contact angles at the air-water interface (θ_{aw}) of > 90° (hydrophobic particles, picture 1) and < 90° (hydrophilic particles, picture 2).

as an anti-foam. It was found that a correlation between the volume of foam destroyed (i.e. anti-foam efficacy) and contact angle existed. Garrett explained this behaviour in terms of a bridging action by the hydrophobic particle across two air-water interfaces.[29] He proposed that film rupture occurs when the particle bridging two air-water interfaces becomes spontaneously dewetted (due to its high contact angle). This action causes a hole to be formed in the foam film before the film finally completely ruptures. This mechanism is now described in more detail.

The bridging-dewetting mechanism is depicted in Figure 1.14. In the following explanation it is assumed that the particles are of a small enough size such that any effects arising from gravity are negligible. Fresh foams generated from foaming solutions containing pre-dispersed solid particles will have particles incorporated into the foam lamellae, (Figure 1.14, picture 1). At this stage, the lamellae are relatively thick compared to the diameter of the solid particle and so the particle will remain fully immersed in the intra-lamella liquid. As the film thins due to liquid drainage (driven mainly driven by gravity) it becomes thinner and providing the particle remains in the lamella, it can potentially enter one of the air-water surfaces. The immersion depth of the particle depends on its hydrophobicity (i.e. contact angle). (Figure 1.14, pictures 2 and 6). Film thinning continues to occur until the film becomes the same thickness as the depth of immersion of the solid particle, at which stage the particle bridges the two air-water surfaces and the lower air-water surface curves towards the particle due to the contact angle (Figure 1.14, pictures 3 and 7). This curvature causes a Laplace pressure which forces liquid away from the region around the particle resulting in enhanced film drainage.

The contact angle of the particle now dictates the fate of the thin film. If the contact angle of the solid particle with the foaming solution $\theta_{aw} < 90^{o}$ then film drainage will continue until the interface becomes planar (Figure 1.14, picture 4). Further drainage will cause the air-water surface to curve as shown in Figure 1.14, picture 5. This causes a Laplace pressure which acts to draw liquid towards the particle region thus opposing further film drainage and causing film stabilisation. If $\theta_{aw} > 90^{o}$, thinning will continue until the particle becomes completely dewetted resulting in a hole being formed in the foam film before subsequent rupture occurs (Figure 1.14, picture 8).

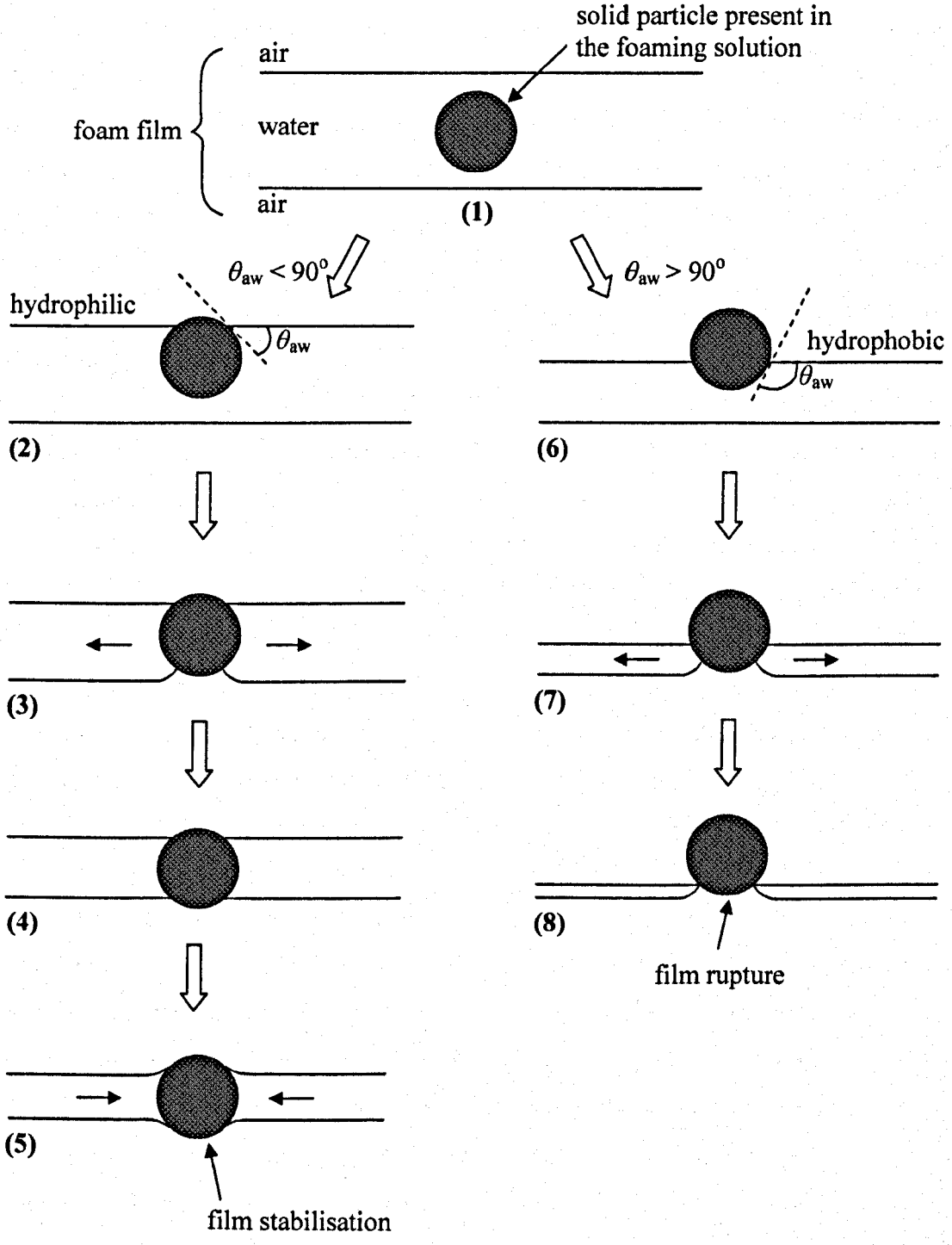

Figure 1.14 Bridging-dewetting mechanism of anti-foam action by solid particles. The fate of the foam film depends upon the contact angle of the particle at the air-water surface measured through the water phase, θ_{aw}.

1.9 Solid particles and oils operating in combination as anti-foams

Many formulated systems contain both oil and solid particles because the overall efficacy of the anti-foaming action is normally greater than if the oil and solid particles are taken separately, i.e. a synergy between the two components of the anti-foam compound is often observed.[6] Kulkarni et al.[30-32] proposed that the oil spreads along the surface of the film carrying particles with it. The particles then rapidly adsorb surfactant rendering them hydrophilic and causing a surface stress which leads to the ultimate rupture of the film. The problem with this view is that a local depletion in surfactant would cause the surface tension to decrease. This would cause a surface tension gradient and liquid would flow towards the area of high surface tension in a Marongoni flow (see section 1.4.5). This type of flow is regarded as a film stabilisation process. Additionally we note that hydrophilic particles are capable of stabilising foam (section 1.8.2). Dippenaar[33] suggested that the particles play the central role in a mixed anti-foam agent by a bridging dewetting mechanism (section 1.8.2). The oil adsorbs at the particle surfaces and simply increases the particle's contact angle. Frye and Berg[34] also proposed that oil coats the surfaces of solid particles in mixed anti-foam compounds. They proposed that these oil coated particles behave as larger hydrophobic particles and rupture films by the bridging-dewetting mechanism (see Figure 1.14). Due to their larger size, they will form a bridge across foam films faster than smaller particles because less liquid drainage from the film has to occur before the immersion depth of the particle is reached by the second interface. Garrett has shown that in a mixed oil/particle anti-foam compound, the solid particles are adsorbed at the oil-water interface.[6] He proposed that in the presence of particles, the ease in which the oil drop can penetrate the oil-water-air film (the pseudoemulsion film, see section 1.6) is increased. He suggested that the pseudoemulsion film is ruptured by the bridging-dewetting action (section 1.8.2). In Figure 1.15 it can be seen that the air-water interface will ultimately meet the oil-water interface causing rupture of the pseudoemulsion film if $\theta_{aw} + \theta_{ow} > 180^{o}$. If $\theta_{ow} > 90^{o}$ then film rupture can occur when $\theta_{aw} < 90^{o}$. If the particle was present in the absence of oil, then this would not occur (see section 1.8.2).[35,36]

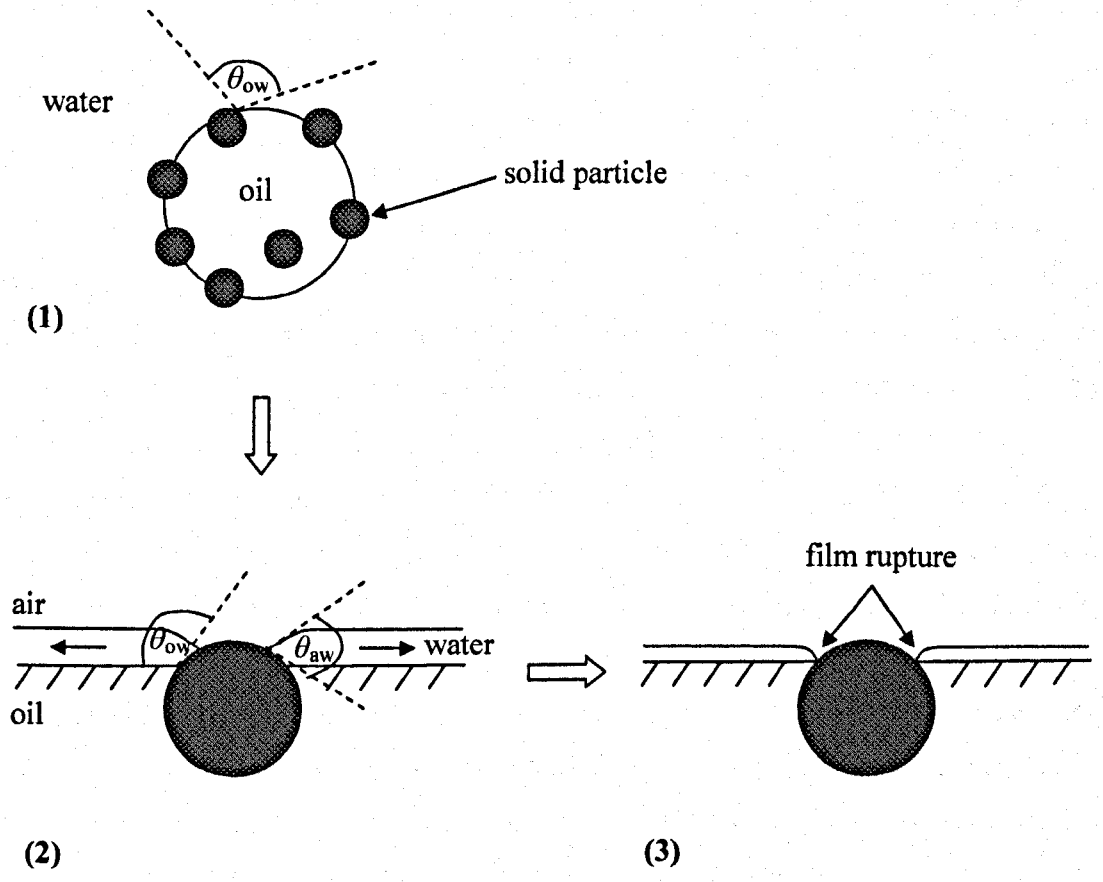

Figure 1.15 Rupture of air-water-oil (pseudoemulsion film) by spherical particles with $90^\circ < \theta_{ow} < 180^\circ$ and $\theta_{aw} > 180^\circ - \theta_{ow}$ so that $\theta_{aw} < 90^\circ$. Diagrams copied from reference 6.

1.10 Presentation of this thesis

Chapter 2 details all of the experimental techniques used in the study. The results of the work are then grouped into 4 main sections. Chapter 3 describes results relating to the foamability and foam stability of a series of pure surfactant homolgues as a function of their headgroup size and tail length. In chapter 4, the effect that oil vapours have on these foams is then presented. This work was carried out to test a possible mechanism to explain the observation that microemulsions can act as anti-foams.[22] Oil-in-water (o/w) microemulsions with nm sized oil droplets are capable of acting as anti-foams where the mechanism cannot be bridging-dewetting because the oil droplets are too small. A possible explanation for the anti-foam effect is that the solubilised oil adsorbs into the foam film surface forming mixed oil/surfactant monolayers. Adding oil in the vapour phase by sparging the gas through oil prior to the surfactant solution leads to oil/surfactant mixed monolayers to be formed directly, i.e. emulsions are not required. These ideas are systematically addressed by measuring the foaming properties of the nonionic surfactants in the presence of oil vapours of different types as a function of surfactant headgroup size and tail length. In chapter 5, the ways in which silica particles of nanometre (nm) size affect foaming solutions of nonionic surfactants are investigated. In the past, research into the effects of solid particles on foam has concentrated on much larger particles (of μm size). Chapter 6 looks at the effect that oils and nm-sized silica particles have on the foaming properties of nonionic surfactant when they are used in combination. Finally, a summary of the work and suggestions for future work are presented in chapter 7.

References

1. A. Waltermo, P. M. Claesson, S. Simonsson, E. Maner I. Johansson and V. Bergeron, Langmuir, (1996), **12**, 5271.
2. A. Bhakta and E. Ruckenstein, *Adv. Colloid Interface Sci.*, (1997), **70**, 1.
3. L. L. Schramm, *The Language of Colloid and Interface Science A Dictionary of Terms*, American Chemical Society, Washington DC, 1993.
4. D. J. Shaw, *Introduction to colloid and Surface Chemistry*, 4th ed., Butterworth Heinemann, Oxford, 1999.
5. K. Shinoda, T. Yamanaka and K. Kinoshita, *J. Phys. Chem.*, (1959), **63**, 648.
6. P. R. Garrett, *Defoaming Theory and Industrial Application*, Marcel Dekker, New York, 1993, pp.2-113.
7. M. J. Schick and E. A. Beyer, *J. Am. Oil Chemists Soc.*, (1963), **40**, 66.
8. G. M. Gantz, in *Nonionic Surfactants*, (M. J. Schick Ed.), Marcel Dekker, New York, 1967, p.739.
9. M. J. Schick and I. R. Schmolka, in *Nonionic Surfactants*, (M. J. Schick Ed.), Marcel Dekker, New York, 1987, pp.836-855.
10. J. H. Clint, *Surfactant Aggregation*, Blackie & Son Ltd, New York, 1992, p.154.
11. R. Aveyard and T. A. Lawless, *J. Chem. Soc., Faraday Trans. 1*, (1986), **82**, 2951.
12. M. N. Fineman, G. L. Brown and R. J. Myers, *J. Phys. Chem.*, (1952), **53**, 963.
13. A. BonfillonColin and D. Langevin, *Langmuir*, (1997), **13**, 599.
14. K. V. Schubert, R. Strey and M. Kahlweit, *J. Colloid Interface. Sci.*, (1991), **141**, 21.
15. N. M. Van Os, J. R. Haak and L. A. M. Rupert, *Physico-Chemical Properties of Selected Anionic, Cationic and Nonionic surfactants*, Elsevier, Amsterdam, 1993.
16. L. Lobo and D. T. Wasan, *Langmuir*, (1993), **9**, 1668.
17. R. Aveyard, B. P. Binks, P. D. I. Fletcher and J. R. MacNab, *Langmuir*, (1995), **11**, 2515.
18. B. P. Binks, D. Crichton, P. D. I. Fletcher, J. R. MacNab, Z. X. Li, R. K. Thomas and J. Penfold, *Colloids and Surfaces A*, (1999), **146**, 299.

19. S. A. Khan and R. K. Prud'homme (Eds.), *Foams Theory, Measurements and Applications*, Marcel Dekker, New York, 1996.
20. N. D. Denkov, P. Cooper and J. Martin, *Langmuir*, (1999), **15**, 8514.
21. N. D. Denkov, *Langmuir*, (1999), **15**, 8530.
22. R. Aveyard, B. P. Binks, S. W. Bird and P. D. I. Fletcher, Unpublished Results, University of Hull, 1996.
23. R. Aveyard, B. P. Binks, P. D. I. Fletcher and J. R. MacNab, *Ber Bunsen Phys. Chem.*, (1996), **100**, 224.
24. R. Aveyard, P. Cooper and P. D. I. Fletcher, *J. Chem. Soc. Faraday Trans.*, (1990), **86**, 3623.
25. J. R. Lu, Z. X. Li, R. K. Thomas, B. P. Binks, D. Crichton, P. D. I. Fletcher, J. R. McNab and J. Penfold, *J. Phys. Chem. B.*, (1998), **102**, 5785.
26. S. G. Mokrushin, *Kolloidn. Zh.* (1950), **12**, 448.
27. N. Dombrowski and R. P. Fraser, *Phil. Trans. Royal Soc. London, Ser. A*, (1954), **247**, 13.
28. A. K. Livshitz and S. V Dudenkov, *Tsvet. Metally*, (1954), **30**, 14.
29. P. R. Garrett, *J. Colloid Interface Sci.*, (1979), **69**, 107.
30. R. D. Kulkarni, E. D. Goddard and B. Kanner, *Ind. Eng. Chem. Fundam.*, (1977), **16**, 472.
31. R. D. Kulkarni, E. D. Goddard and B. Kanner, *J. Colloid Interface Sci.*, (1977), **59**, 468.
32. R. D. Kulkarni, E. D. Goddard and B. Kanner, *Croat. Chem. Acta*, (1977), **50**, 163.
33. A. Dippenaar, *Int. J. Miner. Process*, (1982), **9**, 1.
34. G. C. Frye and J. C. Berg, *J. Colloid Interface Sci.*, (1989), **130**, 54.
35. R. Aveyard, B. P. Binks, P. D. I. Fletcher, T. G. Peck and C. E. Rutherford, *Adv. Colloid Interface Sci.*, (1994), **48**, 93.
36. R. Aveyard, P. Cooper, P. D. I. Fletcher and C. E. Rutherford, *Langmuir*, (1993), **9**, 604.

Chapter 2

CHAPTER 2

Experimental

This chapter consists of two main sections. In the first section (2.1), the materials used in this work are fully described. The second part (sections 2.2 – 2.10) contains full details of the apparatus and experimental techniques used throughout the study.

2.1 Materials

2.1.1 Water

All water was purified by passage through an Elgastat Prima reverse osmosis unit and then through a Milli-Q water reagent system. The surface tension of the processed water was periodically checked and found to be 71.8 ± 0.2 mN m^{-1} at 25.0 °C. This tension is in excellent agreement with published literature values[1] indicating that the water was free from surface active impurities.

2.1.2 Surfactants

a. Polyoxyethylene glycol ethers of general structure $H\text{-}(CH_2)_n(O\text{-}CH_2\text{-}CH_2)_m\text{-}OH$ abbreviated to C_nE_m were obtained from a variety of sources and were all of the highest purity available. The surfactants obtained from Nikkol were chromatographically pure samples. The surfactants obtained from Fluka and Sigma had purities of at least 97 %. Purity of the surfactant samples was checked by comparing the cloud points (Cp.) of 1 weight percent (wt. %) aqueous solutions (see section 2.10.1) with literature values. Data relating to this class of surfactants can be found in Table 2.1.

Table 2.1 Summary of measured and literature values of the cloud points of aqueous solutions (1 wt. %) and literature values for the cmc at 25.0 °C of the different C_nE_m surfactants used in this work. Numbers in parenthesis show reference sources.

Surfactant	Measured Cp. /°C	Literature Cp. /°C	Supplier	Stated purity	cmc /M
C_8E_5	65.0	63.6 [2]	Sigma	99.4 %	6.7×10^{-3} [3]
$C_{10}E_5$	47.0	44.0 [3]	Fluka	> 97 %	8.1×10^{-4} [3]
$C_{12}E_5$	33.5	32.0 [4]	Nikkol	Single peak on GC	6.4×10^{-5} [5]
$C_{14}E_5$	25.5	20.0 [3]	Nikkol	Single peak on GC	1.0×10^{-5} [3]
$C_{12}E_7$	66.0	66.8 [2]	Nikkol	Single peak on GC	8.0×10^{-5} [6]
$C_{12}E_8$	81.4	80.0 [3]	Nikkol	Single peak on GC	9.04×10^{-5} [7]
$C_{12}E_9$	89.5	87.5 [3]	Fluka	> 98 % (TLC)	1.0×10^{-4} [6]

b. n-dodecyl trimethyl ammonium bromide (DTAB) was obtained from Avocado Research Chemicals Ltd and had a stated purity of 97 %. It was used as received without further purification. The literature value for the cmc for DTAB in water is reported as 1.5×10^{-2} M.[8] DTAB has the following structure:

$H\text{-}(CH_2)_{12}\text{-}N(CH_3)_3^+ \; Br^-$

c. Sodium dodecylsulphate (SDS) was obtained from BDH and had a stated purity of ≥ 99 %. It was used as received without further purification. The literature value for the cmc of SDS is water is reported as 8×10^{-3} M.[9] SDS has the following structure:

$H\text{-}(CH_2)_{12}\text{-}SO_4^- \; Na^+$

d. Commercial nonionic surfactants obtained from Unilever, Vlaardingen, The Netherlands were used as received. Unlike the chromatographically pure surfactants described in (a) above, the commercially available non-ionic surfactant described here has a distribution associated with the number of carbons in the hydrophobic chain and the number of ethylene oxide units in the hydrophilic moiety and consequently does not have a specified relative molecular mass. Lutensol AO7 is predominantly composed of $C_{12}E_7$ and as a result, its cmc will be similar to that of $C_{12}E_7$. In this work, all concentrations relating to the commercially available surfactants are quoted in wt. % avoiding the requirement of knowing the precise relative molecular mass.

2.1.3 Oils

The *n*-alkanes used were obtained from Aldrich and had stated purities of at least 98 %. Prior to use they were all passed through a packed column of neutral aluminium oxide (Al_2O_3) twice to remove polar impurities. The purity of the oils is summarised in Table 2.2.

Table 2.2 Purities of the oils used in this work.

Alkane	**Supplier**	**Purity**
hexane	Aldrich	98 %
octane	Aldrich	98 %
decane	Aldrich	> 99 %
dodecane	Aldrich	> 99 %
squalane	Aldrich	99 %

2.1.4 Silica particles

Silica particles with primary particle diameter quoted as 10 – 40 nm were obtained as gifts from Wacker-Chemie and were used as received. They are prepared as follows: first, volatile trichlorosilane is introduced into a hydrogen / oxygen flame. Hydrolysis takes place at about 1200 °C producing fumed silica and hydrogen chloride. This produces primary particles with diameters of the order of 10 nm. In the flame these primary particles fuse into larger units, known as aggregates, of the order of 100 – 500 nm. Upon cooling, these aggregates flocculate to form agglomerates. These agglomerates measure between 10 – 50 μm. The hydrophilicity of the particles is described in terms of the % of residual silanol groups on the particle surfaces. The SiOH groups provide the hydrophilic character of the particles. These SiOH groups can form hydrogen bonds between the silica particles or to other polar substances. For example, the SiOH groups can react with dichlorodimethylsilazane ($(CH_3)_2SiCl_2$), hexamethyldisilazane ($[(CH_3)_3Si]_2NH$) or reactive polydimethylsiloxanes to form hydrophobic silica particles.

Typically, there are 2 SiOH groups per 1 nm^2 on the surfaces of the hydrophilic silica and 1 Si-OH group per 1 nm^2 on the surfaces of the hydrophobic silica.[10] The most hydrophobic silica particles have about 0.5 SiOH groups per 1 nm^2. Figure 2.1 shows the production process of the fumed silica particles and the structure of (i) hydrophilic silica and (ii) hydrophobic silica.[10] Figure 2.2 shows a TEM image of a carbon-coated Cu/Pd grid with hydrophilic silica particles deposited by evaporation from a solution containing dispersed particles in an aqueous solution of $C_{12}E_5$. It can be seen from the figure that the particles tend to aggregate together in solution to form larger units. The TEM confirms that the diameter range of the individual particles is of the order of 20 nm, and that the size distribution of the particles is within the range quoted by the manufacturer.

Table 2.3 summarises the range of different silica particles available according to the % SiOH groups on the particle surfaces.

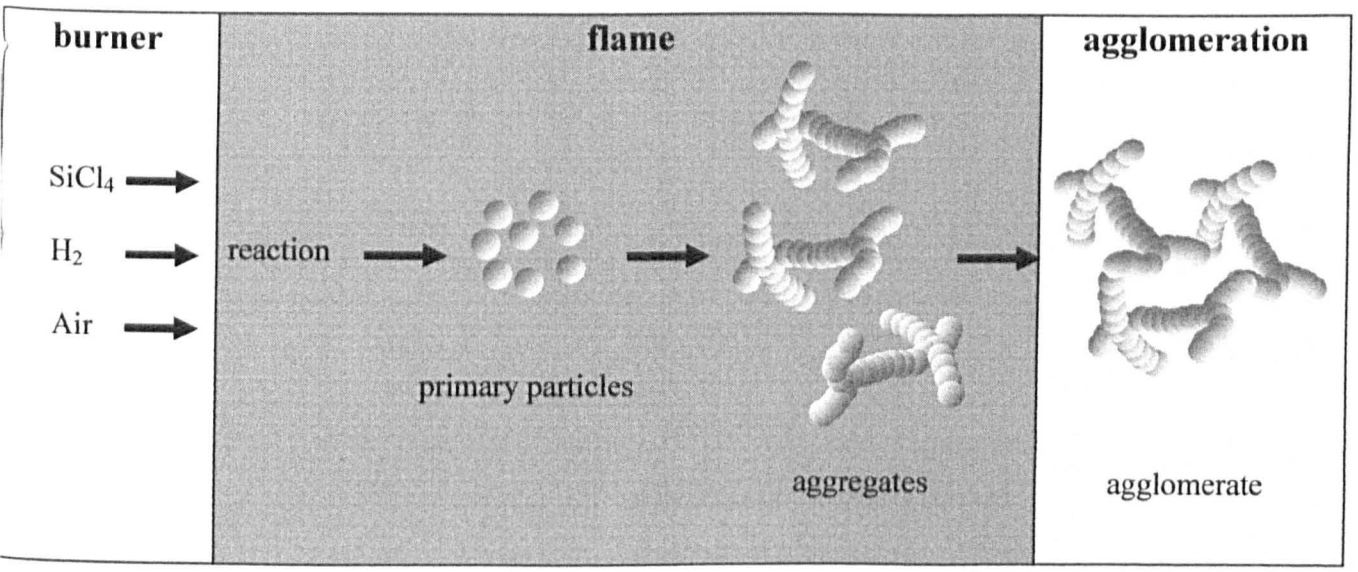

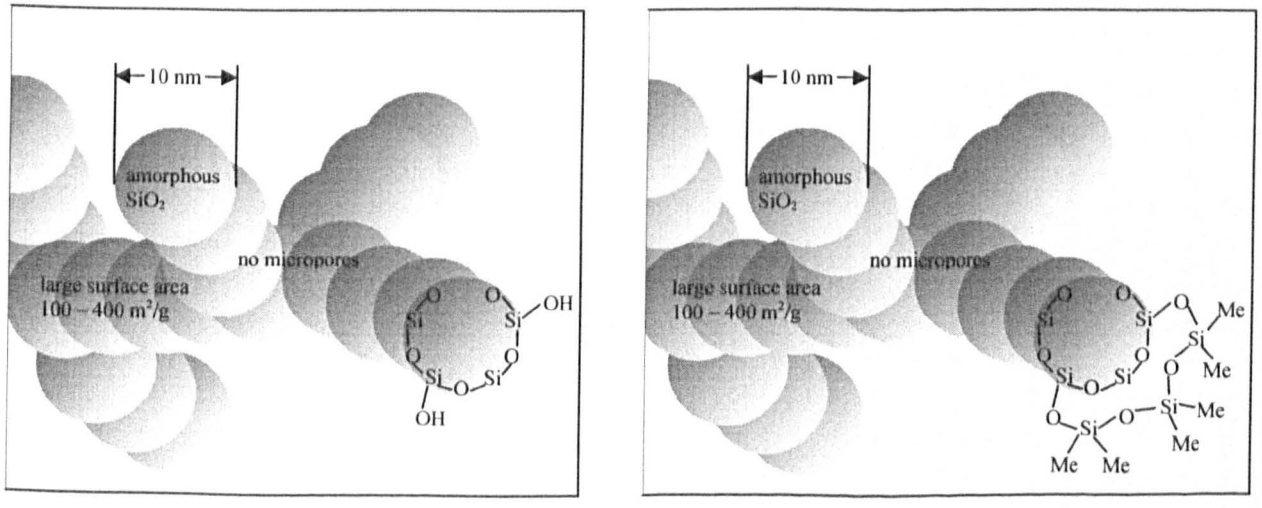

Figure 2.1 The 3-stage production process for fumed silica particles (top diagram) and the structures of the hydrophilic (left) and hydrophobic (right) silica particles (bottom diagram). The diagrams have been copied from reference 10.

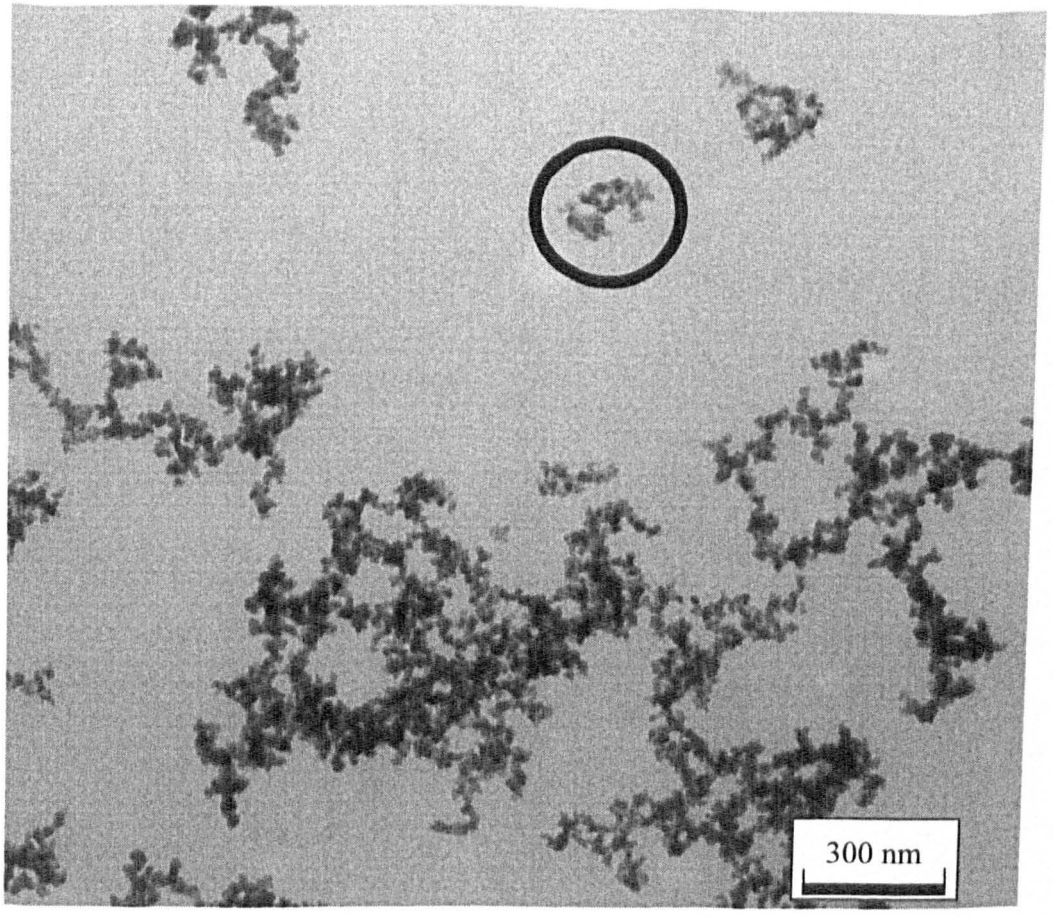

Figure 2.2 Transmission electron micrograph (TEM) of a carbon-coated Cu/Pd grid with silica particles deposited by evaporation from a solution composed of 0.2 wt. % silica (100 % SiOH) dispersed in aqueous $C_{12}E_5$ (1 mM). The scale bar is shown in the Figure. The circle highlights a typical aggregate formed when multiple particles adhere together in solution.

Table 2.3 The range of silica particles used in this work.[10]

Codename	% SiOH	Specific surface area / m^2g^{-1}
N20	100	200
SLM 1466	79.9	200
SLM 1471	65.7	200
SLM 957	57.0	200
SLM 1472	50.9	200
H30	50.0	250
SLM 1467	40.4	200
SLM 091	36.0	200
SLM 1468	24.1	200
SLM 1469	18.3	200
SLM 1470	14.1	200

2.1.5 Miscellaneous materials

In addition to the surfactants, oils and silica particles mentioned above, the following materials were also used in this work.

Table 2.4 Miscellaneous materials used in this study

Material	Supplier	Purity
hexamethyldisilazane (HMDS)	Lancaster	> 99 %
sodium chloride (NaCl)	BDH	99.5 %
potassium hydroxide (KOH)	BDH	AnalaR grade
ethanol (EtOH)	BDH	AnalaR grade
aluminium oxide (Al_2O_3)	Sigma	> 99 %
nitrogen gas (N_2)	Energas	High purity

2.2 Preparation of glassware

All glassware was cleaned by immersing it in a solution of alcoholic KOH (approximate composition is 2 M KOH in 4 parts ethanol to 1 part water) and allowing it to soak for at least 1 hour. The glassware was then removed and rinsed under distilled water before being finally rinsed under ultra pure water (obtained from the Milli-Q water reagent system) and dried in an oven at approximately 60 °C.

2.3 Measuring foam volume and foam stability using a foam column

2.3.1 Foam column description

A thermostatically controlled foam column was constructed as shown in Figure 2.3. The thermostat surrounding the column comprises two concentric glass cylinders with a copper coil in the annular space between them with both sections filled with distilled water. Water was pumped around the copper coil using a thermostat (Grant LT D6G, -20 to 100 °C) capable of temperature control to within 0.1 °C. Before each foaming measurement, the column was washed with a solution of alcoholic KOH and rinsed thoroughly with Milli-Q treated water.

N_2 gas was passed through a Puritube packed with activated charcoal to remove any organic gaseous material, and a 5 - 100 cm^3 min^{-1} gas flowmeter (Platon, Gilmont Instruments) into the inlet manifold at the bottom of the column. The gas flowmeter was calibrated prior to use by setting a constant gas flow rate and measuring the volume swept by a single soap bubble in 1 minute along a graduated burette. This number was plotted as a function of the displayed meter reading at this fixed flow rate (Figure 2.4).

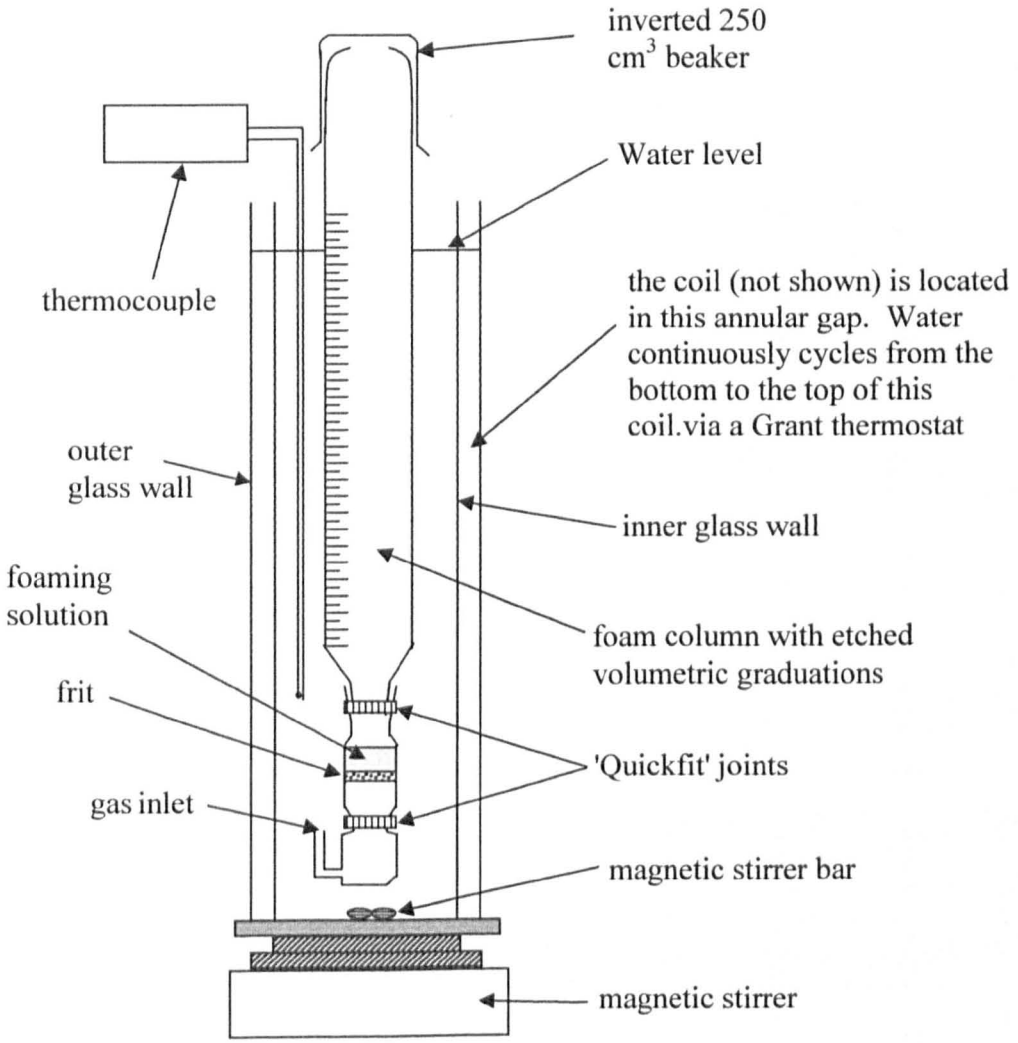

Figure 2.3 Schematic diagram of the foam column and thermostat used for foamability and foam stability measurements.

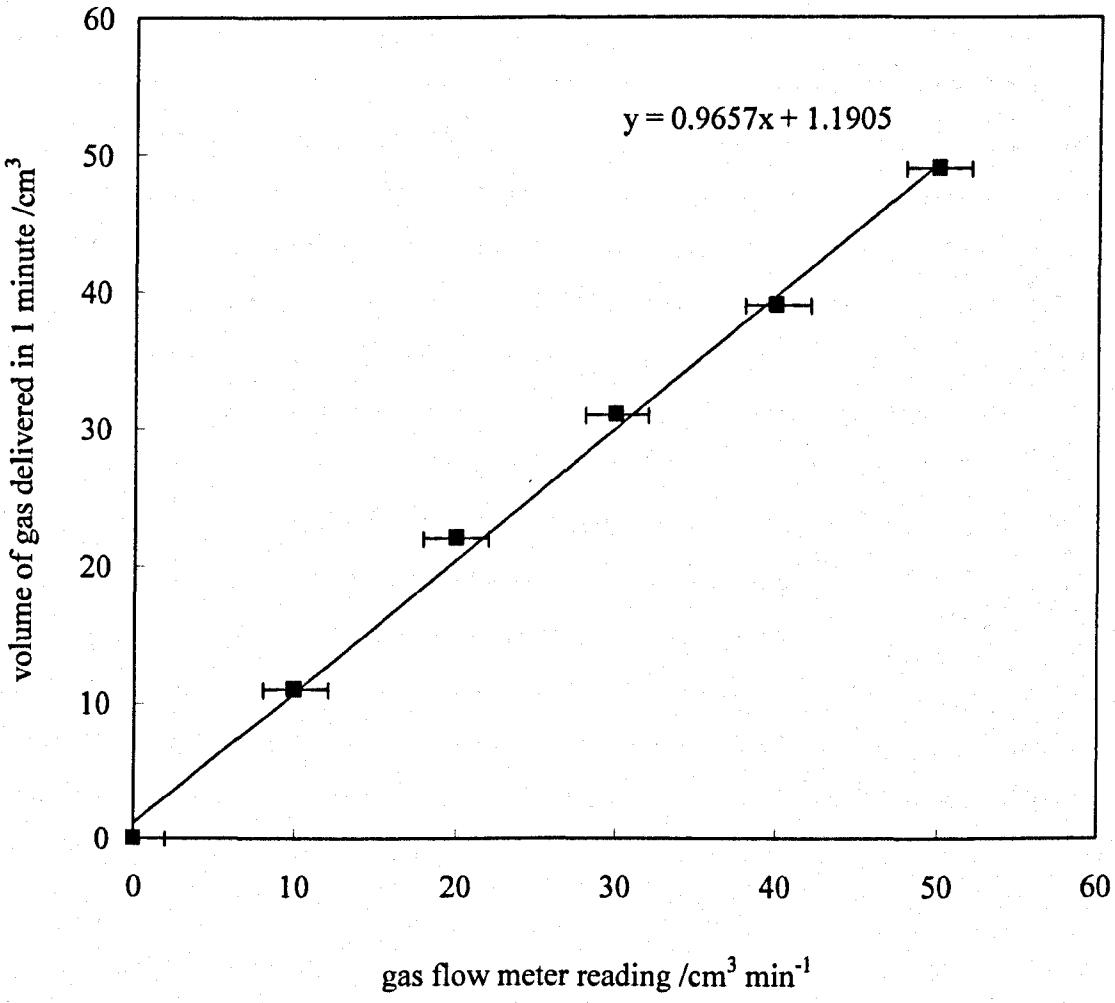

Figure 2.4 Calibration plot for the Plaxton flow meter of gas volume delivered in 1 minute versus the flow meter reading.

2.3.2 *Foam column operation*

The column was first removed from its thermostat and the upper part of the column was removed by unscrewing the Quickfit joint. The gas flow rate was set as low as possible (1 - 2 cm^3 min^{-1}), and the aqueous surfactant solution (15.0 cm^3) was added onto the top of the frit (Pore 1, 90 – 150 μm). No foaming occurs at this stage due to the very low flow rate of gas. The upper part of the column was then screwed back on and the entire column is immersed in the thermostat bath. The inverted beaker at the top of the column acts as a dust cap and also helps to minimise any evaporation of liquid from the top surface of the foam. The temperature was continuously displayed using a type K thermocouple (Eurisem ST-508) capable of measuring to 0.1 °C. The thermocouple was calibrated prior to use with a mercury thermometer (Zeal, England) capable of being read to the same accuracy. Once the temperature of the column and the surfactant solution on the frit had equalised to the temperature of the water thermostat, foaming was initiated by increasing the gas flow rate using the control on the gas flow meter to the desired value (normally 48 cm^3 min^{-1}). The volume of foam produced after a suitable foaming time (typically 10 minutes) was recorded as a function of bulk surfactant concentration using the volumetric gradations on the column giving a measure of foamability for a particular surfactant system. In addition to these measurements, the appearance of the foam was noted and the approximate bubble radius was estimated visually.

2.3.3 *Foam stability measurements using the foam column*

The stability of the foam was assessed by plotting foam volume as a function of time after the foam had been created. Time = 0 was taken as the instant the foam had been produced and the gas supply had been removed after the initial (10 minute) foam production period.

2.4 Delivery of oil vapour to a foam

In order to produce foam made from gas containing oil vapour, the oil vapour delivery system was introduced between the flow meter and the inlet manifold at the bottom of the foam column.

2.4.1 Apparatus

The vapour delivery system comprises three bubblers that are situated in the same thermostatted water bath as the foam column. Fixing the entire foaming system at the same temperature ensures that there are no 'cold spots' in the vapour delivery system where the oil could condense and form droplets. The N_2 gas enters the first oil bubbler and becomes saturated with the alkane of interest. In order to ensure that the N_2 gas was fully saturated with alkane oil vapour, three bubblers were connected together in a serial configuration (Figure 2.5). See section 4.3 for a detailed explanation of the way in which it was verified that 3 bubblers were sufficient to saturate the gas.

2.4.2 Variation of oil vapour activity

Alkane vapour concentrations (expressed as oil vapour activity equal to the ratio of the oil partial pressure to the saturated oil vapour pressure P/P_0) were controlled and set at specific values for some of the foaming measurements by mixing the alkane of interest with the involatile long-chained alkane squalane (C_{30}). For measurements with alkane vapours delivered at values of P/P_0 less than 1, the bubblers contained mixtures of the volatile oil and squalane. The required value of P/P_0 was obtained by adjusting the mole fraction of the alkane relative to the mole fraction of squalane within the bubblers according to the following relationship:

$$P/P_0 = fX \qquad [2.1]$$

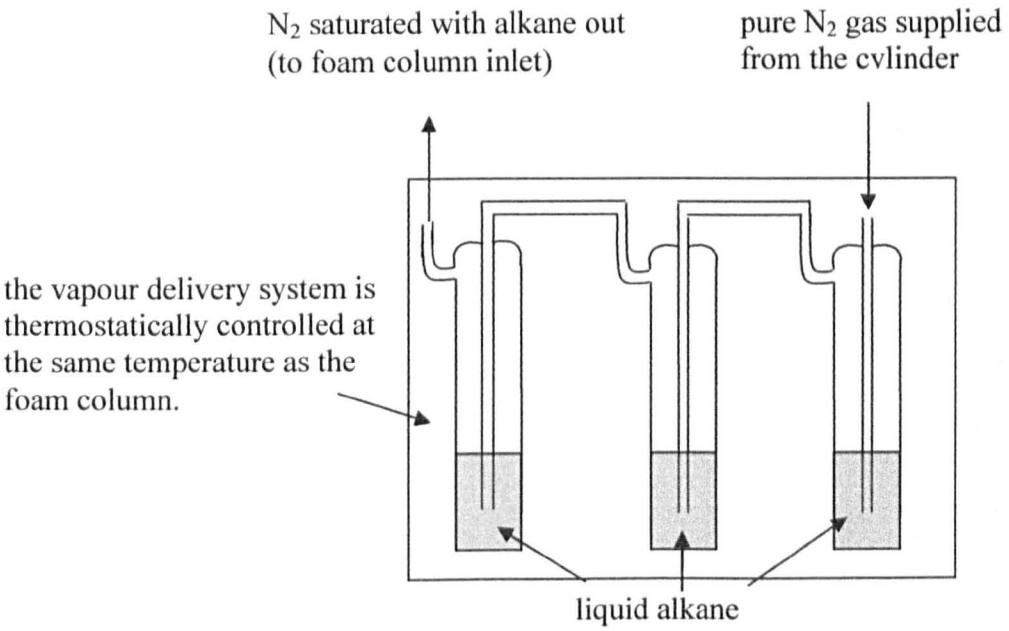

Figure 2.5 A schematic diagram showing the configuration of the three oil bubblers connected in series in order to produce a saturated N_2-alkane vapour stream.

Where X is the mole fraction of the volatile alkane in the squalane mixture and f is the activity coefficient. The necessary activity coefficients are taken from extrapolations of data published in the literature.[11] Previous work undertaken at Hull has established that this procedure reliably produces the correct oil vapour concentration within the flowing gas stream.[12]

2.5 Measuring foamability and foam stability using shake tests

The foamability and foam stability of various foaming solutions were assessed using the "shake test". The shake test provides a quick and quantitative way of assessing both foamability and foam stability. An accurately measured volume of the foaming solution was transferred to a 100 cm^3 measuring cylinder which was then stoppered before being shaken by hand in a reproducible way for 1 minute. Foam volume was measured as a function of time until the foam had fully collapsed to 0 cm^3. The initial volume of the freshly formed foam relates to the foamability of the foaming solution and the time taken for the foam to fully collapse corresponds to the foam stability of the dispersion. In this work foam stability is generally reported as the time taken for the foam to collapse to half its initial volume. All of the shake tests were performed at ambient temperature (19 ± 2 °C).

2.6 Preparation and characterisation of aqueous surfactant-silica dispersions

2.6.1 Dispersion of silica into surfactant solutions

A known mass of silica powder was accurately weighed into a glass bottle of approximate volume 50 cm^3 typically containing 20.0 cm^3 of aqueous surfactant solution. Generally, for the majority of systems containing silica detailed in this thesis, the concentration of dispersed silica was within the range of 0.05 to 0.2 wt. %. The particles were dispersed using a high intensity ultrasonic vibracell processor (Sonics & Materials) with a tip diameter of 3 mm, operating at 20 KHz at a power of between 10 and 40 W for up to 10 minutes. The power and the time were adjusted

depending on the ease with which the particles would disperse (this was judged visually). During the dispersion process it was necessary to immerse the bottle containing the dispersion in an ice bath to prevent excessive heating of the solution.

2.6.2 Characterisation of surfactant-silica dispersions using transmission electron microscopy

Transmission electron microscopy (TEM) was used to characterise various surfactant-silica dispersions. Silica particles were dispersed into the various aqueous surfactant solutions as described in the previous section. They were then allowed to equilibrate overnight in a thermostatted water bath whilst being stirred with a magnetic stirrer. Immediately prior to analysis by TEM, the sample was manually agitated. 1 drop of the undiluted dispersion (*ca.* 10 μL) was then withdrawn and placed onto a 300 support mesh made from Cu/Pd and coated with carbon. The dispersion was then allowed to air dry. The prepared sample was then placed onto a Jeol 100c 80 kV electron microscope. The resulting image was exposed onto a Kodak sheet film which was developed for 4 minutes before being printed at a factor x3 enlargement. It was possible to size any species shown in the print using a ruler as the factors of enlargement and magnification were known.

2.7 Measuring surface tensions using the du Noüy ring method

Surface tensions (γ) were determined by measuring the static, maximum pull on a platinum / iridium (Pt / Ir) du Noüy ring (supplied by Krüss) on a home-built, fully thermostatted tensiometer.

2.7.1 Background theory

A du Noüy ring tensiometer comprises a chemically inert ring suspended from a sensitive balance such that the force required to pull the ring from a liquid's surface (or the interface between two liquids) can be measured. It is essential that the

temperature of the liquid on which the measurements are being performed is accurately controlled (± 0.1 °C or better) and so a thermostat is also an essential component of a tensiometer. The ring is suspended from the balance via supporting stirrups which are an integral part of the ring itself and serve to hold the ring parallel to the plane of the liquid's surface. The ring is initially suspended above the liquid (Figure 2.6, picture 1). The ring is then gradually lowered and contacts the liquid surface causing a meniscus to form. At this stage it is subjected to a slight positive force because of the adhesive force between the ring and the surface (Figure 2.6, picture 2). Due to the surface tension of the liquid, the ring must be pushed through its surface which causes a small negative force (Figure 2.6, picture 3) to be exerted on the ring. Slightly more lowering causes the ring to completely break through the liquid's surface (Figure 2.6, picture 4). The meniscus (now supported by the ring) can be raised to a height above the plane of the liquid by raising the height of the ring. During this height increase, the force acting upon the ring increases until it reaches a maximum value (Figure 2.6, pictures 5-7). This maximum force corresponds to the condition where a tangent constructed at the wetting point on the ring is perpendicular to the plane of the liquid's surface (see picture 7 in Figure 2.6) Raising the height of the ring beyond this point causes the force on the ring to decrease and eventually, the lamella breaks (Figure 2.6, picture 8).

Equation 2.2 describes the situation when the maximum pulling force is present on the ring during a measurement

$$mg = \frac{4\pi R\gamma}{F} \qquad [2.2]$$

m is the mass of the liquid raised above its surface, g is the acceleration due to gravity, R is the average radius of the ring (obtained by adding value of the inner radius of the ring and the radius of the wire making up the ring) and F is a correction factor. F is included in order to allow for the hydrostatic weight of the liquid volume in the meniscus formed underneath the ring.[13] The shape of this meniscus is largely dependent on the geometry of the particular ring used. This means that the precise shape of the meniscus needs to be considered in order to accurately obtain the volume of liquid underneath the ring when the condition of maximum pull is reached. The

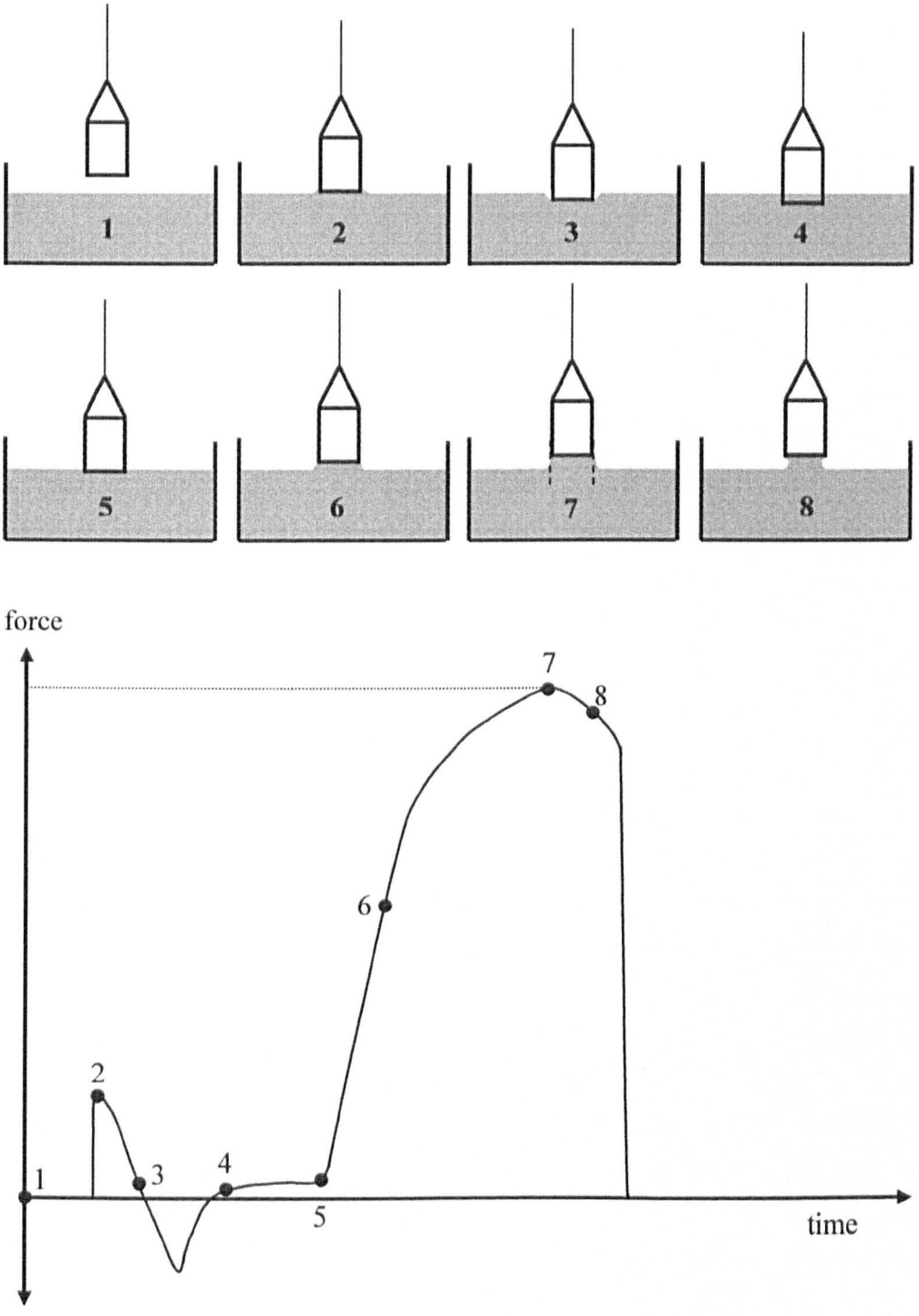

Figure 2.6 Forces subjected to a du Noüy ring at various stages of the surface tension measurement process. The horizontal dashed line shows the maximum pulling force on the ring.

correction factor allows for differences in shape between the meniscus on the outside and inside of the ring. When the condition of maximum pull is attained, the force acting upon the ring is a function of R^3/V and R/r, where r is the cross-sectional radius of the wire of the ring and V is the volume of liquid lifted above the liquid plane in the solution. This volume is given by the following equation

$$V = \frac{\gamma^* 4\pi R}{\Delta\rho g} \qquad [2.3]$$

where γ^* is the uncorrected surface tension and, $\Delta\rho$ is the difference in densities between the two phases (in this work, between air and water) and g is acceleration due to gravity.

R^3/V is calculated for each determination and the corresponding correction factor F is obtained from extrapolating data from published tables in the literature.[13] Once F has been obtained for a given uncorrected surface tension, γ^*, the actual (corrected) surface tension is simply the product $\gamma^* F$.

The correction factor described above is only applicable when the surface tension is above 25 mN m^{-1}. In order to measure surface tensions below these values the correction factor developed by Zuidema and Waters[14] should be used. This factor is an extension of the earlier work by Harkins and Jordan.[13] This factor should be multiplied by the uncorrected surface tension in order to obtain the actual surface tension and it is calculated in the following way

$$F = 0.725 + \sqrt{\frac{0.01425\,\gamma^*}{\frac{L^2}{4}(\rho_1 - \rho_2)} + 0.04532 - \frac{1.679}{\frac{R}{r}}} \qquad [2.4]$$

where L is the wetted parameter of the ring (= $4\pi R$) and ρ_1 and ρ_2 are the densities of the phases with the highest and lowest densities respectively.

2.7.2 Construction and operation of the tensiometer used in this work

A schematic diagram detailing the setup of the tensiometer can be seen in Figure 2.7. The du Noüy ring is suspended from the bottom of the balance. The laboratory jack is heightened such that the du Noüy ring resides in the surface of the solution. The balance is then set to zero. The maximum pull on the du Noüy ring is continuously maintained by adjusting the height of the solution-containing Petri dish using the laboratory jack. The maximum pull, reported as a mass on the balance, is subsequently converted to a force by multiplying it by acceleration due to gravity (g) which is accurately calculated for the specific location of the measurement. The thermostatted jacket has pumped water continuously circulating around it which is pumped directly from a Grant thermostat (not shown in the Figure). This method of temperature control makes it possible to maintain the temperature to within 0.1 °C when the required temperature is within a few degrees of ambient temperature. The entire system is covered with a hood to reduce external disturbance potentially arising from drafts etc. Before each use, the du Noüy ring was cleaned by immersing it in a solution of alcoholic KOH. It was then rinsed in water treated by the Milli-Q water reagent system before being dried in a blue Bunsen burner flame until it glowed red.

The ring used in all of the surface tension measurements had a mean radius of 9.549 mm and was constructed of wire with a cross-sectional radius of 0.185 mm.

2.8 Single soap film lifetimes

2.8.1 Apparatus

The lifetimes of single soap films were measured using the apparatus depicted in Figure 2.8. The apparatus served as a way of making soap films from a foaming solution in a controlled and reproducible way.

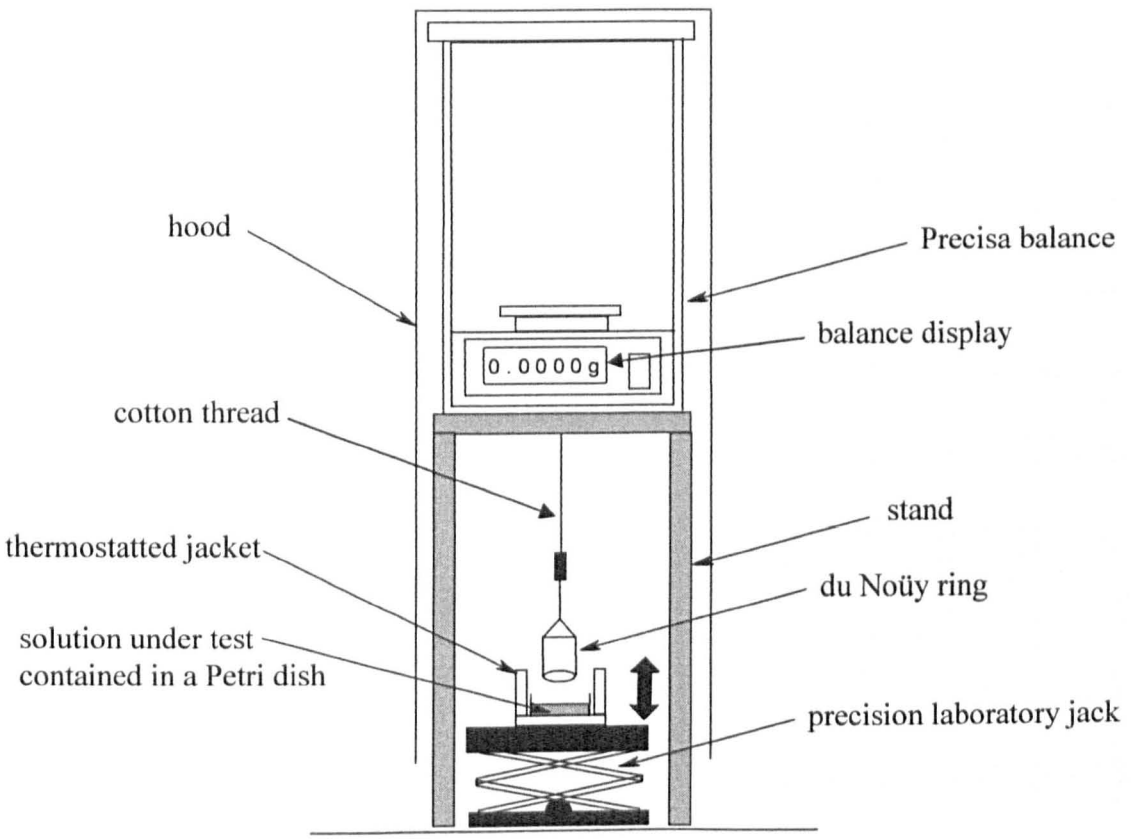

Figure 2.7 Schematic diagram of the home-built tensiometer. Tensions were calculated using the maximum force subjected to the suspended Pt / Ir du Noüy ring.

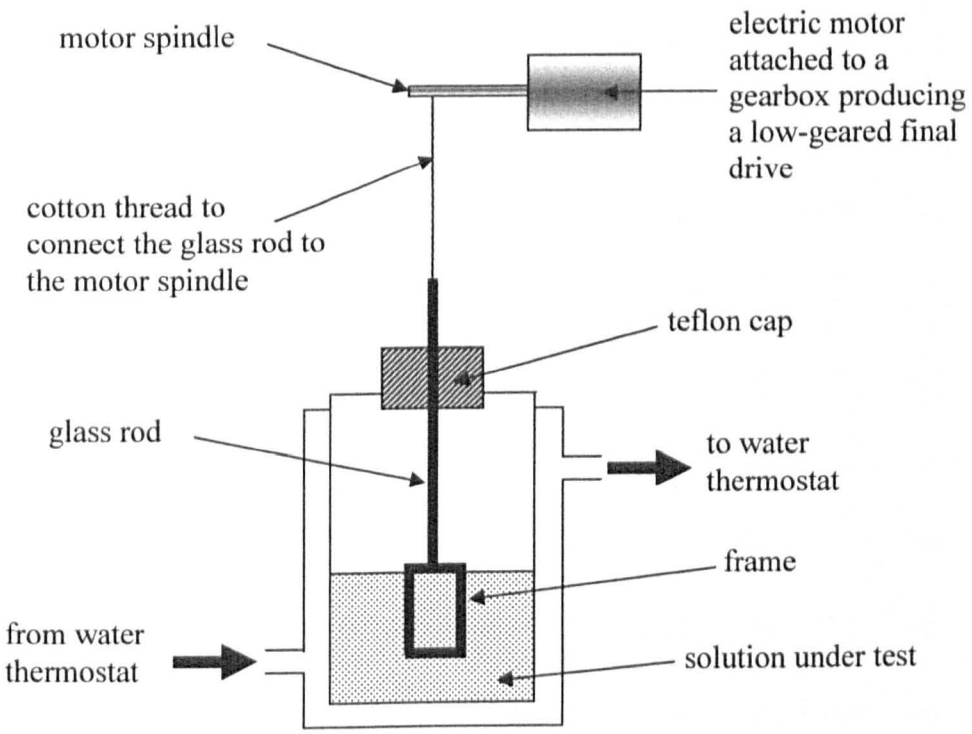

Figure 2.8 Apparatus used for measuring the lifetimes of single soap films.

2.8.2 *Operational procedure*

The thermostatted vessel has an approximate internal volume of 110 cm^3 and an internal height of 70 mm. The vessel has a screw on cap with a rubber bung inside. The bung has a hole through its centre large enough for the glass rod to easily pass through. Films are formed on the glass frame (internal dimensions: 27 mm high x 16 mm wide) constructed of 2 mm diameter glass rod. The frame is attached to a glass rod which passes through the hole in the seal and is attached to some cotton which is rapped around the spindle of an electric motor. The motor is used so that the speed at which the film is drawn is reproducible. The motor is geared in such a way that the frame is lowered and raised at a rate of 10 mm sec^{-1}. 60.0 cm^3 of a $C_{12}E_5$ (1 mM) surfactant solution is placed in the vessel. The glass frame is then placed into the solution such that it is fully immersed. The seal at the top of the container is then screwed on, and the cell is thermostatted at 20.0 °C. The system is then left for 1 hr to allow the headspace above the surfactant solution to become fully saturated. A film is drawn by pulling the glass frame upwards out of the surfactant solution using the motor until the bottom edge of the frame is just below the surface of the solution. This is to ensure that the liquid can drain freely from the film into the bulk solution. Film lifetimes are measured by simply measuring the time taken for the film to pop (this was judged visually and in the cases where the films were clear, it could be identified by a slight disturbance to the solution from which the films were drawn).

2.8.3 *Representation of single film lifetimes*

The lifetimes of single films drawn from aqueous surfactant solutions exhibit a statistical spread even for constant experimental conditions. Figure 2.9 shows the lifetime of different films against film number plotted in the order the films were drawn. It can be seen that the data is extremely scattered. Taking the mean of this data is not very informative because the presence of very few long-lived films will shift the mean lifetime of the films upwards. If however, the fraction of films with a lifetime of t or less is plotted against t, a curve is produced from which the time taken for half of the films to rupture can be obtained (Figure 2.10). When determining film lifetimes, the lifetimes of at least 20 films were measured.

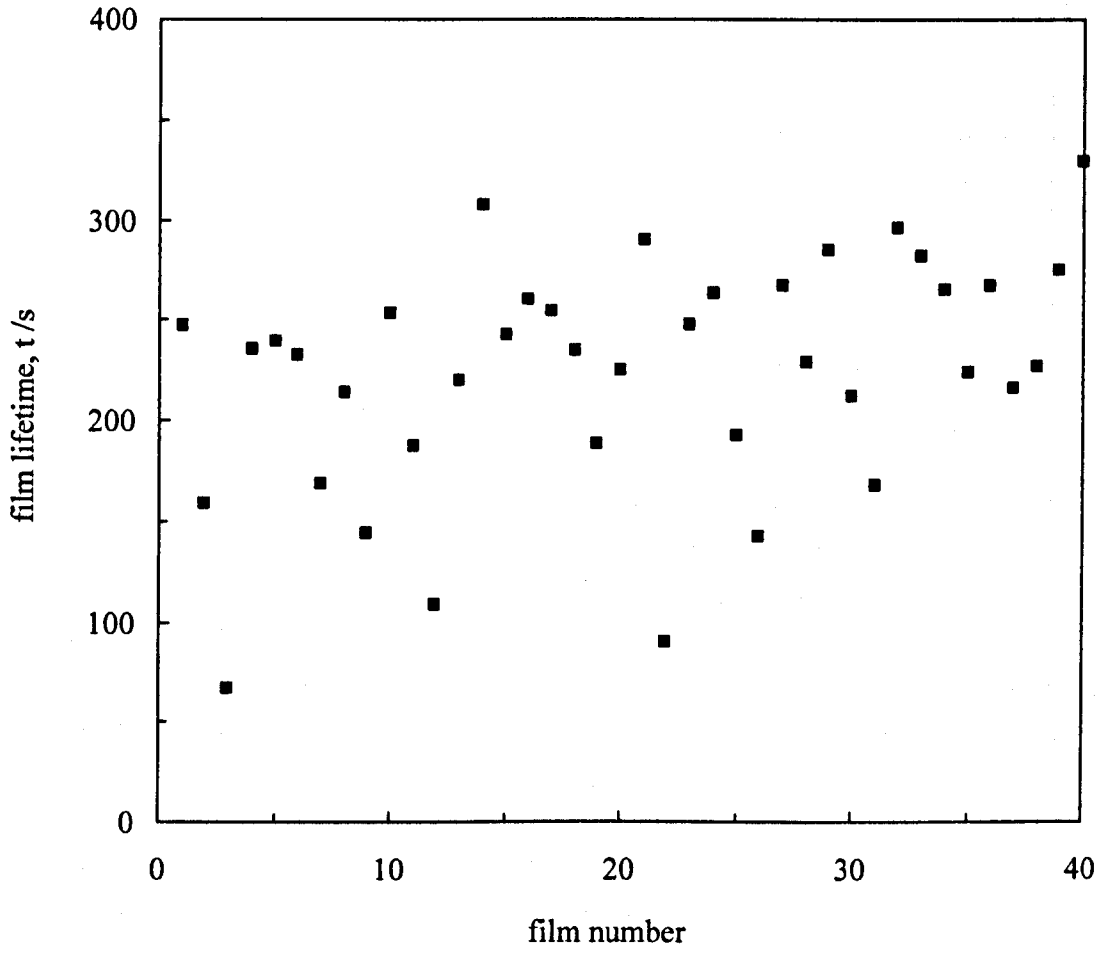

Figure 2.9 Lifetimes of single soap films formed from a solution of 1 mM $C_{12}E_5$ (60.0 cm^3) at 20.0 °C in the absence of silica particles.

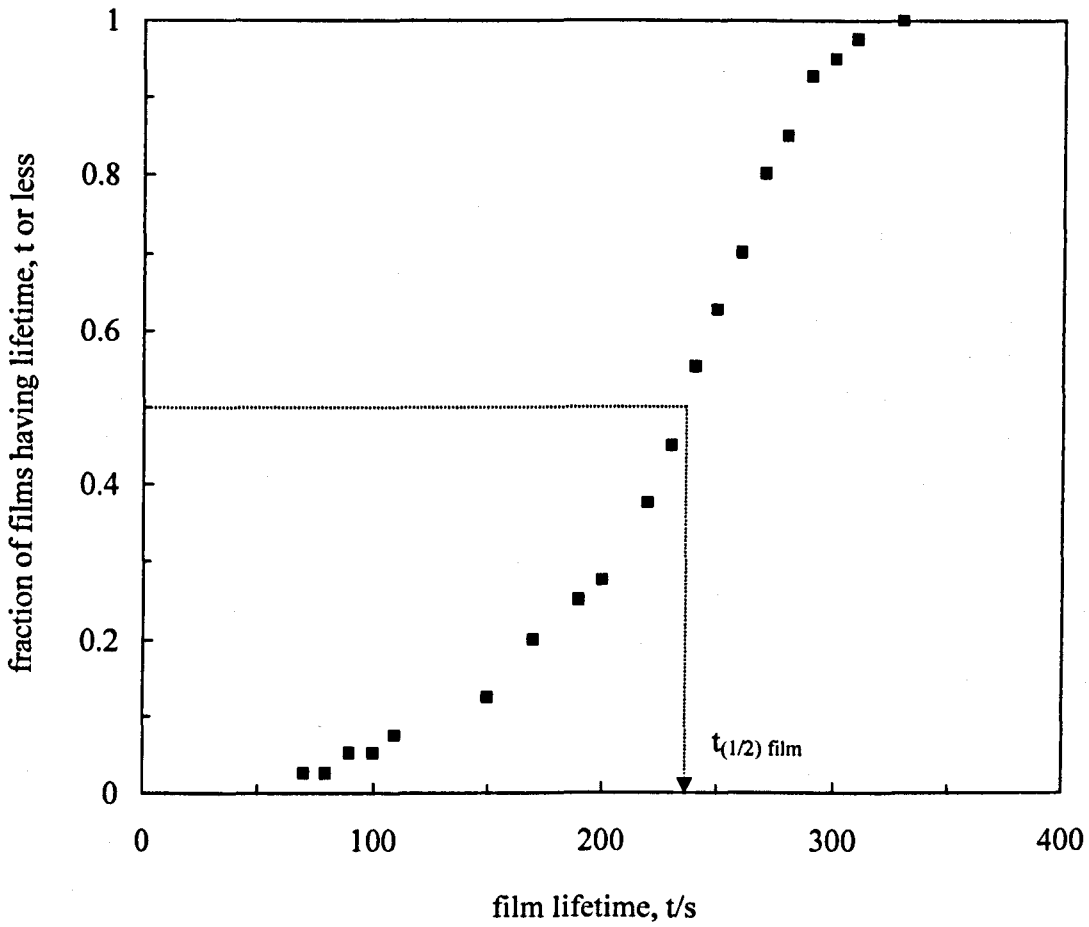

Figure 2.10 Plot of the fraction of films having a lifetime of t or less as a function of film lifetime t. Films formed from a solution of 1 mM $C_{12}E_5$ (60.0 cm^3) in the absence of silica particles at 20.0 °C.

2.9 Silica particles and oil as combined foam control agents

2.9.1 Methods of delivering silica particles and oils to a foaming solution

There are different ways of adding oils and particles to a foaming solution (see Figure 2.11 for a brief summary). In a simple experiment, decane and one of the silica particle types (as powder) were added to a solution of 30 cm^3 of $C_{12}E_5$ (1 mM). Foam shake tests as described previously (Section 2.5), were then undertaken. It is important to note here that the particles were not dispersed into the surfactant solution prior to the shake tests.

In another series of experiments, particles were dispersed in the oil initially using the ultrasonic probe (see section 2.6.1). This resulted in a gel being formed. This gel was then added to an aqueous solution of $C_{12}E_5$ to see what influence it had on both the solution's foamability and foam stability.

The final method of delivering the oil and particles to the foaming solution is to homogenise the oil into a pre-equilibrated surfactant-silica dispersion and this yields a mixed surfactant-silica-oil emulsion. This method is fully described in the next section.

2.9.2 Preparation and characterisation of mixed surfactant-silica-oil emulsions

Emulsions comprising water, surfactant, silica particles and oil were produced in the following way. First, the silica particles were dispersed into an aqueous solution of $C_{12}E_5$ surfactant, using the ultrasonic probe (see section 2.6.1). This surfactant-silica dispersion was then left to equilibrate overnight in a thermostatted water bath at 20.0 °C whilst being gently stirred with a magnetic stirrer bar. Next, 5 vol. % of decane was added to the dispersion and the resulting mixture was then homogenised using an Ultra Turrax T25 homogeniser operating at 11000 r.p.m. for 2 minutes. For each silica particle type, 2 samples of 50 cm^3 of emulsion were made (each containing 47.5 cm^3 surfactant-silica dispersion and 2.5 cm^3 oil). One of the samples was then taken and the emulsion drop sizes were determined using a Laser Diffraction Instrument

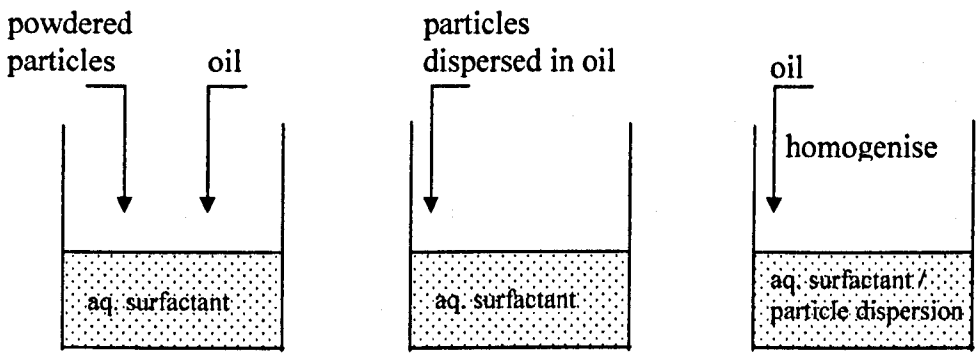

Figure 2.11 The three ways in which silica particles and oil were added to the aqueous solution of nonionic surfactant.

(see section 2.9.3 for a full explanation). Drop sizes were also determined a few hours after emulsion preparation. A small volume of emulsion was taken from the sample and added to a graduated specimen tube so that the stability of the emulsion could be monitored with respect to coalescence and creaming (or sedimentation). In addition to the tests outlined above, foam shake tests were also carried out in the usual way.

The second emulsion sample was diluted by a factor of 10 by using an aqueous sample of $C_{12}E_5$ (1 mM). Using the Laser Diffraction Instrument, the drop size in this diluted emulsion was determined. Again, drop sizes were determined a few hours after the emulsion was prepared. Emulsion stability tests were also carried out on the diluted emulsion sample in exactly the same way as outlined above by using graduated specimen tubes in addition to a foam shake test. This diluted emulsion sample was again diluted by a factor of 10 using aqueous $C_{12}E_5$ (1 mM) and foam shake tests were performed on it. The sample (now diluted by a factor of 100) was further diluted by a factor of 10 and foam shake tests were performed. Emulsion stability tests and drop size measurements could not be performed on the two most diluted emulsion samples (1/100 and 1/1000 of the original) due to the low concentrations of oil present. This entire process was repeated for the range of different silica particles (shown in Table 2.3).

In a second series of similar experiments, emulsions were prepared and analysed using the procedures outlined above except that instead of diluting the emulsions with surfactant alone, the emulsions were diluted with pre-equilibrated surfactant-silica dispersion (prepared in the usual way). Emulsions were only diluted with surfactant-silica dispersions in which the concentration and 'type' of silica (% SiOH on the particle surfaces) were the same as in the emulsion. In this way, only the volume of oil in the emulsion was reduced with each dilution, and the concentrations of the other components (surfactant and silica particles) remained constant.

2.9.3 *Measurement of emulsion drop size distribution*

Emulsion drop size distributions were determined on a Malvern MasterSizer 2000 SM Laser diffractometer. This apparatus can determine drop sizes in the range 10 nm – 1 mm and uses the principles of light scattering and subsequent data analysis using Mie theory to give size distributions. For each measurement, the emulsion of interest was diluted by adding small quantities of it to approximately 50 cm^3 of ultra pure water (the emulsion's continuous phase) contained in a sample handling unit (Hydro 2000 SM(A)) using a Pasteur pipette. The emulsion was gently inverted several times prior to this process and the aliquot was always taken from the middle of the emulsion sample tube in order to get the best possible representation of the system. For all measurements, the stirrer speed on the sample handling unit was set to 850 r.p.m.

2.9.4 *Characterisation of silica particle, oil and surfactant mixtures using optical microscopy*

Samples of systems containing silica particles, oil and surfactant were viewed under an optical microscope (Nikon Labphot). A few drops of the sample were placed onto a glass slide (76 x 26 x 1.0 mm, Blue Star Microslides) using a Pasteur pipette and a cover slip (24 x 24 mm, Scientific Laboratory Supplied Ltd.) was placed over it. The slide was then placed under the microscope and the objective was set to either x10 or x40 magnification. The microscope was coupled to a DIC-U high resolution camera (World Precision Instruments) which was connected to a PC running "DIC-U Imaging Software for Windows 2.2A" (World Precision Instruments). Captured images were then imported into a graphics manipulation package (Adobe Photoshop, version 5.0 LE). The images were rescaled to 650 x 486 pixels and were stored in JPEG format. Images of a calibrated graticule (National Physical Laboratory) were captured under the microscope at the two magnifications used in the same way as described above and these served as a means of sizing features in the images.

2.9.5 Rheological studies of mixed surfactant-silica-oil emulsions

Rheological properties of the emulsions were measured using a Rheometer (CV0 120 high Resolution, Bohlin Instruments). In these experiments, shear stress and viscosity were measured as a function of shear rate which when plotted, yielded so-called flow curves. Samples were preconditioned by applying a fixed shear rate of 1 s^{-1} for 10 s which ensured that all of the emulsions were at similar starting points with respect to creaming before any measurements were made. The measuring system was a double gap 40/50 steel geometry and the gap was automatically set to 0.150 mm. This measuring system was chosen due to its tolerance to particulate materials and the reported good reproducibility of data associated with it.[15] During the measurement process, shear rates were ramped from 0.05226 to 218.9 s^{-1} and the corresponding shear stresses and viscosities were measured. For all of the measurements, the delay time was set to 5 s and the integration time was set to 5 s. All of the measurements were made at 20.0 °C

2.10 Miscellaneous techniques

2.10.1 Surfactant cloud point determinations

1 wt. % samples of aqueous nonionic surfactant were prepared by adding 0.1 g of surfactant to 10 cm^3 of water treated with the Milli-Q water reagent system. Each sample was placed into the water reservoir of a thermostat (Grant LT D6G, -20 to 100 °C) initially set at approximately 15 °C. The temperature of the thermostat was then gradually increased, until the surfactant solution was visually judged to appear cloudy. The temperature was then slightly reduced such that the solution reverted to being clear and colourless. This process of ramping the temperature to above and below the cloud point was repeated lowering the temperature range of the ramping each time until the precise temperature at which the solutions turned cloudy was obtained. This temperature was accurately measured using a mercury thermometer (Zeal, England) capable of being read to 0.1 °C.

2.10.2 Delivery of HMDS to aqueous silica dispersions

N_2 gas was bubbled through HMDS (vapour pressure = 20 mmHg at 20.0 °C) contained in a bubbler at a flow rate of 50 cm^3 min^{-1}. The HMDS-saturated N_2 gas stream was then passed through the bottom of a glass separating funnel which contained a glass frit. Approximately 30 cm^3 of aqueous silica dispersion was added above the frit. In this work, silica particles with 79.9 % SiOH on their surfaces were used. They were dispersed at concentrations of between 1 and 4 wt. %. Figure 2.12 shows the experimental setup of this apparatus.

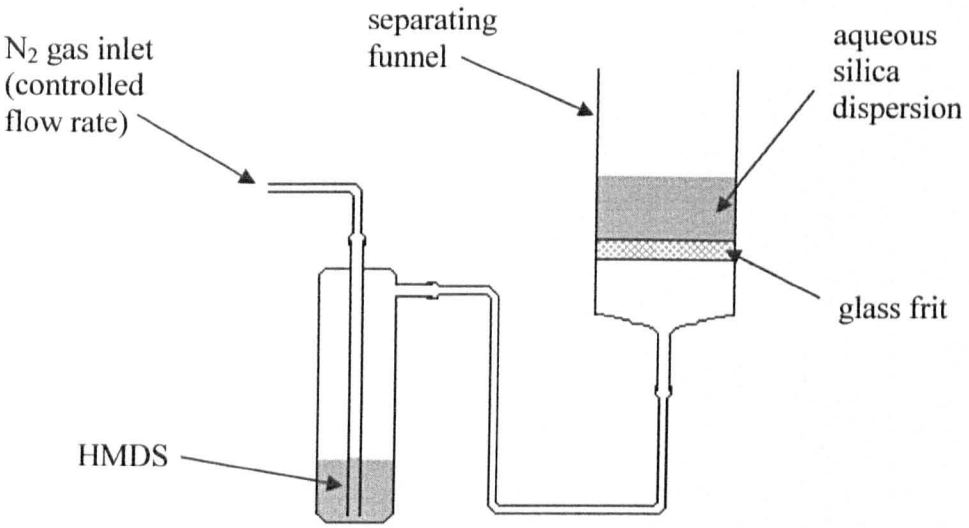

Figure 2.12 HMDS delivery setup. N_2 gas flows through the bubbler where it becomes saturated with HMDS. It then passes through a glass frit and into the aqueous silica dispersion.

References

1. Handbook of Chemistry and Physics, CRC Press, 62nd edition, 1981 – 1982.
2. J. R. MacNab, PhD thesis, University of Hull, 1996.
3. N. M. Van Os, J. R. Haak and L. A. M. Rupert, *"Physico-Chemical Properties of Selected Anionic, Cationic and Nonionic Surfactants"*, Elsevier, Amsterdam, 1993.
4. K. V. Schubert, R. Strey and M. Kahlweit, *J. Colloid Interface. Sci.*, (1991), **141**, 21.
5. M. J. Rosen, A. W. Cohen, M. Dahanayake, and X. –Y. Hua, *J. Phys. Chem.*, (1984), **86**, 541.
6. P. Becherin in *"Nonionic Surfactants"*, M. J. Schick (Ed.), Marcel Dekker, NY, 1966.
7. G. Olofsson, *J. Phys. Chem.*, (1985), **89**, 1473.
8. K. M. McGrath, *Langmuir*, (1995), **11**, 1835.
9. S. F. Turner, S. M. Clark, A. R. Rennie, P. N. Thirtle, D. J. Cooke, Z. X. Li and R. K. Thomas, *Langmuir*, (1999), **15**, 1017.
10. Wacker HDK® Fumed Silica Manufacturers Brochure, Wacker-Chemie GmbH, München, Germany.
11. A. J. Ashworth and D. H. Everett, *Trans. Faraday Soc.*, (1960), **56**, 1609.
12. D. Crichton, Ph.D. thesis, University of Hull, 1998.
13. W. D. Harkins and H. F. Jordan, *J. Am. Chem. Soc.*, (1930), **52**, 1751.
14. H. H. Zuidema and G. W. Waters, *Ind. Eng. Chem. (Anal. Ed.)*, (1941), **13**, 312.
15. "Bohlin CVO 120 HR Users Manual", Bohlin, UK.

Chapter 3

CHAPTER 3

Foaming of nonionic surfactants

3.1 Introduction

Nonionic surfactants are used in a wide variety of foaming applications because their foaming levels can be tailored to cover a broad spectrum.[1] The versatile foaming properties of nonionic surfactants can be ascribed to factors such as the great variety of the hydrophobic groups available and the way in which the hydrophobic characteristics can be balanced with the hydrophilic characteristics of the molecule. Although there is a limited amount of scattered literature on these surfactants[1-3], there is no systematic comparison of the different surfactant homologues in relation to foaming. In this chapter, this lack of literature will be addressed by systematically studying the foaming properties of alkyl ethoxylate surfactants of different head and tail lengths.

3.2 Cloud point determinations of aqueous solutions of nonionic surfactants

As noted in section 1.5.3, at concentrations in excess of their cmc, aqueous solutions of C_nE_m surfactants phase separate into two phases when the temperature exceeds the cloud point (Cp.) of the solution. Phase separated systems show different foaming characteristics compared with single-phase solutions.[4,5] Cloud points arise from the tendency of micelles to aggregate (and form a concentrated phase) at high temperatures. As the temperature rises, forces between the micelles become attractive, because of the loss of the hydration by water of the ethylene oxide headgroups responsible for steric repulsions between the micelles.[6] At a well defined concentration and temperature, the solution phase separates into a micellar-rich phase and a micellar-poor phase. This phase separation occurs slowly and consequently, the solution initially becomes cloudy. It has been shown that drops of the surfactant-rich phase of approximate size 5 μm, can bridge the foam films made from the surfactant-

poor phase and cause the rupture of foam films. This anti-foam action reduces the foamability of the surfactant solution.[4] It is therefore important to compare the foam properties of C_nE_m surfactant solutions at temperatures below their cloud points.

Figure 3.1 shows how the cloud points vary for the two series of nonionic surfactants used in this work (C_nE_5 and $C_{12}E_m$). The top plot shows the effect that varying the number of ethylene oxide groups in the headgroup has on the cloud point when the hydrophobic tail contains 12 methylene units. Increasing the number of ethylene oxide units in the surfactant headgroup increases the temperature at which phase separation occurs. This is due to hydration around the ethylene oxide groups which is higher for the larger headgroups. The water has to be removed before the net force acting between micelles become attractive thus promoting phase-separation. The lower plot in Figure 3.1 shows the influence that the length of the hydrophobic tail has on the cloud point of the surfactant. Here, the number of ethylene oxide units in the surfactant headgroup is fixed at 5. More hydrophobic surfactants have lower cloud points than the less hydrophobic ones since the hydrophobic group is mainly responsible for the attraction between surfactant molecules and their micelles. From Figure 3.1 it can be seen that in order to avoid complications associated with foaming measurements at or above the cloud point temperature, only surfactants in the following range can be studied at 25.0 °C (for surfactant concentrations of 1 wt. %.):

C_nE_5 $\quad n < 14$

$C_{12}E_m$ $\quad m > 5.$

3.3 Foamability

3.3.1 Theoretical considerations

Foamability refers to the effectiveness of a surfactant solution to foam under specified conditions of gas input. The stabilisation of a foam bubble requires a level of surfactant adsorption to occur before the bubble has chance to coalesce with the bulk gas phase. In attempting to correlate surfactant adsorption with the dynamic

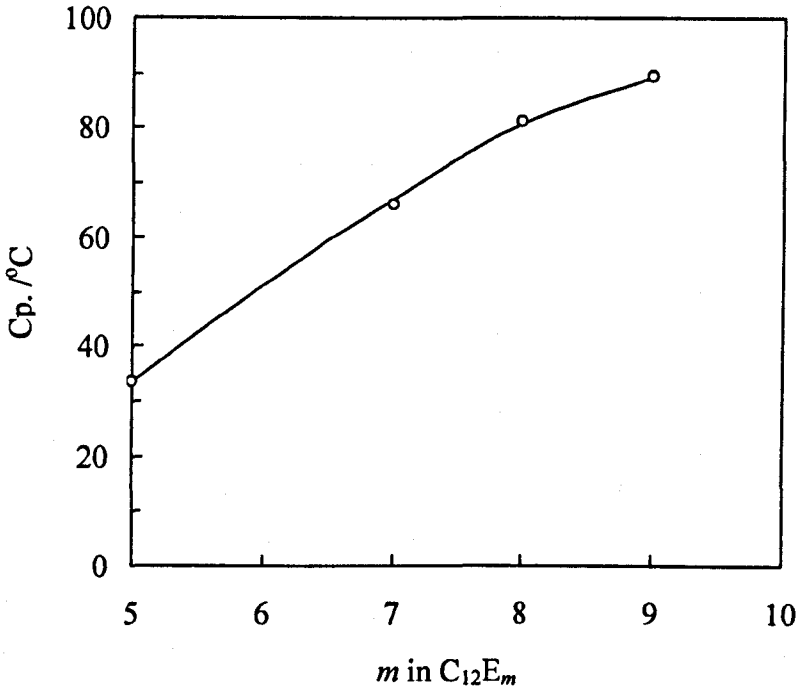

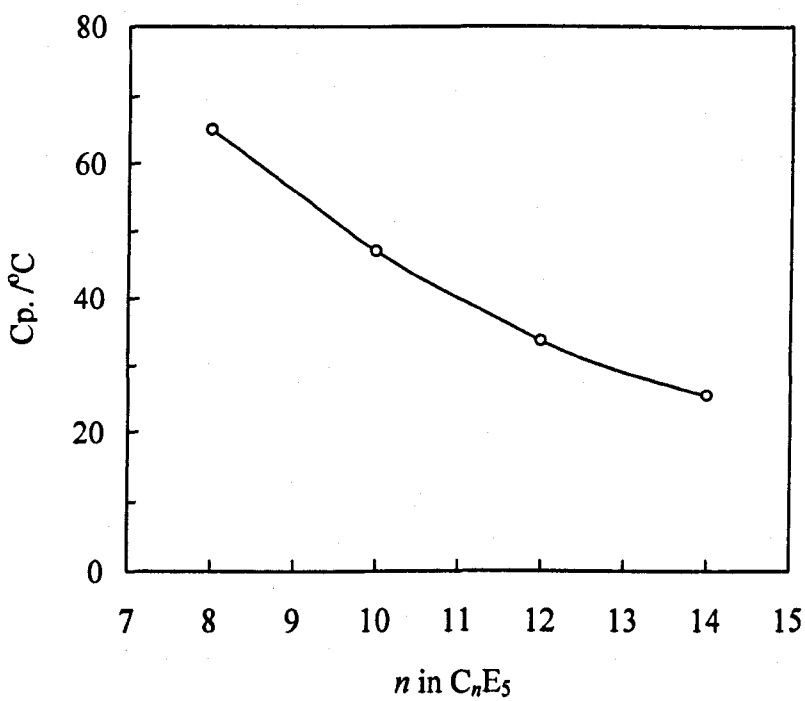

Figure 3.1 Measured cloud points for aqueous solutions of C_nE_m surfactants (1 wt. %) as a function of head group ($C_{12}E_m$, upper plot) and tail group C_nE_5 (lower plot).

processes determining foamability, it is necessary to consider both the equilibrium extent of surfactant adsorption and the adsorption rate relative to the foam dynamics. The equilibrium extent of adsorption of a surfactant at the air-water surface depends on the aqueous phase concentration according to the equilibrium adsorption isotherm. The extent of adsorption increases with increasing concentration up to a critical concentration at which micelles form in the bulk aqueous phase. This concentration is termed the critical micelle concentration (cmc). Since micelles do not adsorb at the air-water surface and surfactant monomer activity remains approximately constant above the cmc, maximum surfactant adsorption is obtained at or close to the cmc and is typically of the order of 2 molecules per nm^2 for single-chained surfactants. The air-water surface tension decreases with increasing surfactant concentration up to the cmc and remains approximately constant with further concentration increases. Both the adsorption isotherm and the cmc may be obtained from measurements of the air-water surface tension (γ) as a function of the surfactant concentration.

The driving force for both adsorption and micellisation results from the tendency of the hydrophobic tail group of the surfactant to de-mix with the water solvent. This common driving force is the origin of the correlation between the cmc and the strength of the adsorption, as noted above. The driving force increases with increasing chain length of the surfactant tail group. For nonionic surfactants containing a single alkyl chain as the tail group, the cmc decreases approximately 10 fold with an increase of two methylene groups in the chain. Values of the cmc for ionic surfactants are higher (typically 2 orders of magnitude) than for nonionic species with the same tail group. Variation in the head group structure for nonionics generally has only a relatively small effect on the cmc. As described above, changes in the adsorption tendency correlate with changes in the cmc. Based on these considerations, one expects surfactants showing low cmc values (corresponding to a high tendency to adsorb) to stabilise foams at correspondingly lower concentrations than a high cmc surfactant.

The formation of foam involves the creation of new air-water surface area at a rate which depends on the gas input rate and the size of the bubbles formed. For the foam to be stable, it seems reasonable to assume that a certain (unknown) minimum level of

surfactant must be adsorbed on the newly created surface. In order to achieve the necessary adsorption, two conditions must be fulfilled. Firstly, the surfactant concentration in the foaming solution must be high enough such that the equilibrium adsorption either equals or exceeds the required level. Secondly, the *rate* of adsorption must be such that the required level is reached within the time in which the new surface area is created during the foam formation, i.e. before the bubble in the solution rises and meets the bulk gas phase.

The rate of surfactant adsorption at the air-water surface depends strongly on surfactant concentration. A time (t_{ads}) characterising the adsorption rate as determined by dynamic tensiometry can be defined as the time required for the dynamic surface tension to reach halfway between the pure solvent tension (corresponding to zero adsorption) and the equilibrium value. Referring to the data of Lin et al.[7] for the adsorption of dodecyl octaoxyethylene glycol ether (abbreviated to $C_{12}E_8$) at the air-water surface, the values of t_{ads} are 13, 250 and 5000 s for concentrations of 1.8×10^{-5}, 2.2×10^{-6} and 1.7×10^{-7} M, respectively. Adsorption times (at corresponding concentrations) for a range of nonionic surfactants are generally similar, e.g. for aqueous solutions of $C_{12}E_5$, values for t_{ads} are 240 and 7200 s for concentrations of 2.0×10^{-6} and 1.0×10^{-7} M respectively.[8] For nonionic surfactants, the rate of adsorption into dilute monolayers is thought to be diffusion controlled. The adsorption rate into concentrated monolayer (at surfactant concentrations approaching the cmc) is thought to be slightly slower than diffusion controlled indicating the presence of a small but significant activation energy barrier.[9]

From the information given above, it can be summarised that in order for a surfactant solution to foam, the following criteria must be fulfilled:

(i) The equilibrium adsorption must be high enough and (ii) the rate of adsorption must be fast enough. This rate is fast for high surfactant concentrations and slow for low surfactant concentrations. For short chain high cmc surfactants, the concentration required for sufficient adsorption is high and therefore the rate of adsorption is high. This means that foamability is likely to be limited by the adsorption isotherm at equilibrium. For long chain low cmc surfactants, the concentration required for surfactant equilibrium adsorption is very low and so the rate of adsorption is slow.

Here, the foamability is likely to be limited by the adsorption rate (t_{ads}). Hence, one expects two regimes with possible crossover between the two behaviours as a function of surfactant tail length. In regime 1 (adsorption control), foamability should correlate with the cmc. In regime 2 (kinetic control), foamability should be independent of the cmc of the surfactant.

3.3.2 Results - variation of surfactant tail length

Figure 3.2 shows the foam volume after 10 minutes as a function of bulk surfactant concentration for C_nE_5, where n = 14, 12, 10 and 8. The foam was produced by sparging N_2 gas through 15.0 cm^3 of surfactant solution at a flow rate of 48 cm^3 min^{-1} for 10 minutes. At sufficiently low surfactant concentrations, none of the surfactants produce any foam after the 10 minute foaming period. As the surfactant concentration is increased, a transition from non-foaming to foaming behaviour is observed which is clearly different for each surfactant in the series. The upward arrows show the cmc for each surfactant. The downward arrow shows the parameter $C(1/2)$ for $C_{14}E_5$. $C(1/2)$ represents the mid-point concentration at which the transition from non-foaming to foaming behaviour occurs for a given surfactant. The value of $C(1/2)$ is equal to the concentration corresponding to half of the maximum foam volume plateau value. $C(1/2)$ will be used as a universal measure of foamability throughout this work. Surfactants with low values of $C(1/2)$ are considered to be of a higher foamability than those with a higher value of $C(1/2)$. Increasing the number of methylene units in the hydrophobic chain (whilst fixing the number of ethylene oxide units in the headgroup) lowers the value of $C(1/2)$ progressively across this series of C_nE_5 surfactants. This shows that a higher concentration of C_8E_5 is required to produce foam than $C_{14}E_5$ for example. This is due to the lower adsorption of short chain surfactants as discussed above.

Figure 3.3 is derived from Figure 3.2 and shows the volume of foam produced after the 10 minute foaming period (V_{max}) as a function of the number of methylene groups in the surfactant tail group. V_{max} would be equal to 480 cm^3 if the surfactant was 100 % efficient at trapping all of the N_2 gas during foam production (10 min. x 48 cm^3 min^{-1} = 480 cm^3). The theoretical maximum volume of 480 cm^3 is denoted by the

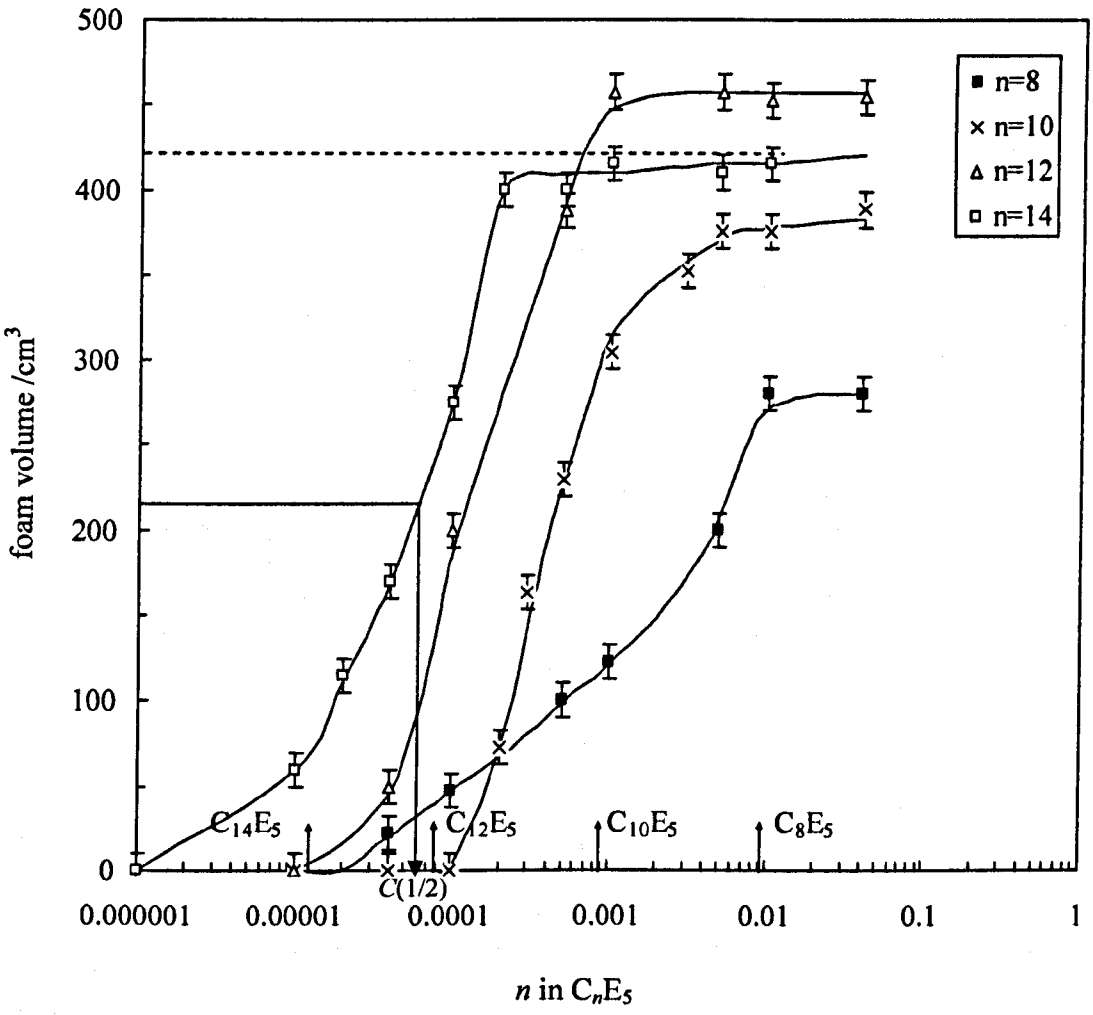

Figure 3.2 Foam volume immediately after 10 minutes of gas sparging as a function of surfactant concentration for C_nE_5 surfactants with n = 8, 10, 12 and 14. The N_2 gas flow rate was 48 cm^3 min^{-1} and the initial volumes of surfactant used were 15.0 cm^3. The upward arrows denote the cmc of the different surfactants. The solid lines are guides for the eye.

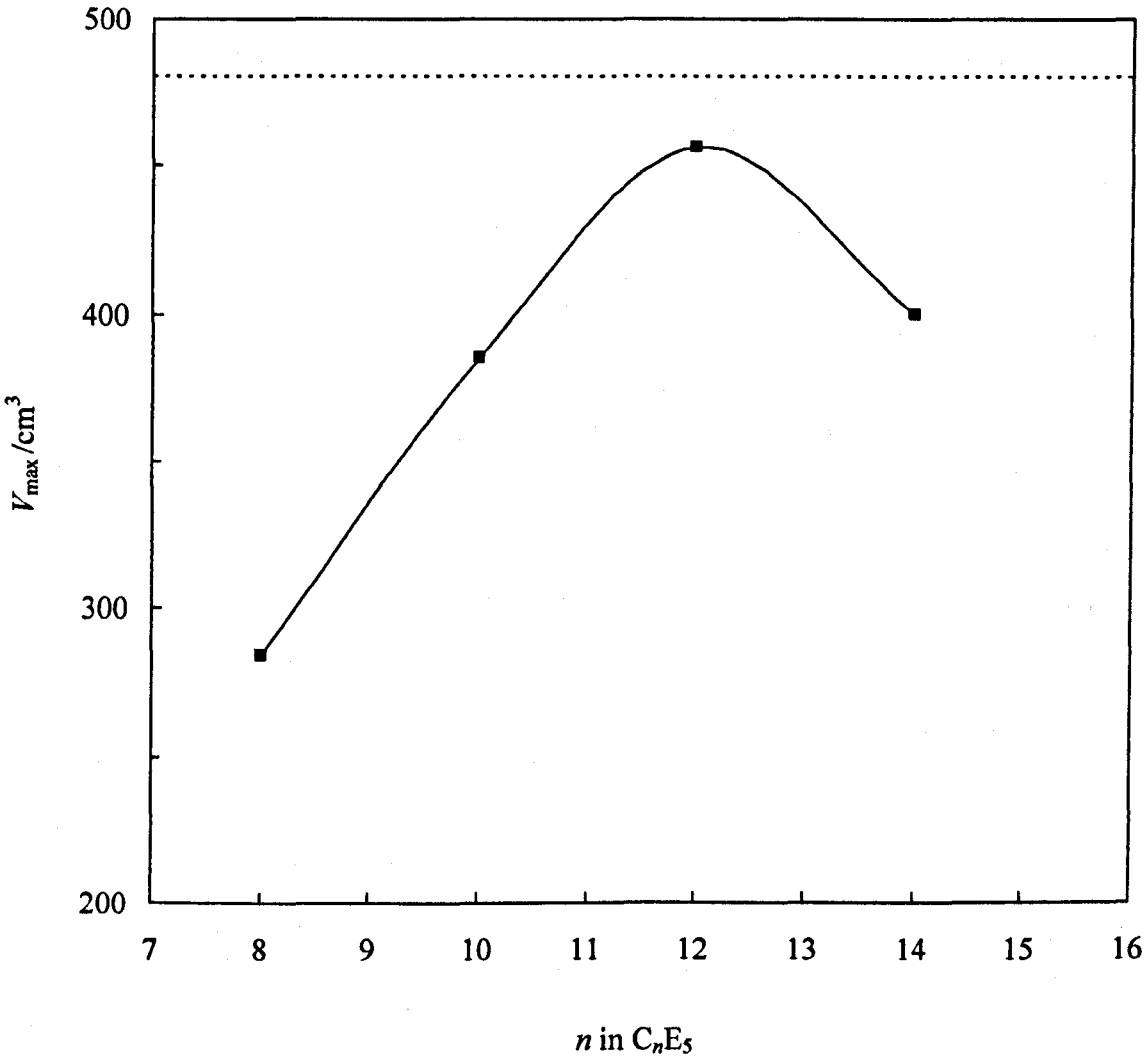

Figure 3.3 Foam volume (V_{max}) obtained after sparging N_2 gas through 15.0 cm^3 of surfactant solution at a flow rate of 48 cm^3 min^{-1} for 10 minutes as a function of surfactant tail length. The horizontal dashed line shows the maximum possible foam volume after 10 minutes using these experimental parameters.

horizontal dashed line in Figure 3.3. V_{max} is seen to increase with increasing surfactant tail length, until a maximum is reached when n = 12, before starting to decrease again as n is raised to 14. A possible explanation for this decrease in V_{max} is that the cloud point of $C_{14}E_5$ is very close to the experimental temperature of 25.0 °C when measured at 1 wt. %. When cloud points are measured as a function of surfactant concentration and the data is plotted, a parabola exhibiting a minimum value is obtained. The cloud point temperature of $C_{14}E_5$ measured at 1 wt. % may not necessarily correspond to the lowest possible cloud point for $C_{14}E_5$ which may be obtained at higher or lower concentrations than 1 wt. % (depending on whether 1 wt. % corresponds to a position on the negative or positive slope on the parabola (see section 1.5.3 for a more detailed account of this). Although the surfactant can still clearly foam, some of the foam could be being broken by the bridging action described in section 3.2 as it is being formed due to the experimental temperature being lower than the cloud point for this surfactant concentration regime. The onset of the turbidity caused by the cloud point could be masked by the agitation in the surfactant solution induced by the gas sparging.

Figure 3.4 is a summary of the foamability behaviour of the C_nE_5 series of surfactants and shows how the values of $C(1/2)$ and the cmc vary in relation to the number of carbons in the hydrophobic moiety of the surfactant molecule. As shown the values of $C(1/2)$ for surfactant tails containing less than 11 methylene units fall below the cmc curve whereas those for the higher tail lengths are higher than the corresponding cmc values. Although C_nE_5 surfactants with n values higher than 14 could not be measured due to complications arising from the cloud point phenomena, the value of $\log(C(1/2)/M)$ for $C_{16}E_6$ (possible to measure because of the higher cloud point arising from having 6 ethylene oxides in the headgroup) was found to be approximately -4. The data suggests that there is a crossover in foamability behaviour as a function of surfactant tail length. Prins measured equilibrium and dynamic surface tension and foamability as a function of bulk concentration.[10] It was found that the dynamic surface tension correlated with the foamability of the solution. This corresponds to a condition where foamability is governed by the surfactant adsorption rate not by equilibrium adsorption.

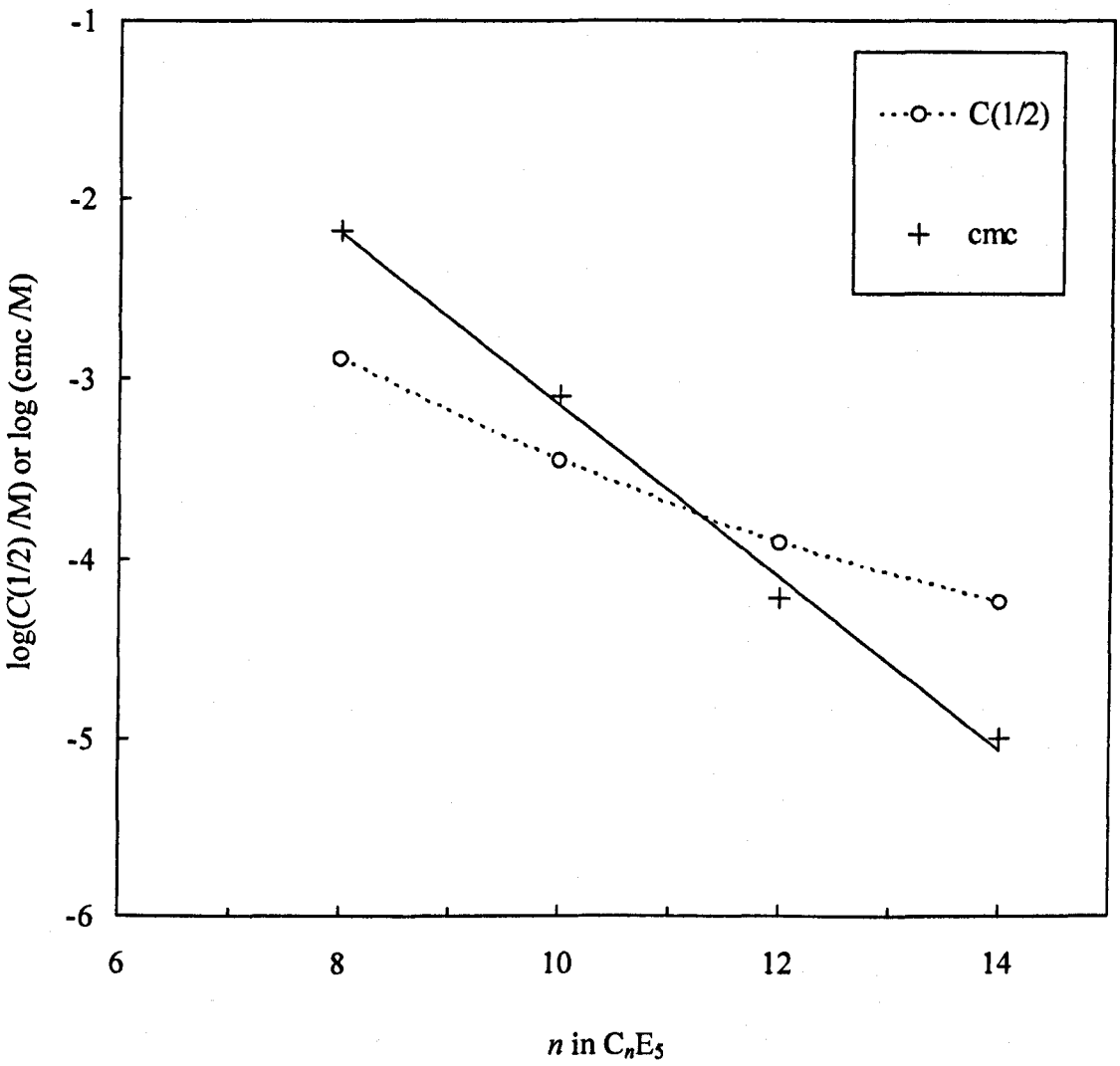

Figure 3.4 Comparison of the variation of $C(1/2)$ and cmc with surfactant chain length n.

3.3.3 *Results - variation in surfactant headgroup size*

Figure 3.5 shows the foam volume after 10 minutes as a function of bulk surfactant concentration for the $C_{12}E_m$ series of nonionic surfactants. The cmc of these surfactants is very similar across the series because the hydrophobic moiety remains constant (12 methylene groups). All of the foamability curves can be superimposed. The data supports the idea that foamability is related to factors linked to the adsorption of a particular surfactant (the adsorption for all of the surfactants in the $C_{12}E_m$ series is similar due to similar cmc values). Figure 3.6 shows the maximum foam volume obtained after 10 minutes of foaming (V_{max}). It can be seen that there is no dependence of V_{max} on the number of ethylene oxide units in the surfactant headgroup signified by the horizontal linear nature of the data (within experimental uncertainty).

Figure 3.7 is a summary of the foaming behaviour of the $C_{12}E_m$ series of surfactants and shows $C(1/2)$ values in relation to the surfactant cmc. The cmc is only slightly dependent on the number of ethylene oxide groups in the surfactant headgroup and values of $C(1/2)$ are always above the corresponding cmc.

3.3.4 *Theoretical treatment of foamability limiting conditions*

From the experimental findings in this chapter, it is postulated that foamability can be limited by either adsorption dynamics or equilibrium adsorption, and the tail length of the surfactant dictates which particular regime is acting to limit the foamability.

Short-tailed surfactants have chain length dependent $C(1/2)$ values equal to a fraction of the corresponding cmc whereas long-tailed surfactants have a chain length independent $C(1/2)$ value, which is higher than the corresponding cmc. For short-tailed surfactants, $C(1/2)$ values are relatively high and thus surfactant adsorption to the gas bubble surfaces during foam generation is predicted to be fast. When surfactant adsorption is fast relative to bubble formation time, foam production will occur when the *equilibrium* adsorption exceeds a critical value (Γ_{crit}) required for bubble stability. For surfactants with different cmc values, this will happen at a

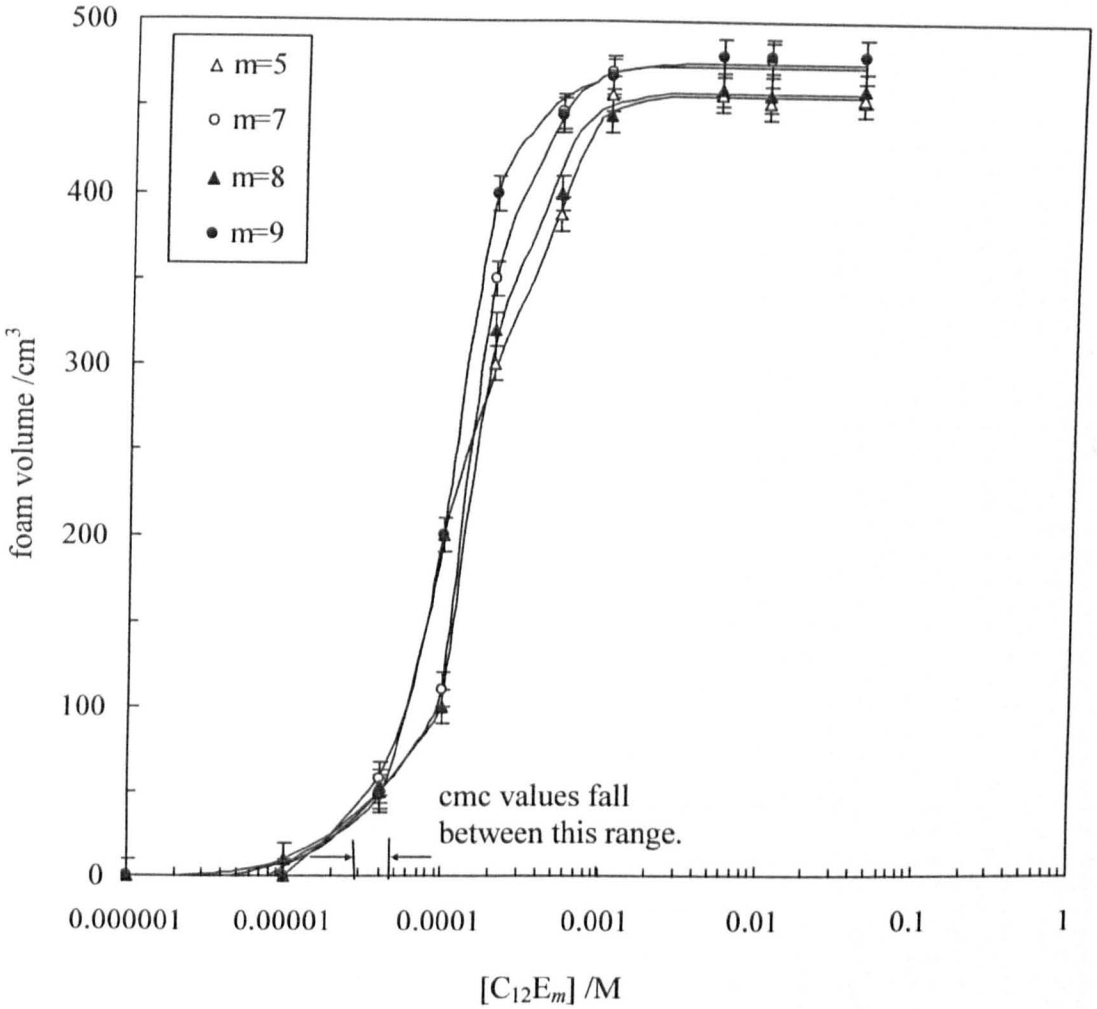

Figure 3.5 Foam volume immediately after 10 minutes of gas sparging as a function of surfactant concentration for $C_{12}E_m$ surfactants with m = 5, 7, 8 and 9. The N_2 gas flow rate was 48 cm^3 min^{-1} and the initial volumes of surfactant used were 15.0 cm^3. The horizontal arrows denote the range of cmc values of the different surfactants. The solid lines are guides for the eye.

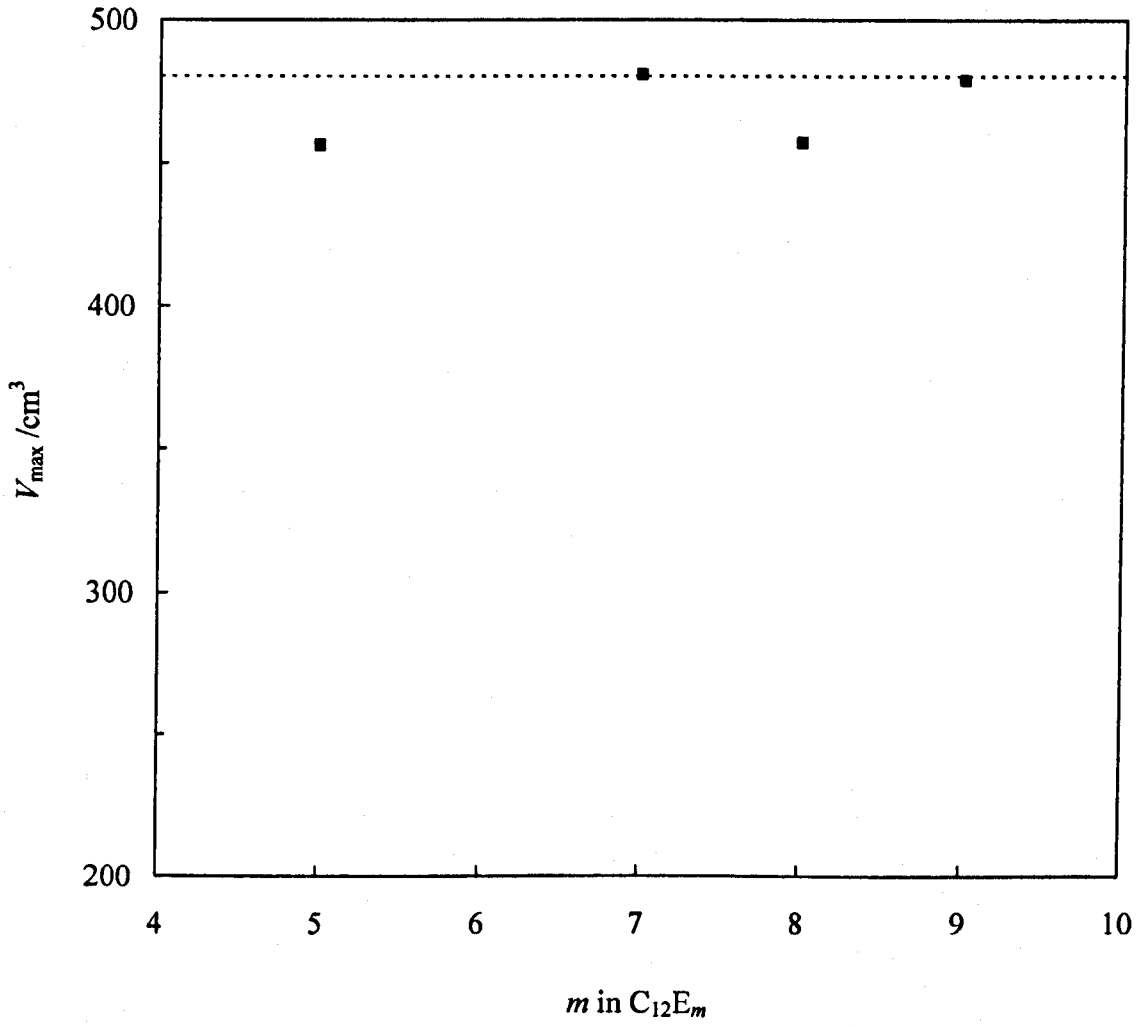

Figure 3.6 Foam volume (V_{max}) obtained after sparging N_2 gas through 15.0 cm^3 of surfactant solution at a flow rate of 48 cm^3 min^{-1} for 10 minutes as a function of the number of ethylene oxide groups in the headgroup. The horizontal dashed line shows the maximum possible foam volume after 10 minutes using these experimental parameters.

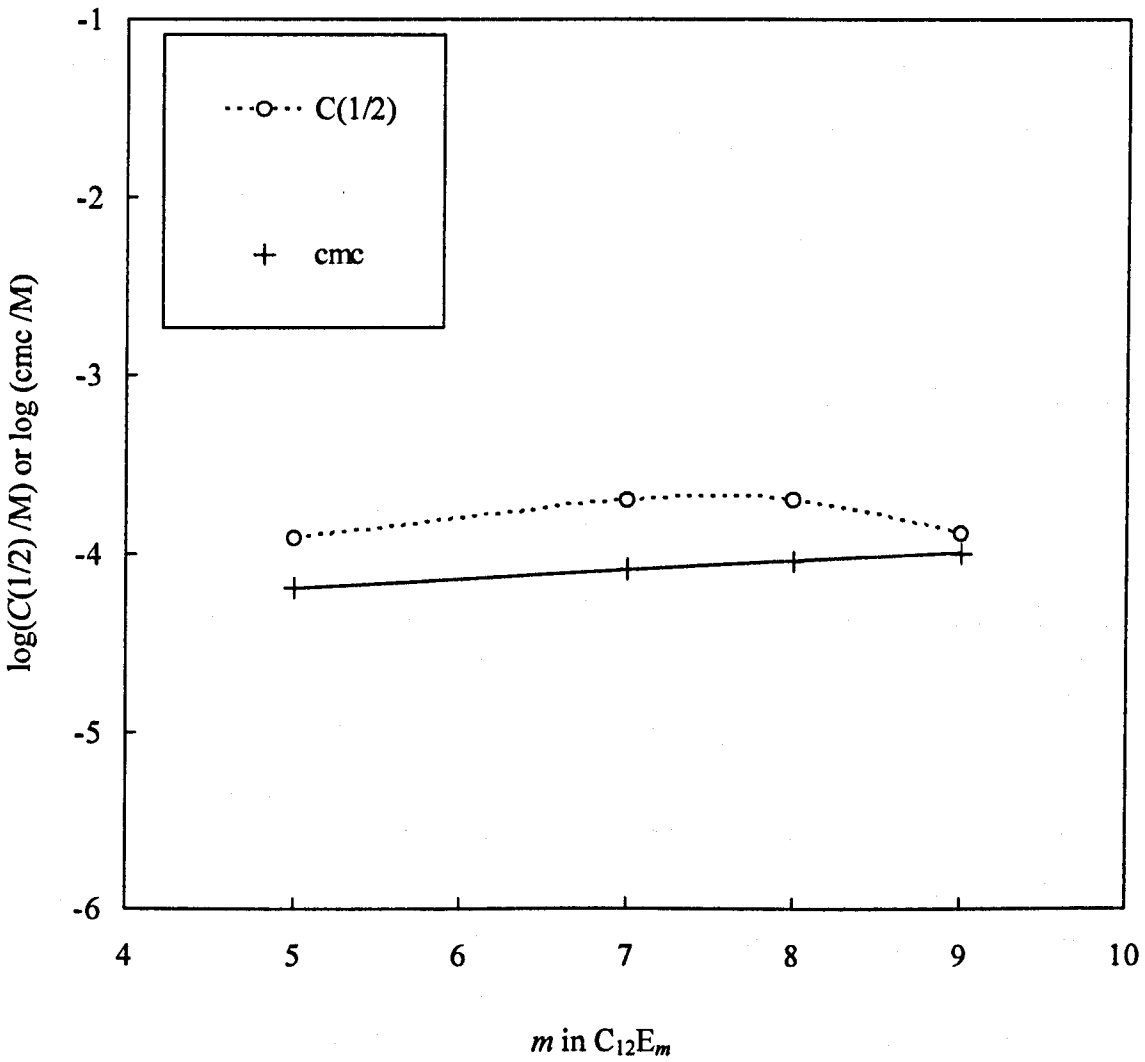

Figure 3.7 *C*(1/2) values and cmc values as a function of the number of ethylene oxide groups in $C_{12}E_m$ in the absence and presence of co-adsorbed decane.

surfactant concentration which is a reasonably constant fraction of the corresponding cmc. Bubble formation time is estimated to be approximately equal to the rise time of the bubbles from the sinter to the surface of the foaming solution. Ybert et al.[11] studied ascending air bubbles in protein solutions. They concluded from their studies that during bubble ascent, surface active substances accumulate at the air/liquid interface and contribute to the bubbles rigidity. Bubble rise time was estimated to be of the order of 10 ms in this work calculated using the Stokes velocity (U_{st}) equation:

$$U_{st} = \frac{2r^2 \rho g}{9\eta} \qquad [3.1]$$

where, r is the bubble radius (1 x 10^{-3} m), ρ is the liquid density at 25.0 °C (1 x 10^3 kg m^{-3}), g is acceleration due to gravity (9.81 m s^{-2}) and η is the liquid viscosity at 25.0 °C (8.91 x 10^{-4} Pa s).[12] Substituting these values into equation [3.1] yields a bubble Stokes velocity (U_{st}) of 2.45 m s^{-1}. The bubble travels approximately 2.5 x 10^{-2} m through the surfactant solution and so the time taken is obtained by dividing distance by U_{st}, giving a time of 1 x 10^{-2} s.

This calculation assumes that there is no increase in the acceleration of the bubble as it rises through the surfactant solution. Recently Liger-Belair et al.[13] observed that champagne bubbles expand as they rise through solution. They also observed that the bubbles become more spaced as they approach the top of the solution indicating that the bubbles are accelerating as they adsorb surface active material. Although the findings from their work show that bubbles accelerate as they travel through a surfactant solution, it was decided to ignore this in the calculation described above.

Since the equilibrium adsorption scales as [surfactant] /cmc, for adsorption controlled foamability $C(1/2)$ values are expected to be a constant fraction of the corresponding cmc as observed here. For long-tailed surfactants, the concentrations required for sufficient equilibrium adsorption are very low and the adsorption kinetics will be slowed. In the situation that bubble stability during foam generation is controlled by adsorption dynamics, $C(1/2)$ expected to be higher than the corresponding cmc and to be approximately independent of the tail length. Thus, the observed variation of $C(1/2)$ with surfactant chain length is qualitatively consistent with a crossover from

equilibrium adsorption control (short tail lengths) to dynamic adsorption control (long tail-lengths).

It was decided to check the validity of these ideas by calculating theoretical values of $C(1/2)$ for the C_nE_5 series of surfactants for different t_{ads} times. Data for equilibrium and dynamic adsorption of $C_{12}E_5$ at the air-water surface is available in the literature.[8] The data for $C_{12}E_5$ can be extrapolated to yield equilibrium and dynamic adsorption data for the other surfactants in the C_nE_5 series by applying empirical fits to the experimental data. In doing this, it is assumed that the surfactant concentration is the only determinant of adsorption rate which is approximately true for surfactants in the range studied here i.e. that the diffusion coefficients of the C_nE_5 surfactants are all approximately equal. This is likely to be true within 30 % or so. Additionally, the following assumption was made when extrapolating the equilibrium adsorption data. Maximum adsorption (Γ_{max}) occurs at or close to the cmc (this is true). A lower surfactant concentration (C_{eq}) is required for the surfactant to reach the critical level of adsorption required to stabilise a bubble (Γ_{crit}). Dividing Γ_{max} by Γ_{crit} yields a factor (Γ_{factor}). Dividing the cmc by C_{eq} yields a second factor (cmc_{factor}). It is assumed that Γ_{factor} and cmc_{factor} are constants, regardless of the surfactant used.

Values of C_{eq} were calculated for each surfactant using a Visual Basic Application (VBA) written to operate within Microsoft Excel[14] (this used the empirical equations fitted to the $C_{12}E_5$ data). This VBA thus yields the concentration of each surfactant required to attain an equilibrium adsorption level equal to Γ_{crit}. A value of Γ_{crit} is set by the user.

A second VBA was written[14] to calculate whether this level of adsorption could be reached within time t_{ads} (set by the user) at a concentration equal to C_{eq}. This concentration was termed the dynamic surfactant concentration (C_{dyn}). If C_{eq} was high enough to permit Γ_{crit} being attained within time t_{ads}, then C_{dyn} was set equal to C_{eq}, the VBA was terminated and the value of C_{dyn} was returned. If however, C_{eq} was too low to allow Γ_{crit} to be attained within time t_{ads}, the concentration of C_{dyn} was slightly increased. This cycle was repeated until C_{dyn} was high enough to allow Γ_{crit} to be reached in time t_{ads}.

C_{eq} is then compared to C_{dyn} and the highest concentration is the calculated value of $C(1/2)$ for the particular surfactant. By comparing C_{eq} and C_{dyn} and taking the highest value to be $C(1/2)$, $C(1/2)$ corresponds to the lowest (limiting) concentration at which the required equilibrium adsorption (Γ_{crit}) can be reached and this level of adsorption can be attained in time t_{ads}. The values of t_{ads} and Γ_{crit} can be changed in order to obtain the best possible agreement between calculated and experimental values of $C(1/2)$. The values of these two variables corresponding to the best fit of the data should correspond to the minimum allowed adsorption time and a realistic surface excess concentration for the stabilisation of a foam bubble in the context of the actual foaming system.

The code contained within the VBAs used to calculate C_{eq} and C_{dyn} and hence $C(1/2)$, can be found in Appendix A.

Figure 3.8 shows calculated $C(1/2)$ values as a function of surfactant tail length. Experimental values of $C(1/2)$ are also shown on the plot for comparison purposes. It can be seen that the model correctly predicts the shape of the $C(1/2)$ curve and predicts $C(1/2)$ values below the cmc for short tailed surfactants and $C(1/2)$ values above the cmc for longer tailed surfactants. In order to get this particular fit of the data, Γ_{crit} was set equal to 1.26 nm^{-2} and t_{ads} was set equal to 2.8 s. The value of Γ_{crit} is reasonable because it is 60 – 70 % of Γ_{max}. The value for t_{ads} is nearly a factor of 300 times larger than the estimated bubble rise time through the surfactant solution of 10 ms. One possible explanation for this is that the bubbles do in fact have longer to adsorb surfactant than the rise time through the surfactant solution. If a sufficient level of surfactant can adsorb to a bubble's surface during the bubble rise time such that the bubbles are stable on the surface of the surfactant for a few seconds, then more surfactant can adsorb while the bubble is in contact with the surfactant solution making it stable enough for the system to be considered a foaming one. A bubble is in contact with the surfactant solution until the surface of the surfactant solution is covered with a single layer of bubbles. At this stage new bubbles forming on the surface promote the (now) older bubbles up the vessel to take their place. This process continues as the foam is produced. t_{ads} is therefore the minimum time for adsorption which is a summation of the bubble rise time and an additional time (unknown from first principles, but estimated from the calculation to be of the order

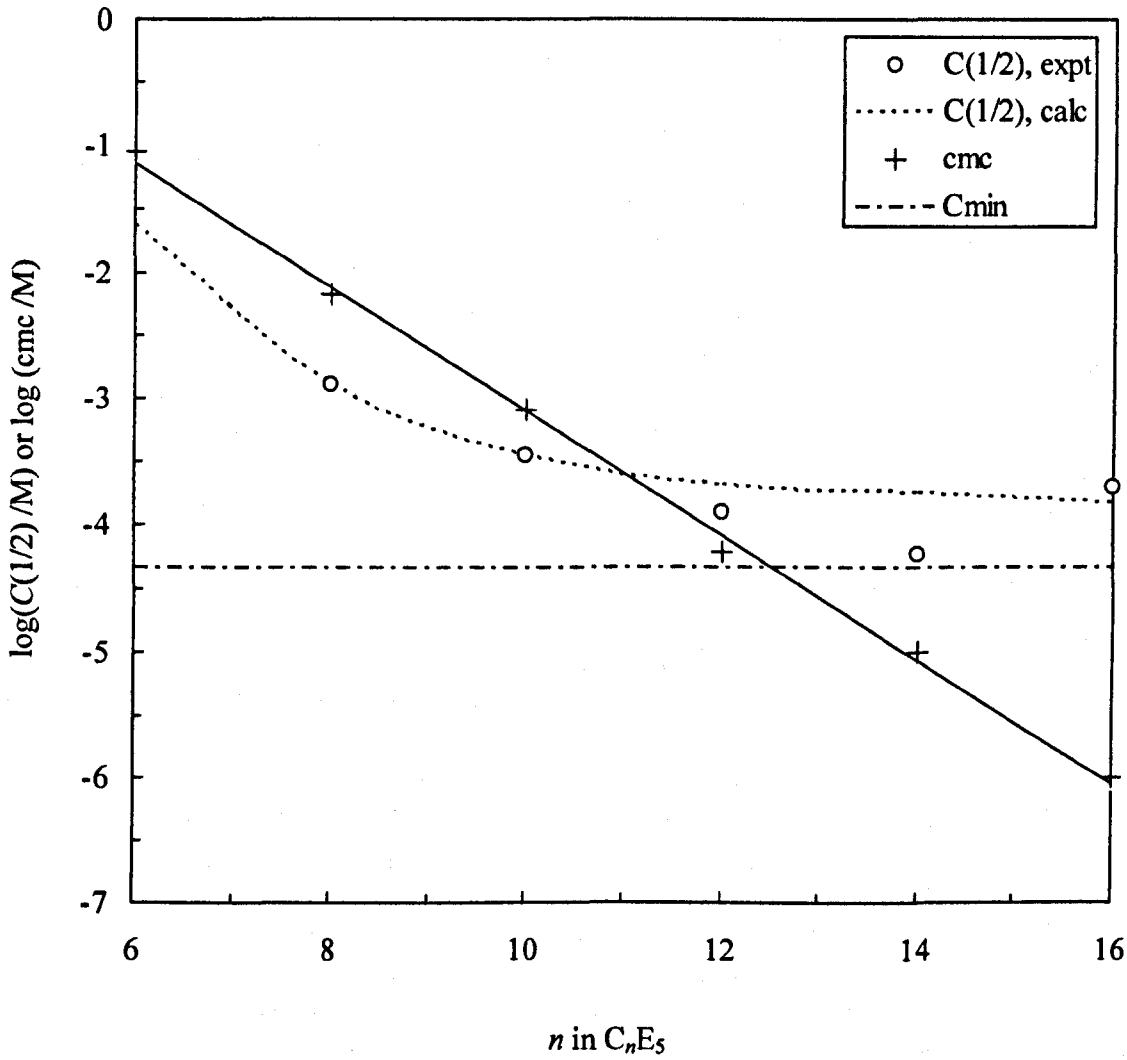

Figure 3.8 Comparison of the variation of $C(1/2)$ and cmc with surfactant chain length n and the value of C_{min} (horizontal dash-dotted line) and $C(1/2)$ calculated values (dotted line). (Data also included for $C_{16}E_6$).

of a couple of seconds or so) for further surfactant adsorption to occur in order for the adsorption to reach Γ_{crit}. This additional time may be approximately equal to the time the freshly formed bubble is in contact with the surfactant solution.

Although the explanations discussed above are plausible, there is an alternative explanation which is possible. For long-tailed surfactants at low concentrations, the foaming solution can be significantly depleted of surfactant during foam generation. For 15.0 cm^3 of foaming solution, the minimum surfactant concentration (C_{min}) required to stabilise 200 cm^3 of foam with bubble radius 2 mm and Γ_{crit} = 1.5 molecules nm^{-2} is approximately $10^{-4.3}$ M.[15] C_{min} is shown by the horizontal dashed line of Figure 3.8. It appears that surfactant depletion of the foaming solution may also be a major determinant of the high tail-length limiting value of $C(1/2)$ for the particular experimental foamability conditions used here.

Using the experimental setup described in this work, it would be impossible to investigate these ideas further. There is no provision for the control of bubble rise time in the current apparatus and the surfactant reservoir is not large enough to hold a sufficient volume of surfactant such that depletion is negligible during the 10 minute foam production period for the long-tailed surfactants. However, in the future work section (Chapter 7) a method is briefly summarised which would permit the idea of a crossover in foamability behaviour as a function of surfactant tail length to be investigated further without depletion giving an ambiguity to the interpretation of the data.

3.3.5 Foaming of commercially available surfactants

Preliminary foaming measurements have been carried out Lutensol AO7, a commercially available surfactant used in various consumer products. Lutensol AO7 is a nonionic surfactant with average structure $C_{12}E_7$ except that it contains a distribution of tail length and number of EO groups in its headgroup. Lutensol AO7 has a distribution of between 11 and 13 carbons in the hydrophobic moiety and 7 ethylene oxide units in the hydrophilic group. It should therefore have a cmc very close to that of $C_{12}E_7$. The cmc and relative molecular mass of $C_{12}E_7$ are 8.0×10^{-5} M

and 494 g mol^{-1} respectively. The cmc of $C_{12}E_7$ can therefore be expressed as 3.95 x 10^{-3} wt. %.

Figure 3.9 shows the foamability of Lutensol AO7 as a function of its concentration according to a series of shake tests (see section 2.5 for full details of this procedure). There is a dramatic increase in foamability at a specific concentration which is the same trend observed for all of the nonionic surfactants in the homologous series investigated in this chapter. In Figure 3.9, it can be seen that there is a dramatic increase in the foamability of the surfactant by shake tests at a concentration similar to $C(1/2)$ measured for $C_{12}E_7$ on the foam column.

The findings in this chapter are therefore likely to be applicable to commercial surfactant equivalents and hence industrial applications.

3.4 Foam stability

Foam stability refers to the persistence of foam once formed. The longer it takes to decay then the more stable it is. Often foam stability is assessed by generating foam and measuring its volume as a function of time. From these decay plots a half-life can be readily obtained which corresponds to the time taken for the foam to decay to half its original volume.

3.4.1 Variation of surfactant tail length

Foam stability (as judged by foam half-life) was measured as a function of the number of methylene groups in the hydrophobic chain when the number of ethylene oxide units in the surfactant head was fixed at 5. Foam half-life was derived from plots of foam volume as a function of time (see Figure 3.10 for a typical decay curve). All of the foams were created from an initial surfactant concentration of 0.04 M (well in excess of the cmc for all of the surfactants studied). The resulting stability plot is shown in Figure 3.11. Increasing the number of methylene groups in the hydrophobic tail from 8 to 14 increases the time taken for the foam to fall to half its initial volume

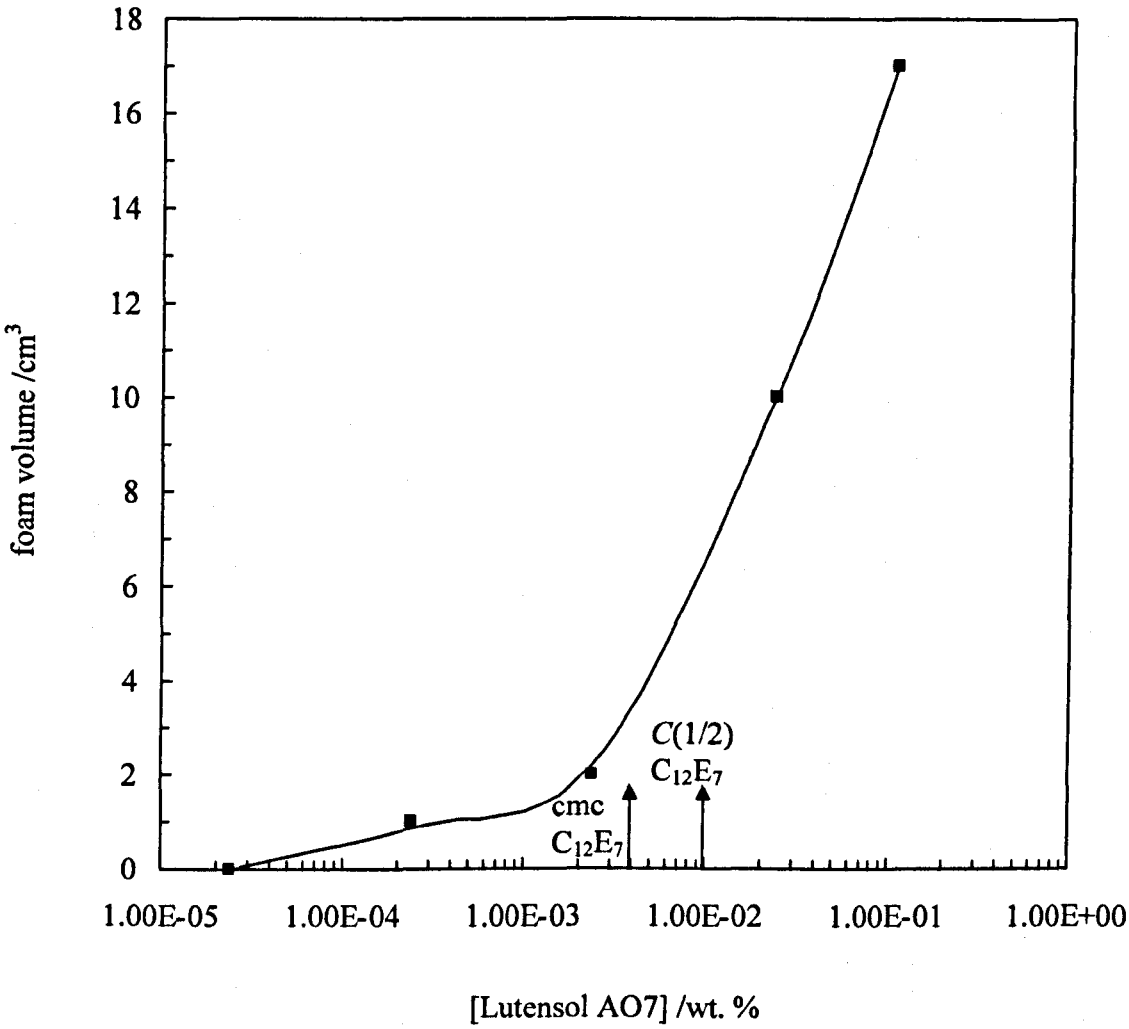

Figure 3.9 Foam volume as a function of surfactant concentration for Lutensol AO7. Foam created by shaking 20.0 cm^3 of aqueous surfactant solution in a 100 cm^3 stoppered measuring cylinder. All measurements made at ambient temperature. The upward arrows denote values for the cmc and $C(1/2)$ for $C_{12}E_7$.

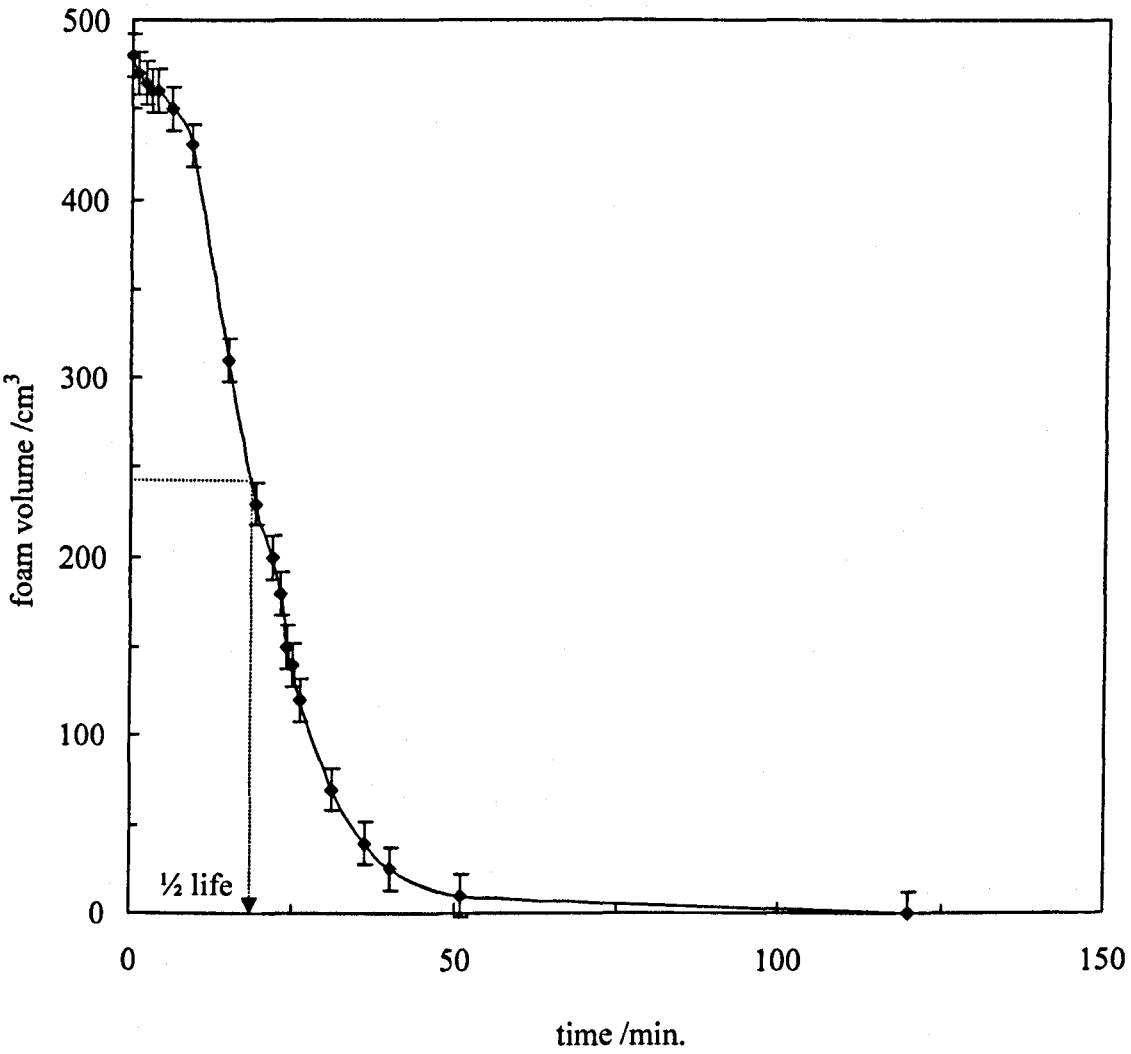

Figure 3.10 Foam volume as a function of time for an aqueous $C_{12}E_5$ stabilised foam. Foam created by sparging N_2 gas through 15.0 cm^3 of surfactant solution (0.04 M) for 10 minutes at a gas flow rate of 48 cm^3 min^{-1}. The measurements were made at 25.0 °C.

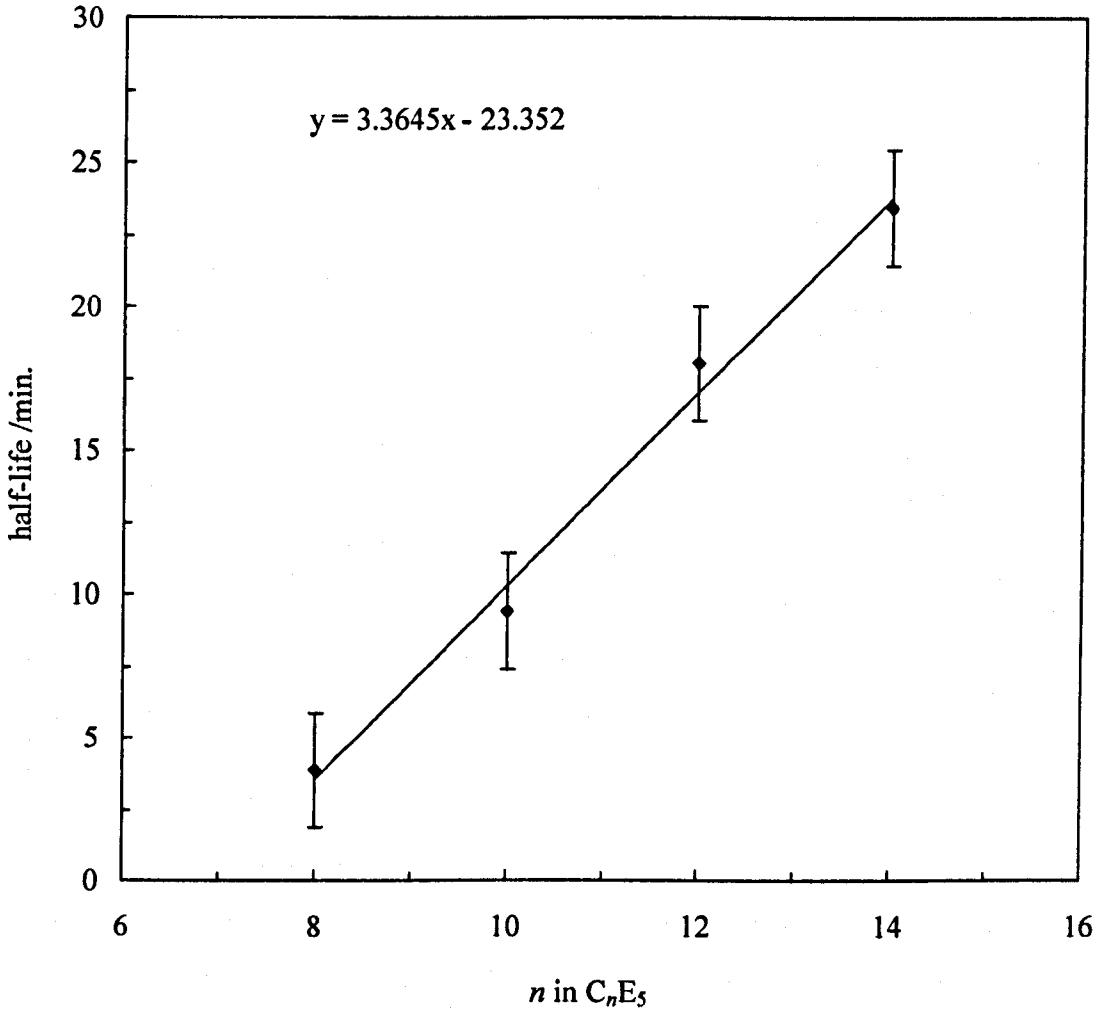

Figure 3.11 Foam stability as a function of n in C_nE_5. Foam created by sparging N_2 gas through 15.0 cm^3 of surfactant solution for 10 minutes at a flow rate of 48 $cm^3\ min^{-1}$. [surfactant] = 0.04 M, temperature = 25.0 °C.

by a factor of approximately 5. This figure illustrates that the hydrophobicity of the surfactant (and hence how strongly it adsorbs) is an important factor in dictating the stability of the resulting foam.

3.4.2 Variation in surfactant headgroup size

The foam stability of the $C_{12}E_m$ series of surfactants is now considered. Figure 3.12 shows foam half-life as a function of the number of ethylene oxide units in the surfactant headgroup. There is only a weak dependence of the number of ethylene oxide groups on foam stability. However, there is a slight increase in foam stability as the number of units in the hydrophilic headgroup is increased and there may even be a slight maximum observed in the stability of the foam when the number of ethylene oxide groups is equal to 8. The data implies that there could be optimum ratio of the number of ethylene oxide units to the number of carbons in the hydrophobic tail corresponding to a maximum in foam stability. As discussed in section 1.5.1, Schick and Beyer studied the effect of ethylene oxide chain length on foam formation (foamability) and foam stability for molecularly distilled (i.e. pure) nonionic surfactants prepared with five different hydrophobic groups.[3] They produced foam using the standard Ross and Miles test[16], using 1 mM of foaming solution. They found that in each series, the foam height and foam stability passed through a maximum at a mole ratio of ethylene oxide which they termed the critical hydrophilic-hydrophobic balance (CHHB). When the hydrophobic group contained 12 carbons, they found that maximum foam stability was observed for 7 ethylene oxide groups. The data in Figure 3.12 also passes through such a maximum at a similar number of ethylene oxide groups and hence a similar CHHB.

Another possible reason for the increase in foam stability as a function of the number of units in the hydrophilic headgroup is due to the fact that the concentration at which black films (C_{bl}) form, decreases with increasing hydrophilic group. It is known that C_s (the surfactant concentration corresponding to stable foams coincides with C_{bl}. Surfactants with longer hydrophilic groups therefore have lower C_s values and so at a fixed concentration (in the case of these experiments 0.04 M), foams stabilised by surfactants with longer hydrophilic groups may be expected to be more stable than

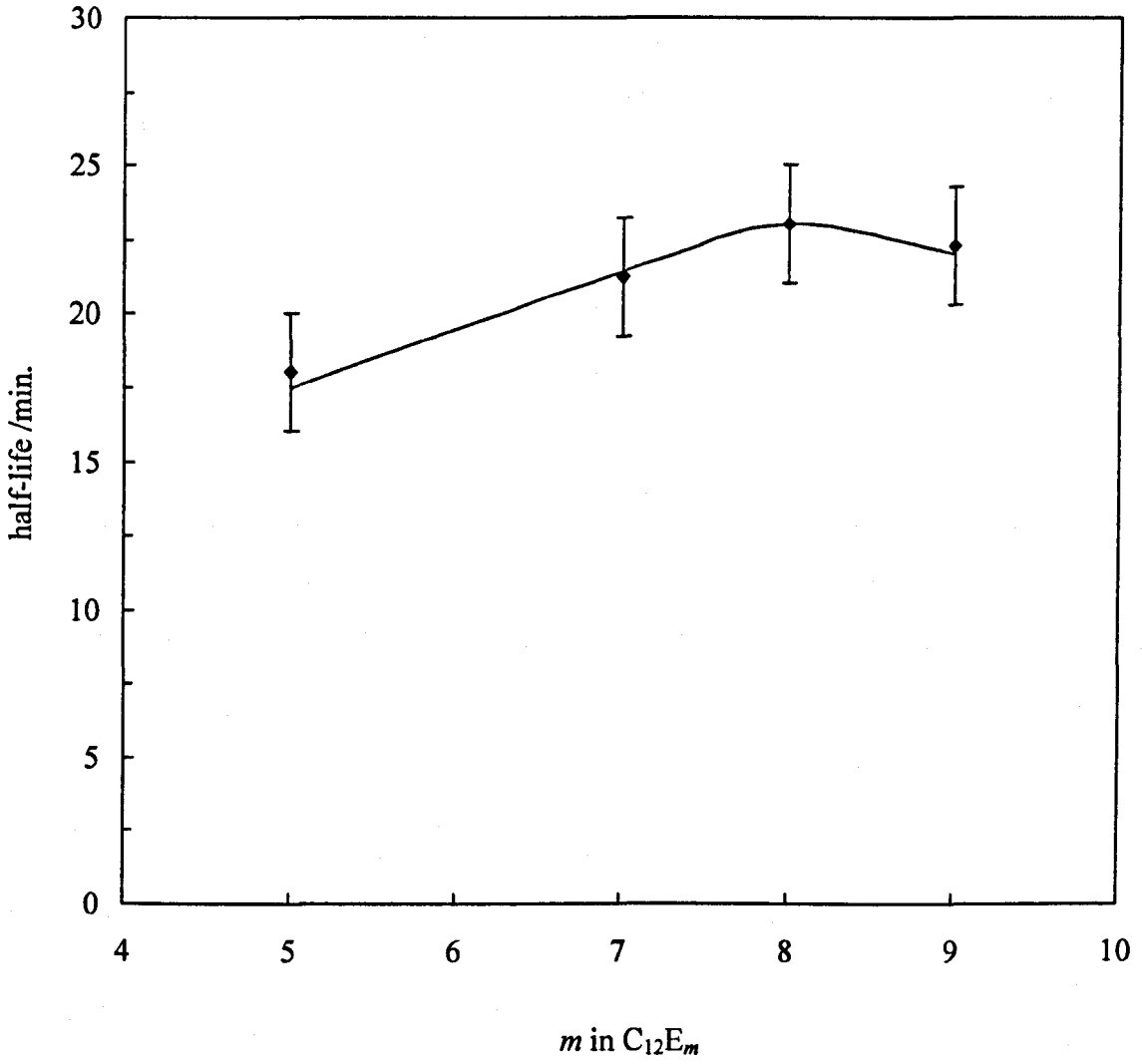

Figure 3.12 Foam stability as a function of m in $C_{12}E_m$. Foam created by bubbling N_2 gas through 15.0 cm^3 of surfactant solution for 10 minutes at a flow rate of 48 $cm^3\ min^{-1}$. [surfactant] = 0.04 M, temperature = 25.0 °C.

foams stabilised surfactants with shorter hydrophilic groups. This is due to the surfactants with larger headgroups being present at concentrations relatively higher than their corresponding C_s values compared to surfactants with smaller headgroups. Yamanaka[17] studied the kinetics of black films and found a virtually linear increase in the decay constants with the rate of growth of black films in a foam stabilised by a nonionic surfactant.[18] These rates of formation of black films will presumably be concentration-dependent.

3.5 Temperature dependence of foaming using $C_{12}E_5$

Figure 3.13 shows the foamability profiles of $C_{12}E_5$ at 20.0 °C and 25.0 °C presented in the form of foam volume after 10 minutes as a function of surfactant concentration. This data shows that decreasing the temperature of the foaming experiments by 5.0 °C (closer to room temperature) does not affect the surfactants tendency to foam. This finding will be capitalised upon in later chapters when the foamability of $C_{12}E_5$ in the presence of foam modifying agents will be measured using shake tests at room temperature.

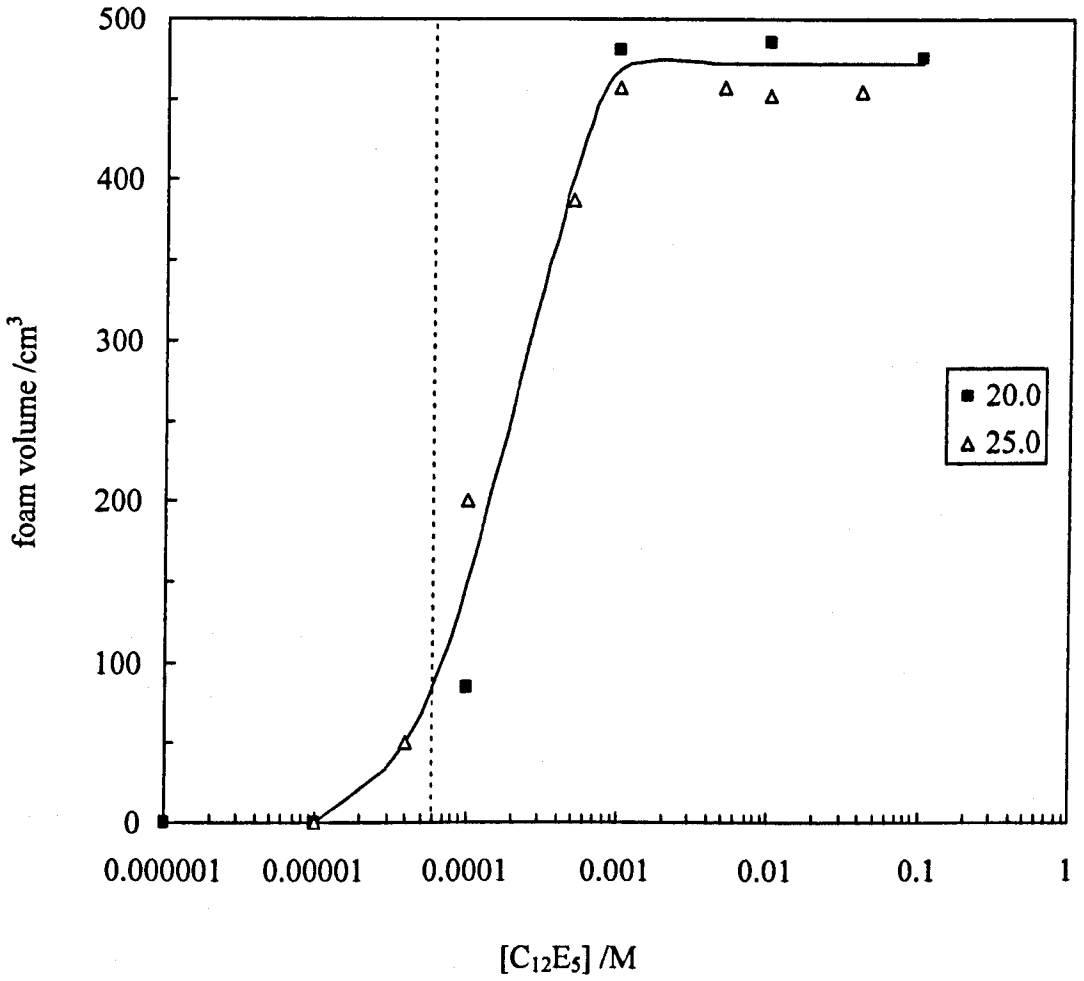

Figure 3.13 Foam volume immediately after 10 minutes gas sparging as a function of surfactant concentration for aqueous samples of $C_{12}E_5$ at 20.0 and 25.0 °C. Foam created by sparging N_2 gas through 15.0 cm^3 of the surfactant solution at a flow rate of 48 cm^3 min^{-1} for 10 minutes.

3.6 Conclusions

- The foamability of the C_nE_m series of surfactants depends on the hydrophobic tail length. Increasing the tail length of the surfactant increases the surfactant's foamability.

- The foamability of the C_nE_m series of surfactants does not depend on the hydrophilic chain length.

- For C_nE_m surfactants, $C(1/2)$ (the concentration corresponding to the transition from non-foaming to foaming behaviour) is below the cmc for short chain surfactants (suggesting equilibrium adsorption control of the foamability) and above the cmc for long chain surfactants, suggesting dynamic adsorption control and/or surfactant depletion.

- At a fixed surfactant concentration in excess of the cmc, increasing the hydrophobic tail length of a surfactant increases the resulting foam's stability.

- At a fixed surfactant concentration, increasing the size of the hydrophilic head group initially increases the resulting foam's stability, to a maximum value at an intermediate number of headgroups. The foam stability is then seen to decrease as the size of the headgroup is increased further.

- In the context of foamability, the commercially available surfactant (Lutensol AO7) behaves similarly to the equivalent pure surfactant homologue ($C_{12}E_7$).

References

1. G. M. Gantz in "*nonionic surfactants*", (M. J. Schick Ed.), Marcel Dekker, New York, 1967, chapter 21.
2. K. Shinoda, T. Yamanaka, and K. Kinoshita, *J. Phys. Chem.*, (1959), **63**, 648.
3. M. J. Schick and E. A. Beyer, *J. Am. Chemists' Soc.*, (1963), **40**, 66.
4. A. Bonfillon-Colin and D. Langevin, *Langmuir*, (1997), **13**, 599.
5. Z. Nemeth, G. Racz, K. Koczo, *J. Colloid Interf. Sci*, (1998), **207**, 386.
6. J. H. Clint, *Surfactant Aggregation*, Blackie & Son Ltd, New York, 1992, p.154.
7. S. Lin, R. Tsay, L. Lin and S. Chen, *Langmuir*, (1996), **12**, 6530.
8. B. P. Binks, P. D. I. Fletcher, V. N. Paunov and D. Segal, *Langmuir*, (2000), **16**, 8926.
9. J. Eastoe, J. S. Dalton, P. G. A. Rogueda, E. R. Crooks, A. R. Pitt and E. A. Simister, *J. Coll. Int. Sci.*, (1997), **188**, 423.
10. A. Prins, *Chem. Ing. Tech.*, (1992), **64**, 73.
11. C Ybert and J. M. di Meglio, *Eur. Phys. J. B.*, (1998), **4**, 313.
12. Viscosity value taken from "*Physical Chemistry*", (P. W. Atkins), Fifth Edition, OUP, Oxford, 1995, p. 833.
13. G. Liger-Belair, R. Marchal, B. Robillard, T. Dambrouck, A. Maujean, M. Vignes-Adler and P. Jeandet, *Langmuir*, (2000), **16**, 1889.
14. Code for the VBA written by P. D. I. Fletcher, University of Hull.
15. The value of r represents a measured bubble radius and the value of Γ_{crit} is an estimate of the level of surfactant adsorption required to stabilise a bubble.
16. J. Ross and G. D. Miles, *Oil and Soap*, (1941), **18**, 99.
17. T. Yamanaka, *Bull Chem. Soc. Japan*, (1970), **43**, 633.
18. M. J. Schick and I. R. Schmolka in "*nonionic surfactants*", (M. J. Schick Ed.), Marcel Dekker, New York, 1987, chapter 14.

Chapter 4

CHAPTER 4

Foaming of nonionic surfactants in the presence of *n*-alkane vapours

4.1 Introduction

The control of foam by either the addition of foam boosters or foam inhibitors to a foaming solution or addition of foam breakers to preformed foam is important in a wide range of products and processes. Micron sized emulsion drops of oil can act as foam inhibitors, either through formation of an unstable liquid oil bridge or by oil drop entry into the foam film surface which may be followed by spreading of the oil over the foam film surface[1-5] (see section 1.6 for a more detailed explanation of the various mechanisms proposed for oil anti-foam action). For many foam control applications, the most effective foam inhibitors consist of solid hydrophobic particles dispersed within an oil-in-water emulsion which is added to the foaming solution. With such complex formulations, a variety of mechanisms may contribute to the overall effectiveness in inhibiting the foam production.[6-11] One possible contribution to foam inhibition arises from the presence within the gas phase of the foam of oil vapour which can co-adsorb at the air-water surface with the primary surfactant stabilising the foam films and thus potentially alter both the foamability and the foam stability. Hadjiiski et al.[11] have observed that co-adsorption of oils into surfactant monolayers causes significant changes in the barrier to entry of micro-sized oil drops into the air water surface which they have shown can be an important determinant of anti-foam activity. Although this observation suggests there can be important differences in behaviour between surfactant monolayers with and without co-adsorbed oil, there have been no studies of the influence of oil co-adsorption on the foaming properties of aqueous surfactant solutions. In this chapter, the effect of oil vapours, in the absence of any additional foam control components, has been systematically studied in relation to the foamability and foam stability of pure nonionic surfactants.

4.2 Mixed oil / surfactant monolayers

As discussed in section 1.7.1, oils can co-adsorb with primary surfactant to form mixed oil surfactant monolayers.

At the surface of pure water, linear alkanes of chain length equal to pentane or shorter can wet the surface. This corresponds to an infinite extent of adsorption by the oil at the water–vapour surface.[12] The maximum adsorption (i.e. at a partial pressure corresponding to the equilibrium vapour pressure) of higher alkanes decreases sharply with increasing chain length with alkanes such as decane showing negligible adsorption. However, longer chain length vapours do adsorb significantly at the surface of an aqueous surfactant solution, which contains an adsorbed monolayer of surfactant. A mixed adsorbed film containing both oil and surfactant is formed at equilibrium. Following the pioneering work of Hauxwell and Ottewill[13], alkane vapour adsorption at the surface of surfactant solutions has been systematically investigated using surface tensiometry[14-19] and neutron reflection methods[20-23] for varying surfactant structures and concentrations, different oils and varying oil vapour concentrations (expressed as oil vapour activity equal to the ratio of the oil partial pressure to the equilibrium oil vapour pressure P/P_0). Measurement of the surface tension as a function of P/P_0 has been used to determine the adsorption isotherms of the oils. Neutron reflection studies using selective deuteration of the components of the mixed oil-surfactant films have enabled the determination of the microstructures of selected adsorbed films. For high chain length oils showing negligible adsorption on pure water, the key features of oil adsorption into surfactant monolayers relevant to this work are summarised below:

1. The surface excess concentration of oil Γ_{oil} generally increases approximately linearly with P/P_0 to reach a maximum value $\Gamma_{oil,max}$ at $P/P_0 = 1$. The maximum extent of surface tension reduction $\Delta\gamma$ caused by the addition of oil vapour at $P/P_0 = 1$ is typically in the range 1 – 10 mN m^{-1}.

2. For surfactants with the same tailgroup but different headgroups, $\Gamma_{oil,max}$ is largest for the surfactants with the largest area per adsorbed molecule, i.e. $\Gamma_{oil,max}$ increases with increasing headgroup size of the surfactant.

3. For a homologous series of surfactants with a constant hydrophilic headgroup and varying hydrophobic tailgroup, $\Gamma_{oil,max}$ increases with increasing surfactant chain length.

4. For a particular surfactant, decreasing the surfactant concentration causes the area per adsorbed surfactant to increase, eventually to infinity when the concentration is zero. With increasing area per adsorbed surfactant, the oil adsorption at $P/P_0 = 1$ passes through a maximum before decreasing to zero adsorption for the pure water surface.

5. For a particular surfactant, $\Gamma_{oil,max}$ increases with decreasing molar volume of the adsorbing oil.

6. Oil vapour adsorption generally causes only a slight (typically 10 % or less) increase in the area per adsorbed surfactant molecule. Within the mixed film, the adsorbed oil molecules are mainly located within the surfactant chain region. Oil adsorption causes only a slight increase in the average thickness of this region.

From the summary above, it can be concluded that the oil molecules co-adsorb with the primary-stabilising surfactant by occupying the maximum space available in the tail region of the surfactant. This view explains why $\Gamma_{oil,max}$ varies in the ways summarised above when factors relating to the surfactants or the oil are changed and is consistent with neutron reflection data.

It is also relevant to note here that Eastoe and co-workers[24] have found that adding an alkane into a surfactant monolayer changes the sign of the dilational viscosity (ε') of the monolayer from negative to positive. They propose that this occurs due to the

stabilisation of the dilational (longitudinal) waves. These waves propagate from capillary (longitudinal) waves which are driven by surface tension due to the presence of an interfacial film. There is an adsorption barrier for the stability of dilational waves expressed as a ratio (Z) of two characteristic times, (i) for the adsorption of a surfactant at an interface (t_{ads}) and (ii) for diffusion from bulk surfactant to an interface (t_{diff}). An increase in adsorption barrier therefore increases the value of ratio Z. Dilational wave stability can be expressed in terms of the Marangoni elasticity number (M). By changing the sign of the dilational viscosity, surface elastic properties are altered and these are likely to strongly affect foam stability.

4.3 Delivery of oil vapour to the foam

For measurements in the presence of oil vapour at $P/P_0 = 1$, the N_2 gas steam was passed through a series of 3 oil bubblers held within the thermostat tank so as to produce a saturated vapour stream prior to entry of the foam column. For measurements with oil vapours at P/P_0 less than 1, the bubblers contained mixtures of the volatile oil plus the involatile species squalane. The required value of P/P_0 was obtained by adjustment of the squalane concentration within the bubblers according to $P/P_0 = fX$, where X is the mole fraction of the volatile oil in the squalane mixture and f is the activity coefficient taken from reference 25. Values for P_0 were taken from reference 26. See the experimental section for full details of this method.

Due to the fact that a low molecular weight *n*-alkane evaporates at a faster rate than a higher molecular weight one (due to its higher vapour pressure), it was anticipated that there could potentially be a lower limit to the molecular weight of the oils accessible for use in these experiments. This limit would arise because of the oil being depleted (by evaporation) during the bubbling of gas through the oil mixture causing the value of P/P_0 to change significantly with respect to time because of the change in mole fractions (the mole fraction of the lower weight alkane would decrease with time). It was decided to investigate this further before proceeding with any foaming measurements. This was achieved by fixing the value of P/P_0 at 0.2 for hexane, octane, decane and dodecane by mixing the appropriate mass of each alkane with a fixed mass of squalane in order to obtain the necessary overall mole fraction

for the particular oil required to make the value of P/P_0 equal to 0.2. Nitrogen gas was then bubbled through each oil mixture at a flow rate of 48 cm^3 min^{-1} and the total mass of the mixture was measured at 15 minute time intervals for 90 minutes. It was assumed that all of the mass loss was due to depletion of the low molecular weight alkane by evaporation. From this data, modified mole fractions were calculated based on the masses of the two species at time t and hence values for P/P_0 were obtained at the 15 minute time intervals. Figure 4.1 shows how the values of P/P_0 (initially fixed as closely as possible to 0.2) vary with respect to time for hexane, octane, decane and dodecane. When using low molecular weight alkanes containing less than 8 carbons in their chain, P/P_0 varies significantly over the course of the 90 minute time period. The value to which P/P_0 was lowered after 15 minutes was plotted in the form of the percentage of its initial value as a function of the number of carbons in the alkane's chain. From this data (Figure 4.2) it can be seen that the lowest alkane that can realistically be used in the series is octane otherwise the drop in P/P_0 is too significant during a 10 minute foam generation experiment.

Based on previous work[27], it was decided to connect 3 bubblers in series with one another to ensure that the N_2 gas was fully saturated with the oil vapour. In order to verify that 3 bubblers was a sufficient number to allow the N_2 gas to become fully saturated under the experimental conditions used in this work, the expected mass loss of alkane was calculated with respect to time using equation [4.6], which was derived in the following way

the ideal gas equation

$$PV = nRT \qquad [4.1]$$

can be rearranged to

$$n = \frac{PV}{RT} \qquad [4.2]$$

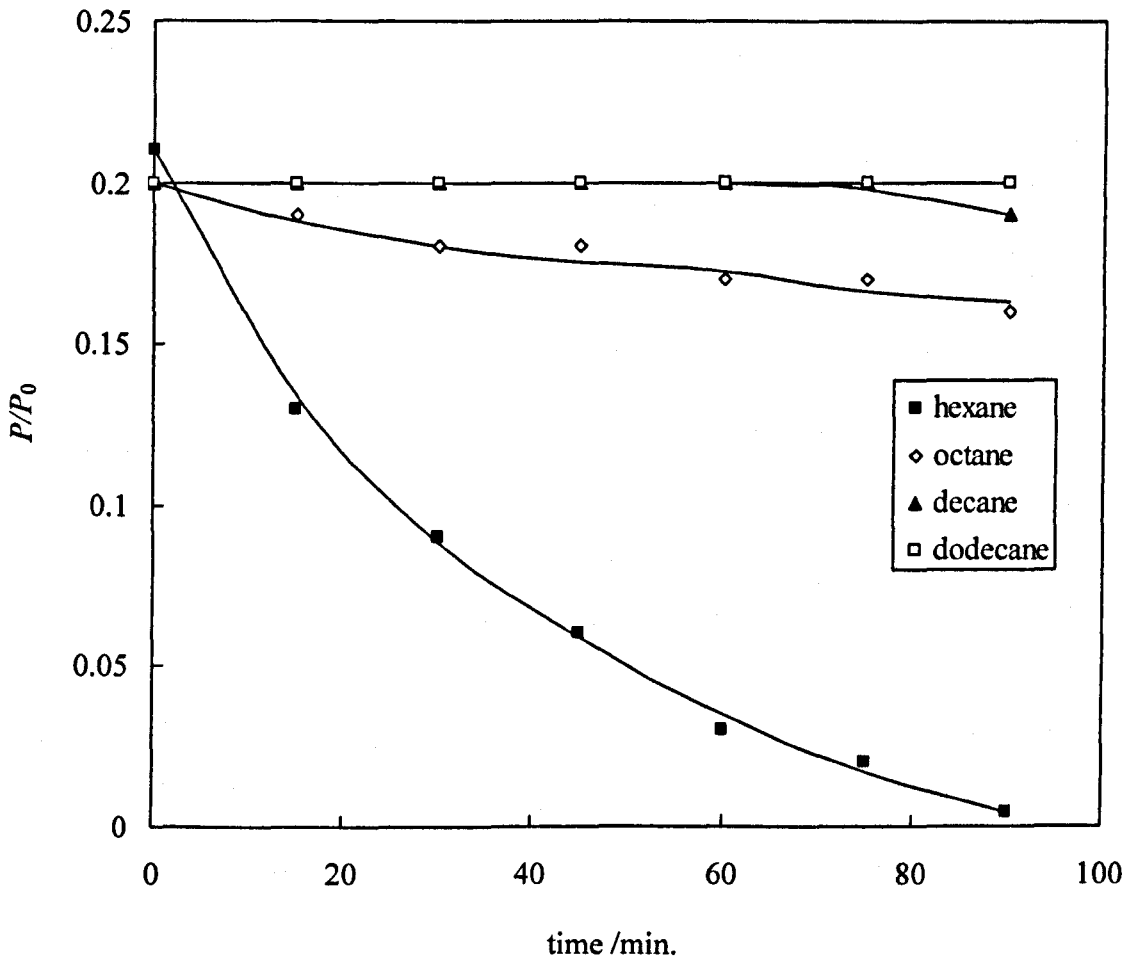

Figure 4.1 P/P_0 as a function of time for low molecular weight alkanes (hexane, octane, decane and dodecane) mixed with squalane such that the value of P/P_0 at time = 0 is approximately 0.2 for each alkane. Nitrogen gas was bubbled through each mixture at a flow rate of 48 cm^3 min^{-1}. All measurements were made at 25.0 °C.

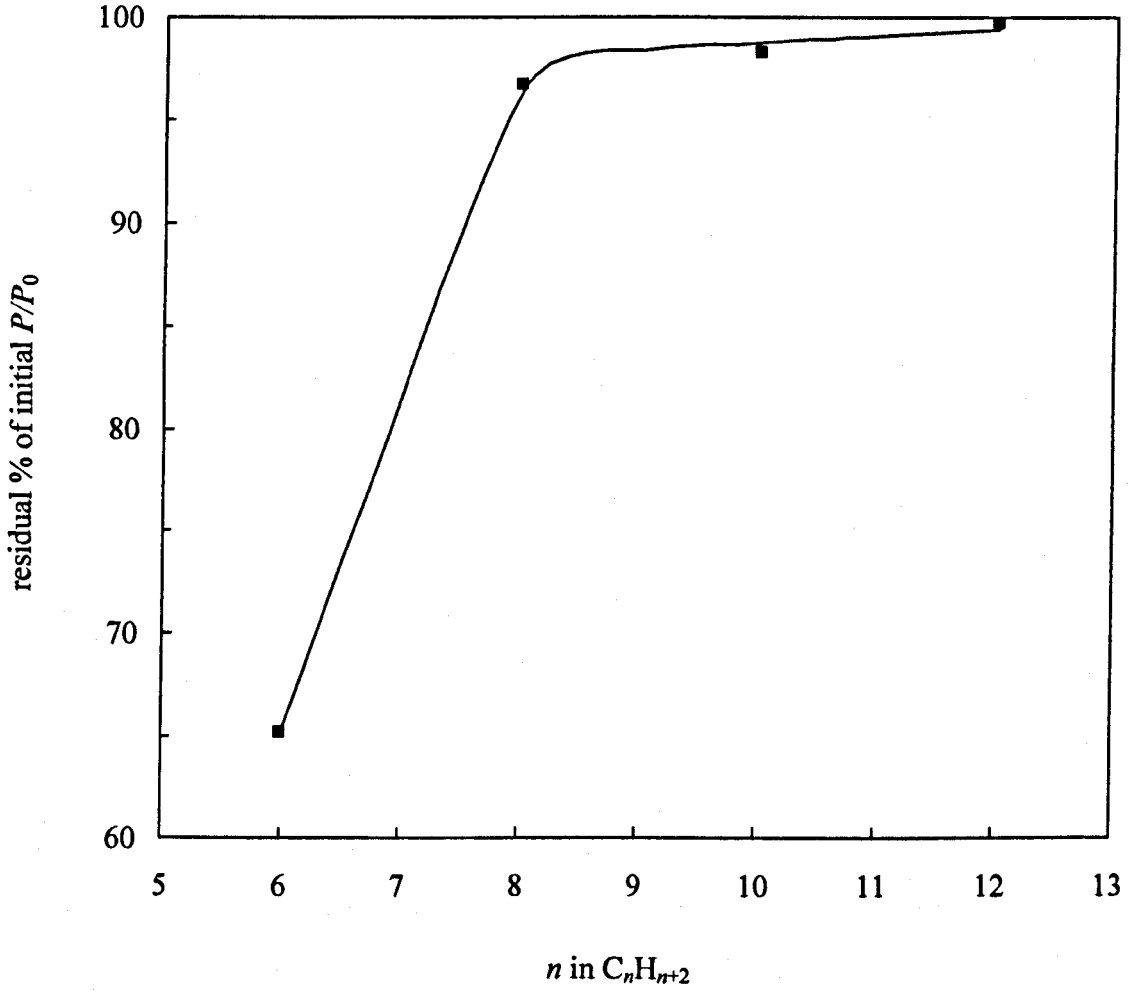

Figure 4.2 Percentage of P/P_0 (initially set at 0.2) remaining as a function of the number of carbons in an alkane chain after bubbling nitrogen gas through mixtures of the alkane and squalane at a gas flow rate of 48 $cm^3\ min^{-1}$ for 15 minutes. All measurements were made at 25.0 °C.

the volume of gas (V) delivered in a given time (t) is equal to the flow rate (F)t

$$n = \frac{PFt}{RT} \qquad [4.3]$$

number of moles (n) can be expressed as mass (m) / relative molecular mass (M)

$$\frac{m}{M} = \frac{PFt}{RT} \qquad [4.4]$$

the change in mass (m_t - $m_{t=0}$) is to be calculated with respect to change in time (t-t_0)
[m_t - $m_{t=0} \equiv dm$, t - $t_0 \equiv dt$]

$$\frac{dm}{M} = \frac{PFdt}{RT} \qquad [4.5]$$

rearranging equation [4.5] yields

$$\frac{dm}{dt} = \frac{MPF}{RT} \qquad [4.6]$$

Where t is the time, m is the mass of the alkane accumulated at time t, M is the relative molecular mass of the alkane, P is the pressure of the alkane (obtained by multiplying the alkane's equilibrium vapour pressure by the value of P/P_0), F is the gas flow rate, R is the gas constant and T is the absolute temperature.

Plotting mass loss as a function of time interval (t-t_0) yields a linear line where dm / dt is the gradient. The measured mass loss of vapour delivery systems containing 1, 2 and 3 bubblers was then plotted on the same chart. This data is shown in Figure 4.3. The dashed line shows the expected mass loss of octane with respect to time. When using a single bubbler, the measured mass loss is lower than the expected (calculated) mass loss. This indicates that the N_2 gas is not becoming saturated with octane and hence P/P_0 will have a lower actual value than the calculated value. Connecting two bubblers in series results in more of the N_2 gas becoming saturated with the alkane and using 3 bubblers in series ensures that gas becomes fully saturated with the

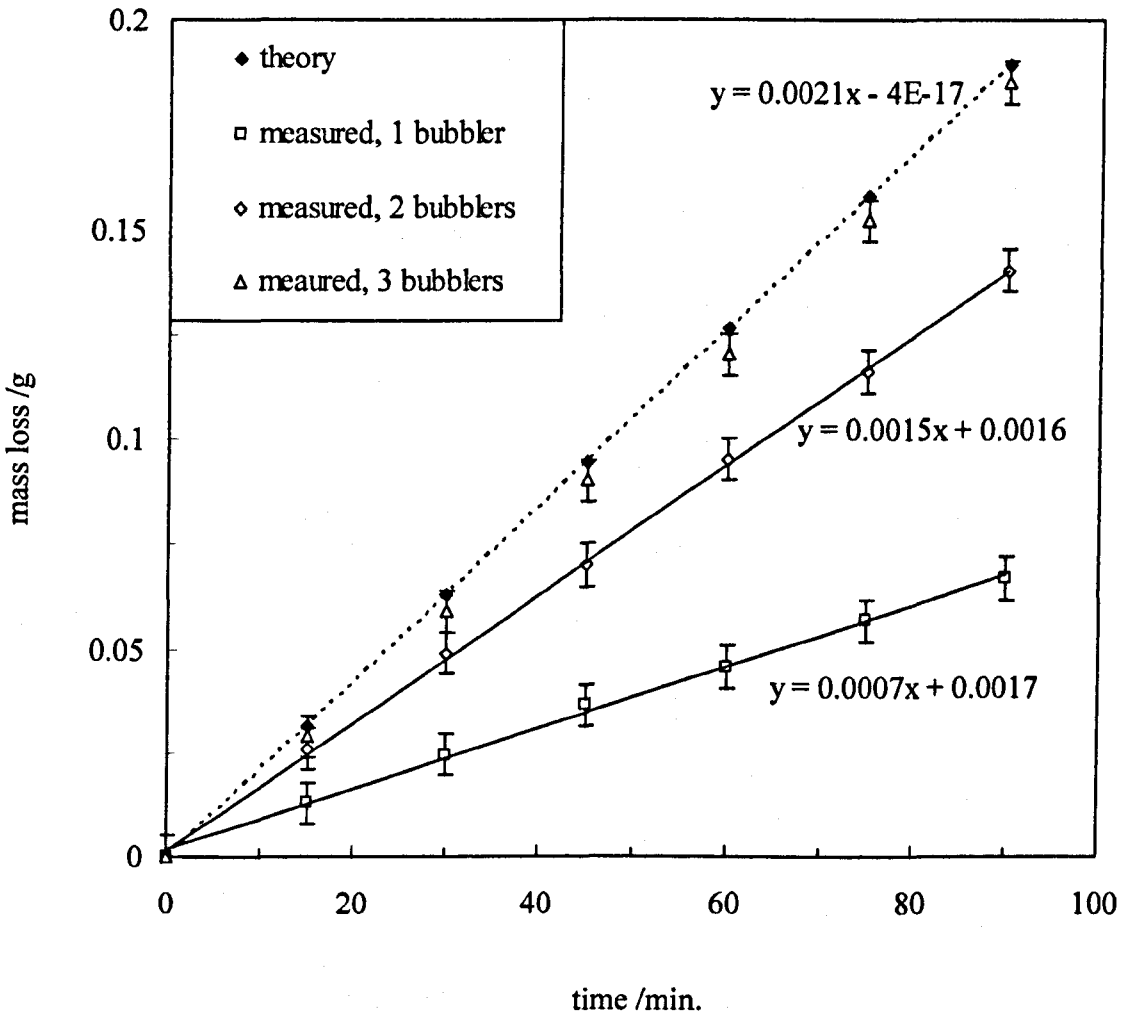

Figure 4.3 Theoretical mass loss as a function of time for octane, and measured mass loss for 1, 2, and 3 bubblers in series. Values of P/P_0 initially set at 0.2.

alkane. This is reflected by the fact that the measured mass loss data series can be superimposed with the calculated mass loss series within experimental uncertainty.

4.4 Variation of surfactant tail length

4.4.1 Foamability

Figures 4.4 – 4.7 show the foamability of the C_nE_5 series of surfactants with and without decane vapour at $P/P_0 = 1$. At low concentrations of surfactant, in the presence of oil vapour, no foam is produced. As the concentration of surfactant is increased there is a transition from non-foaming to foaming behaviour for each of the surfactants. Qualitatively, these are the same trends observed for surfactant solutions foamed in the absence of oil vapour (see chapter 3). Where the difference lies is in the higher concentrations of surfactant required to achieve the transition from non-foaming to foaming behaviour relative to the no oil vapour case for a particular surfactant. This is reflected in the fact that all of the foamability curves in the presence of decane vapour are shifted upwards by approximately 1 order of magnitude yielding higher values of $C(1/2)$ in the presence of decane vapour in comparison to the same systems containing no oil. Based on this, it can be concluded that decane vapour strongly reduces the foamability of the C_nE_5 series of nonionic surfactants.

Figure 4.8 shows comparisons of values of $C(1/2)$ with and without decane vapour relative to the cmc for different length tail groups. For C_8E_5, $C(1/2)$ is increased by decane vapour by a factor of 17 whereas this factor decreases with increasing n to give a factor of 4.5 for $C_{14}E_5$. In contrast, the maximum extent of equilibrium adsorption of oil into surfactant monolayers (measured at surfactant concentrations in excess of the cmc) is known to increase with increasing chain length of the surfactant.[18] Hence there appears to be no clear correlation between the foam inhibition effect by oil vapours and the extent of oil adsorption. There are however certain factors that should be taken into account which may explain why there is no clear correlation. Firstly, the foam inhibition effects are measured at surfactant concentrations close to $C(1/2)$ whereas the equilibrium oil vapour adsorption

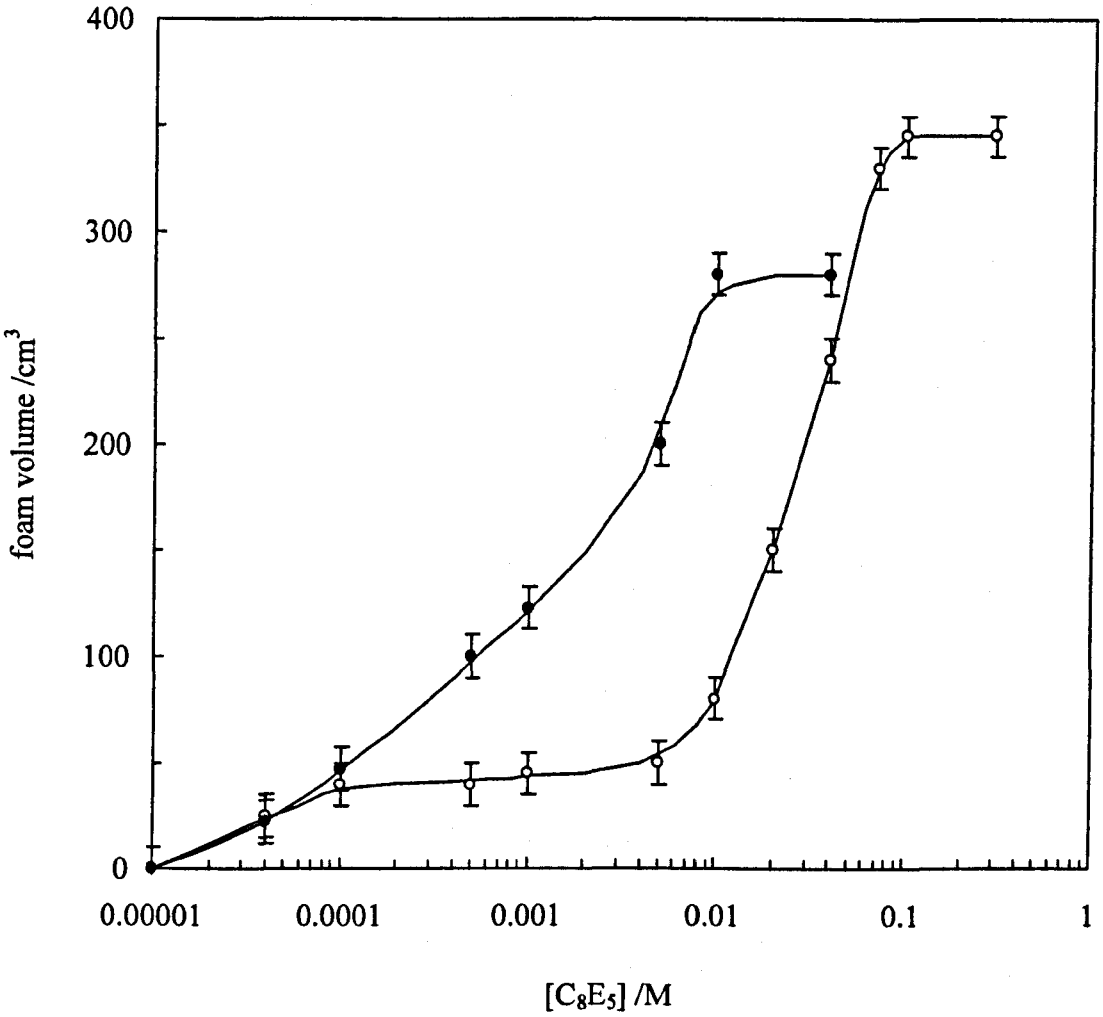

Figure 4.4 Foam volume immediately after 10 minutes gas sparging as a function of surfactant concentration for C_8E_5 with (open circles) and without (filled circles) saturated decane vapour. The nitrogen gas flow rate was 48 cm^3 min^{-1} and the initial volume of surfactant solution was 15.0 cm^3. The solid lines are guides for the eye.

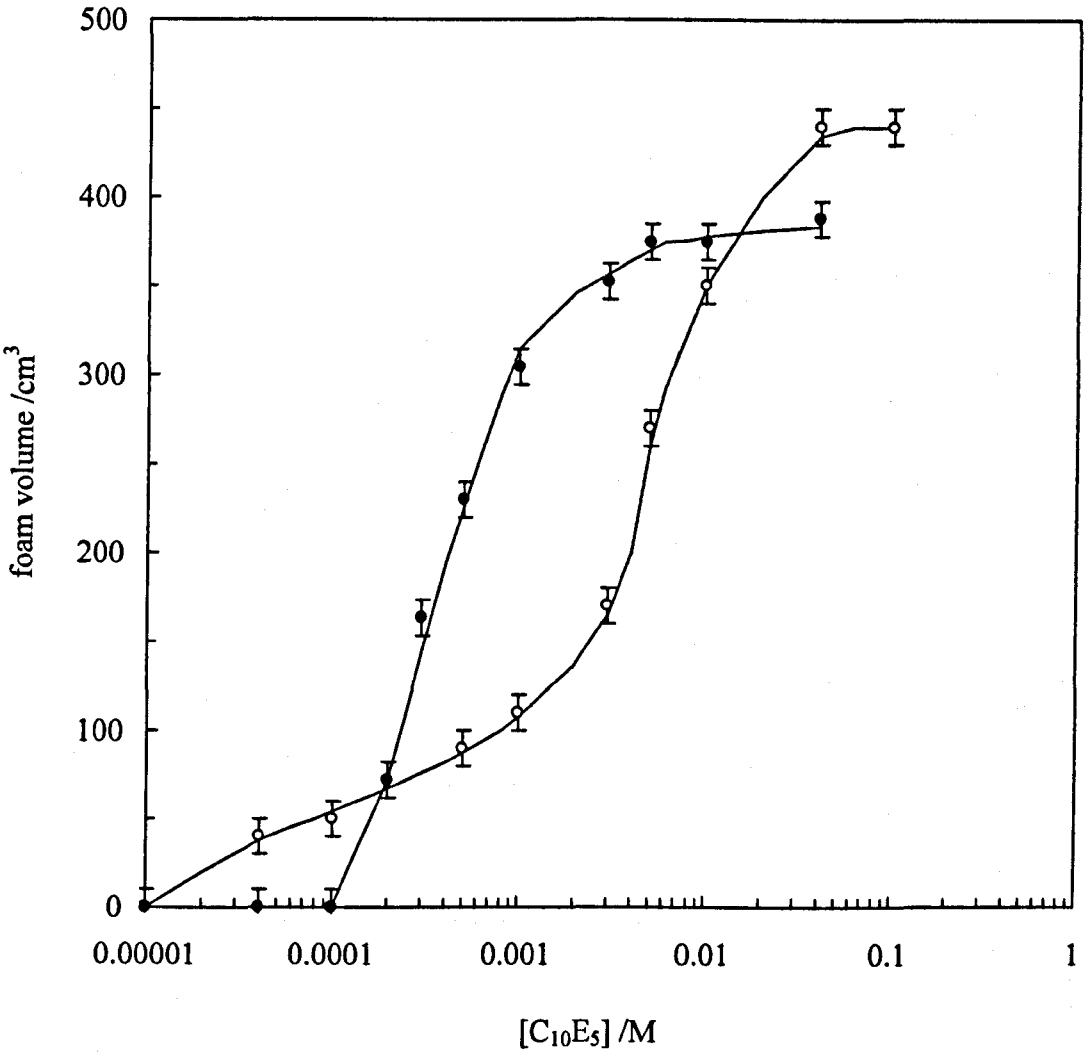

Figure 4.5 Foam volume immediately after 10 minutes gas sparging as a function of surfactant concentration for $C_{10}E_5$ with (open circles) and without (filled circles) saturated decane vapour. The nitrogen gas flow rate was 48 cm^3 min^{-1} and the initial volume of surfactant solution was 15.0 cm^3. The solid lines are guides for the eye.

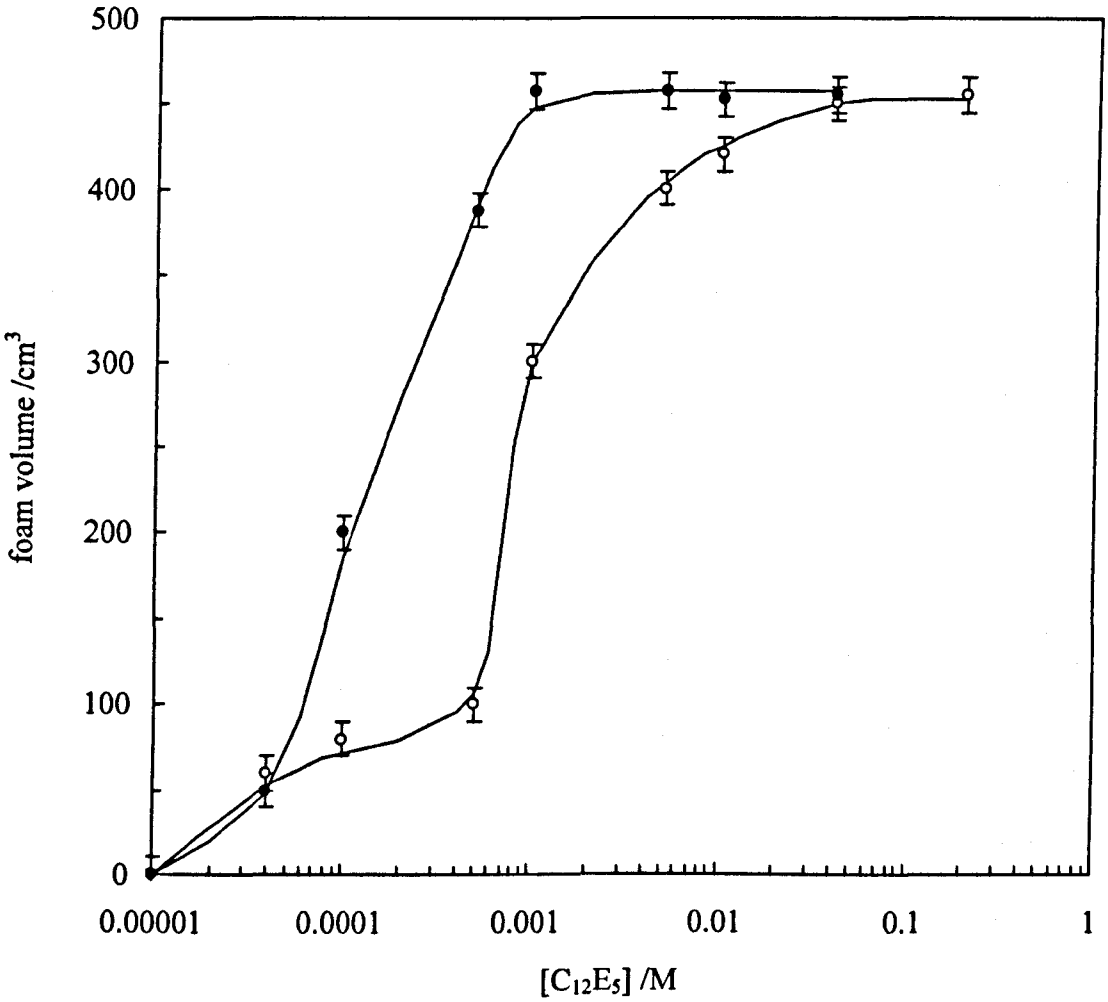

Figure 4.6 Foam volume immediately after 10 minutes gas sparging as a function of surfactant concentration for $C_{12}E_5$ with (open circles) and without (filled circles) saturated decane vapour. The nitrogen gas flow rate was 48 cm^3 min^{-1} and the initial volume of surfactant solution was 15.0 cm^3. The solid lines are guides for the eye.

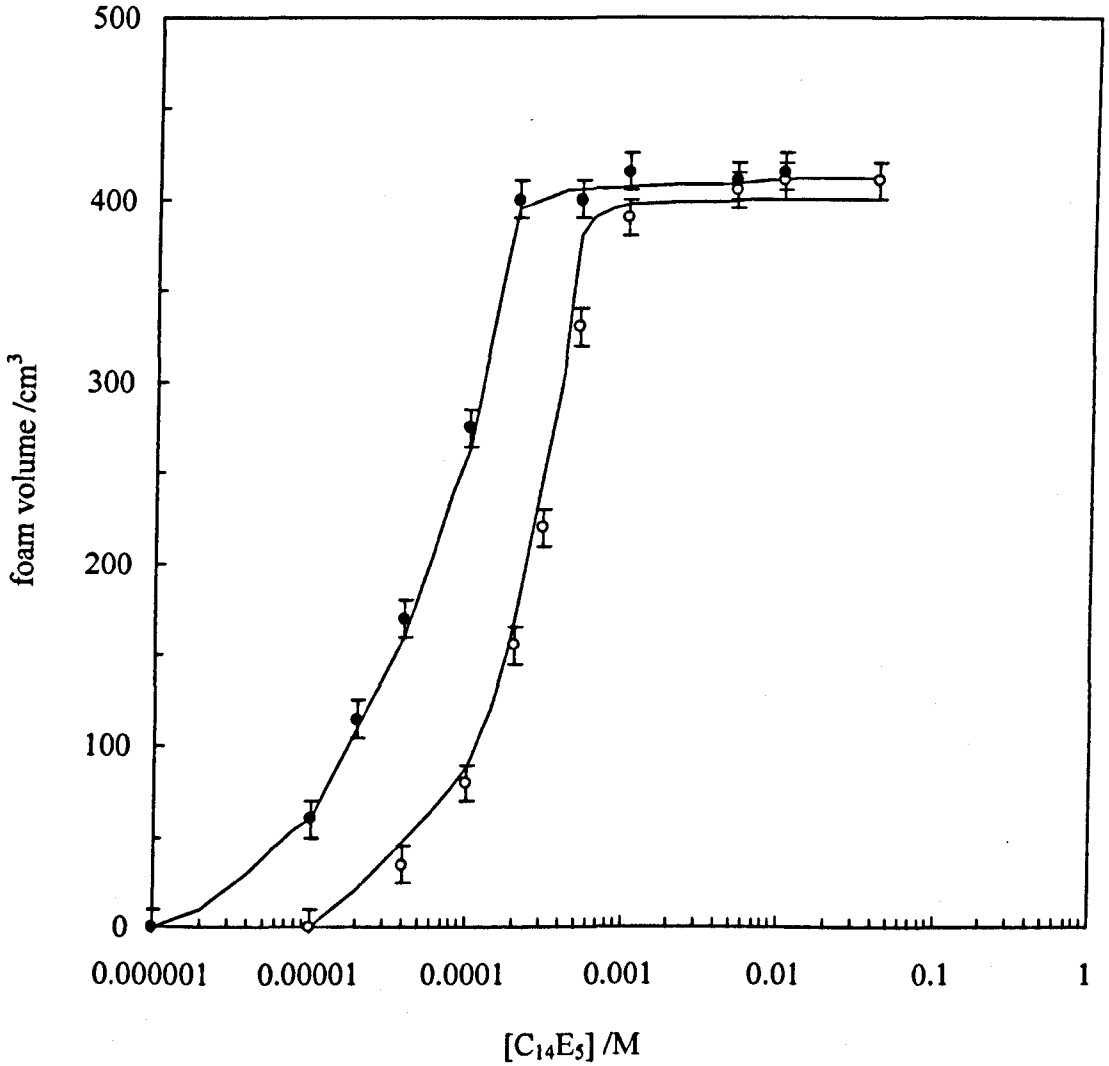

Figure 4.7 Foam volume immediately after 10 minutes gas sparging as a function of surfactant concentration for $C_{14}E_5$ with (open circles) and without (filled circles) saturated decane vapour. The nitrogen gas flow rate was 48 cm^3 min^{-1} and the initial volume of surfactant solution was 15.0 cm^3. The solid lines are guides for the eye.

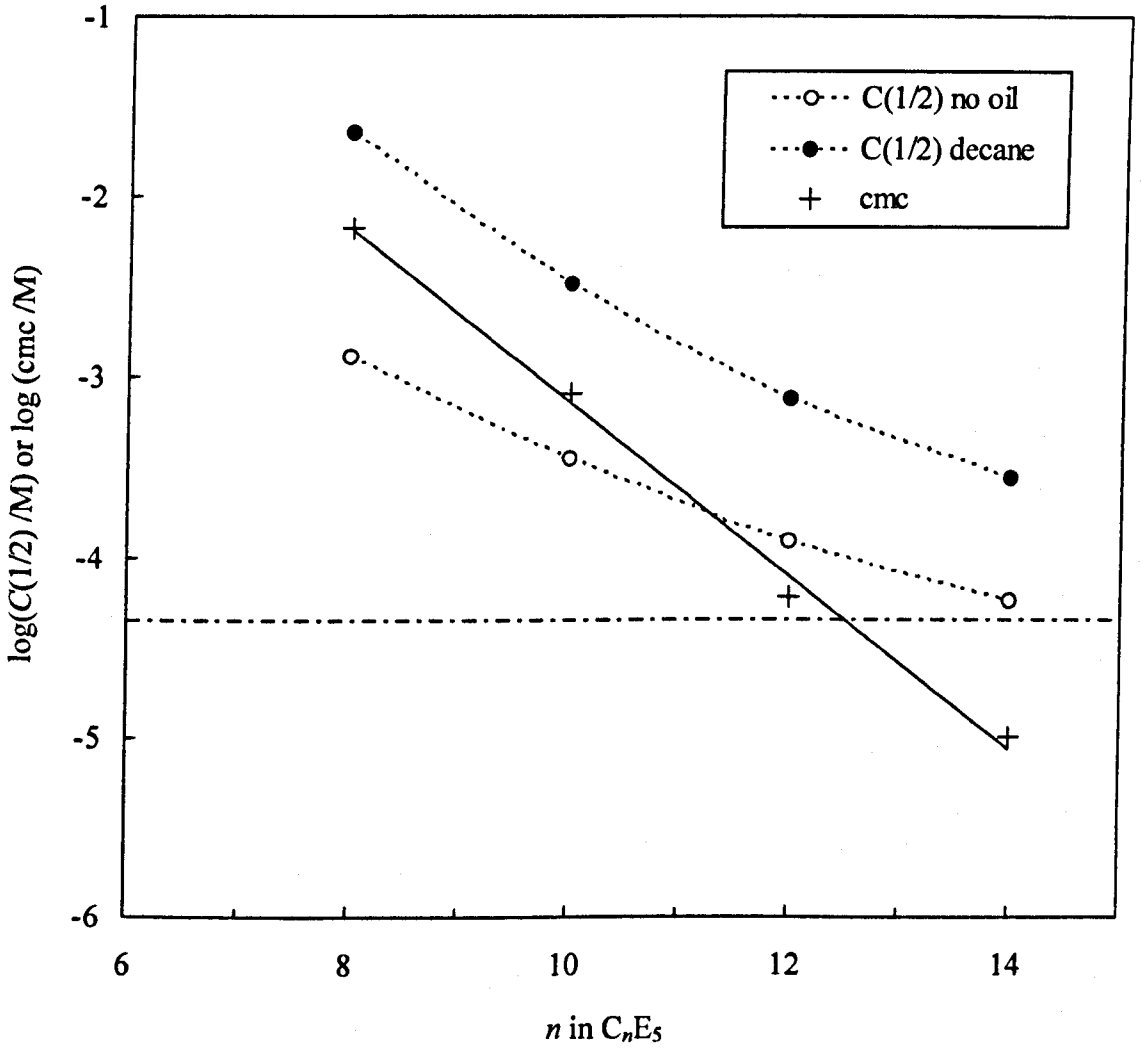

Figure 4.8 Comparison of the variation of $C(1/2)$ with surfactant chain length n with (filled circles) and without (open circles) decane vapour. The plot also shows the variation of the surfactant cmc in the absence of added oil vapour (crosses, solid line) and the value of C_{min}, (see section 3.3.4) horizontal dash-dotted line.

measurements refer to surfactant concentrations well in excess of the cmc. Additionally, for high chain length surfactants, for which $C(1/2)$ > cmc, potential solubilisation of the oil within the micelles present may further complicate the comparison. The hydrophobicity of the surfactants also changes as the tail length of the surfactant is increased. These factors will be discussed in more detail in section 4.6.

Figure 4.9 shows how V_{max} (the volume of foam formed immediately after 10 minutes gas sparging) varies as a function of surfactant tail length in the absence and presence of co-adsorbed decane (delivered at P/P_0 =1). It can be seen that the same trend exists in the presence of decane vapour as in the pure surfactant case i.e. there is a maximum in V_{max} values for the case where there are 12 methylene groups in the surfactant tail length. For lower surfactant tail lengths, 12 and below, the decane appears to increase the maximum volume of foam formed after the 10 minutes foam production period.

4.4.2 Foam stability

Figure 4.10 shows how foam volume varies as a function of time, once the foam has been produced from $C_{12}E_5$ at a concentration of 0.04 M (above the cmc), in the presence and absence of co-adsorbed decane. Decane was delivered at a P/P_0 value of 1. The half-life, defined as the time taken from the foam volume to decrease to half of its initial value, is lower for the foam containing co-adsorbed decane in the stabilising surfactant monolayer. From plots of foam volume as a function of time (as shown for $C_{12}E_5$ in Figure 4.10), half-life values were determined as a function of the number of methylene groups in the surfactant tailgroup (Figure 4.11). The concentrations of surfactant were fixed at 0.04 M for all of these foaming solutions which is higher than the cmc for the all of surfactants.

The addition of oil decreases the stability of all of the foams relative to the corresponding pure surfactant case. In the case of foam stabilised with surfactant and co-adsorbed decane, the half-life is seen to increase with increasing tail length which is the same trend observed in the absence of oil.

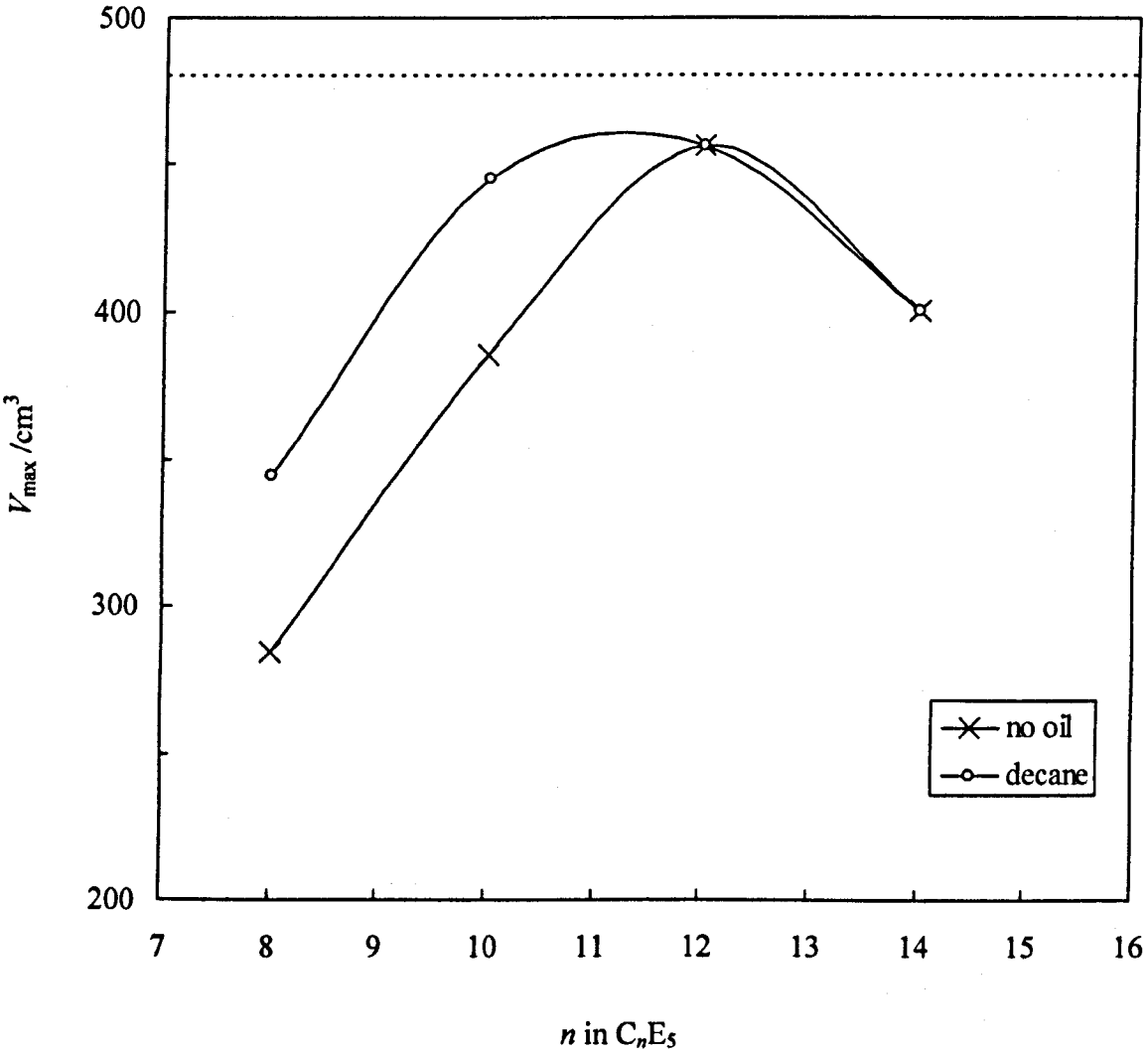

Figure 4.9 Foam volume (V_{max}) obtained after sparging N_2 gas through 15.0 cm^3 of surfactant solution at a flow rate of 48 cm^3 min^{-1} for 10 minutes as a function of surfactant tail length in the absence and presence of decane vapour (P/P_0 = 1). The horizontal dashed line shows the maximum possible foam volume after 10 minutes using these experimental parameters.

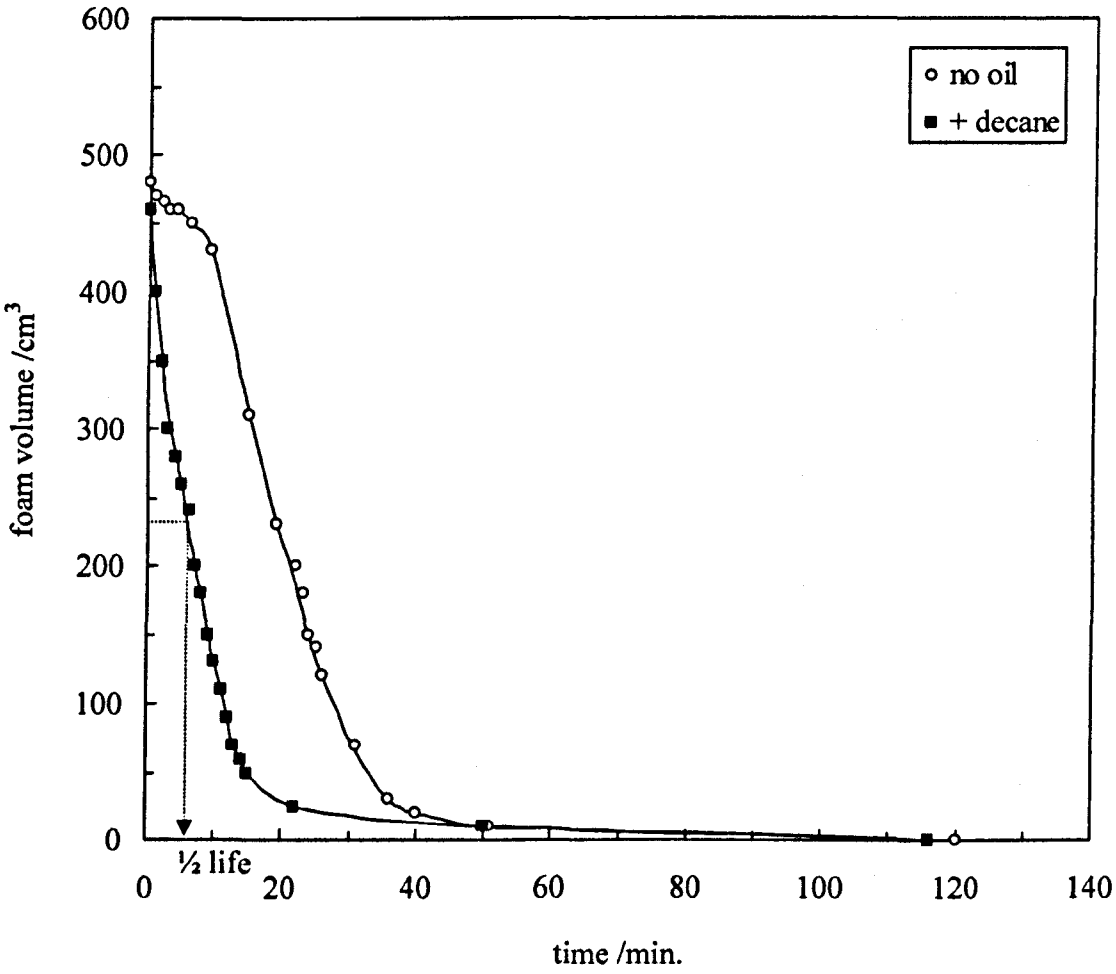

Figure 4.10 Foam stability of $C_{12}E_5$ in the absence and presence of decane. Foam created by sparging N_2 gas through 15 cm^3 of aqueous $C_{12}E_5$ solution at a flow rate of 48 cm^3 min^{-1} for 10 minutes. The concentration of $C_{12}E_5$ was set at 0.04 M and the temperature was set at 25.0 °C.

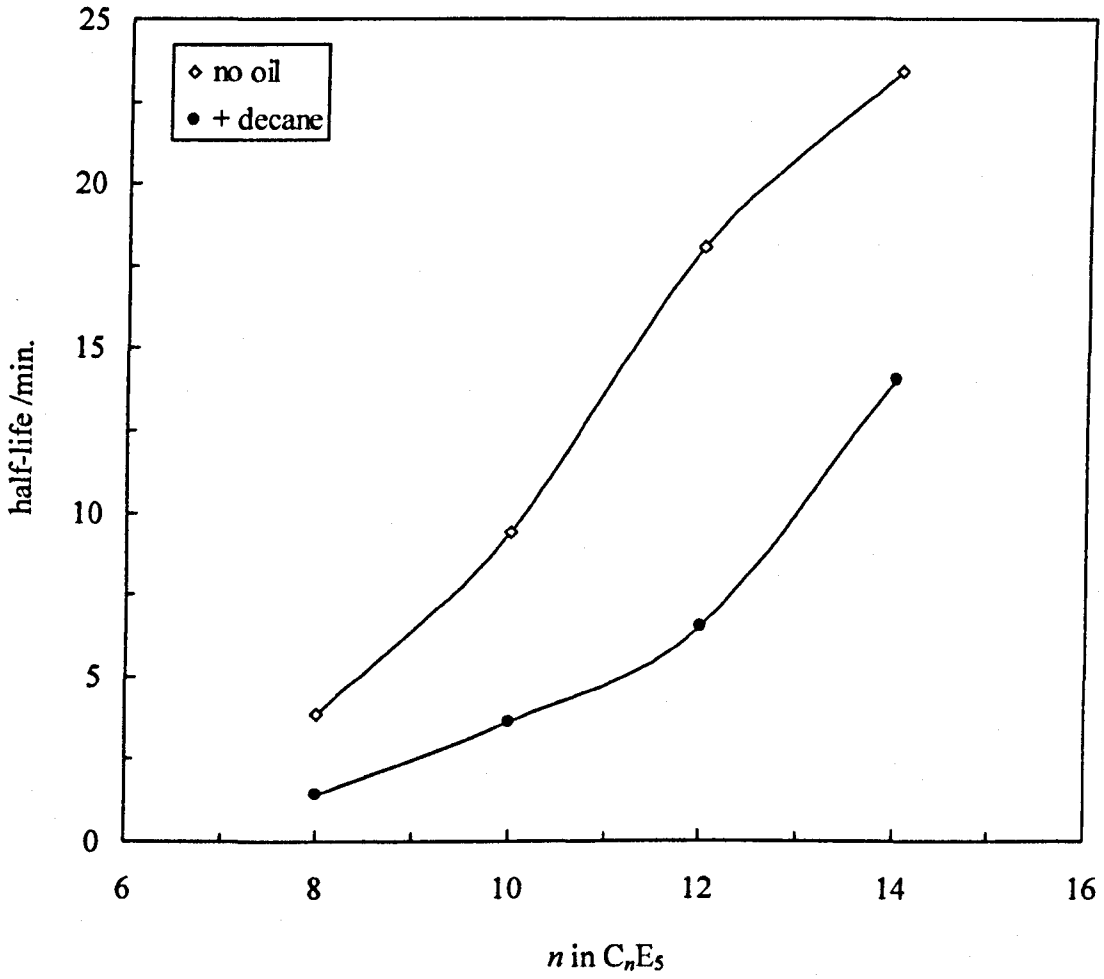

Figure 4.11 Foam half-lives in the absence and presence of decane ($P/P_0 = 1$) as a function of surfactant tail length. Foams created by sparging N_2 gas through 15.0 cm^3 of surfactant solution at a flow rate of 48 cm^3 min^{-1} for 10 minutes. The concentration of surfactant was 0.04 M and the temperature was 25.0 °C.

4.5 Variation of surfactant head group size

4.5.1 Foamability

Foamability curves for the $C_{12}E_m$ series of surfactants with m = 5, 7, 8 and 9 are shown in Figure 4.12. When decane vapour is added to the gas stream at P/P_0 = 1, $C(1/2)$ is increased by approximately 1 order of magnitude for m = 5, 7 and 8. The shift for m = 9 is larger and is consistent with the idea that increasing the surfactant headgroup size results in a larger area per adsorbed surfactant molecule, increased oil vapour adsorption and hence a larger foam inhibition effect. On this basis however, it remains unclear why the shift between m = 8 and 9 is larger than between m = 5 and 8.

Figure 4.13 is a summary of the behaviour noted above and shows how values of $C(1/2)$ vary in the absence and presence of co-adsorbed decane for the $C_{12}E_m$ series of surfactants.

Figure 4.14 shows the volume of foam produced immediately after 10 minutes gas sparging (V_{max}) as a function of the number of ethylene oxide groups in the surfactant headgroup. There is no clear correlation between maximum foam volume obtained after 10 minutes and headgroup size in the presence of co-adsorbed decane in the surfactant monolayer.

4.5.2 Foam stability

Foam stability is now considered in relation to the number of ethylene oxide groups in the surfactant headgroup. Figure 4.15 shows how, upon the addition of decane, foam stabilities (as judged by half-life) are lowered relative to the corresponding pure surfactant cases regardless of the number of ethylene oxide groups in the surfactant headgroup. The concentration of surfactant was fixed at 0.04 M for all of the foaming systems. The least stable foams in Figure 4.15 are those stabilised by $C_{12}E_7$, $C_{12}E_8$ and $C_{12}E_9$ with co-adsorbed decane. These all have slightly lower stabilities (of the order of 4 minutes) compared with $C_{12}E_5$ (6.5 minutes).

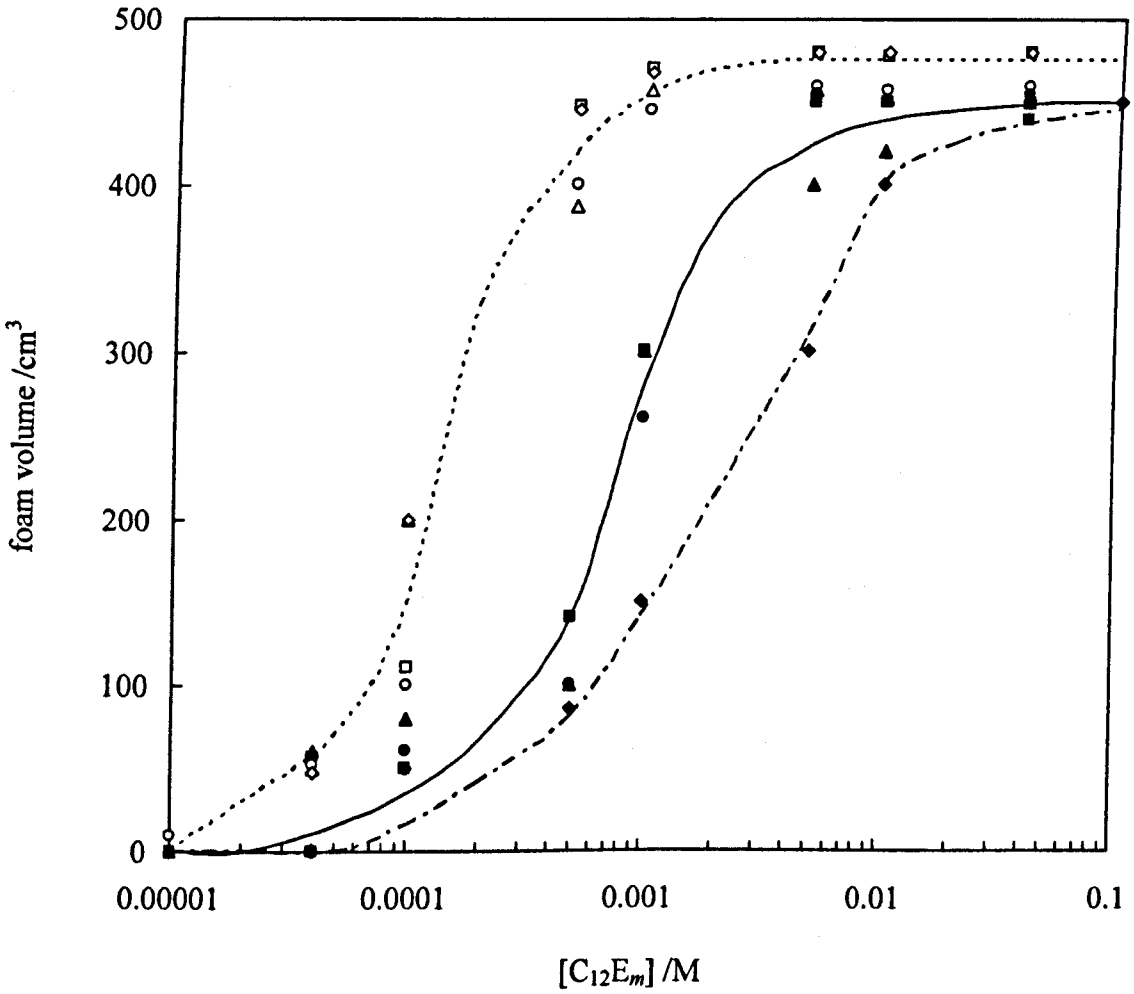

Figure 4.12 Foam volume immediately after 10 minutes of gas sparging as a function of surfactant concentration for the $C_{12}E_m$ series with m = 5 (triangles), 7 (squares) 8 (circles) and 9 (diamonds). Open symbols refer to the absence of oil vapour and filled symbols correspond to saturated decane vapour. The lines are guides for the eye and correspond to all four surfactants in the absence of decane (dotted line), $C_{12}E_5$, $C_{12}E_7$ and $C_{12}E_8$ with decane vapour (solid line) and $C_{12}E_9$ with decane vapour (dash-dotted line).

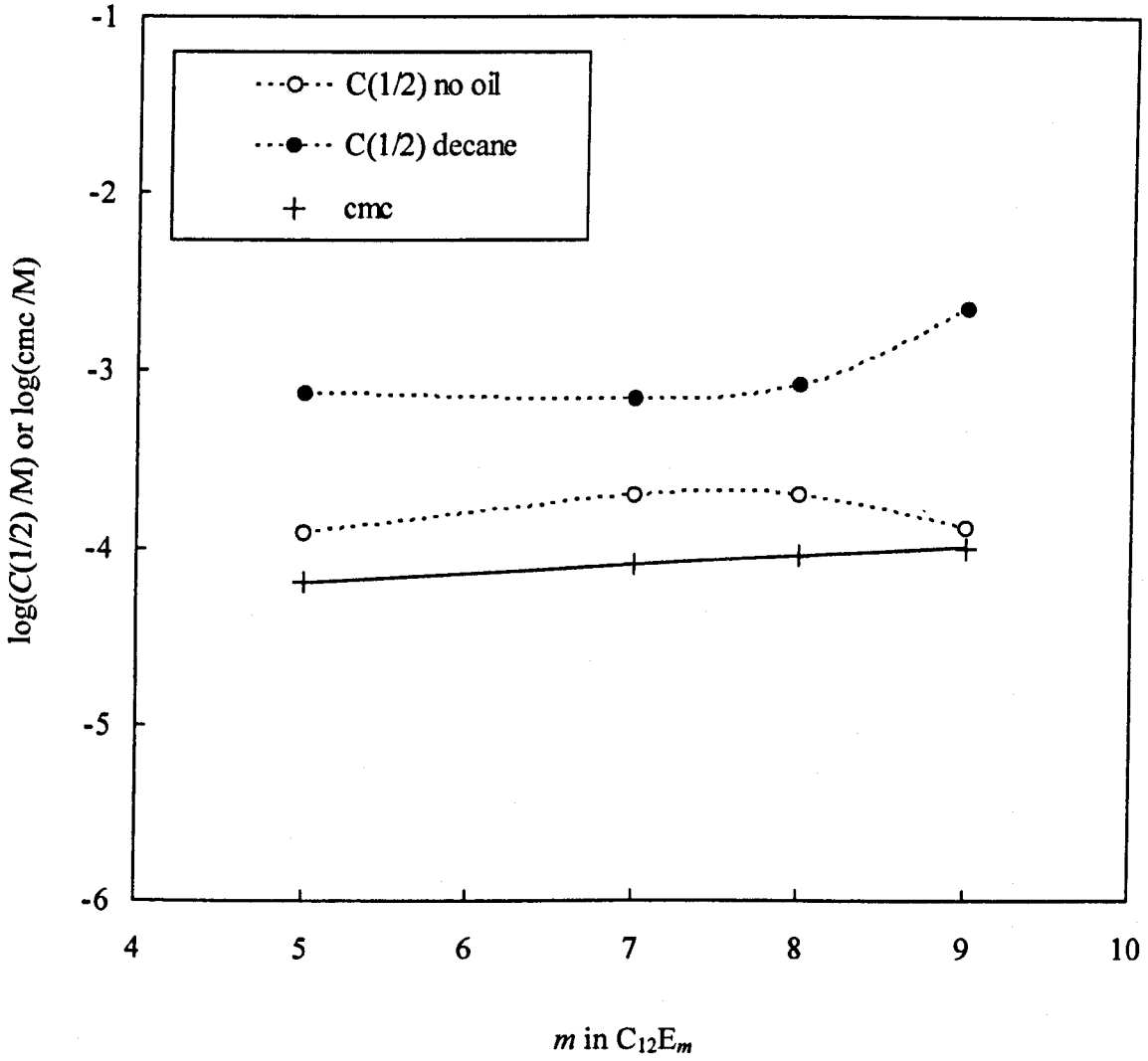

Figure 4.13 Comparison of the variation of $C(1/2)$ with surfactant chain length m with (filled circles) and without (open circles) decane vapour. The plot also shows the variation of the surfactant cmc (crosses, solid line).

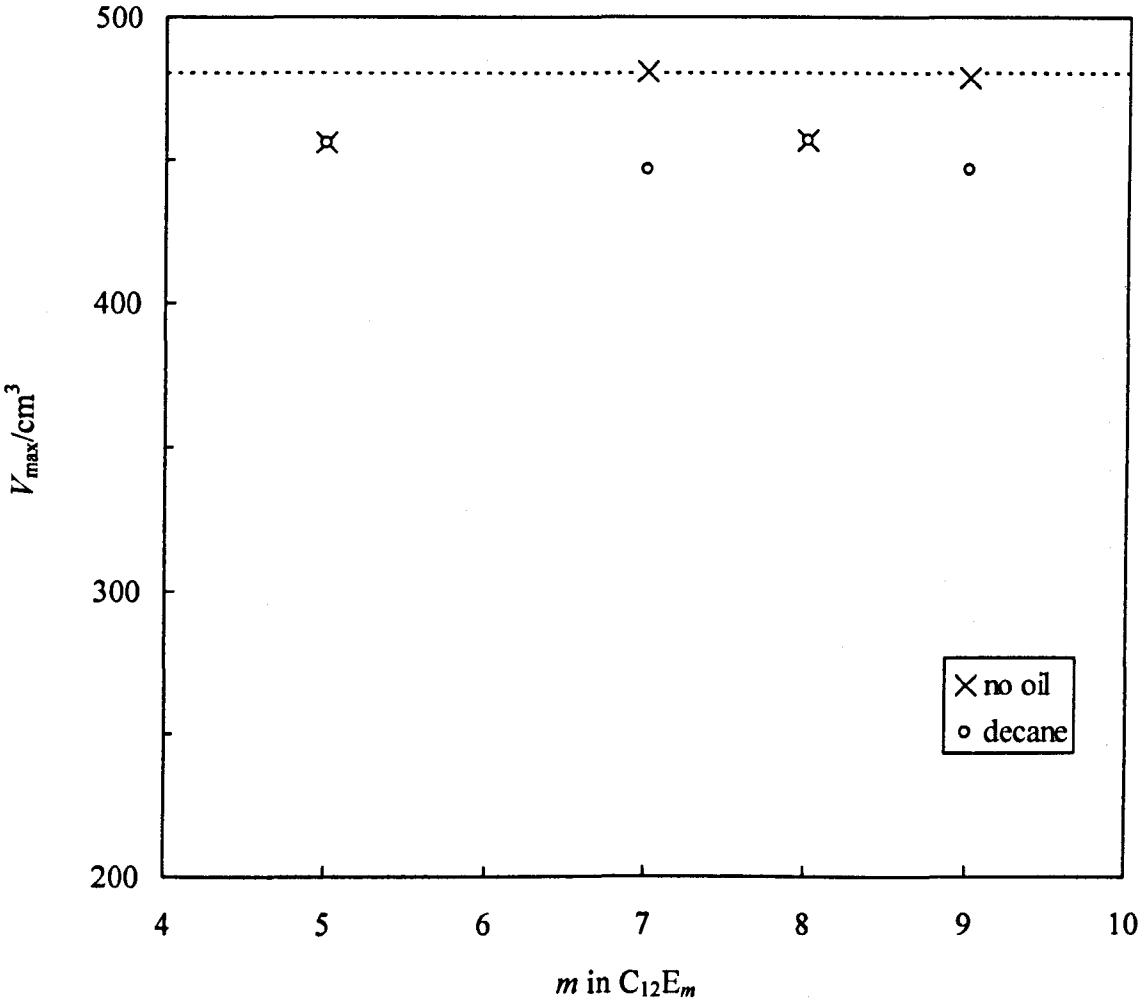

Figure 4.14 Foam volume (V_{max}) obtained after sparging N_2 gas through 15.0 cm^3 of surfactant solution at a flow rate of 48 cm^3 min^{-1} for 10 minutes as a function of surfactant headgroup size in the absence and presence of decane vapour (P/P_0 = 1). The horizontal dashed line shows the maximum possible foam volume after 10 minutes using these experimental parameters.

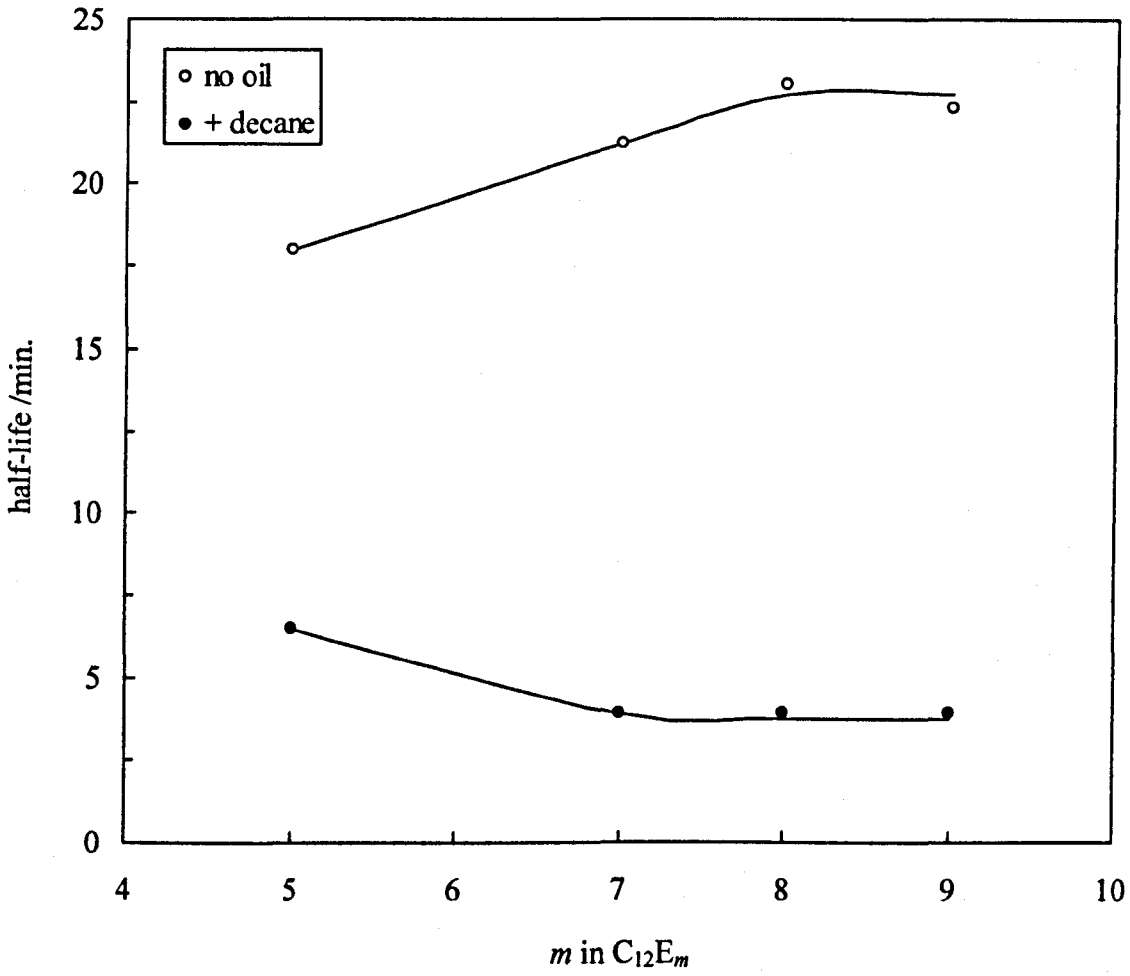

Figure 4.15 Foam half-lives in the absence and presence of decane ($P/P_0 = 1$) as a function of surfactant headgroup size. Foams created by sparging N_2 gas through 15.0 cm^3 of surfactant solution at a flow rate of 48 cm^3 min^{-1} for 10 minutes. The concentration of surfactant was 0.04 M and the temperature was 25.0 °C.

4.6 Foamability, foam stability and the extent of oil adsorption into surfactant monolayers

In this section, the anti-foam action of co-adsorbed oil (in relation to both foamability and foam stability) is considered in relation to its surface excess concentration in the monolayer (Γ_{oa}). As we have already seen, foamability inhibition is quantified by the extent to which $C(1/2)$ is increased in the presence of oil vapour relative to the pure surfactant case. Thus we can define a ratio ($R_{foamability}$) which represents the level of anti-foam action for a particular system in the presence of co-adsorbed oil as follows

$$R_{foamability} = C(1/2)_{oil} / C(1/2)_{no\ oil} \qquad [4.7]$$

The ratio $R_{foamability}$ increases with increasing foamability reduction caused by the addition of co-adsorbed oil due to a higher value of $C(1/2)_{oil}$ relative to $C(1/2)_{no\ oil}$.
In a similar way, the effect that co-adsorbed oil changes the foam stability of the system can be expressed in a ratio ($R_{stability}$) by using foam half-lifes ($t(1/2)$) as follows:

$$R_{stability} = t(1/2)_{no\ oil} / t(1/2)_{oil} \qquad [4.8]$$

Here, the ratio $R_{stability}$ increases with increasing foam stability reduction caused by co-adsorbed oil.

4.6.1 Foamability and foam stability of C_nE_5 series

First, we consider how the foamability and foam stability of the C_nE_5 series of surfactant change when decane is delivered at $P/P_0 = 1$ in relation to the level of co-adsorbed decane in the monolayer (Γ_{oa}) (values of Γ_{oa} were extrapolated from reference 19).

Figure 4.16 shows how $R_{foamability}$, $R_{stability}$ and Γ_{oa} change with n in C_nE_5.

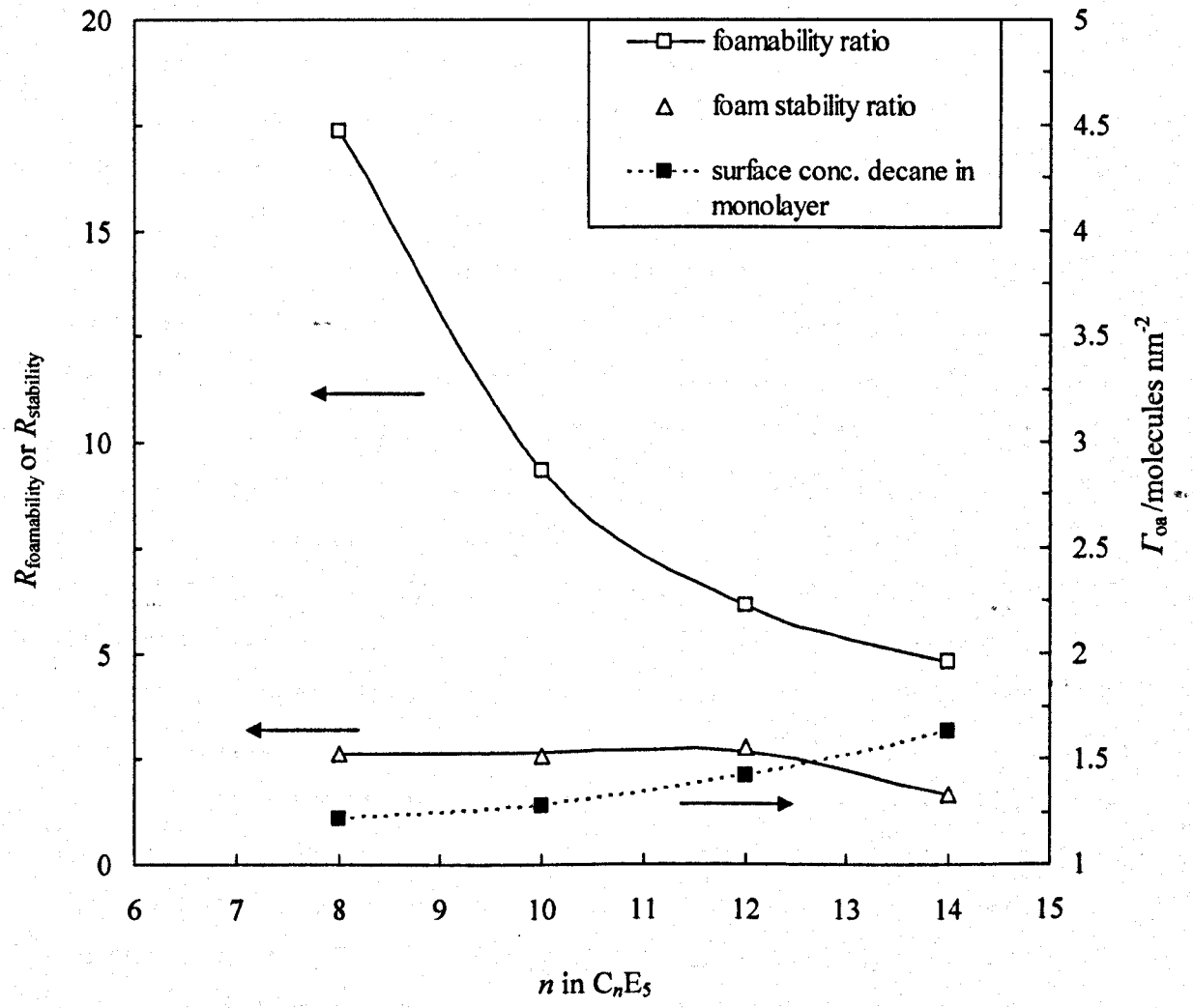

Figure 4.16. Surface concentration of adsorbed decane (Γ_{oa}) and ratios of $C(1/2)$ and t(1/2) values in the absence and presence of co-adsorbed decane ($P/P_0 = 1$) as a function of n in $C_{12}E_n$.

The plot shows that $R_{foamability}$ decreases with increasing surfactant tail length, although the level of adsorbed oil in the monolayer increases. This shows that although there is more oil adsorbed in the tail region of the $C_{14}E_5$ compared to say C_8E_5, the foam inhibition effect is larger for C_8E_5 than for $C_{14}E_5$. This observation is not consistent with the level of oil co-adsorbing with the surfactant in the monolayer.

As one expects decane to co-adsorb more in the tail region of $C_{14}E_5$ than C_8E_5, it is expected that $C_{14}E_5$ should be relatively less stable than its corresponding no oil case compared to C_8E_5. This situation would be reflected in the half-life ratio (defined above) being higher for $C_{14}E_5$ than for C_8E_5. From Figure 4.16, it is clear that this is not the case. The half-life ratio remains approximately constant with respect to surfactant tail length until the number of methylene groups equals 12. The ratio then starts to decrease as the number of methylene units are increased to 14, so in the presence of decane, the stability of foam stabilised by surfactants with longer tail groups tends towards the corresponding no oil cases There are two possible explanations for this discrepancy. Firstly, the surfactant concentration at which all of these determinations were performed was the same for all of the surfactants (0.04 M). As mentioned above, this corresponds to a concentration in excess of the cmc of all the surfactants. This means that oil could potentially become solubilised within the micelles present in the solution. The number of micelles present in a solution of $C_{14}E_5$ is greater than the number present in the same concentration of a solution of C_8E_5 solution (due to the lower cmc of $C_{14}E_5$). This means that more oil could be solubilised by the $C_{14}E_5$ solution, resulting in less oil co-adsorbing in the surfactant monolayer. The second reason is that although potentially more oil can co-adsorb with $C_{14}E_5$ than C_8E_5 case, $C_{14}E_5$ is more strongly adsorbing than C_8E_5 (due to its lower cmc). This increased foam stabilisation effect (due to the higher adsorption) may be greater than the foam destabilisation effect due to the higher oil adsorption.

Effects arising from surfactant hydrophobicity can be (crudely) removed by diving ratios of the values of $C(1/2)$ by the surfactant cmc.

Figure 4.17 shows how [$R_{foamability}$, $R_{stability}$] /cmc and Γ_{oa} change with n in C_nE_5. As discussed above, Γ_{oa} increases as surfactant tail length increases and the ratio $R_{foamability}$ and $R_{stability}$ decreases with increasing tail length. When values of $R_{foamability}$

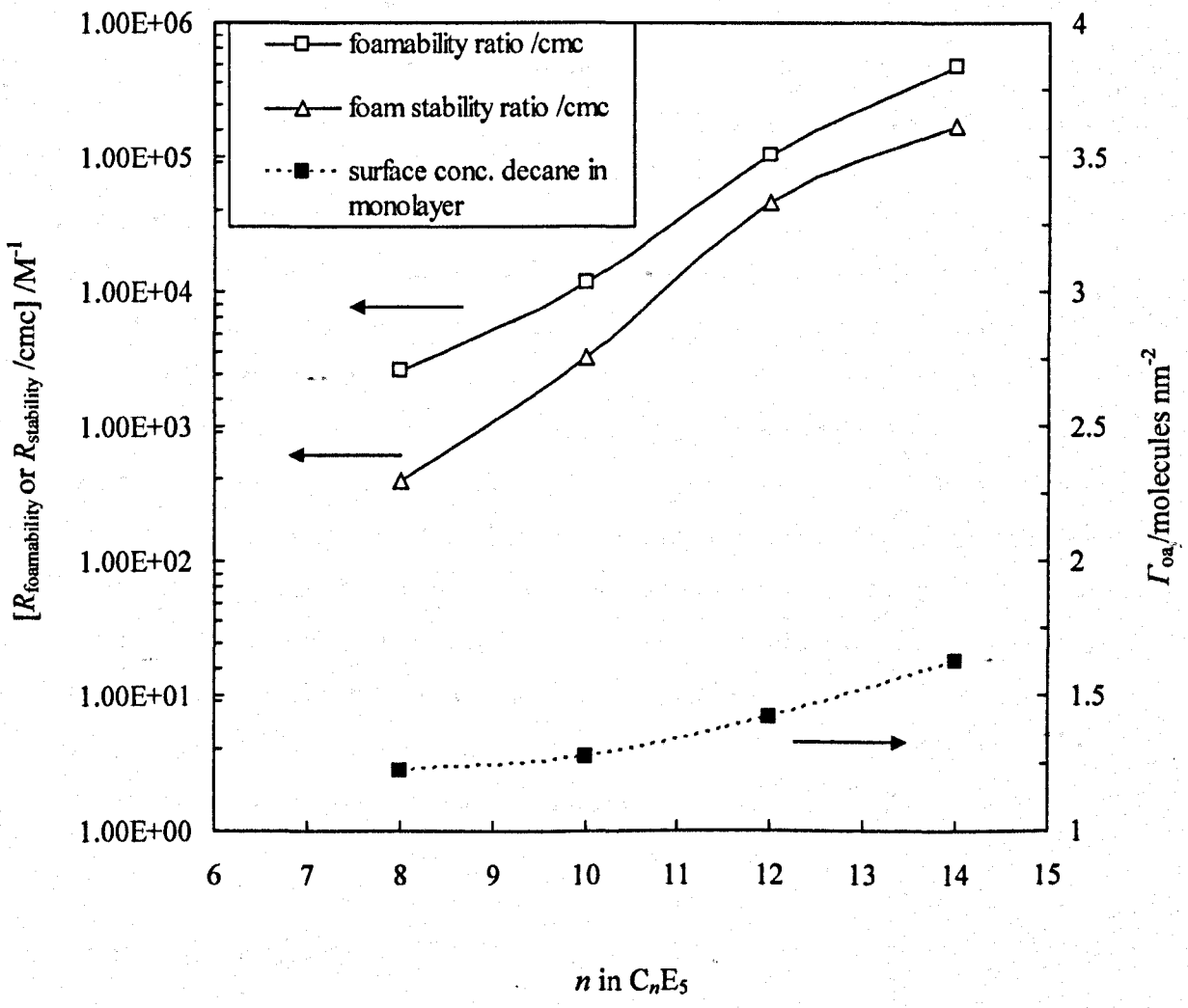

Figure 4.17 Surface concentration of adsorbed decane (Γ_{oa}) and ratios of $C(1/2)$ and t(1/2) values in the absence and presence of co-adsorbed decane ($P/P_0 = 1$) as a function of n in $C_{12}E_n$. Ratios normalised to surfactant hydrophobicity by dividing by the surfactant cmc.

and $R_{stability}$ are divided by the corresponding cmc of the surfactant (to normalise surfactant hydrophobicity) the plot now shows that the factor increase in surfactant concentration required to achieve the transition from non-foaming to foaming behaviour and the reduction in foam stability between the no oil and oil cases increases with increasing tail length. This trend is consistent with the idea that more oil co-adsorbed in the tail region of the surfactant corresponds to a situation where a greater anti-foam effect is observed. In chapter 3 it was argued that when values of $C(1/2)$ were above the cmc of the corresponding surfactant, then foamability may be controlled by surfactant adsorption dynamics i.e. foamability is limited by kinetic control as opposed to equilibrium adsorption control. In Figure 4.8 it was seen that values of $C(1/2)$ were always above the values of the corresponding values of the cmc values in the presence of co-adsorbed oil in the surfactant monolayer. This implies that in the presence of co-adsorbed oil, foamability is always in the kinetic control foamability regime. It therefore follows that oil vapour may reduce the foamability of a particular surfactant by increasing the time taken for surfactant to adsorb at the air / water interface. In order to achieve the necessary level of adsorption within the required time for a foam to be stabilised, the value of $C(1/2)$ needs to be increased in the presence of oil vapour relative to the pure surfactant case in order for the surfactant solution to stabilise foam. This is observed experimentally.

4.6.2 Foamability and foam stability of $C_{12}E_m$ series

Figure 4.18 shows how $R_{foamability}$, $R_{stability}$ and Γ_{oa} change with m in $C_{12}E_m$.

As expected, Γ_{oa} increases with increasing headgroup (due to the larger area adsorbed per surfactant molecule), and a relatively higher concentration of surfactant is required to achieve the transition from non-foaming to foaming behaviour for surfactants with larger headgroups in the presence of co-adsorbed decane. Additionally, the presence of co-adsorbed decane reduces the stability of surfactants with larger headgroups relatively more than surfactants with smaller headroups. Due to the fact that cmc does not depend significantly on surfactant headgroup size, this interpretation is not complicated because of differences in adsorption between the different surfactants in the $C_{12}E_m$ series.

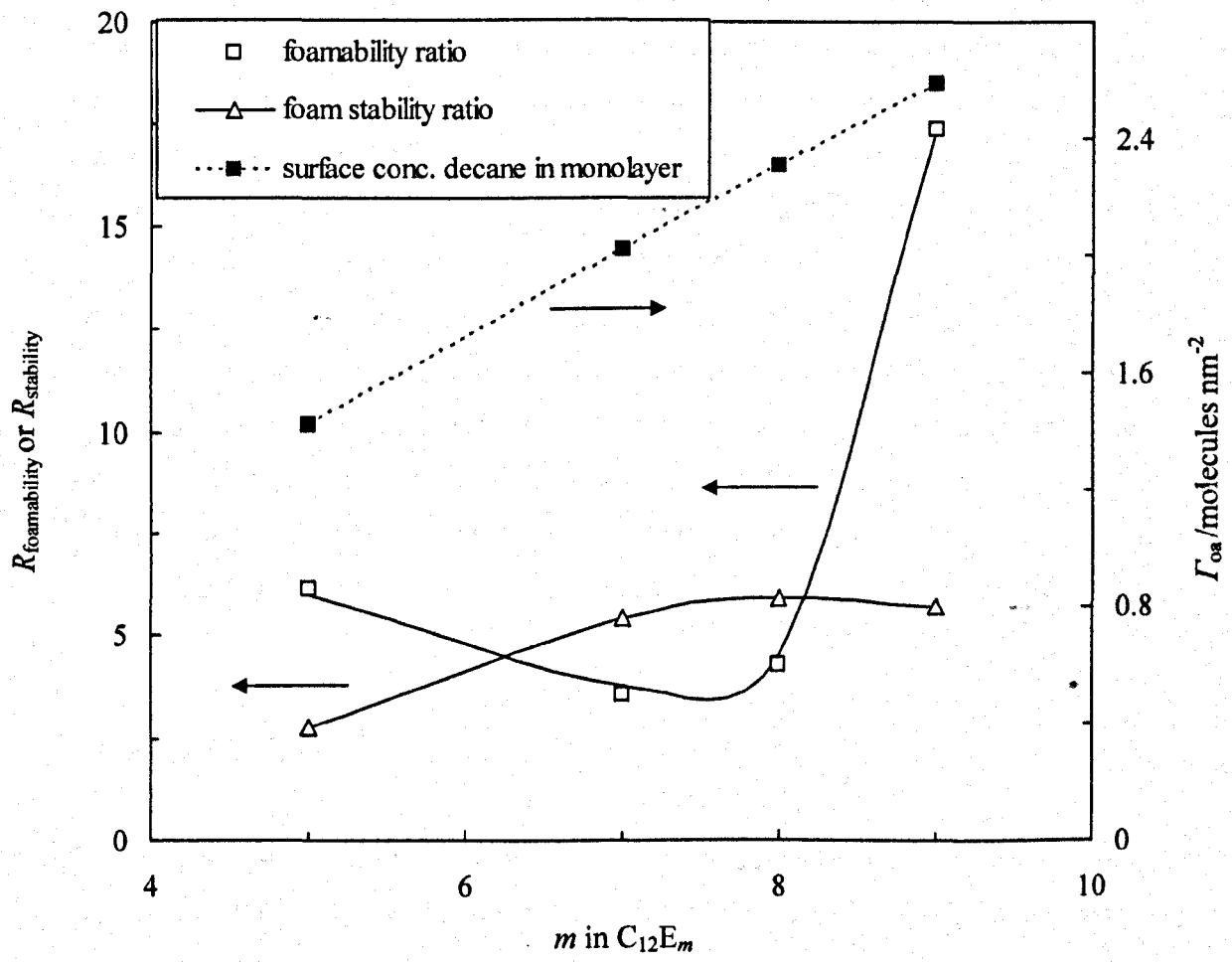

Figure 4.18 Surface concentration of adsorbed decane (Γ_{oa}) and ratios of $C(1/2)$ and t(1/2) values in the absence and presence of co-adsorbed decane ($P/P_0 = 1$) as a function of m in $C_{12}E_m$.

4.6.3 Co-adsorbed oil and the foamability regime of C_nE_m surfactants

In Chapter 3, it was postulated that when values of $C(1/2)$ were higher than the corresponding surfactant cmc, foamability was limited by adsorption dynamics. Therefore, a possible explanation for the observation that $C(1/2)$ values with oil are all greater than the corresponding surfactant cmc is that slow adsorption may control the foamability. The limiting volume of foam obtained at high surfactant concentrations is not greatly affected and, as shown in Figure 4.9, may even be slightly enhanced. It appears that foamability properties of mixed oil-surfactant films are similar to those of pure surfactants at lower surfactant concentrations. Studies of the dynamic surface properties of mixed monolayers containing dodecane with cetyl trimethylammonium bromide have shown that oil addition alters the dilational viscosity in a manner which is thought to be consistent with an increase in the energy barrier to surfactant adsorption.[24] Jayalakshmi and Langevin investigated the effect of dodecane addition on monolayers of dodecyl trimethylammonium bromide an found that oil addition increased the viscoelasticity of the monolayer.[28]

4.7 Effect of molar volume of oil on foaming

Figure 4.19 shows the effects that different oil vapours (delivered to the foaming systems at $P/P_0 = 1$) on the foamability curve for $C_{10}E_5$. The foam inhibition, quantified as the extent to which $C(1/2)$ is shifted upwards, increases with decreasing molar volume of oil. This sequence corresponds with the magnitude of $\Gamma_{oil,max}$ which similarly increases with decreasing oil size. The curves also show a slight increase (with decreasing oil chain length) in the maximum foam volume obtained at high surfactant concentrations.

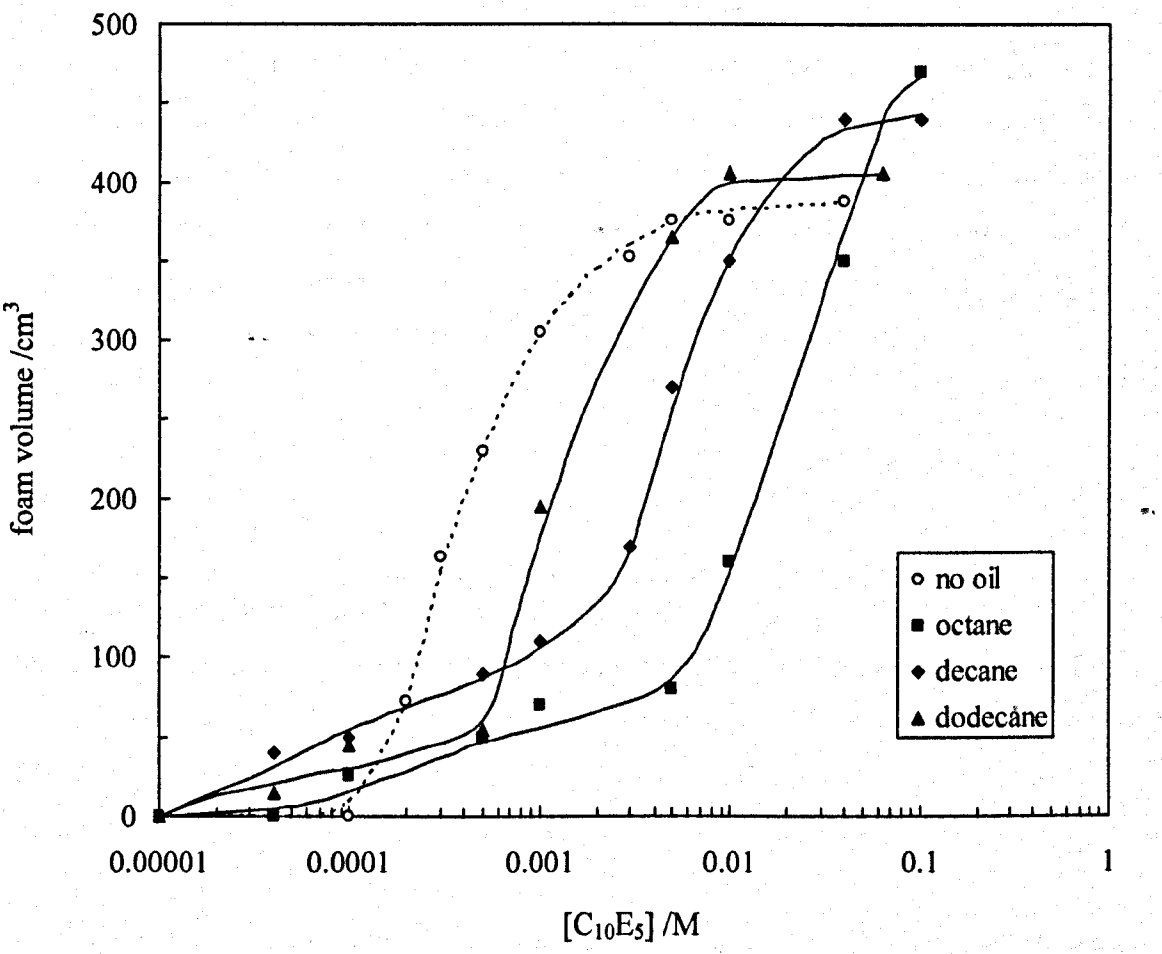

Figure 4.19 Foam volume immediately after 10 minutes gas sparging as a function of surfactant concentration for $C_{10}E_5$ in the absence of oil vapour (open circles, dotted line) and in the presence of octane (filled squares), decane (filled circles) and dodecane (filled triangles) vapours at P/P_0 = 1. The solid and dotted lines are guides for the eye.

4.8 Variation of oil vapour activity

4.8.1 Foamability

For foaming solutions containing 5 x 10^{-4} M $C_{12}E_5$ (a factor of approximately 10 times the cmc), the effect of adding oil vapours with varying P/P_0 was examined using bubblers containing mixures of the volatile oil with the involatile species squalane. As shown in Figure 4.20, increasing P/P_0 causes a progressive decrease of foam volume from the value corresponding to no oil (P/P_0 = 0) to the value P/P_0 =1, for both decane and dodecane. This is due to the higher vapour concentration of oil available for co-adsorption with the primary foam-stabilising surfactant.

4.8.2 Foam stability

The effect of oil vapours delivered at different values of P/P_0 on the stability of the foam was examined by generating the foam in the presence of the required vapour for 10 minutes and then monitoring the subsequent decay of the foam. Figure 4.21 shows the decay of foam stabilised by 5 x 10^{-4} M $C_{12}E_5$ in the presence of co-adsorbed decane.

Adding even a low oil vapour concentration in the foam causes a sharp increase in the rate of decay of the foam. In considering foam decay, it is relevant to note that oil adsorption causes the surface tension to decrease. At the upper surface of the foam, the inner surface of the bubbles contain oil and hence have a lower surface tension compared with the outer bubble surface for which the oil vapour is lost due to diffusion. This unequal tension across the foam films of the topmost layer of bubbles in the foam may contribute to an accelerated decay rate. Valkovska et al. have observed that film instability can result from diffusional flux of oil across an asymmetric liquid film.[29]

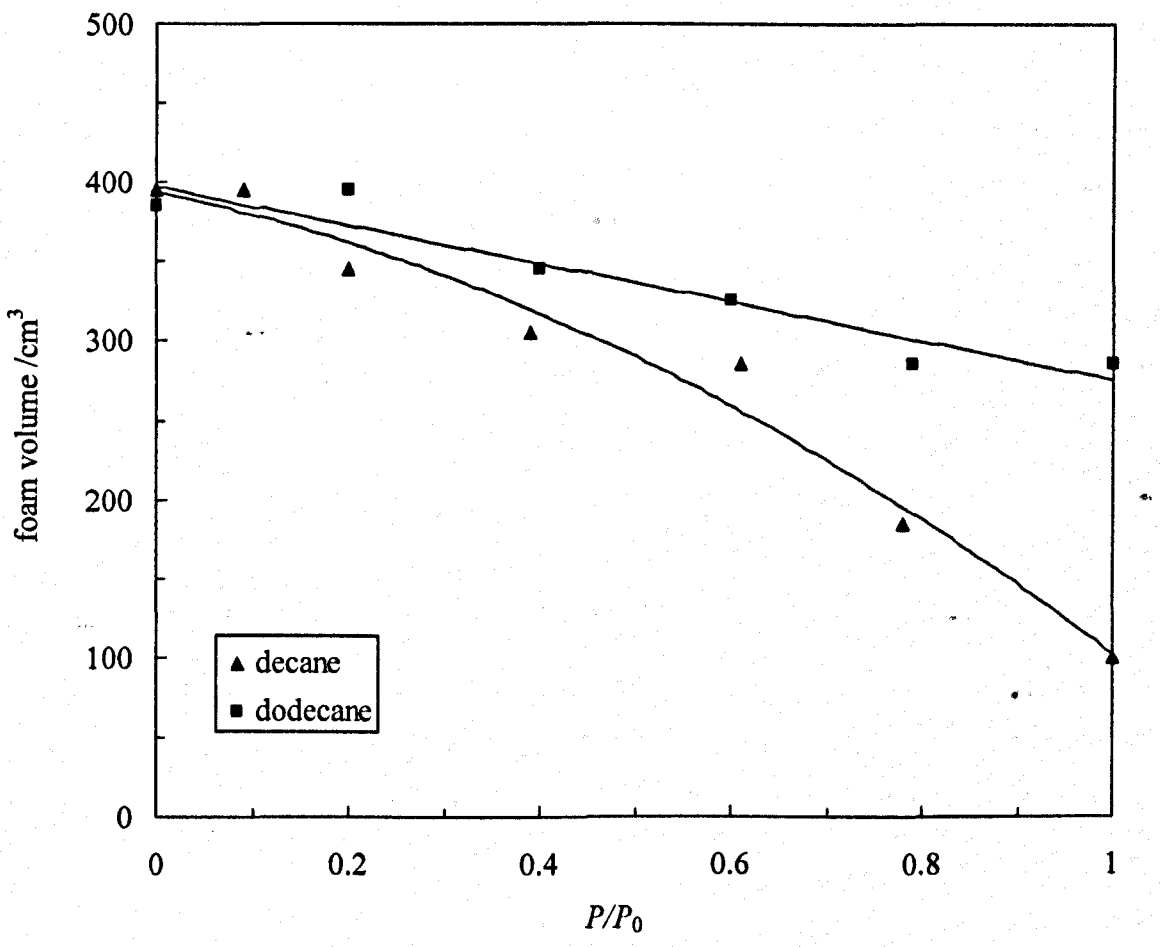

Figure 4.20 Foam volume immediately after 10 minutes gas sparging as a function of P/P_0 for decane and dodecane. Foam created by sparging N_2 gas through 15.0 cm^3 of $C_{12}E_5$ (5 x 10^{-4} M) for 10 minutes at a flow rate of 48 cm^3 min^{-1}.

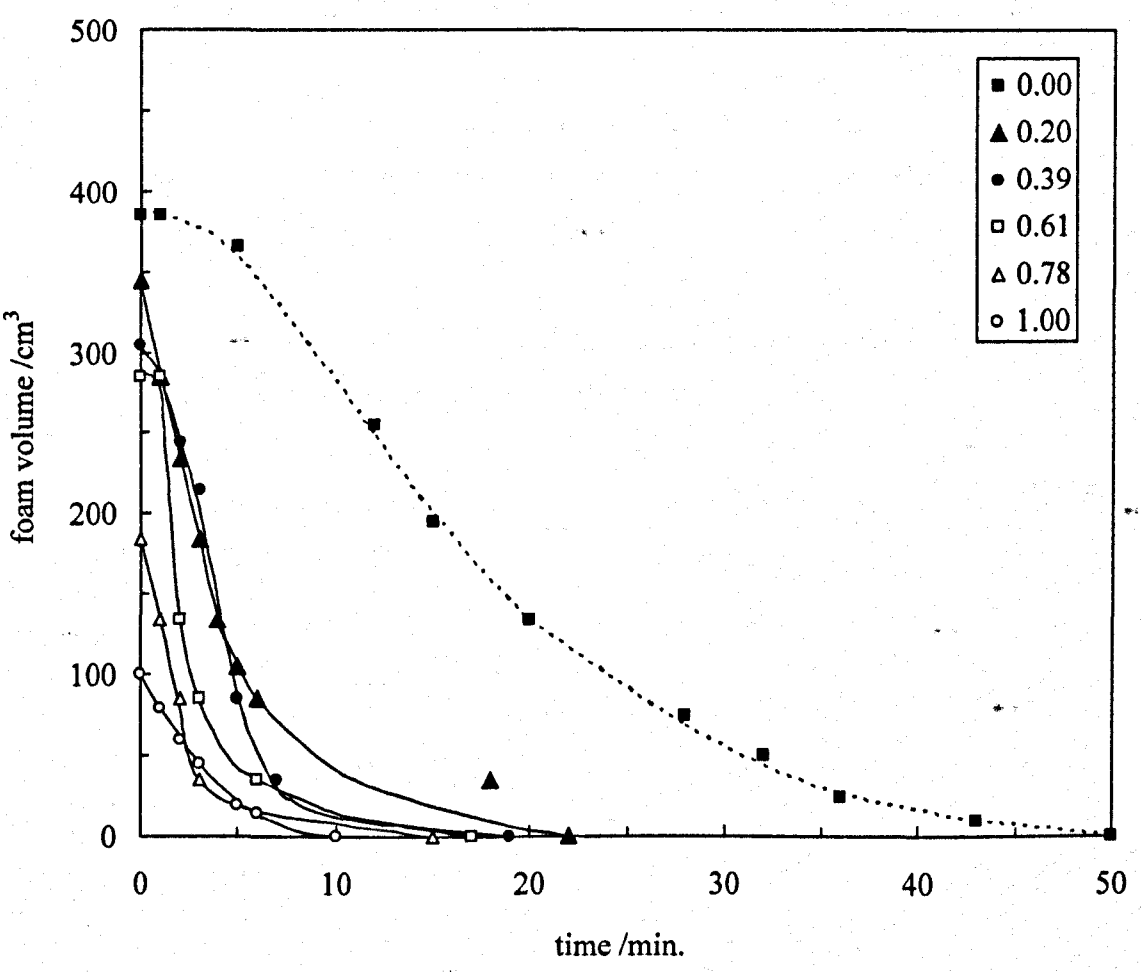

Figure 4.21 Decay of foam following generation for 10 minutes with 5 x 10^{-4} M $C_{12}E_5$ in the presence of decane vapour at the P/P_0 values shown in the legend.

4.9 Conclusions

- The main effect of incorporating oil vapours during foam generation with nonionic surfactant is that the surfactant concentration required to achieve the transition from non-foaming to foaming behaviour $C(1/2)$ is increased.

- In the presence of oil vapour, $C(1/2)$ is higher than the cmc for the range of oil + surfactant systems studied here. Following foam generation, its decay is accelerated by the presence of oil vapour.

- Increasing the oil vapour concentration causes a progressive decrease in both the foamability and stability of foam stabilised.by $C_{12}E_5$.

- Decreasing the molar volume of oil increases the foam inhibition effect for foams stabilised by $C_{10}E_5$.

References

1. K. Koczo, L. A. Lobo and D. T. Wasan, *J. Colloid Interface Sci.*, (1992), **150**, 492.
2. R. Aveyard, B. P. Binks, P. D. I. Fletcher, T, -G. Peck and P. R. Garrett, *J. Chem. Soc. Faraday Trans.* (1993), **89**, 4313.
3. B. K. Jha, S. P. Christiano and D. O. Shah, *Langmuir*, (2000), **16**, 9947.
4. L. Arnaudov, N. D. Denkov, I. Sercheva, P. Durbutt, G. Broze and A. Mehreteab, *Langmuir*, (2001), **17**, 6999.
5. A. Hadjiiski, S. Tcholakova, N. D. Denkov, P. Durbutt, G. Broze and A. Mehreteab, *Langmuir*, (2001), **17**, 7011.
6. R. Aveyard, P. Cooper, P. D. I. Fletcher and C. E. Rutherford, *Langmuir*, (1993), **9**, 604.
7. P. R. Garrett (Ed.), "*Defoaming, Theory and Industrial Applications*", Surfactant Science Series, vol 45 (Chapter 1), Marcel Dekker, New York, 1993.
8. K. Koczo, J. E. Koczone and D. T. Wasan, *J. Colloid Interface Sci.*, (1994), **166**, 225.
9. N. D. Denkov, P. Cooper and J. –Y. Martin, *Langmuir*, (1999), **15**, 8514.
10. T. Tamura, M. Kageyama, Y. Kaneko, T. Kishino and M. Nikaido, *J. Colloid Interface Sci.*, (1999), **213**, 179.
11. A. Hadjiiski, S. Tcholakova, I. B. Ivanov, T. D. Gurkov and E. F. Leonard, *Langmuir*, (2002), **18**, 127.
12. K. Ragil, J. Meunier, D. Broseta, J. O. Indekeu and D. Bonn, *Phys. Rev. Lett.*, (1996), **18**, 1532.
13. F. Hauxwell and R. H. Ottewill, *J. Colloid Interface Sci.*, (1970), **34**, 473.
14. R. Aveyard, P. Cooper and P. D. I. Fletcher, *J. Chem. Soc., Faraday Commun.*, (1990), **86**, 211.
15. R. Aveyard, B. P. Binks, P. Cooper and P. D. I. Fletcher, *Prog. Colloid Polymer Sci.*, (1990), **81**, 36.
16. R. Aveyard, P. Cooper and P. D. I. Fletcher, *J. Chem. Soc. Faraday Trans.*, (1990), **86**, 3623.
17. R. Aveyard, B. P. Binks, P. Cooper and P. D. I. Fletcher, *Adv. Colloid Interface Sci.*, (1990), **33**, 59.

18. R. Aveyard, B. P. Binks, P. D. I. Fletcher and J. R. MacNab, *Langmuir*, (1995), **11**, 2515.

19. R. Aveyard, B. P. Binks, P. D. I. Fletcher, and J. R. MacNab, *Ber. Bunsenges. Phys. Chem.*, (1996), **100**, 224.

20. J. R. Lu, R. K. Thomas, R. Aveyard, B. P. Binks, P. Cooper, P. D. I. Fletcher, A. Sokolowski and J. Penfold, *J. Phys. Chem.*, (1992), **96**, 10971.

21. J. R. Lu, R. K. Thomas, B. P. Binks, P. D. I. Fletcher and J. Penfold, *J. Phys. Chem.*, (1995), **99**, 4113.

22. J. R. Lu, Z. X. Li, R. K. Thomas, B. P. Binks, D. Crichton, P. D. I. Fletcher, J. R. MacNab and J. Penfold, *J. Phys. Chem. B*, (1998), **102**, 5785.

23. B. P. Binks, D. Crichton, P. D. I. Fletcher, J. R. MacNab, Z. X. Li, and R. K. Thomas, *Colloids and Surfaces A*, (1999), **146**, 299.

24. D. Sharpe and J. Eastoe, *Langmuir*, (1995), **11**, 4636.

25. A. J. Ashworth and D. H. Everett, *Trans. Faraday Soc*, (1960), **56**, 1609.

26. *Selected Values of Properties of Hydrocarbons and Related Compounds*, Thermodynamics Research Centre, AP144, Texas A&M University 1978.

27. D. Crichton, Ph.D. thesis, University of Hull, 1998.

28. Y. Jayalakshmi and D. Langevin, *J. Colloid Interface Sci.*, (1997), **194**, 22.

29. D. S. Valkovska, P. A. Kralchevsky, K. D. Danov, G. Broze and A. Mehretab, *Langmuir*, (2000), **16**, 8892.

Chapter 5

CHAPTER 5

Foam control by nanometre sized silica particles

5.1 Introduction

In this chapter, the ways in which nanometre (nm)-sized silica particles of different hydrophobicities modify the foaming properties of aqueous solutions of the pure nonionic alkyl ethoxylate surfactant $C_{12}E_5$ when dispersed in the initial foaming solution will be examined. This addresses the fact that at present, there are no reports available in the literature documenting the effect that nm-sized silica particles of different hydrophobicities have on the foaming properties of nonionic surfactant solutions.

5.2 Mode of action of solid particles – new developments

The bridging-dewetting mechanism was presented in Chapter 1 and was developed by Garrett[1], and has been confirmed experimentally by various workers.[2-5] The bridging mechanism is still the most documented mechanism of anti-foam action by solid particles. When operating in a bridging mechanism, hydrophobic particles, that is particles with contact angles, $\theta_{aw} > 90^{o}$ (measured through the aqueous phase) decrease the stability of foam providing they are large enough to bridge the films. For this to occur their diameters must fall within the μm size range. Particles can also increase the stability of a foam via the bridging mechanism when $\theta_{aw} < 90^{o}$.

Although the bridging mechanism is widely accepted, it is not the only mechanism that has been proposed for the way in which solid particles can destabilise (or stabilise) foam. This is reflected in published reports where variations or exceptions to the bridging mechanism have been found and alternative views have been proposed. For example, the fundamental bridging mechanism predicts that foam destabilisation should always occur in hydrophobic particle-containing foaming

systems. Experimental findings have shown that this is not always the case. Aveyard et al. found that for certain systems, particles with contact angles slightly above and below 90° were capable of increasing foam stability.[5] The observed foam stabilisation observed for systems containing particles with contact angles slightly greater than 90°, was ascribed to the net effect of two opposing processes. Although the bridging mechanism was still operational and was acting to destabilise the foam, another process was simultaneously occurring which acted to retard film drainage by blocking Plateau borders and hence slow the film thinning process.

In this section, findings documented in the literature will be presented which provide alternative explanations for when the bridging mechanism cannot be operational. These views are not presented to disprove the bridging mechanism. They can however, be used to explain observations which are not necessarily consistent with the bridging mechanism. They are also relevant to the work presented in the results section of this chapter because the bridging mechanism was developed to explain the action of solid particles in the size range 1 to 100 μm whereas the particles used in this work are much smaller (of the order of 20 nm). Consequently, the particles used in this work could function in ways other than by the bridging mechanism, and the foaming of surfactant solutions containing these nm-sized silica particles may be different compared to the same surfactant solutions containing larger particles of equivalent hydrophobicies.

As stated above, in certain cases hydrophobic particles incorporated in a foam can act in alternative ways to a bridging mechanism. For example, Kulkarni et al.[6] noted that spraying hydrophobic silica particles onto some foam resulted in the rapid destruction of the bubbles contacted by the solid particles. They proposed that the particles form weak spots in the film by depletion of the foam stabilising surfactant as a result of the surfactant adsorbing onto the solid surfaces.

The opposite effect to anti-foam action is enhanced foam stability which was the effect observed by Torikata et al. for foams containing hydrophobic particles.[7] They found that increasing the concentration of polystyrene particles in the foaming solution retarded the liquid drainage which, they stated, was reflected by an increase in foam stability. Tang et al.[8] also reported that hydrophobic solid particles can

enhance the stability of a foam. They studied hydrophobic silica particles in the diameter range 20 to 700 nm. They found that for foams stabilised by sodium dodecyl sulfonate in alkaline aqueous medium, the smaller the particle size, the stronger the observed stabilisation. They showed that hydrophobic particles delayed the time taken for foam collapse, although they did not propose a clear mechanism for this delay.

Another way in which particles can affect the stability of foam films according to their hydrophobicity was reported by Johansson et al.[9] They noted that particles of intermediate hydrophobicities acted to stabilise foam films by streaming along the air/solution lamellae during drainage of the film. The effect of particles concentrating along the edges of the Plateau borders appeared to increase the rigidity of the interface and hence the overall stability of the foam structure. Particles of greater hydrophobicities penetrated the interface to a much greater extent and ruptured the film. More hydrophilic particles remained dispersed in the lamellae and did not appear to have much influence on the foam's stability.

From the summary presented above, it is clear that even if the nm-sized silica particles are not large enough to bridge foam films, there are still other possibilities for the ways in which they can change the foaming properties of aqueous surfactant solutions.

5.3 Surfactant-silica particle dispersions

Although the surfaces of the particles used in this study are produced with different levels of hydrophobicity (varied by treating their surfaces to different extents with a silane reagent), (see section 2.2.4 for more details) it needs to be confirmed that changing the % SiOH on the particle surfaces changes the resulting hydrophobicity of the particle in a predictable way. This allows a systematic study of the effect that particle hydrophobicity has on the foaming properties of $C_{12}E_5$ by using particles with different residual % SiOH values. Any differences observed in foaming solutions containing these particles can then be confidently attributed to the hydrophobicity of the particles. Recently, Binks et al. have shown that these nm-sized silica particles

can stabilise emulsions in the absence of any surfactant.[10-13] Here, the wettability of the particles (as judged by the contact angle, θ) is one of the key factors in dictating whether the resulting emulsion will be stable. If the particles are either too hydrophilic (low θ, high % SiOH) or too hydrophobic (high θ, low % SiOH), they will tend to remain dispersed in either the aqueous or oil phase respectively and give rise to unstable emulsions. It is only when θ (measured through the aqueous phase and controlled by the % SiOH on the particle surfaces) is slightly less than 90° that the particles will be held at the liquid-liquid interface and stabilise oil-in-water (o/w) emulsions, or, for θ slightly greater than 90°, that water-in-oil (w/o) emulsions can be formed. This work shows that the particle contact angles can be used to finely control whether the particles remain dispersed in water or in oil and that these silica particles can be used in a systematic study of particle hydrophobicity effects because the % SiOH on the particle surfaces (and hence values of θ) have been shown to be capable of being finely tuned.

All of the nm-sized silica particles can be dispersed in 1 mM of aqueous $C_{12}E_5$ solution (approximately 17 times its cmc) up to concentrations of 0.2 wt. % regardless of their initial % SiOH content, using ultrasound (see section 2.6.1 for full details of this procedure). Above this concentration, only the most hydrophilic (% SiOH $\geq$ 65.7) particles disperse in the solution regardless of the power or the duration of the applied ultrasound.

All of the dispersions are clear but exhibit a very slight blue tint and they all foam upon shaking. Once the foam has broken, the dispersions, upon shaking, produce the same volume of foam once again. This implies that the dispersions remain stable throughout the foam production and foam breaking processes and that the action of the particles is not affected by the foam production process.

5.3.1 Characterisation using transmission electron microscopy

Figures 5.1 – 5.5 show transmission electron micrographs (TEMs) of a selection of the silica dispersions. The scale of the image is shown in each Figure. Figure 5.1 shows the way in which the particles appear when deposited from dispersions of pure

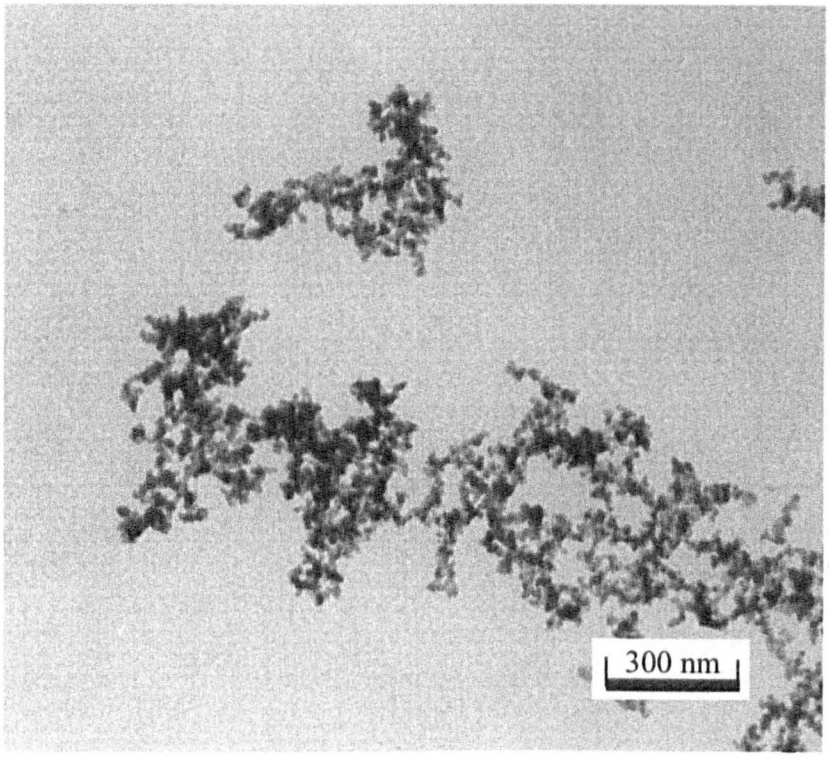

Figure 5.1 Transmission electron micrograph (TEM) of a carbon-coated Cu/Pd grid with silica particles deposited by evaporation from a solution composed of 0.2 wt. % silica (100 % SiOH) dispersed in water. The scale bar is shown in the Figure.

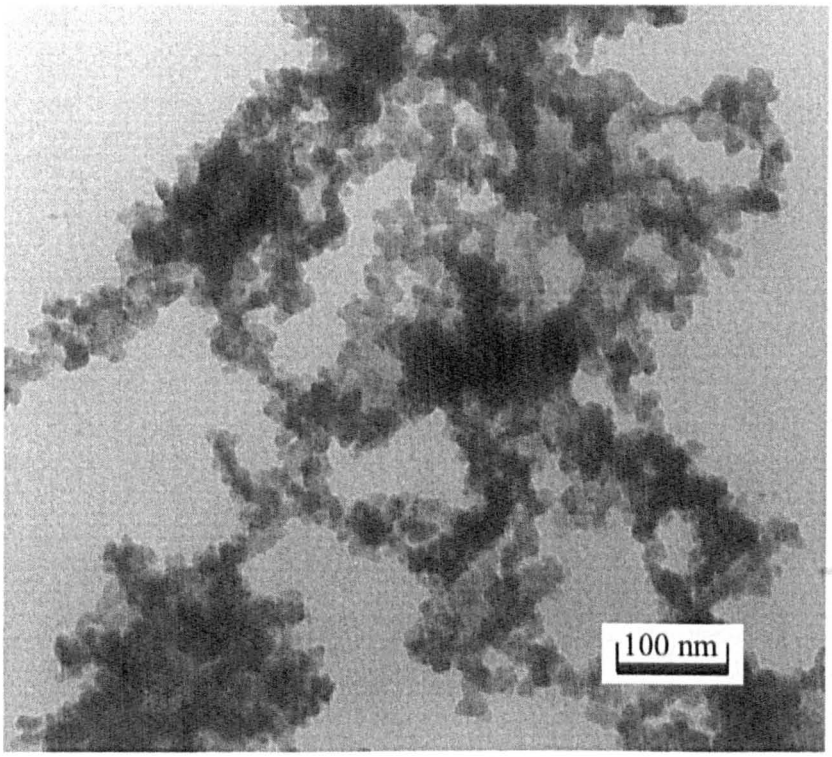

Figure 5.2 Transmission electron micrograph (TEM) of a carbon-coated Cu/Pd grid with silica particles deposited by evaporation from a solution composed of 0.2 wt. % silica (79.9 % SiOH) dispersed in 6.1 x 10^{-6} M $C_{12}E_5$. The scale bar is shown in the Figure.

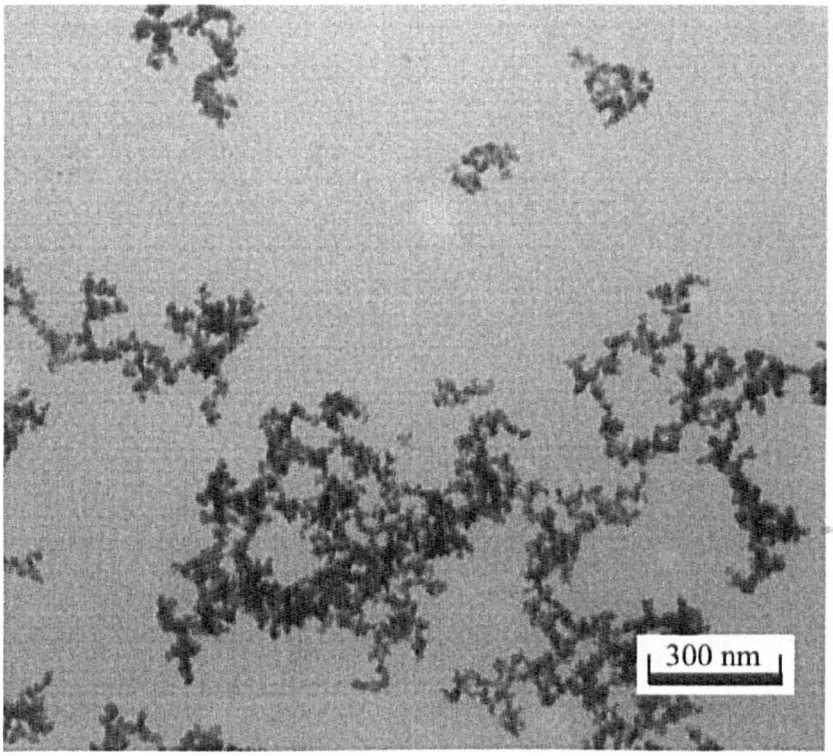

Figure 5.3 Transmission electron micrograph (TEM) of a carbon-coated Cu/Pd grid with silica particles deposited by evaporation from a solution composed of 0.2 wt. % silica (100 % SiOH) dispersed in 6.0×10^{-6} M $C_{12}E_5$. The scale bar is shown in the Figure.

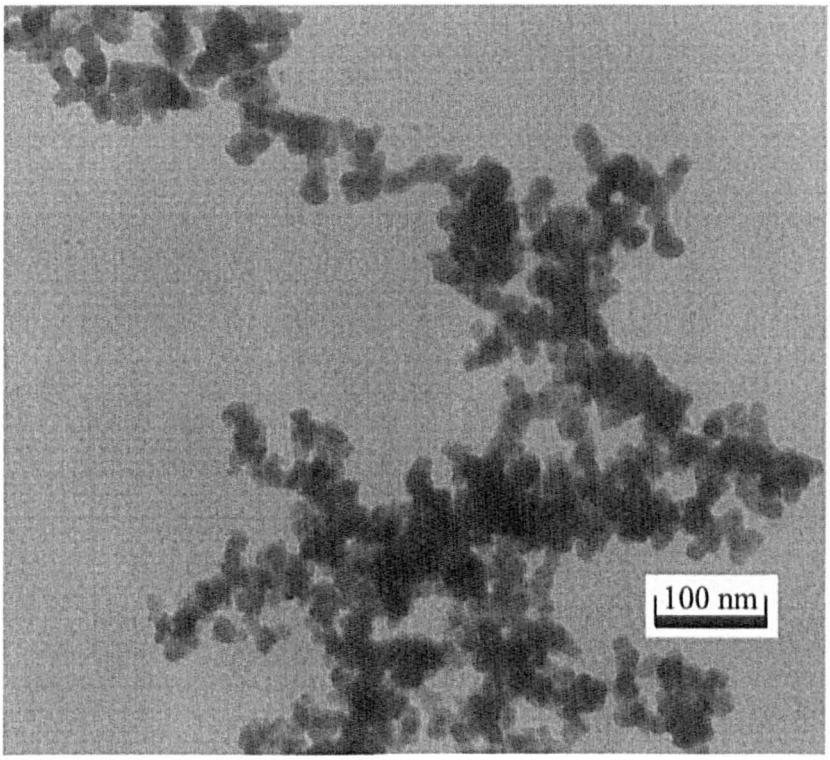

Figure 5.4 Transmission electron micrograph (TEM) of a carbon-coated Cu/Pd grid with silica particles deposited by evaporation from a solution composed of 0.2 wt. % silica (79.9 % SiOH) dispersed in 1 mM $C_{12}E_5$. The scale bar is shown in the Figure.

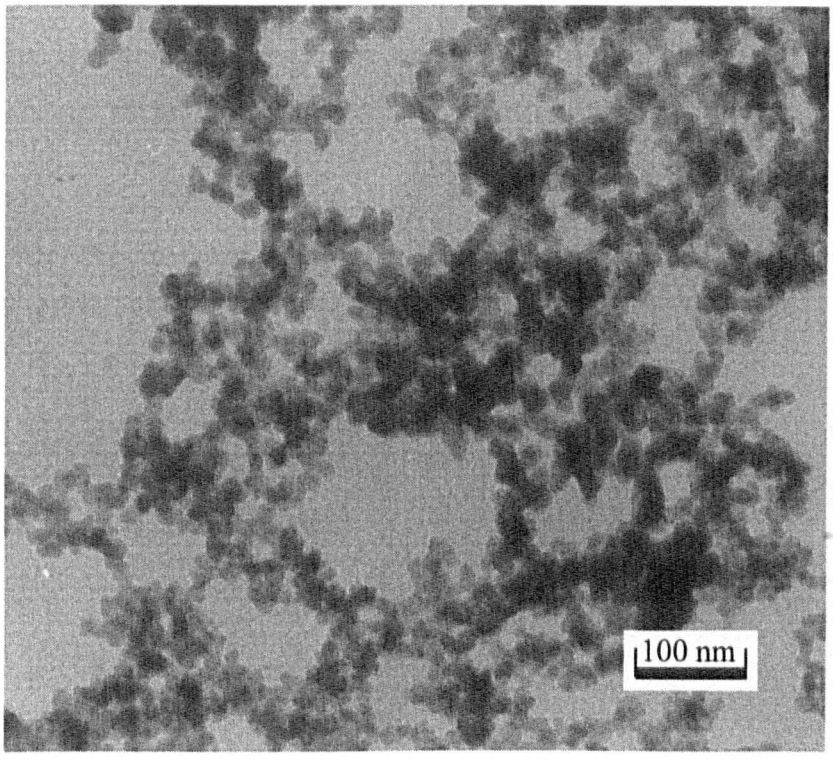

Figure 5.5 Transmission electron micrograph (TEM) of a carbon-coated Cu/Pd grid with silica particles deposited by evaporation from a solution composed of 0.2 wt. % silica (100 % SiOH) dispersed in 1 mM $C_{12}E_5$. The scale bar is shown in the Figure.

water. As shown in the Figure, the particles may to form networks throughout the solution if the TEM is representative of the solution. Figures 5.2 – 5.5 show that the silica particles may form networks and small aggregates when dispersed in aqueous $C_{12}E_5$ surfactant solutions, regardless of whether the concentration of the surfactant solution is higher or lower than its cmc. These observations are consistent with the manufacturer's data (see section 2.1.4).

5.4 Adsorption isotherms of $C_{12}E_5$ onto silica particles in water

As briefly discussed in section 5.2.1, silica particles can deplete surfactant from an aqueous solution because the surfactant can adsorb onto the particle surfaces. The fact that even the most hydrophobic silica particles can be dispersed in the nonionic surfactant solution but not in pure water implies that there must be at least some adsorption of surfactant onto these particle surfaces. This adsorption could have a significant impact on the foamability of the nonionic surfactant solution if the adsorption is high enough to significantly reduce the equilibrium surfactant concentration. The adsorption of surfactant onto the silica particle surfaces could also change the hydrophobicity of the particles which could impact on both the foamability and the foam stability of the solution as discussed in section 5.2. Before any foaming measurements are presented, the adsorption of $C_{12}E_5$ onto the silica particle surfaces will first be investigated.

There have been several studies reported in the literature where researchers have focussed specifically on the adsorption of nonionic surfactant onto hydrophobic and hydrophilic silica surfaces. Alexeev et al. found that micellar surfactant solutions can enhance the stability of dilute silica dispersions. Concentrated dispersions were also found to be stable provided that the particles remain separated by at least one layer of surface adsorbed micelles.[14,15] Giordano-Palmino et al.[16] also concluded from their studies that micelle-like aggregates were present on silica suspensions in nonionic surfactant solutions. Levitz et al. found that at low coverages, isolated molecules are adsorbed by hydrogen bonding between the headgroup of the surfactant and the surface silanols. Further adsorption occurs by an aggregation process between surfactant molecules leading to surface micelles.[17-20] Lindheimer et al. showed that

silica acts as a precursor to micelle formation below the cmc.[21] van den Boomgard et al. found that the adsorption isotherms of nonionics onto silica exhibited well-defined plateaus in excess of the cmc.[22] Although it is clear from this collection of work that nonionic surfactant does readily adsorb onto the surface of silica, more detailed information is required regarding the factors governing it (e.g. surfactant structure) and the result that the adsorption has on the resulting hydrophobicity of the particles. Portet et al. found that preferential adsorption of nonionic surfactants onto silica occurred for surfactants with smaller headgroups.[23] Some researchers suggest that a bilayer is formed for surfactants with a small headgroup. For example, Böhmer et al. found that $C_{12}E_6$ adsorbed onto silica forming a bilayer just below the cmc. They concluded that the net attraction between surfactant tails is of crucial importance for the structure of adsorbed layers of nonionic surfactants.[24] They also stated in their paper, that nonionic surfactant does not readily make hydrophilic surfaces hydrophobic. Somasundaran et al.[25] stated that at low adsorption densities, surfactants with large headgroups (e.g. C_8E_{40}) impart hydrophobicity to the silica surface. Further adsorption restores particle hydrophilicity. These changes are not observed for surfactants with a smaller headgroups. They suggest that these differences in hydrophobicity effects are related to the conformational behaviour of adsorbed molecules. In addition to this, Lee et al.[26] showed by neutron reflection studies that $C_{12}E_6$ forms a bilayer on quartz, with headgroups at the surface of the solid and at the film-solution surface. The headgroups are separated by a hydrophobic layer. It is interesting to note the result of Scales et al.[27] who investigated the contact angle changes for hydrophobic and hydrophilic surfaces induced by nonionic surfactants. They prepared hydrophilic (α-quartz) and hydrophobic (siloxanated and silanated α-quarz) plates with contact angles from 0 to 90° measured through the aqueous phase. They found that a "characteristic normalisation of wetting behaviour" was obtained for all of the surfaces, which was independent of the natural wettability of the original surface. They concluded that the orientation of the adsorbed surfactant molecule is such that its headgroup is directed towards the aqueous phase when the adsorption density approaches the maximum for that surfactant. Recently, Grant et al.[28] investigated the configuration of adsorbed C_nE_m surfactants onto hydrophilic and hydrophobic silica. They reported that $C_{10}E_5$, $C_{10}E_6$, $C_{12}E_5$, $C_{12}E_8$, $C_{14}E_6$ and $C_{16}E_6$ all formed continuous layers on the surface of hydrophobic silica. However, they found that $C_{10}E_5$, $C_{10}E_6$, $C_{12}E_8$ and $C_{16}E_6$ formed globular structures on hydrophilic

silica whereas $C_{12}E_5$ and $C_{14}E_6$ formed a flat continuous layer on hydrophilic silica. Tiberg[29] found that $C_{12}E_5$ adsorbed onto hydrophilic silica at higher densities than $C_{12}E_8$. He attributed this behaviour to the higher *n*:*m* ratio of $C_{12}E_5$ compared to $C_{12}E_8$. $C_{16}E_5$ has an even higher *n*:*m* ratio than $C_{12}E_5$ and a longer tail than $C_{14}E_6$, yet it forms globular structures on the surfaces of silica. From this finding, they therefore stated that they could not provide a broadly applicable molecular explanation of the surface-phase behaviour of C_nE_m surfactants on silica. However, they stated that generally, for a variety of nonionic surfactants, globular micelles were formed on hydrophilic silica and a laterally continuous layer was formed on the hydrophobic silica. They concluded that the structure on hydrophilic silica is similar to that formed in bulk above the cmc, probably because the silica surface contained hydroxyl groups, which can in some ways substitute for the hydrogen bonds in water. The structure on hydrophobic silica is a large perturbation of the solution structure, probably because the substrate introduces a new energy term: a minimisation of substrate-water area. Mixing of the surfactant and diethyloctylsilane hydrocarbon chains may also contribute to the change in shape from the solution structure. They gave no insight into the resulting hydrophobicity of the silica after the adsorption of nonionic surfactant had occurred.

From the summary above, it is clear that there are various possibilities for the ways in which nonionic surfactant can adsorb onto silica surfaces (either surface micelles can form or a bilayer can be built up). The structure of adsorbed surfactant structure depends upon the hydrophobicity of the silica particles and the size of the surfactant headgroup in relation to the length of the tail group. As explained in section 5.1, the hydrophobicity of the particles can play an important role on how they affect the foaming of surfactant solutions. From the collection of work presented above, it remains unclear as to how the initial % SiOH content on the particles would influence the level (and mode) of adsorption of $C_{12}E_5$ onto the nm-silica particle surfaces. At low % SiOH coverages, $C_{12}E_5$ may adsorb so as to form a continuous layer. At higher values of % SiOH $C_{12}E_5$ may form globular units on the surface of the silica. This adsorption of surfactant will inevitably change the hydrophobicity of the particles which could affect the way in which they influence foaming behaviour. In addition to the resulting hydrophobicity of the silica particles, this adsorption will also cause surfactant depletion which can impact on foaming. The level of surfactant adsorption

onto the particle surfaces as a function of their initial % SiOH content is determined and discussed in the following sections.

5.4.1 Surface tension measurements

The adsorption isotherms for the three most hydrophilic silica particle types (65.7, 79.9 and 100 % SiOH) were determined by surface tension measurements. In doing this, it is assumed that the dispersed silica particles do not affect the air-water tensions other than by depletion of surfactant by adsorption. Measuring the surface tension in the absence of silica particles as a function of surfactant concentration yields a calibration curve. By measuring the surface tension as a function of surfactant concentration in the presence of a known mass of dispersed particles, another curve will be obtained which, providing there is a high enough level of surfactant adsorption, should be displaced to higher concentrations relative to the curve for samples with no particles. Equilibrium surfactant concentrations in the presence of particles can be found by comparing surfactant concentrations which give the same value of surface tension on each curve. The difference in these concentrations arises from the adsorption of the surfactant onto the silica, i.e. in the presence of silica a higher surfactant concentration is required to recover the same equilibrium surface tension. This difference in concentrations can be converted to the number of moles of $C_{12}E_5$ adsorbed onto a unit mass of silica at the equilibrium surfactant concentration in the pure surfactant case (this is the concentration of surfactant corresponding to the fixed surface tension on the calibration curve). By taking different values of surface tension and comparing the corresponding concentrations between the two curves, an adsorption isotherm can be constructed for silica particles with particular % SiOH contents on their surface. Isotherms were determined for the 3 most hydrophilic silica particle types because of the limitation that the more hydrophobic particles cannot be dispersed in dilute surfactant solutions (below the cmc).

Figures 5.6 – 5.9 show the surface tension as a function of time for each of the surfactant-silica dispersions for a range of surfactant concentrations. It can be seen that the surface tension – time dependence for all of the dispersions are approximately horizontal. Although there are small changes in surface tension with time, these are

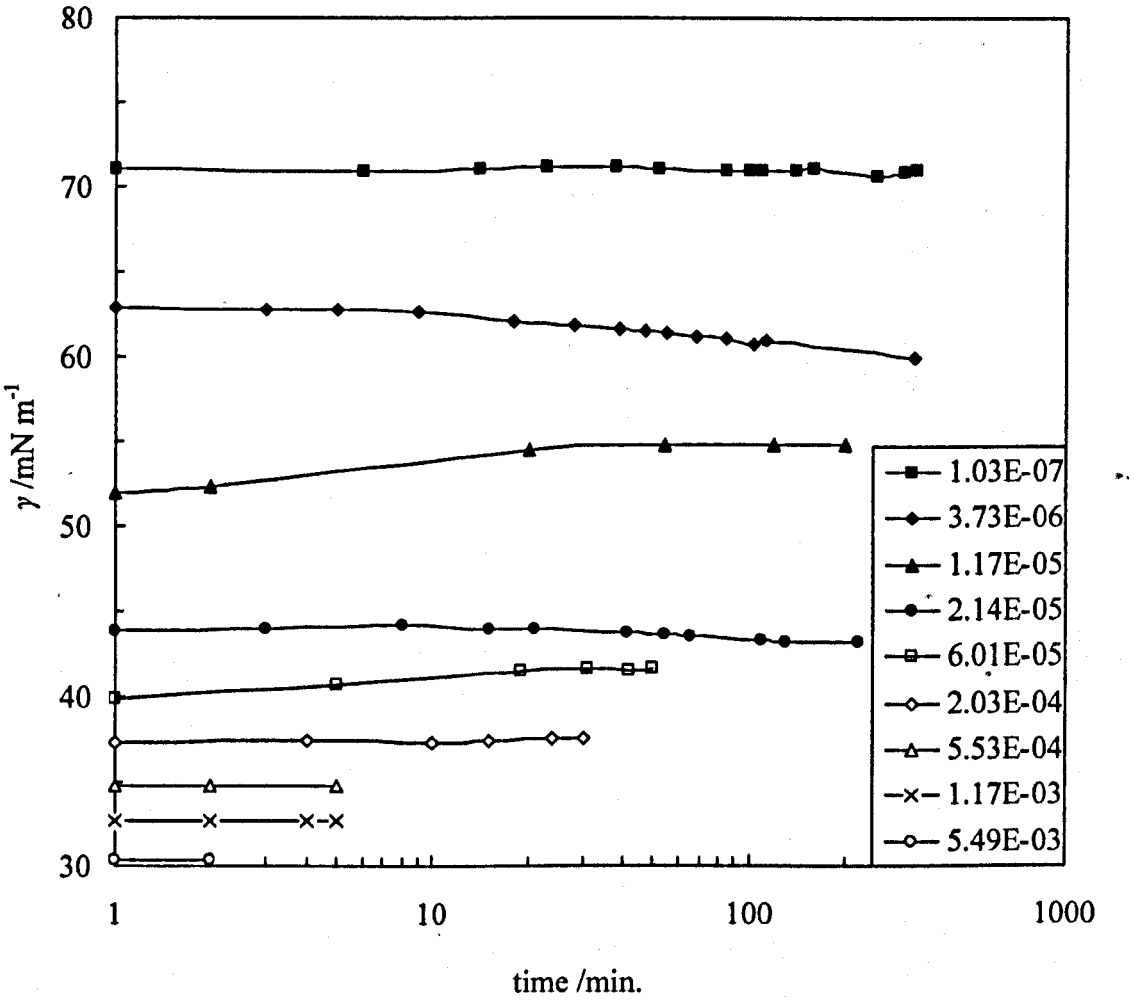

Figure 5.6 Variation of surface tension with time for $C_{12}E_5$ with 0.2 wt. % of silica particles (% SiOH = 100) dispersed at different surfactant concentrations (concentrations in the legend in M). All of the measurements were made at 20.0 °C.

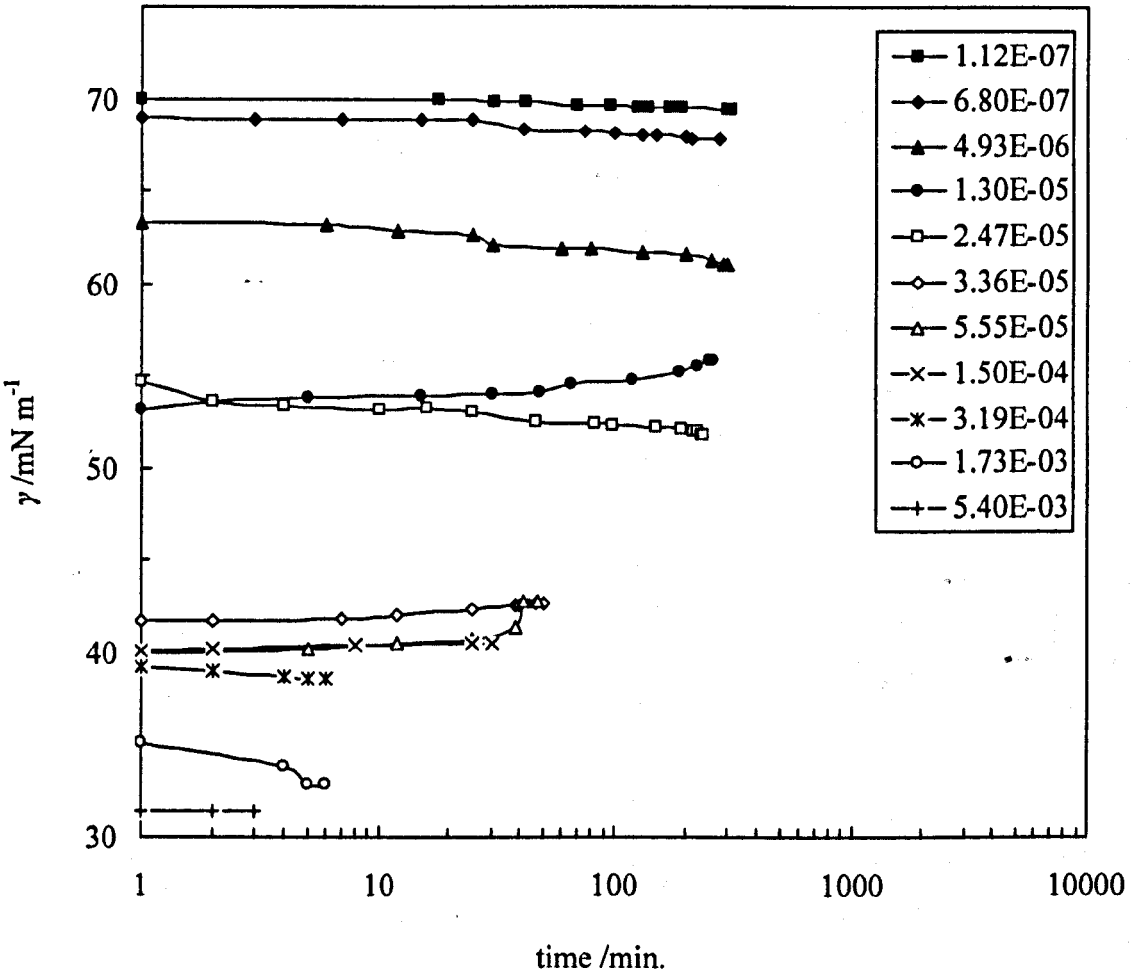

Figure 5.7 Variation of surface tension with time for $C_{12}E_5$ with 0.4 wt. % of silica particles (% SiOH = 100) dispersed at different surfactant concentrations (concentrations in the legend in M). All of the measurements were made at 20.0 °C.

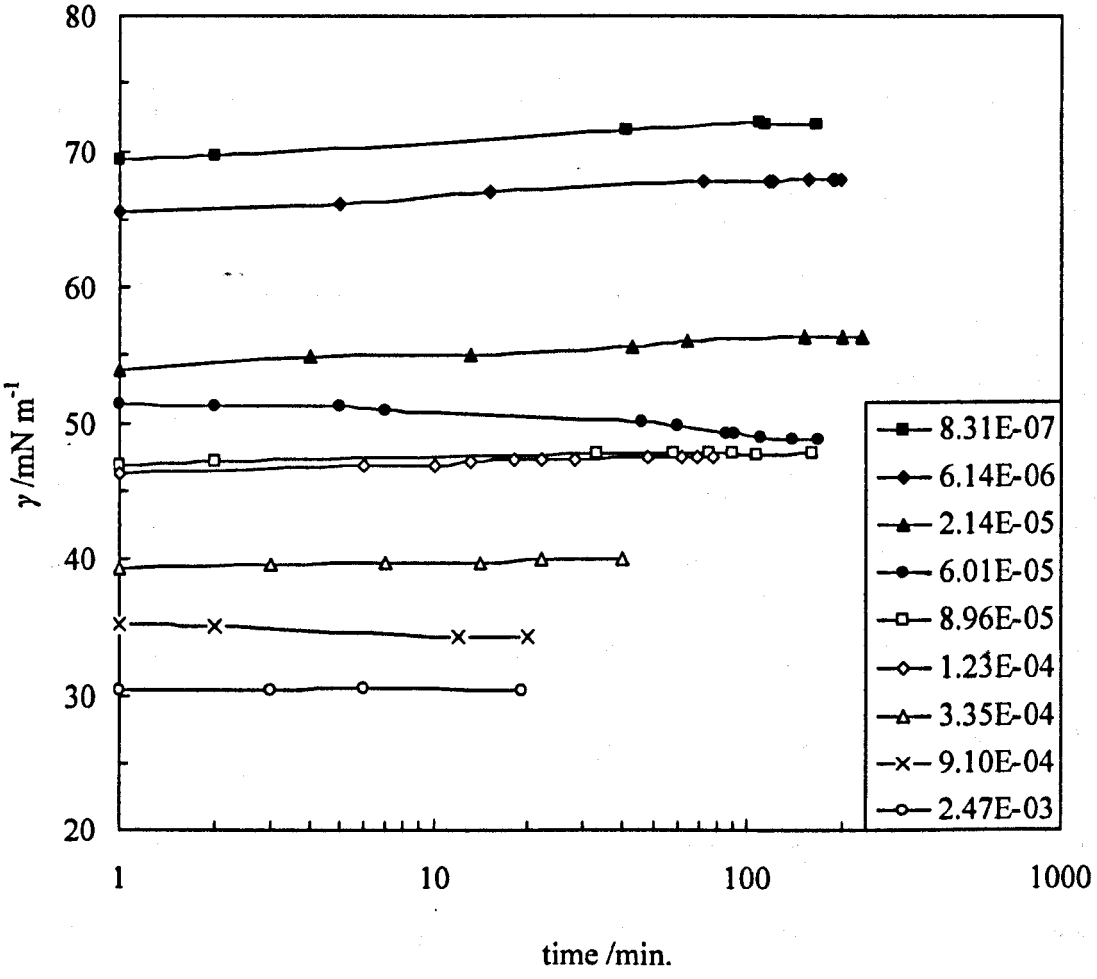

Figure 5.8 Variation of surface tension with time for $C_{12}E_5$ with 0.2 wt. % of silica particles (% SiOH = 79.9) dispersed at different surfactant concentrations (concentrations in the legend in M). All of the measurements were made at 20.0 °C.

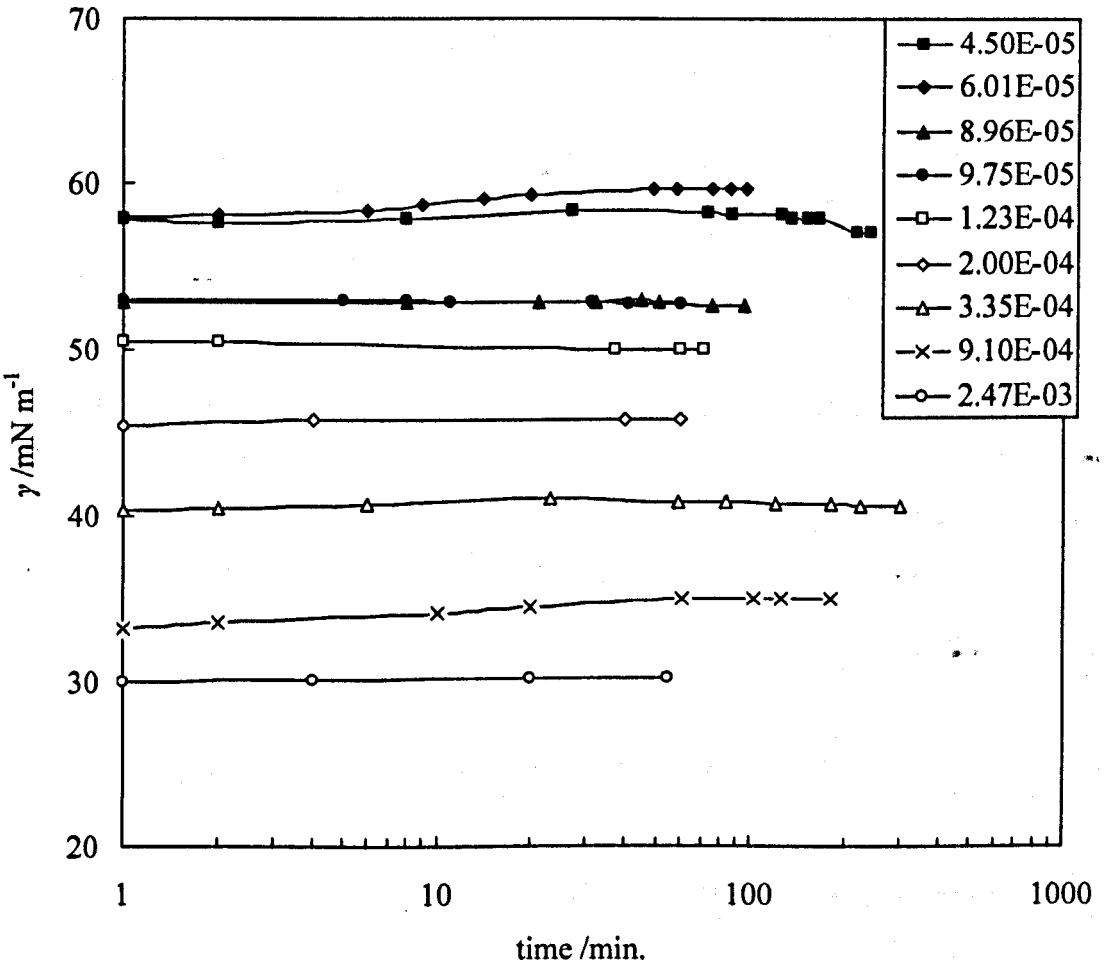

Figure 5.9 Variation of surface tension with time for $C_{12}E_5$ with 0.2 wt. % of silica particles (% SiOH = 65.7) dispersed at different surfactant concentrations (concentrations in the legend in M). All of the measurements were made at 20.0 °C.

likely to be due to drift in the balance of the tensiometer. It appears that an equilibrium surface tension is reached within 1 minute or so for all of the dispersions. This is in complete contrast to pure $C_{12}E_5$ where equilibrium adsorption times range from 10 minutes for 1 x 10^{-5} M to 400 minutes for 1 x 10^{-7} M.[30]

Figure 5.10 illustrates this difference in adsorption rates by showing two surface tension – time dependence curves. Although the equilibrium surface tensions for both systems is approximately the same, it can be seen that for the surfactant sample containing the dispersed silica, the tension drop occurs almost immediately and is of the order of 1 or 2 mN m^{-1}. For the pure surfactant case containing no silica, the sharp decrease in surface tension occurs over a period of 25 minutes or so and the tension drop is far larger than for the sample containing silica (of the order of 17 mN m^{-1}). One idea that explains this observation is that the dispersed silica acts as a surfactant reservoir. This is plausible because $C_{12}E_5$ will adsorb onto the surface of each of the silica particle types used above. The silica is fully dispersed in the surfactant solution and may aid in the transport of the surfactant to the air-water interface.

Figure 5.11 shows the surface tension as a function of bulk surfactant concentration for $C_{12}E_5$ alone and for a series of $C_{12}E_5$-silica dispersions. The Figure shows that regardless of the % SiOH coverage on the particles or the concentration at which the particles are dispersed, there is a concentration of surfactant at which the surface tension reaches a constant value. This is very similar for all of the systems shown.

For tensions higher than this constant value, a higher concentration of surfactant is required to recover the same surface tension when dispersed particles are present. This concentration increases with decreasing % SiOH content on the particle surfaces. For silica with 100 % SiOH on its surface, the surfactant concentration required to achieve the same surface tension as pure $C_{12}E_5$ is higher when the particles are dispersed at 0.4 wt. % than when they are dispersed at 0.2 wt. %. For each of the dispersions, there is a concentration of surfactant at which the surface tension becomes approximately constant before falling again to a limiting value (approximately 30 mN m^{-1}). A possible explanation for this is the formation of a bilayer on the surface of the silica. (Recall from earlier in this section that Böhmer et

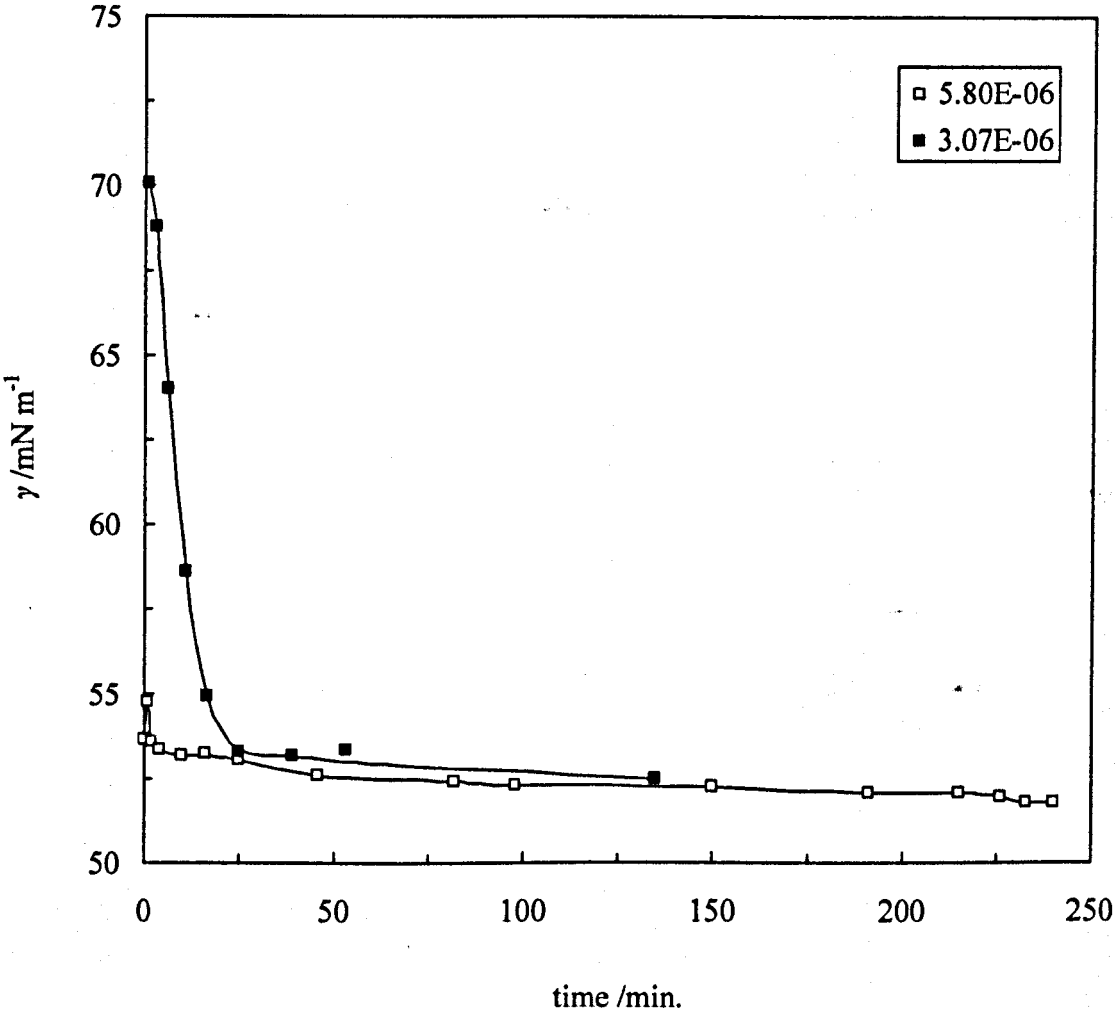

Figure 5.10 Surface tension as a function of time for $C_{12}E_5$ in the absence of silica particles (filled squares) and in the presence of silica particles (100 % SiOH) dispersed at 0.4 wt. % (open squares). Numbers in the legend show the equilibrium concentration of $C_{12}E_5$. The equilibrium concentration of $C_{12}E_5$ in the presence of particles was determined using the surface tension plot for 0.4 wt. % 100 % SiOH (Figure 5.11).

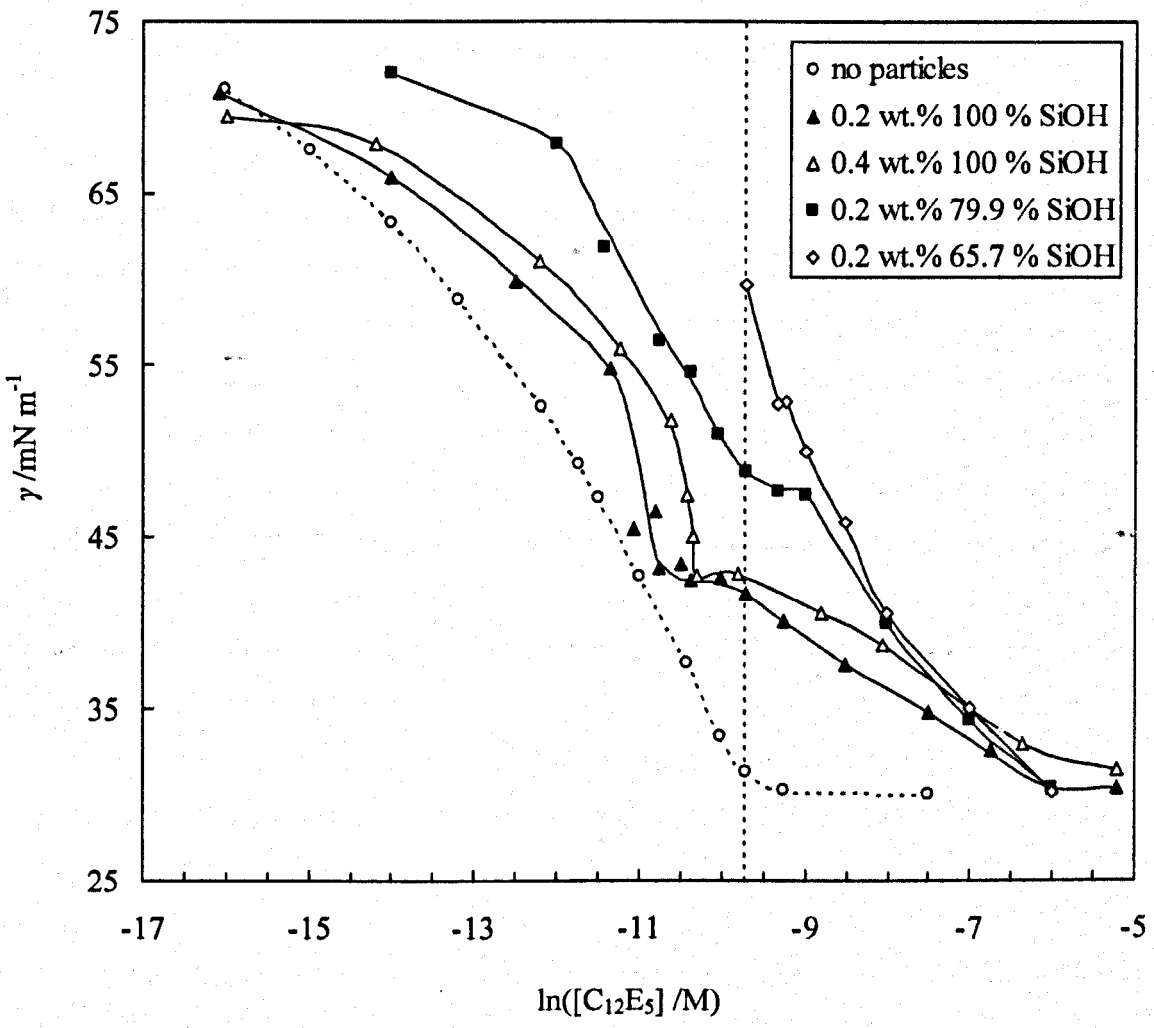

Figure 5.11 Variation of equilibrium surface tension with aqueous $C_{12}E_5$ concentration. The symbols in the legend and the solid lines refer to the concentration of dispersed silica particles and the residual % SiOH on their surfaces and the open circles and dashed line refers to the pure surfactant case. The horizontal dashed line shows the cmc of pure $C_{12}E_5$. All of the measurements were made at 20.0 °C.

al. predicted that a bilayer formation occurred after the stepwise addition of $C_{12}E_6$ onto hydrophilic silica.[24])

5.4.2 Nonionic adsorption isotherms onto silica nano-particles in water

Figure 5.12 shows the adsorption isotherms derived from the surface tension measurements. As the surfactant concentration is increased, the number of moles of $C_{12}E_5$ adsorbing onto unit mass of silica gradually increases. The maximum number of moles of $C_{12}E_5$ which can adsorb onto the silica is the same for all silica types and is approximately 1200 μ mol /g SiO_2. It should be noted here that any further adsorption beyond this point cannot be determined using the surface tension method because further increases in surfactant concentration do not lower the surface tension (which is now at its lowest possible value for a fixed surfactant) as the cmc of the surfactant has been reached. The level of adsorption does however seem to be of the correct order when compared to the value of around 600 μ mol /g reported for Ludox AS40 (precipitated colloidal silica with spherical particles) obtained by Böhmer et al.[24] The silica used in their study had a specific surface area of 140 m^2 /g which is approximately half that of the silica used in this study (200 - 250 m^2 /g as stated by the manufacturer, see Table 2.3).

In order to check the derived adsorption isotherm, the most hydrophilic silica particles were dispersed at a higher concentration (0.4 wt. %), and the resulting surface tensions were measured for the range of surfactant concentrations. Although a higher concentration of surfactant was required to recover the same surface tension compared to the lower particle concentration dispersion, both derived adsorption isotherms for that particle type (% SiOH = 100) could be superimposed as expected (Figure 5.13)

The overall finding from this part of the work is that $C_{12}E_5$ adsorbs onto the surface of the more hydrophobic silica particles more than the hydrophilic silica particles. Although all of the particles become hydrophilic in nature after the adsorption of nonionic surfactant onto their surfaces, it remains unclear as to whether there is a variation in hydrophilicity as a function of the initial % SiOH on their surfaces or

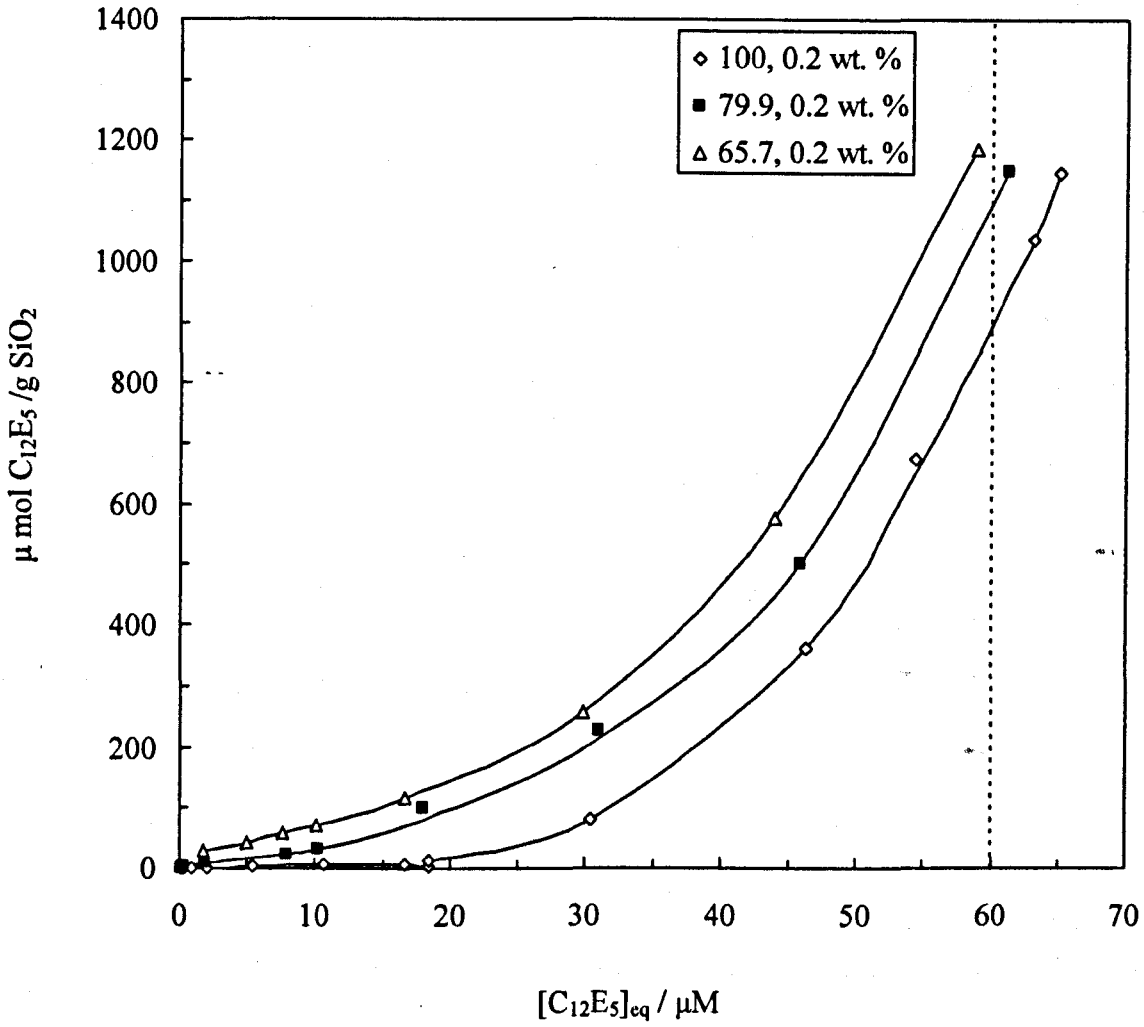

Figure 5.12 Number of moles of $C_{12}E_5$ adsorbed onto 1 g of silica with various % SiOH on their surfaces as a function of equilibrium surfactant concentration at 20.0 °C. Numbers in the legend show the SiOH coverage and the concentration of the dispersed particles. The vertical dashed line shows the cmc of pure $C_{12}E_5$.

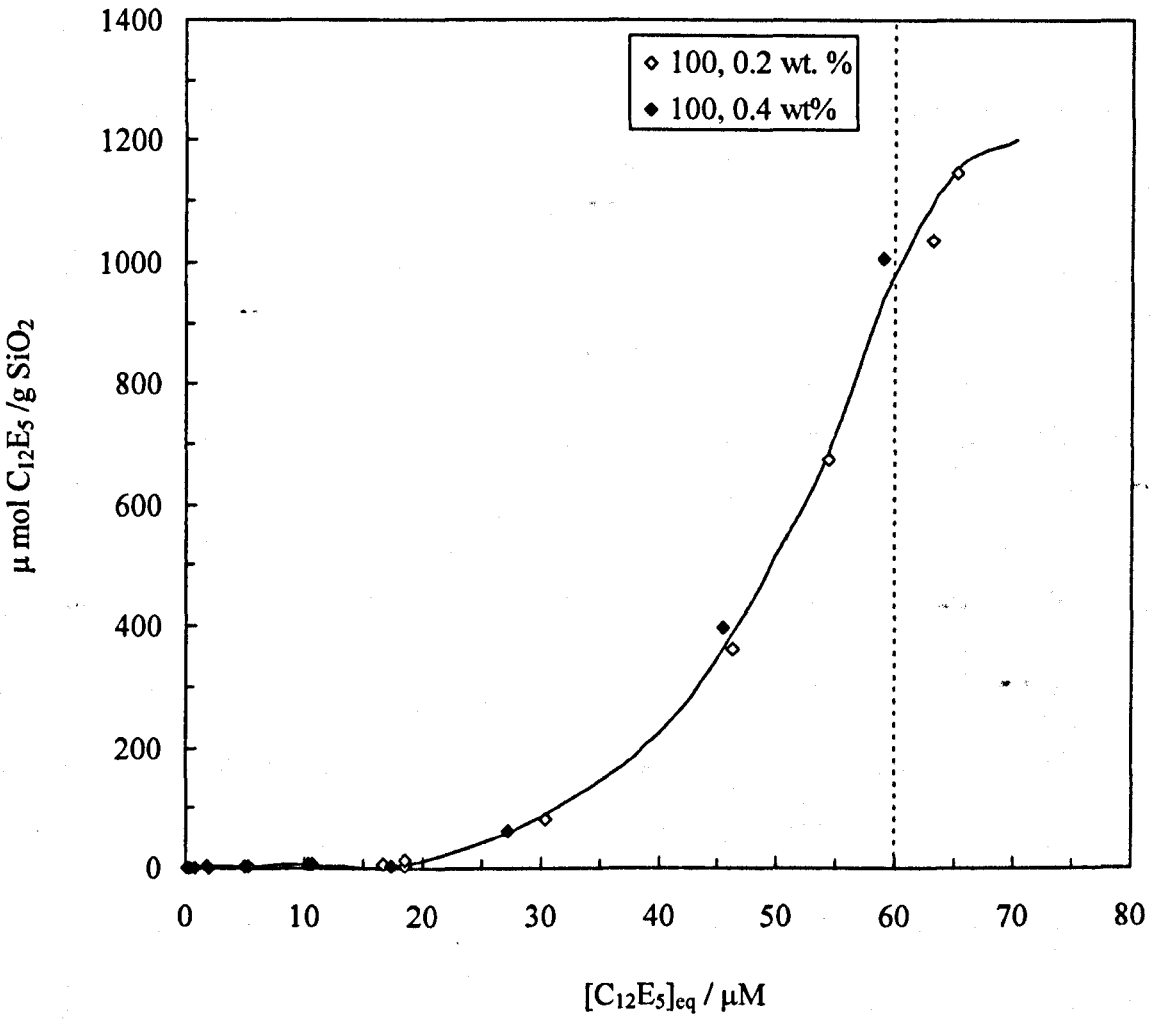

Figure 5.13 Number of moles of $C_{12}E_5$ adsorbed onto 1 g of silica with 100 % SiOH on its surface when dispersed at 0.2 and 0.4 wt. % as a function of equilibrium surfactant concentration at 20.0 °C. Numbers in the legend show the SiOH coverage and the concentration of the dispersed particles. The vertical dashed line shows the cmc of pure $C_{12}E_5$.

whether the wettabilities have all been made equal as reported for the systems studied by Scales et al.[27] after the adsorption of surfactant.

5.5 Foamability of aqueous $C_{12}E_5$-silica dispersions

The foamability of aqueous $C_{12}E_5$ solutions containing dispersed silica particles with different % SiOH contents on their surfaces, dispersed at different concentrations is now considered.

5.5.1 Shake test measurements

Shake tests (as described in section 2.5) were initially used to investigate the foamability of the various surfactant-silica dispersions. Figure 5.14 shows the relative foam volume as a function of the % SiOH on particle surfaces for three silica particle concentrations. Relative foam volume is defined as the volume of foam produced in the presence of particles divided by the volume of foam produced in the absence of particles. Hence, a relative foam volume of 1 corresponds to a foam volume identical to the volume produced in the absence of particles, i.e. surfactant alone. For 20.0 cm^3 of 1 mM aqueous $C_{12}E_5$ contained in a 100 cm^3 stoppered measuring cylinder, the volume of foam produced after shaking for 1 minute was 23 cm^3. Each run was repeated 3 times and the error bars on the y-axis represent the maximum deviation in foam volumes between these three runs. Solutions of $C_{12}E_5$ containing dispersed silica particles have different foamabilities compared to the equivalent systems containing no particles. All of the particles reduce the foamability of the solution regardless of their hydrophobicity (as judged by the % SiOH on the particle surfaces) and the concentration at which they are dispersed. In the presence of particles, foamability decreases with increasing particle concentration for fixed particle hydrophobicity. At a fixed concentration of dispersed particles, decreasing the hydrophobicity of the particles (by increasing the % SiOH on the particle surfaces) increases the resulting foamability of the surfactant solution.

These observations can be explained by considering the adsorption of surfactant onto the silica particle surfaces. This adsorption process lowers the concentration of free

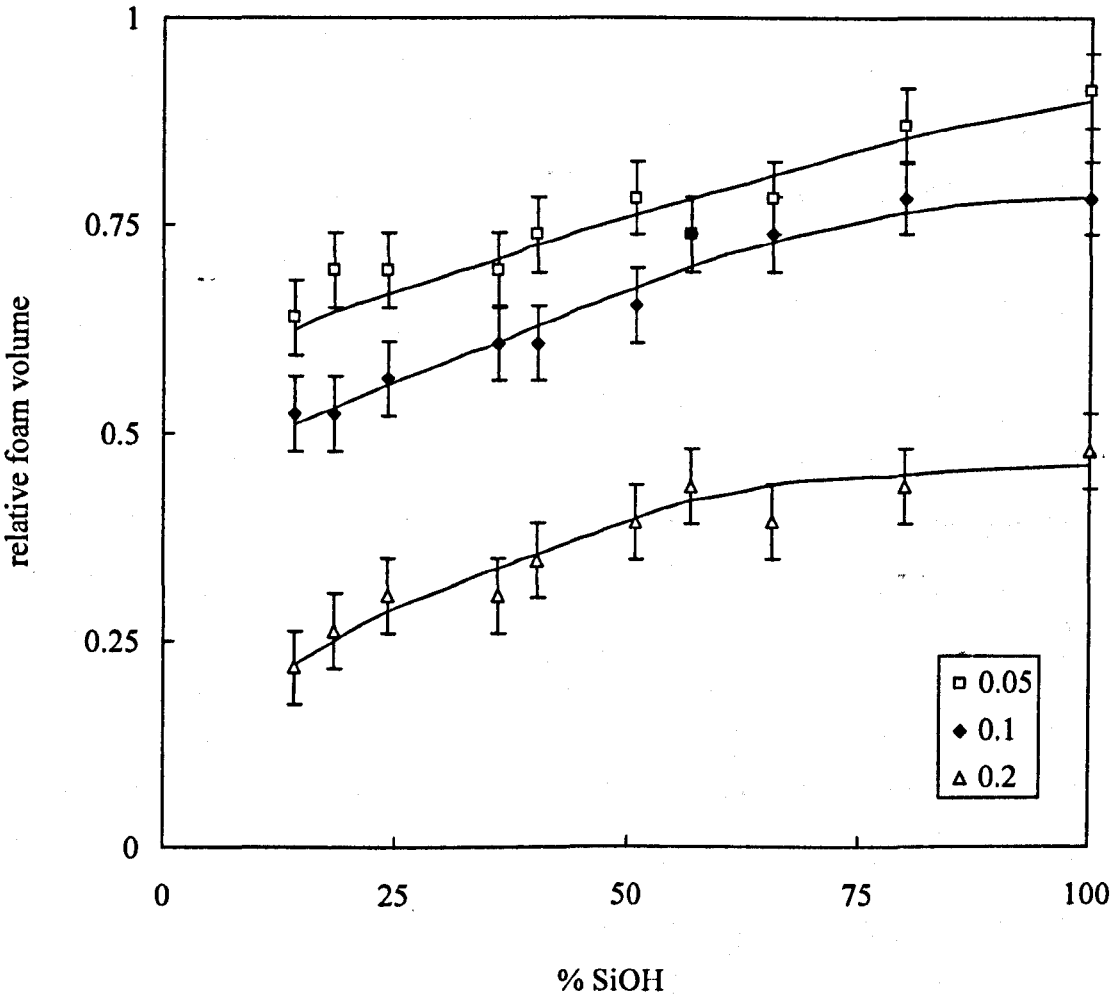

Figure 5.14 Relative foam volume as a function of % SiOH on silica particle surfaces dispersed in 20.0 cm^3 aqueous $C_{12}E_5$ (1 mM). The numbers represent the concentration (in wt. %) of dispersed particles. All of the measurements were made at ambient temperature.

surfactant monomers in the solution, thus changing the equilibrium surfactant concentration. As discussed in chapter 3, lowering the concentration of a surfactant solution can reduce its foamability. We recall from chapter 3 that $C(1/2)$ is the surfactant concentration corresponding to the transition from non-foaming to foaming behaviour for a particular surfactant. At values slightly below $C(1/2)$ foam can be formed but the volume is significantly lower compared to the maximum volume obtainable for a particular surfactant and foam production method. Referring to Figure 5.6, for a system containing 1 mM of $C_{12}E_5$, the equilibrium surfactant concentration is lowered to approximately 5 x 10^{-5} M in the presence of silica particles (100 % SiOH) dispersed at 0.2 wt. %. This is a lower concentration than the value of 1.22 x 10^{-4} M obtained for the $C(1/2)$ value of $C_{12}E_5$.[31] The foamability of $C_{12}E_5$ is predicted to be limited by the surfactant adsorption rate and so $C(1/2)$ may have a slightly different value when foam is produced at different rates, i.e. by using a shake test as opposed to the foam column. Even considering this possible discrepancy, the fact that the silica particles lower the equilibrium surfactant concentration to a value close to $C(1/2)$ could explain why foamability is reduced in the presence of particles. In section 5.4.2, it was concluded from the derived adsorption isotherms that $C_{12}E_5$ adsorbed onto silica particles with a lower % SiOH on their surfaces more than particles with a higher % SiOH on their surfaces. In the presence of dispersed particles, the equilibrium surfactant concentration will therefore be lower for the particles with lower % SiOH on their surfaces. This qualitatively agrees with the trend in foamability, where particles with the lowest % SiOH values dispersed at the highest concentrations reduce the foamability the most.

5.5.2 Foam column measurements

Figure 5.15 shows the foam volume immediately after 10 minutes gas sparging as a function of particle hydrophobicity for 3 different particle concentrations obtained using the foam column. Dispersing the silica particles with high % SiOH content into the surfactant solution does not appear to significantly reduce the foamability of the solution. Particles of the highest hydrophobicity (low % SiOH coverage) do however decrease the foamability of the surfactant solution. This effect is at its largest when the silica particles are dispersed at the highest concentration of 0.2 wt. %.

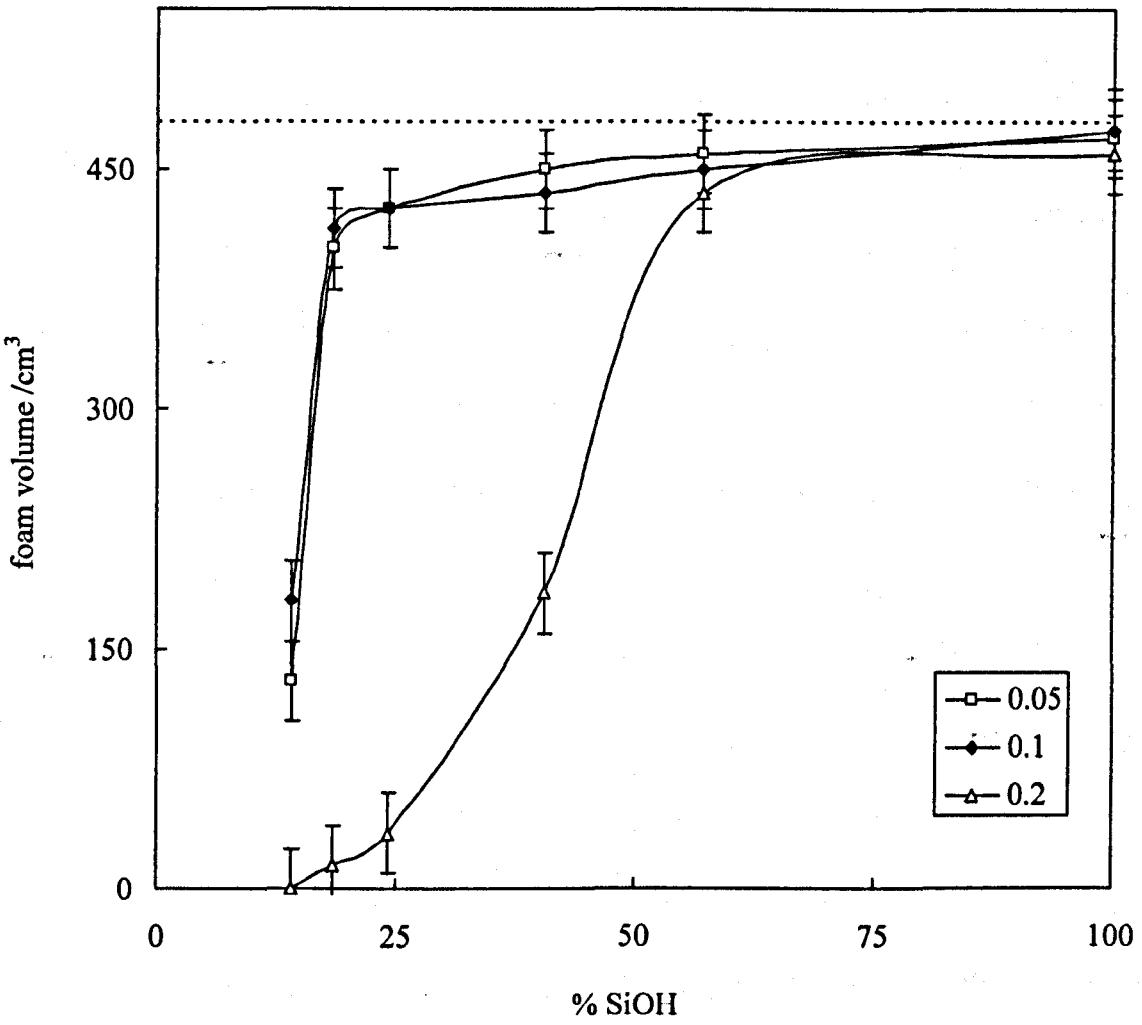

Figure 5.15 Foam volume immediately after 10 minutes of gas sparging as a function of % SiOH on the particle surfaces at different particle concentrations. Foam created by sparging N_2 gas through 15.0 cm^3 of aqueous $C_{12}E_5$ (1 mM) solution for 10 minutes at a flow rate of 48 cm^3 min^{-1}. The dotted line represents the volume of foam produced in the absence of particles. All of the measurements were made at 20.0 °C.

Foamability is completely inhibited when the most hydrophobic silica is dispersed at 0.2 wt. %. The foamability curves are the same (within experimental error) for both the 0.05 and 0.1 wt. % dispersions. At a SiOH content of approximately 20 %, there is a sharp transition from very low foamability to very high foamability for these two particle concentrations. When the particles are dispersed at 0.2 wt. %, the transition is more gradual between 25 to 60 % SiOH. These effects can also be attributed to the value of $C(1/2)$ for $C_{12}E_5$. It is likely that the value of $C(1/2)$ for $C_{12}E_5$ of 1.22×10^{-4} M is the same as the equilibrium surfactant concentration when the silica particles with a % SiOH value of approximately 50 are dispersed into 1 mM of $C_{12}E$ at 0.2 wt. %. The same equilibrium surfactant concentrations are obtained for silica particles with lower values of % SiOH on their surfaces (of the order of 15) when they are dispersed at lower concentrations (0.05 wt. %). This explanation is plausible because although the particles with lower % SiOH on their surfaces can adsorb more surfactant per unit mass, they are dispersed at lower concentrations which probably results in similar equilibrium surfactant concentrations compared to systems containing particles dispersed at 0.2 wt. % with lower adsorption of $C_{12}E_5$ per unit mass.

5.6 Foam stability of aqueous $C_{12}E_5$-silica dispersions

Figure 5.16 shows the way in which the half-life of foams created from the same concentration and type of surfactant can be very different depending on the hydrophobicity and the concentration of the dispersed silica particles. The most hydrophilic particles dispersed at the highest concentrations stabilise the foam more than the most hydrophobic particles dispersed at low concentrations.

Figure 5.17 shows the dependency of foam stability (half-life) on both the hydrophobicity of the particle, and the concentration at which they are dispersed in the aqueous surfactant solution according to a series of shake tests. For the systems containing silica particles dispersed at concentrations of 0.05 and 0.1 wt. %, there is a destabilisation of the foam in the presence of hydrophobic particles relative to the foaming solution containing no particles. Systems containing particles with approximately 25 % SiOH on their surfaces, dispersed at low concentration, produce

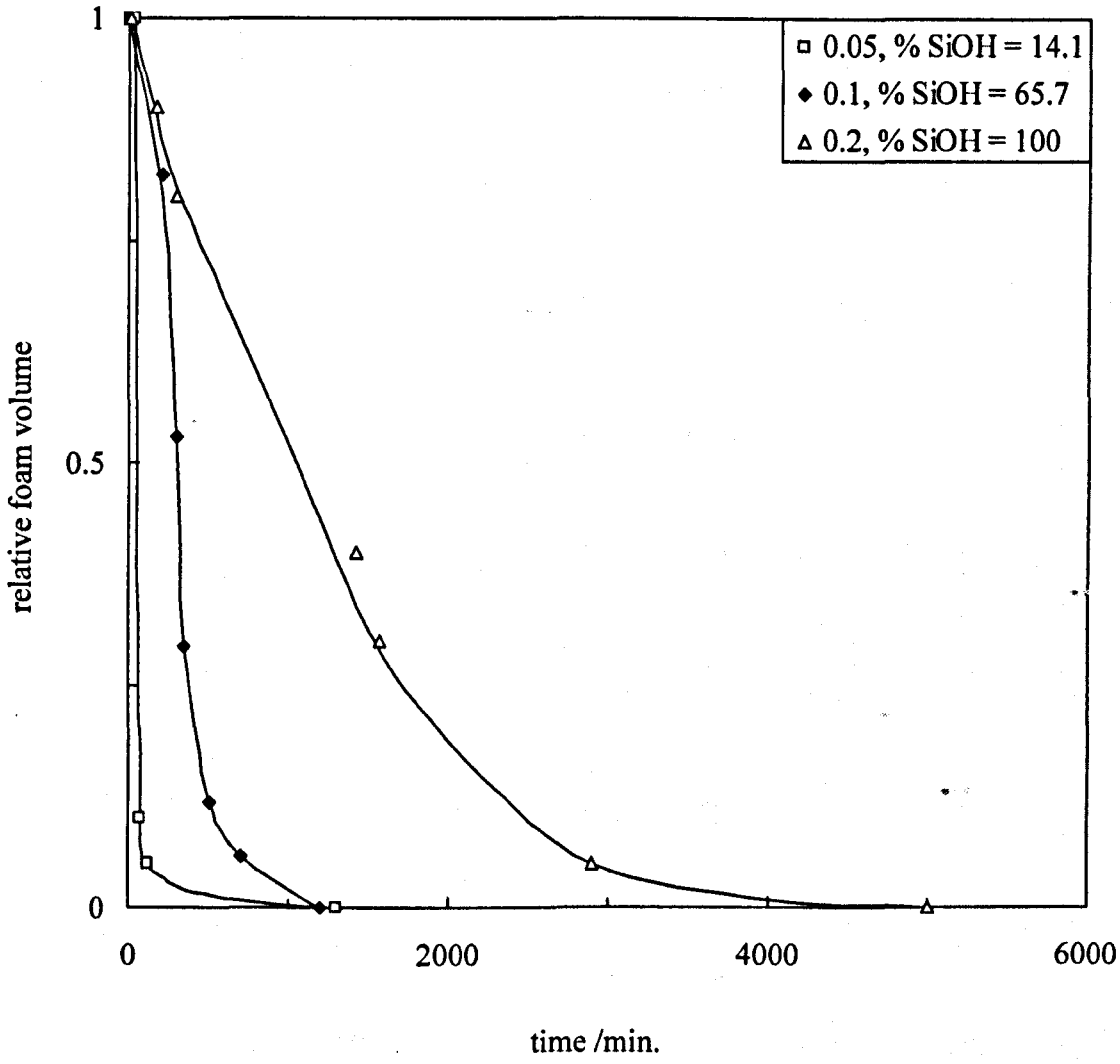

Figure 5.16 Relative foam volume (foam volume at time t / initial foam volume) as a function of time after generation for foam of low stability (open squares), intermediate stability (filled diamonds) and high stability (open triangles). Numbers show the particle concentration and % SiOH on the silica surface. The foams were created by shaking 20.0 cm^3 of aqueous $C_{12}E_5$ (1 mM) containing dispersed silica particles in a stoppered measuring cylinder. All of the measurements were made at ambient temperature.

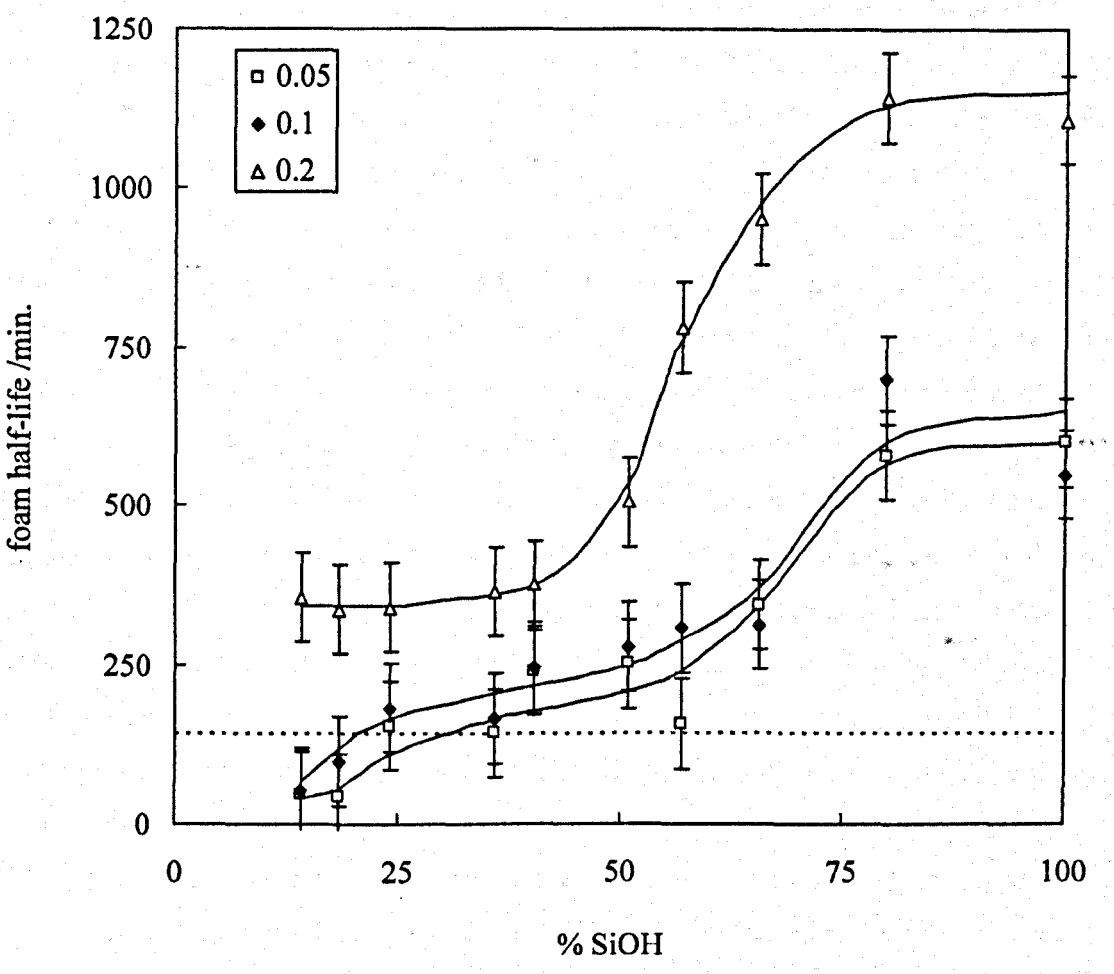

Figure 5.17 Foam half-life of 20.0 cm^3 of aqueous $C_{12}E_5$ (1 mM) containing dispersed silica particles (0.05, 0.1 and 0.2 wt. %) as a function of % SiOH on the particle surfaces. The horizontal dashed line shows the half-life of aqueous $C_{12}E_5$ in the absence of dispersed silica particles. All of the measurements were made at ambient temperature.

foam with half-lives approximately equal to the no particle case. Particles dispersed at 0.2 wt. % stabilise the foam relative to the solution containing no particles, regardless of their % SiOH contents. The maximum enhancement in stability caused by the introduction of silica particles is around a factor of 9. At a SiOH content of between 50 and 60 %, there is a dramatic increase in foam stability for all of the particle concentrations. There is no further increase in stability beyond a SiOH content of about 80 %. There appears to be little difference in the foam stability profiles between the 0.05 and 0.1 wt. % dispersions, i.e. the curves can be superimposed within experimental uncertainty. On increasing the dispersion concentrations from 0.1 to 0.2 wt. % however, there is a significant increase in foam stability for a given % SiOH content. One possible explanation for the observed differences in stability is the location within the foam where the particles reside. Particles with a high % SiOH are more hydrophilic and therefore have a higher tendency to reside in the aqueous liquid phase contained within the Plateau border region of the foam. The Plateau borders act as a drainage network throughout a foam. As the liquid drains from the foam under the force of gravity (and eventually capillary pressure) the foam films thin until they reach a critical thickness. Further thinning causes film rupture and subsequent collapse of the foam. Therefore, any retardation of this liquid flow will promote increased foam stability. It is possible that the hydrophilic particles partially block these drainage channels (due to their location) and increase liquid drainage times. The more hydrophobic particles may adsorb to the liquid-vapour interface and have less of an effect on foam stability because they impede liquid drainage less, (Figure 5.18). This will be reflected in a lower overall foam stability, which has been shown experimentally. It should be noted here however, that $C_{12}E_5$ adsorption onto the particles renders them hydrophilic. It remains to be seen whether the particles exhibit a range of hydrophilicities as a function of their initial % SiOH content after the adsorption of nonionic surfactant in which case there could be differences as to where the particles reside in a foam), or whether their wettabilities have been made equal by the adsorption of the surfactant.

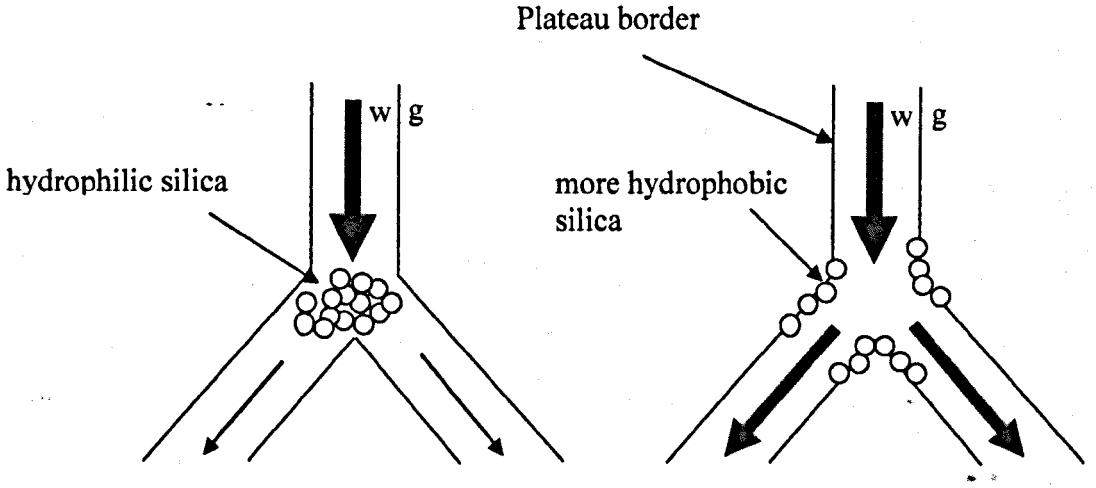

Figure 5.18 Possible fates of particles in surfactant foam films. The left diagram shows a way in which hydrophilic silica particles may act to retard liquid drainage within a Plateau border. The right diagram shows how more hydrophobic silica particles may be adsorbed at the air-water surface and retard liquid drainage less.

5.7 Fixing the equilibrium surfactant concentration in the presence of particles

In order to investigate the idea that particles stabilise foam by residing in the Plateau borders retarding drainage and reduce the foamability by depleting surfactant and lowering the concentration, experiments were carried out in the presence and absence of particles where the equilibrium surfactant concentrations were the same in both cases. In this way, differences observed in stability can be attributed solely to the particles hydrophobicities and not to differences in surfactant concentration induced by particles with different % SiOH on their surfaces. These experiments were also designed to show if there are any differences in the hydrophobicities of particles containing adsorbed surfactant. If there are no differences in foam stabilitiy as a function of the initial % SiOH present on the particles in these experiments, then it shows that the particles add stability to the foam (possibly by retarding drainage) but the differences observed for different % SiOH values for a particular particle concentration are due to bulk surfactant concentration differences not the position of the particles in the foam due to their possible differing hydrophobicities after the adsorption of surfactant.

5.7.1 Shake test measurements

Figure 5.19 shows that the addition of silica particles does not change the foamability of the surfactant when the residual surfactant concentration is the same. The addition of particles does, however, increase foam stability. As discussed earlier, this could be due to the particles residing in the Plateau borders of the foam and restricting liquid drainage thus retarding the thinning of the foam films.

Figure 5.20 reinforces the observation that foamability depends on the residual surfactant concentration which is not adsorbed on the silica. The foam stability is approximately the same for both the 100 % and 79.9 % SiOH silica but is seen to decrease when particles containing 65.7 % SiOH are present. This qualitatively follows the same trend as for the systems shown in Figure 5.17, where the foam stabilities are indistinguishable for 79 and 100 % SiOH coverage but decrease for 65.7 % SiOH. The data therefore suggests that the particles with higher % SiOH

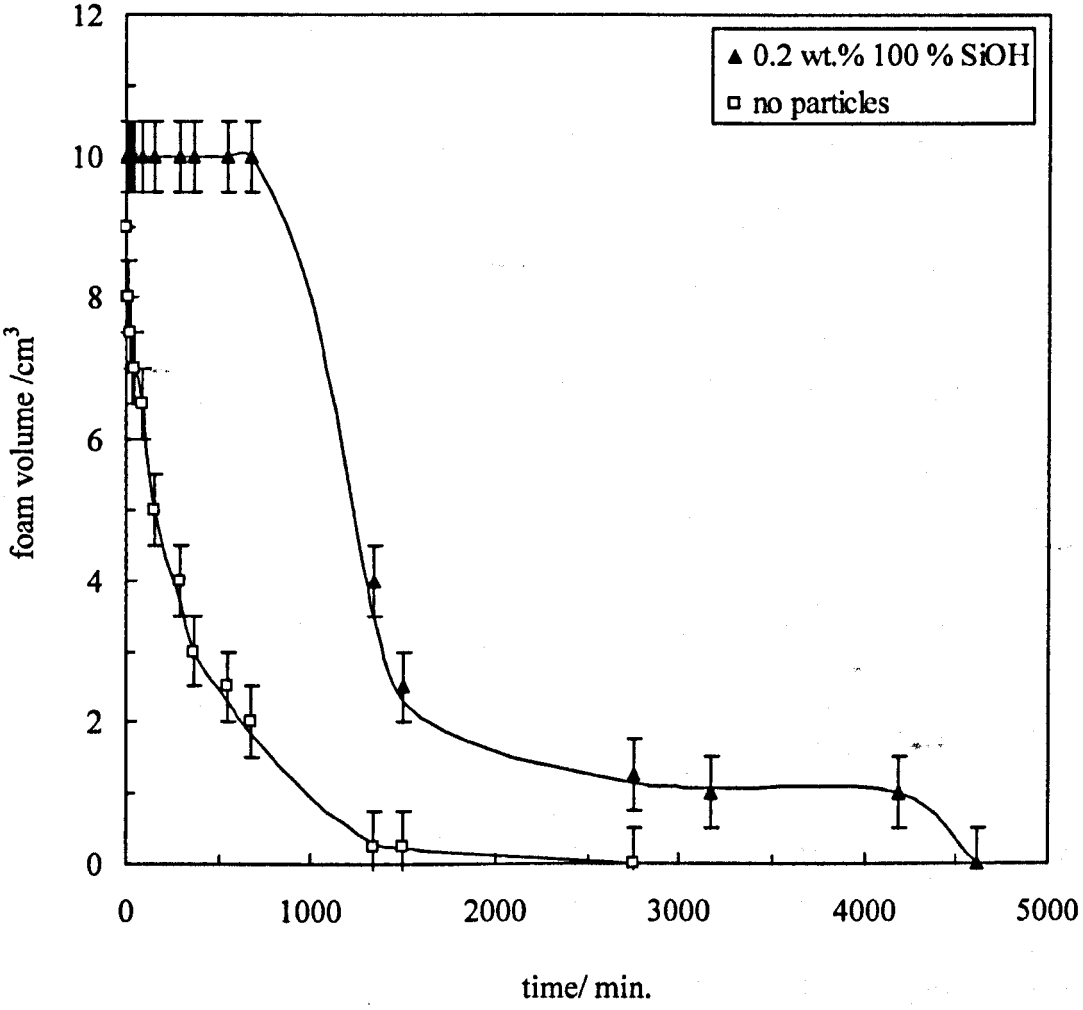

Figure 5.19 Foam volume as a function of time for 20.0 cm^3 of $C_{12}E_5$ with and without dispersed silica. Overall $[C_{12}E_5]$ = 4.11 x 10^{-5} M (open squares) and $[C_{12}E_5]$ = 7.03 x 10^{-4} M (filled squares). Surface tension of both systems = 34.13 mN m^{-1} corresponding to $[C_{12}E_5]_{eq}$ = 4.11 x 10^{-5} M. All of the measurements were made at ambient temperature.

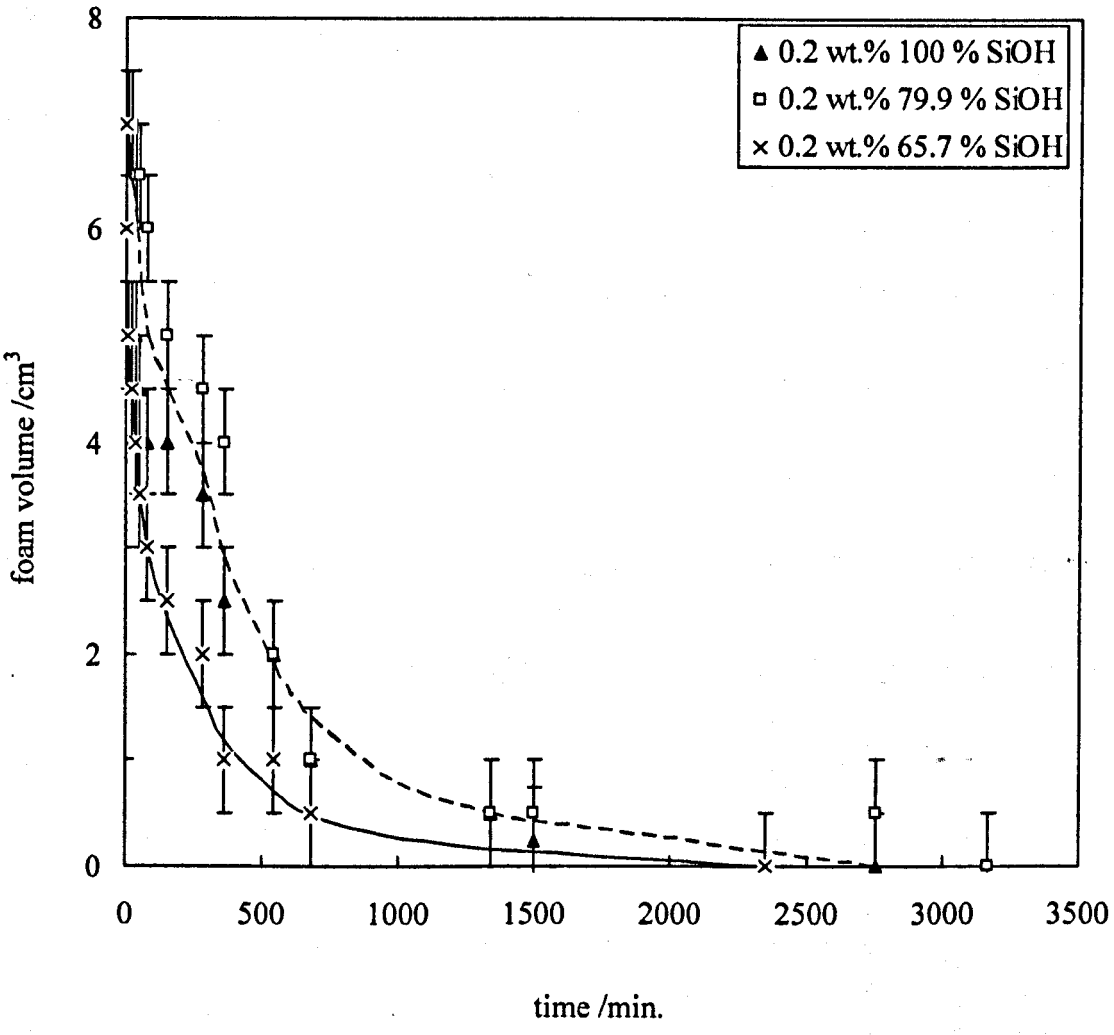

Figure 5.20 Foam volume as a function of time for 20.0 cm^3 of $C_{12}E_5$ with dispersed silica particles present. Overall $[C_{12}E_5] = 7.49 \times 10^{-5}$ (filled triangles), $[C_{12}E_5] = 2.86 \times 10^{-4}$ M (open squares) and $[C_{12}E_5] = 3.8 \times 10^{-4}$ M (crosses). The solid line is a guide for the eye for silica with 65.7 % SiOH on its surface and the dashed line is a guide for the eye for silica with 79.9 and 100 % SiOH on their surfaces. Surface tension of all systems = 41.1 mN m^{-1} corresponding to $[C_{12}E_5]_{eq} = 2.09 \times 10^{-5}$ M. All of the measurements were made at ambient temperature.

coverages stabilise foams more than particles with lower % SiOH coverages because they are more hydrophilic and therefore block the Plateau borders more. This also indicates that adsorbing $C_{12}E_5$ onto the surfaces of the various silica particles does not completely normalise their wettabilities (although hydrophobic particles are rendered more hydrophilic). The fact that in Figure 5.17 surfactant concentration increases with % SiOH on the particle surfaces for a fixed particle concentration (due to lower adsorption), may also contribute to the fact that foam stability increases with % SiOH. The foamability of the systems in Figure 5.20 is less than in those of Figure 5.14 because of the lower free surfactant concentration available in the former.

5.7.2 Foam column measurements

Having measured foamability and foam stability for systems with equivalent equilibrium surfactant concentrations with shake tests, it was decided to make measurements of a similar nature using the foaming column. Figure 5.21 shows the foam volume after 10 minutes as a function of bulk surfactant concentration with and without silica particles (% SiOH = 100) dispersed at 0.2 wt. %. The "[C12E5]eq" data series refers to the residual concentrations of surfactant obtained in the presence of particles i.e. the equilibrium surfactant concentration.

In the presence of particles one may expect the foamability curve to be displaced to the right showing that to produce the same volume of foam in the presence of particles, a higher concentration of surfactant would be required than to produce the same volume of foam in the absence of particles. This is expected because a higher concentration of surfactant is required to attain the same equilibrium surfactant concentration in the presence of silica particles than in the absence of them (due to adsorption).

When the surfactant concentrations are converted to equilibrium surfactant concentrations, to allow for the reduction in concentration due to the dispersed particles, the foam volumes produced after 10 minutes for a particular equilibrium surfactant concentration (in the presence of particles) were expected to be the same as the volume produced using the same surfactant concentration in the absence of

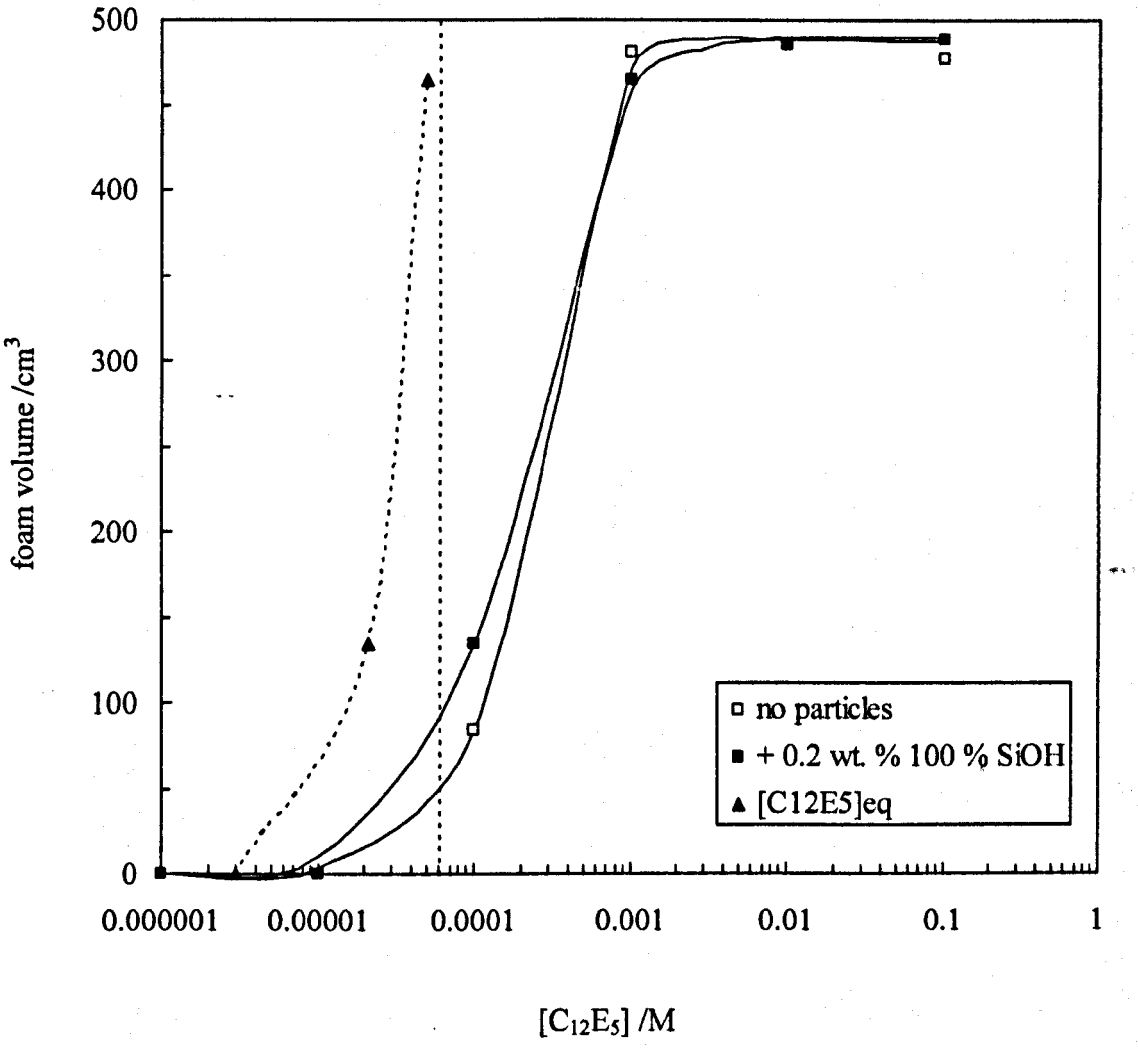

Figure 5.21 Comparison of foamabilities for $C_{12}E_5$ alone and with silica (% SiOH = 100) dispersed at 0.2 wt. %. Foam created by sparging N_2 gas through 15.0 cm^3 of surfactant solution at a flow rate of 48 cm^3 min^{-1} for 10 minutes. The "[C12E5]eq" series shows the equilibrium surfactant concentration in the presence of silica particles calculated using Figure 5.11. The horizontal dashed line shows the cmc of pure $C_{12}E_5$. All of the measurements were made at 20.0 °C.

particles. This is clearly not the case. It is known from the foam stability work that dispersed silica particles can stabilise the foam. In the absence of particles at sufficiently low surfactant concentrations, a small amount of foam is made, but this is unstable and breaks. After 10 minutes of foaming, the foam volume is recorded as 0. If the presence of dispersed particles enhances the stability of this unstable foam, then after 10 minutes a certain volume of foam may persist at this concentration in the presence of particles (even though the concentration of surfactant is slightly lower due to adsorption). Thus, the particles are not enhancing the foamability of the surfactant, but they are stabilising the foam as it is being made. On the foam column this can deceptively appear as an enhancement in foamability but it should be remembered that over a 10 minute foaming period, there will inevitably be breaking of the foam as it is being created. This breaking will occur more readily in the absence of dispersed silica particles.

Figure 5.22 shows the half-life values associated with the foams created. It can be seen that there is a concentration of surfactant in the absence of particles where there is a large increase in foam stability. In the presence of dispersed silica particles, the half-life of each foam is seen to increase relative to the no particle case. The "[C12E5]eq" data series shows the equilibrium surfactant concentration calculated by considering the adsorption of surfactant onto the silica particle surfaces. Higher surfactant concentrations in the plateau region of the series cannot be corrected because they all give constant surface tensions (of the order of 30 mN m^{-1} or so).

5.8 Foamability of aqueous $C_{12}E_5$-silica dispersions in the presence of electrolyte

The effect of adding electrolyte to the initial surfactant solution before dispersing the silica was investigated. Adding NaCl to aqueous $C_{12}E_5$ lowers the cloud point of the solution. At 0.1 M NaCl, this reduction in cloud point is only 1 – 2 °C, which is still well above room temperature and so addition of salt at this concentration will have no effect on the foamability of an aqueous solution $C_{12}E_5$ containing no additives. The addition of salt could however change the foaming of silica particle-surfactant dispersions by reducing the charge on the particles. This may cause dispersed particles to adsorb at the air-water surfaces. They may then co-adsorb with the

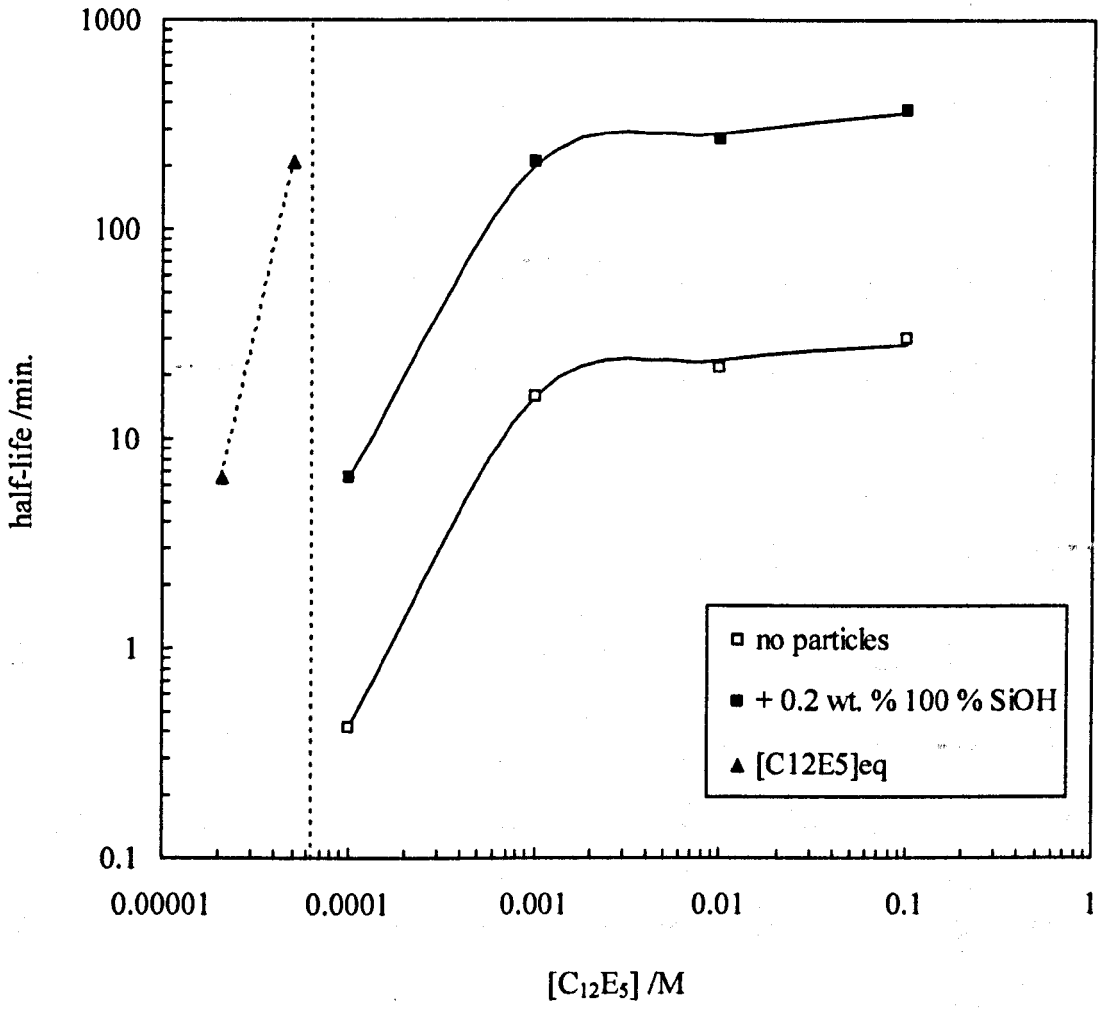

Figure 5.22 Foam half-life time as a function of surfactant concentration with and without dispersed silica particles. Foam created by sparging N_2 gas through 15.0 cm^3 of $C_{12}E_5$ at a flow rate of 48 cm^3 min^{-1} for 10 minutes. The "[C12E5]eq" series shows the equilibrium surfactant concentration in the presence of silica particles calculated using Figure 5.11. The horizontal dashed line shows the cmc of pure $C_{12}E_5$. All of the measurements were made at 20.0 °C.

surfactant which could change the foamability of the system. This postulation is reinforced by recent findings from Paunov et al. who have found that the addition of salt to a silica suspension causes depletion of the silica. This depletion increases with salt concentration and particle contact angle.[32]

Referring to Figure 5.23, it can be seen that adding salt to this particular system does not change its foamability to any noticeable degree and added salt causes no apparent coagulation of any of the dispersions. This finding supports the idea that the foamability of the $C_{12}E_5$-silica dispersions depends on the level of surfactant depletion from the solution as opposed to the location of the particles within the foam.

5.9 Foaming properties of charged surfactants

5.9.1 Charged surfactant adsorption onto silica

In order to try and isolate changes in foaming induced by dispersed particles causing surfactant depletion, it was decided to make some foaming measurements on SDS and DTAB in the absence and presence of dispersed silica particles. The reason for choosing SDS is because it is an anionic surfactant and due to the negative charge on its headgroup, it is not expected to adsorb significantly onto silica surfaces (silica surfaces are also negatively charged at pH > 2.5). Any changes in foamability or foam stability arising from the addition of silica particles are therefore induced by the silica particles acting via another mechanism. DTAB is a cationic surfactant and is expected to adsorb strongly onto the surface of silica due to the positive charge on its headgroup.

Figures 5.24 – 5.27 show TEMs of when silica particles dispersed in SDS and DTAB above and below the cmc of each are deposited onto a carbon coated Cu/Pd mesh. It can be seen that the silica particles appear to form networks regardless of the surfactant type or concentration. The TEMs are effectively indistinguishable from those obtained when depositing $C_{12}E_5$-silica dispersions onto the mesh (Figures 5.2 – 5.5).

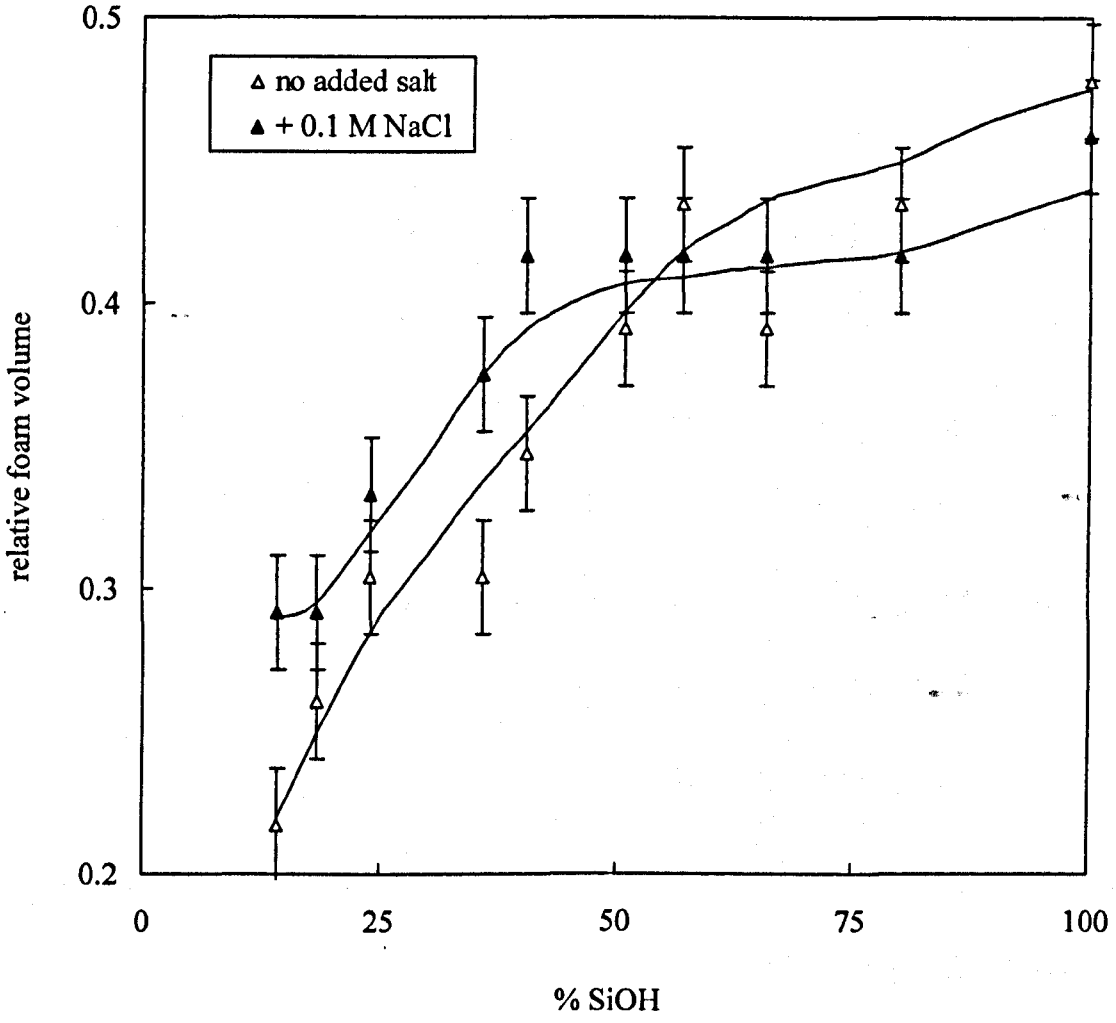

Figure 5.23 Relative foam volume of 20.0 cm^3 aqueous $C_{12}E_5$ (1 mM) as a function of % SiOH on particle surfaces (0.2 wt. %) in the absence a presence of added electrolyte. All of the measurements were made at ambient temperature.

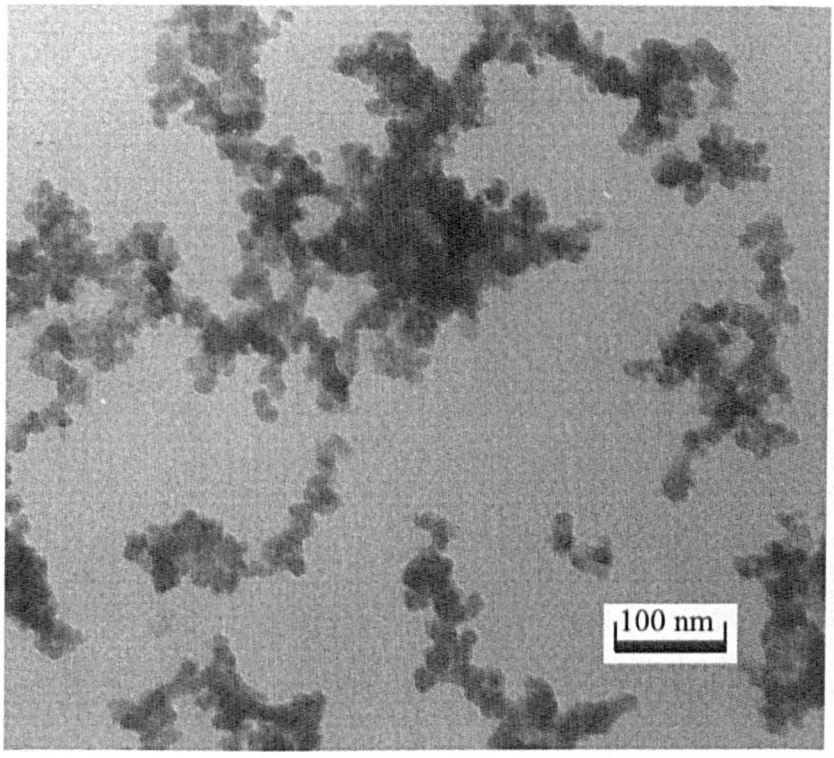

Figure 5.24 Transmission electron micrograph (TEM) of a carbon-coated Cu/Pd grid with silica particles deposited by evaporation from a solution composed of 0.2 wt. % silica (100 % SiOH) dispersed in 4.0×10^{-4} M SDS. The scale bar is shown in the Figure.

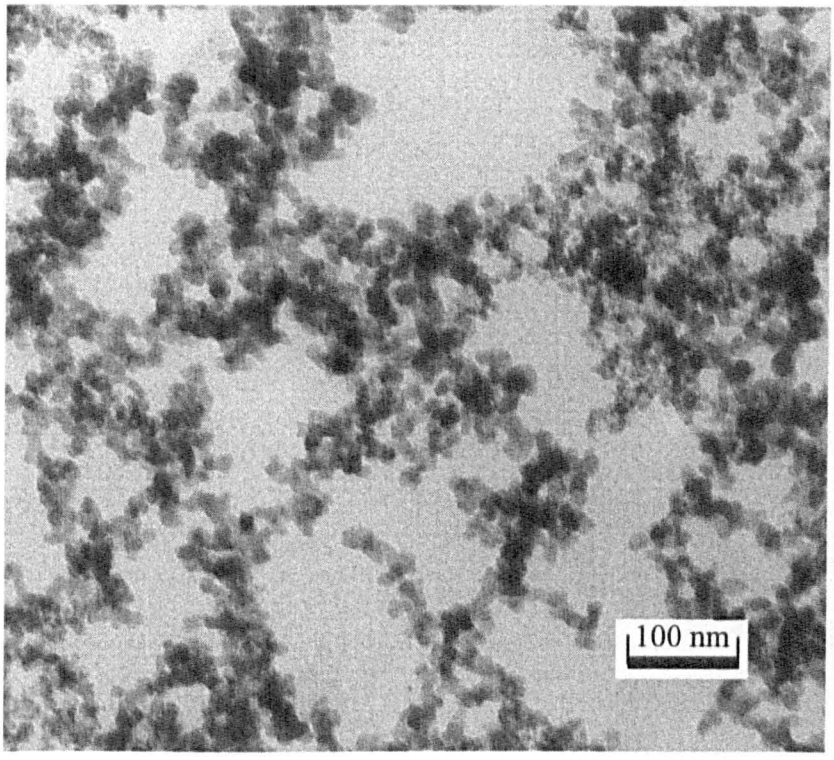

Figure 5.25 Transmission electron micrograph (TEM) of a carbon-coated Cu/Pd grid with silica particles deposited by evaporation from a solution composed of 0.2 wt. % silica (100 % SiOH) dispersed in 1.6×10^{-2} M SDS. The scale bar is shown in the Figure.

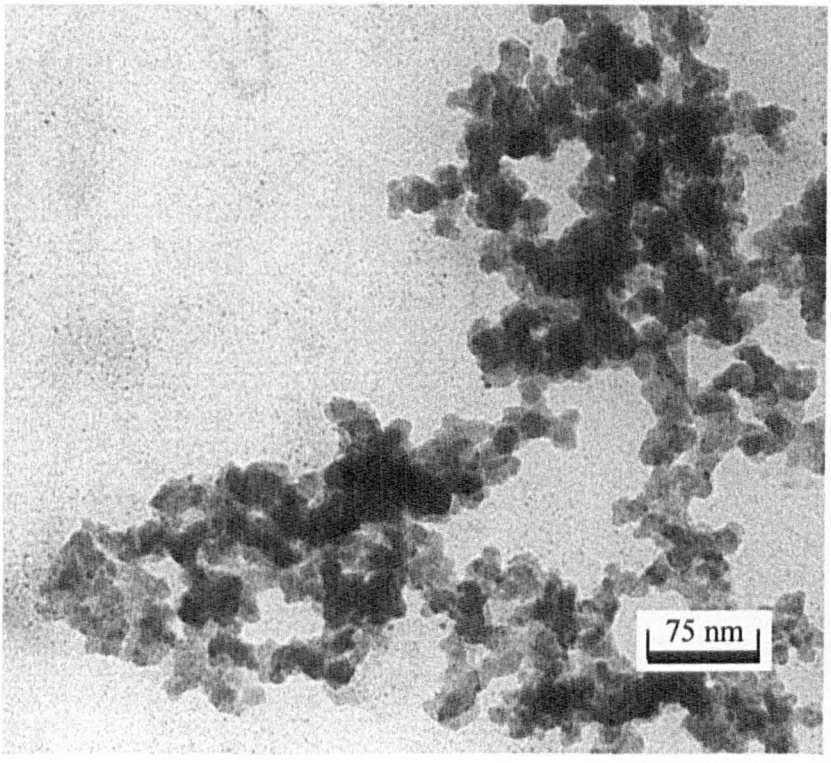

Figure 5.26 Transmission electron micrograph (TEM) of a carbon-coated Cu/Pd grid with silica particles deposited by evaporation from a solution composed of 0.2 wt. % silica (100 % SiOH) dispersed in 7.5 x 10^{-3} M DTAB. The scale bar is shown in the Figure.

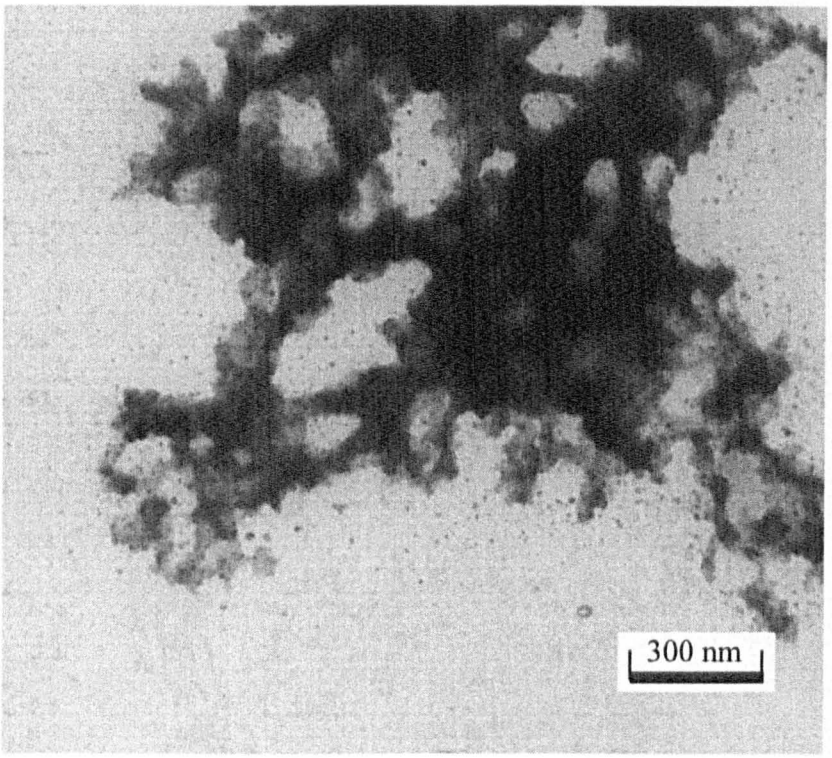

Figure 5.27 Transmission electron micrograph (TEM) of a carbon-coated Cu/Pd grid with silica particles deposited by evaporation from a solution composed of 0.2 wt. % silica (100 % SiOH) dispersed in 3.0 x 10^{-2} M DTAB. The scale bar is shown in the Figure.

Before undertaking any foaming measurements it was decided to verify that SDS will not significantly adsorb onto the surfaces of silica. The surface tensions of SDS above and below the cmc were measured both with and without silica particles dispersed at 0.2 wt. %. Below the cmc surface tensions are similar. Above the cmc however, there appears to be an increase in surface tension. This increase is at its greatest when the lower % SiOH silica is dispersed. This indicates that SDS may in fact slightly adsorb onto the surface of the silica particles above the cmc. See Table 5.1 for the results of this experiment.

Table 5.1 Surface tensions of pure SDS surfactant solutions and SDS-silica dispersions measured above and below the cmc. All measurements made at 20.0 °C, and all tensions in mN m^{-1}.

	No particles	**+ 0.2 wt. % 79.9 % SiOH**	**+ 0.2 wt. % 100 % SiOH**
0.004 M (= cmc /2)	41.5	44.0	41.5
0.016 M (= cmc x 2)	34.1	38.4	35.2

5.9.2 Foamability and foam stability of SDS

Figure 5.28 shows the foamability of SDS solutions above and below the cmc of 8 mM. When making measurements on this system, it was found that 10.0 cm^3 of 0.004 M SDS produced foam containing fairly coarse bubbles at the top (diameter of 10 mm or so). When the coarse bubbles ruptured, a large volume of foam was lost immediately. This caused difficulties in reproducing foamability measurements. The shake tests carried out at the higher concentration (0.016 M) produced foam with small bubbles and so the problem of catastrophic foam collapse was avoided. Above the cmc the addition of particles always reduces the foamability of SDS. This is the same general observation seen for $C_{12}E_5$. In the case of $C_{12}E_5$, 0.2 wt. % 100 % SiOH silica gives the largest foam volume for silica-containing systems. For foam stabilised by SDS, the 100 % SiOH dispersion gives the lowest foam volume. Below the cmc of SDS (0.004 M), the foamability is also generally reduced in the presence

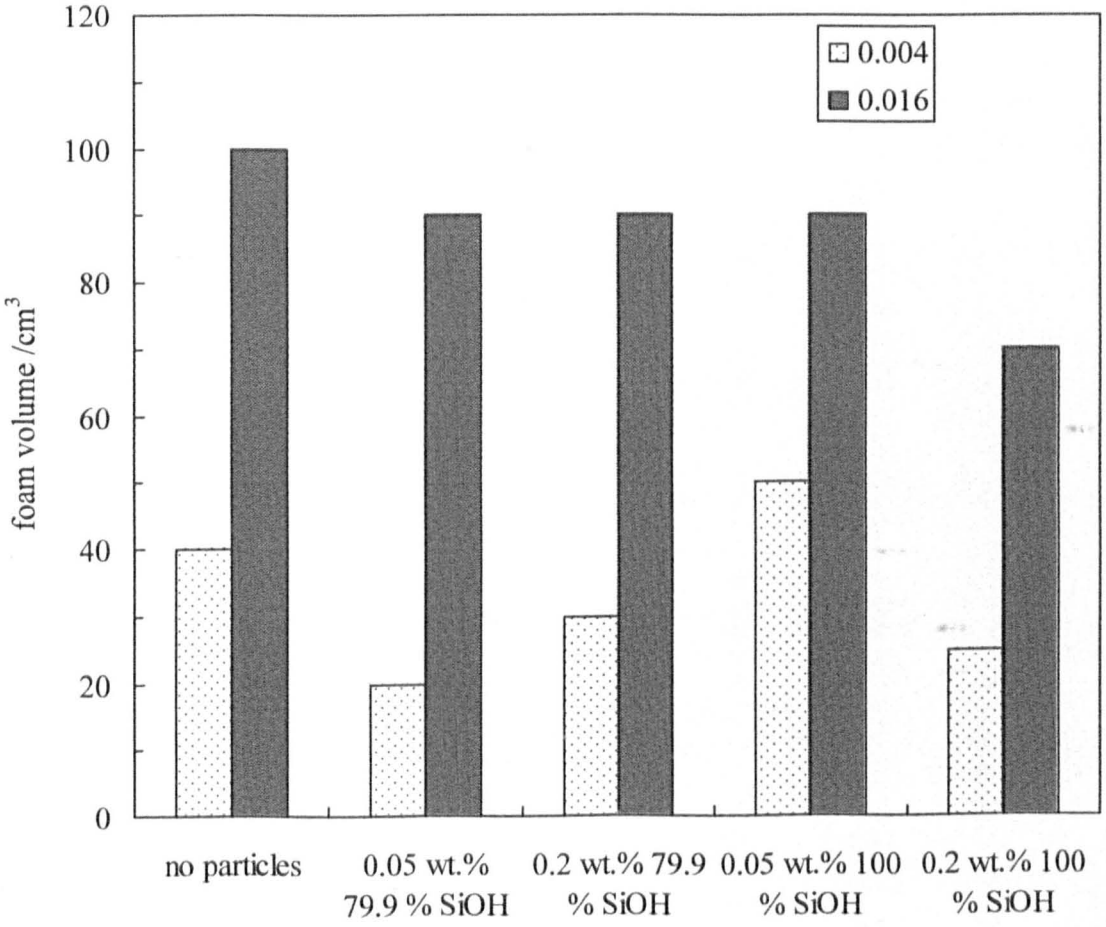

Figure 5.28 Initial foam volume of SDS solutions versus dispersion type. Foam created by shaking 10.0 cm^3 of dispersion in a 100 cm^3 stoppered measuring cylinder. Numbers in the legend show the concentrations of SDS used in M. All of the measurements were made at ambient temperature.

of particles although there is a single exception (0.05 wt. % 100 % SiOH silica). Due to the problems with forming coarse foam explained above these results should be treated with caution. However, the overall trend is that silica particles slightly reduce the foamability of SDS.

We now consider the stability of foam stabilised by SDS both above and below the cmc (Figure 5.29). The higher concentration of SDS always produces more stable foam both in the absence and presence of dispersed silica particles. The particle concentration appears to be the most important factor in dictating the overall stability of the foam. The 0.2 wt. % silica dispersions stabilise the foam relative to the no particle case above and below the cmc. This trend is also observed for $C_{12}E_5$. When silica containing 79.9 and 100 % SiOH is dispersed at the lower concentration of 0.05 wt. % the foam becomes less stable relative to the no particle case. For $C_{12}E_5$, silica particles with 79.9 and 100 % SiOH on their surfaces stabilised the foam relative to the pure surfactant case regardless of their concentration and so SDS behaves differently to $C_{12}E_5$ in this respect. Silica particles of high hydrophilicity > 79.9 are capable of destabilising the foam. Only very hydrophobic particles (SiOH < 20 %) dispersed at 0.05 wt. % destabilised $C_{12}E_5$ foams.

5.9.3 Foamability and foam stability of DTAB

In order to obtain foam volumes below 100 cm^3 in the stoppered measuring cylinders, the initial volume of DTAB had to be reduced to 7.0 cm^3. After repeating the measurements, it became clear that the experiments were irreproducible. Figure 5.30 shows the deviation between two runs of the same experiment where the concentration of DTAB was approximately half that of its cmc (15 mM). It can be seen from Figure 5.30 that both the foamability and the foam stability are very different between two runs. The reason that these experiments were very difficult to repeat was because even small deviations in the initial surfactant volume caused very large differences in the total volume of foam produced (due to DTAB's high foamability).

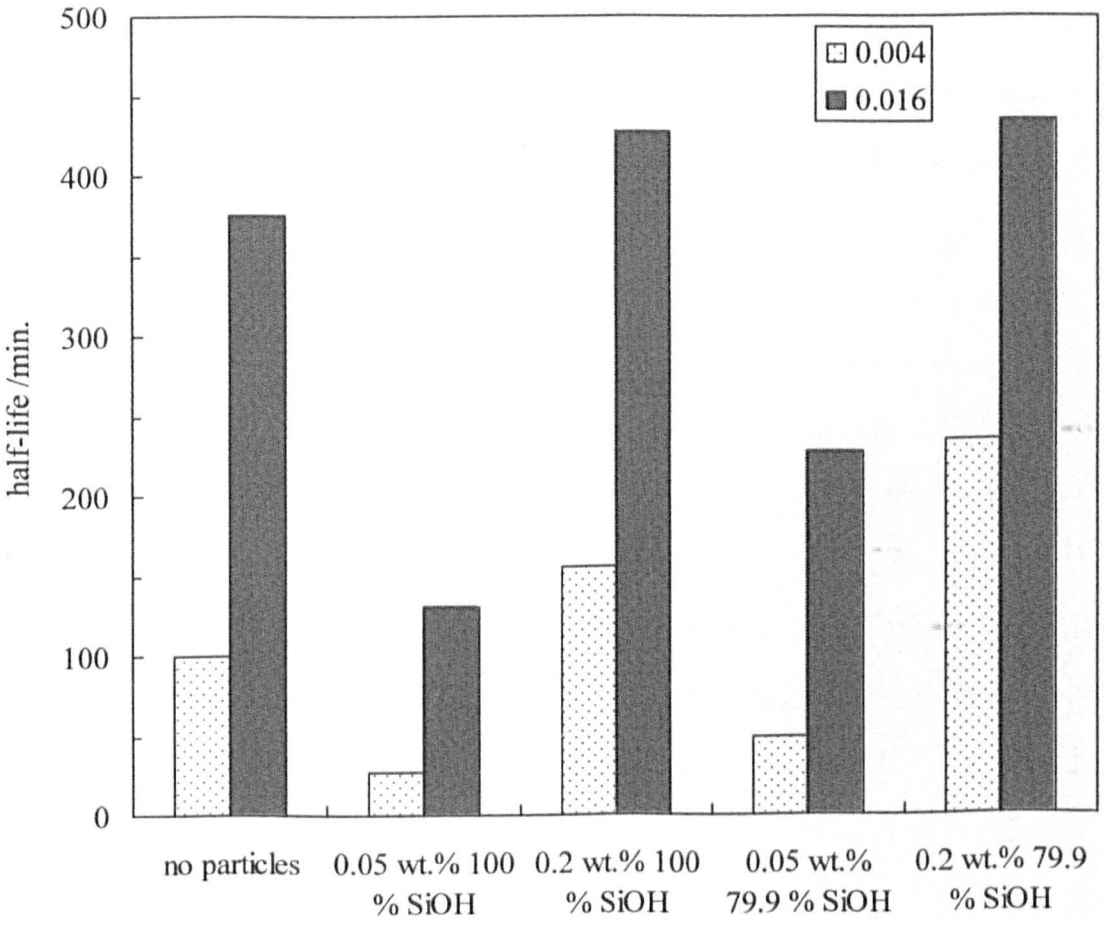

Figure 5.29 Foam stability of SDS solutions versus dispersion type. Foam created by shaking 10.0 cm^3 of dispersion in a 100 cm^3 stoppered measuring cylinder. Numbers in the legend show the concentration of SDS used. All of the measurements were made at ambient temperature.

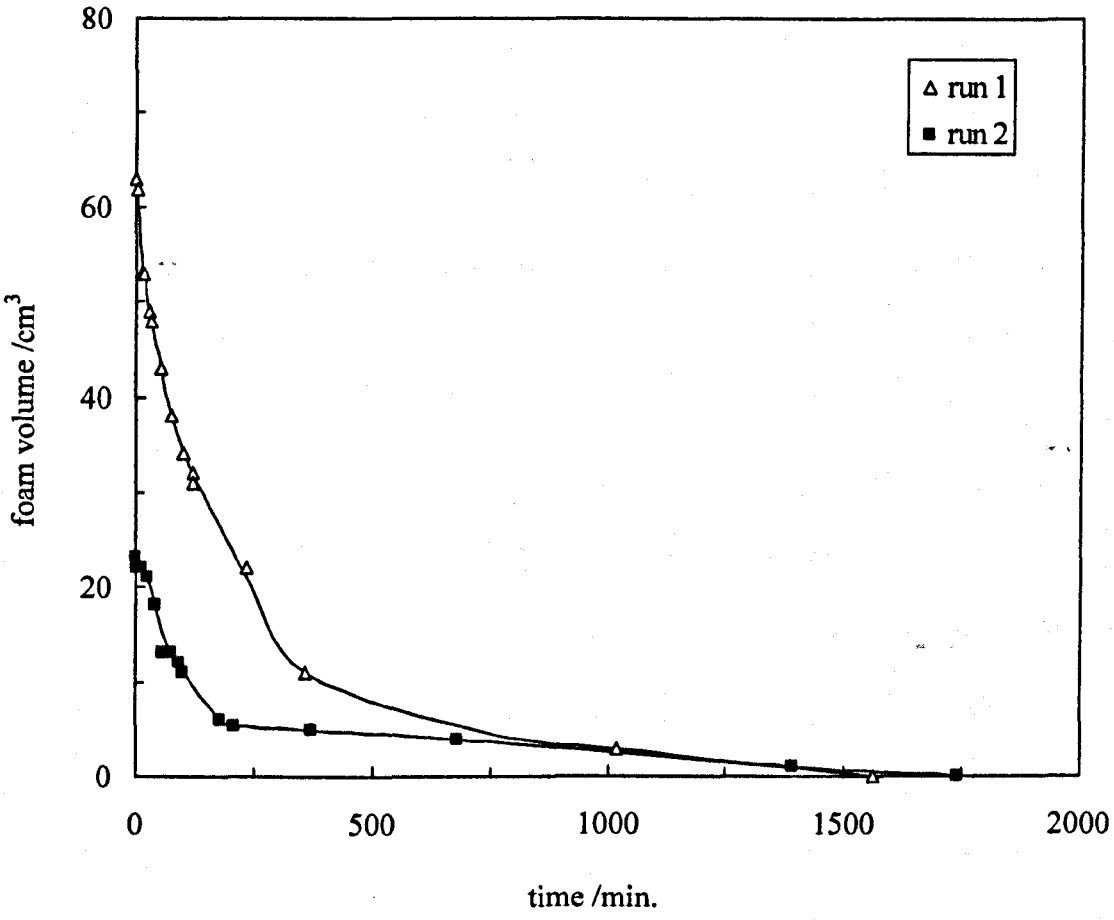

Figure 5.30 Foam volume as a function of time for 7.5 x 10^{-3} M DTAB in the absence of particles. Foam created by shaking 7.0 cm^3 of surfactant in a 100 cm^3 stoppered measuring cylinder. All of the measurements were made at ambient temperature.

Figure 5.31 shows that even slightly above the cmc, 2 runs of the same experiment do not agree. The reasons for the irreproducibility are the same as described above. It should be noted that for 1 run of a particular experiment, silica particles did seem to boost the foamability of the surfactant. In the next section, a comparison between the three classes of surfactant is carried out at fixed surfactant concentrations and this proves to be the case.

5.10 Comparison of the foaming properties of $C_{12}E_5$, SDS and DTAB

Since differences in the foaming behaviour of SDS and DTAB in the absence and presence of particles exist, it was decided to compare the foamabilities and foam stabilities of $C_{12}E_5$, SDS and DTAB using the same concentrations and initial surfactant volumes. As shake test data for 20.0 cm^3 of 1 mM of $C_{12}E_5$ had been collected previously it was decided to fix these two parameters for SDS and DTAB. This also meant that the DTAB experiments were less susceptible to the large errors induced by the high dependency of foam volume on the initial surfactant concentration which was observed at lower surfactant concentrations.

5.10.1 Foamability

Figure 5.32 shows the foamability of the three classes of surfactants (nonionic, cationic and anionic) in the absence and the presence of silica particles dispersed at two different concentrations (0.05 and 0.2 wt. %). The foamability of SDS is slightly enhanced in the presence of silica particles containing 79.9 % SiOH on their surfaces. Although the silica containing 79.9 % SiOH on its surface results in more foam being formed than when silica containing 100 % SiOH on its surface is used (reinforcing previous findings, see Figure 5.28) the overall effect is different because an enhanced foamability is observed relative to the no particle case. It should be noted however, that the concentration at which these experiments were carried out at are lower than those in Figure 5.28 and so there may be valid reasons why this increase in foamability is seen at lower concentrations of SDS in the presence of particles.

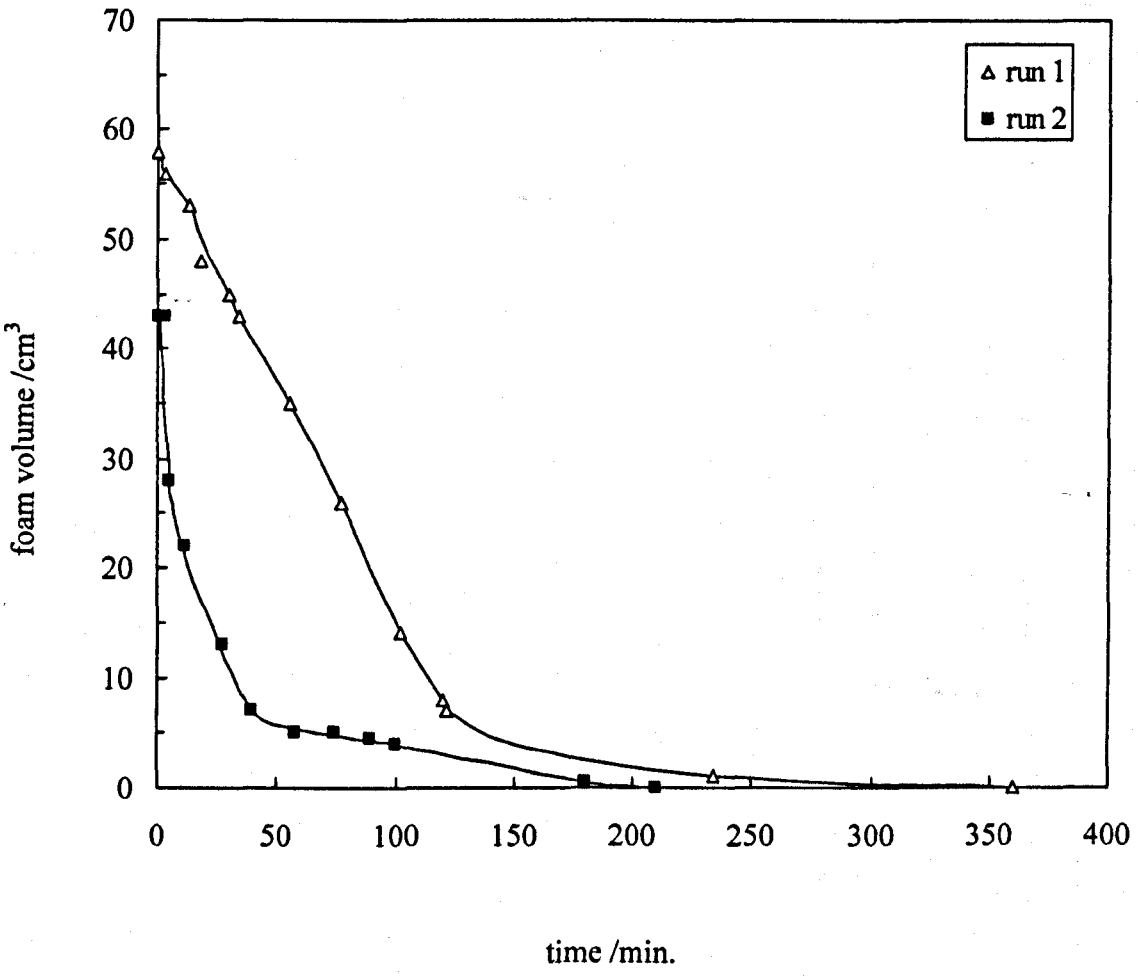

Figure 5.31 Foam volume as a function of time for 3 x 10^{-2} M DTAB in the absence of particles. Foam created by shaking 7.0 cm^3 of surfactant in a 100 cm^3 stoppered measuring cylinder. All of the measurements were made at ambient temperature.

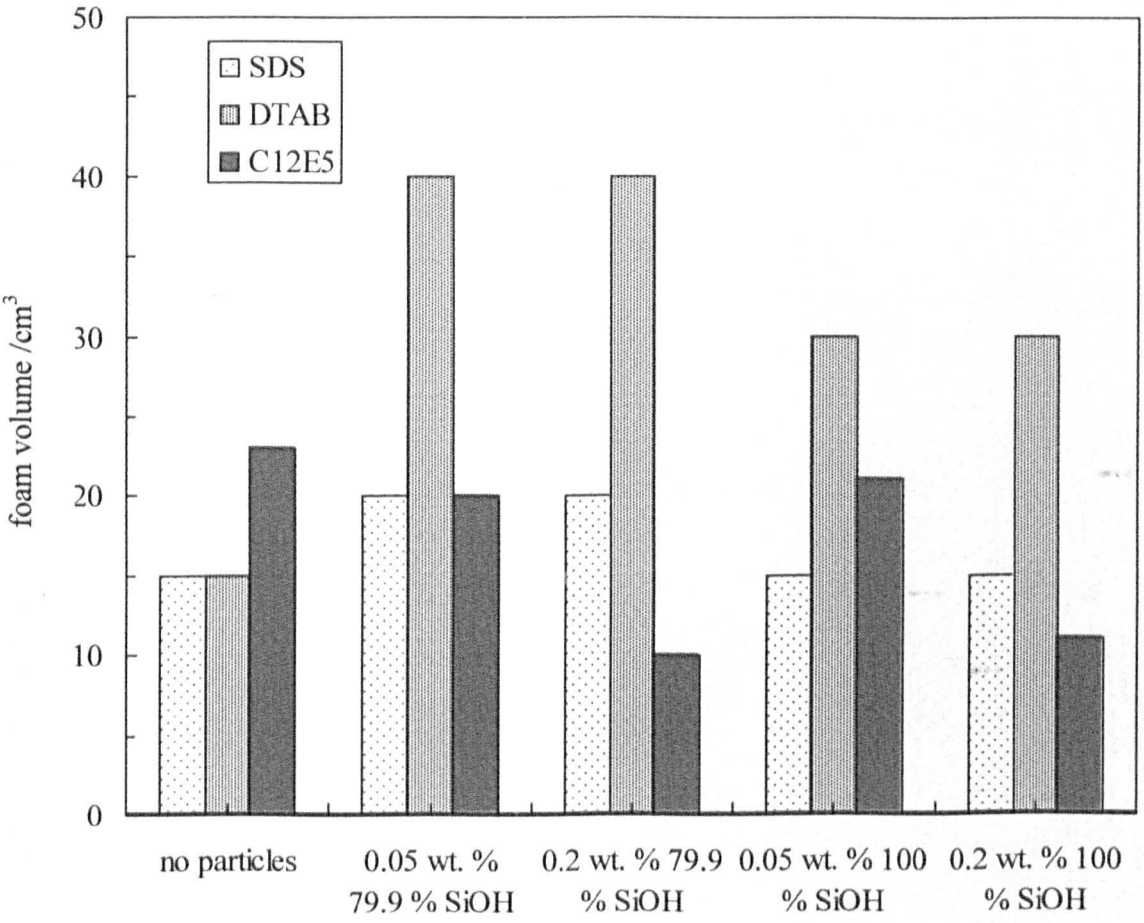

Figure 5.32 Initial foam volume versus dispersion type using 1 mM of each surfactant ($C_{12}E_5$, SDS, DTAB). Foam created by shaking 20.0 cm^3 of the dispersion in a 100 cm^3 stoppered measuring cylinder. All of the measurements were made at ambient temperature.

The foamability of DTAB follows a very different trend to that of $C_{12}E_5$ in that foamability is always increased in the presence of particles. The maximum volume of foam is produced when the 79.9 % SiOH silica is dispersed in the surfactant solution and in there are no differences in foamability induced by changing the concentration of dispersed particles. Frye and Berg[4] found that the contact angle of solid particles plays a critical role in determining the ability of solid particles to act as anti-foams. They found that the addition of ground glass particles to a solution of cationic, anionic and nonionic surfactant often resulted in no foam being formed. For PDMS-treated spherical glass particles (5 – 50 μm) it was found that at contact angles < 80°, antifoam action was reduced to about 50 %. Antifoam efficiency was reduced further for contact angles of less than this. In their studies, there was no evidence of enhanced foaming of a cationic surfactant (hexadecyltrimethyl ammonium bromide abbreviated to HTAB) by adding glass particles as observed in this study. They stated that the rate at which adsorption equilibrium is attained at the air-liquid surface is an important parameter affecting anti-foam action. If the rate is low, the contact angles occurring during the dynamic process of film formation and drainage will be much larger than the equilibrium contact angle resulting in better film rupturing action than expected. Thus antifoam action will be better for surfactants with slow adsorption kinetics. As discussed previously, dispersing silica particles into a $C_{12}E_5$ surfactant solution may increase the rate of adsorption of surfactant to the air-water interface. It is possible that silica acts as a surfactant reservoir for DTAB and speeds up adsorption times in the same way and preventing them working as antifoams. In addition to this, adsorbing DTAB onto the silica may render the particles more hydrophobic. This will promote them to foam bubble surfaces where they can co-adsorb with the primary surfactant and further enhance foaming. Recently it has been shown that when these silica particles have intermediate % SiOH content on their surfaces, aqueous dispersions can stabilise foam in the absence of any other surface active agent.[33] The results of this study indicate that the particles can adsorb at air-water interfaces providing that the hydrophobicity is of a (critical) intermediate value.

5.10.2 Foam stability

Figure 5.33 shows the differences in foam stability between the 3 different surfactants as judged by their half-life values. The stability of SDS remains approximately the same regardless of particle concentration or % SiOH on the particle surfaces.

When stabilising foam using DTAB, the addition of dispersed silica particles always enhances foam stability. This increase in stability is the greatest for the 0.2 wt. % dispersions. This is the same effect as that observed for $C_{12}E_5$. For a particular concentration of dispersed particles, the 79.9 % SiOH silica gives the most stable foam. For $C_{12}E_5$, differences in foam stability cannot be measured between 79.9 % and 100 % SiOH in a fixed particle concentration regime. The magnitude of the stability increase should also be noted for the DTAB case. In the absence of particles, the foam breaks almost immediately (half-life is less than 1 minute). On the addition of 0.2 wt. % 79.9 % SiOH silica, its half-life is increased to several hundred minutes.

5.10.3 Summary of foaming properties of $C_{12}E_5$, SDS and DTAB

SDS: At concentrations lower than the cmc, foamability is slightly increased by the addition of 79.9 % SiOH silica. Particles dispersed at different concentrations with the same % SiOH on their surfaces have the same effects on foamability. Above the cmc, foamability is always decreased (like $C_{12}E_5$) relative to the no particle case. This decrease in initial foam volume is greater for the 100 % SiOH than the 79.9 % SiOH (the opposite to $C_{12}E_5$). Below the cmc, the foam stability remains largely unaffected by the presence of dispersed silica particles. At higher concentrations, SDS is destabilised by 79.9 and 100 % SiOH silica particles dispersed at 0.05 wt. % and stabilised by 79.9 and 100 % SiOH particles dispersed at 0.2 wt. %.

DTAB: The foamability of DTAB is always increased by the addition of silica particles. This increase is the greatest for the 79.9 % silica dispersions and no difference is observed in increasing the particle concentration from 0.05 to 0.2 wt. % for a particular silica type. The particles may be co-adsorbing with the surfactant resulting in greater foaming. Foam stability is always increased in the presence of

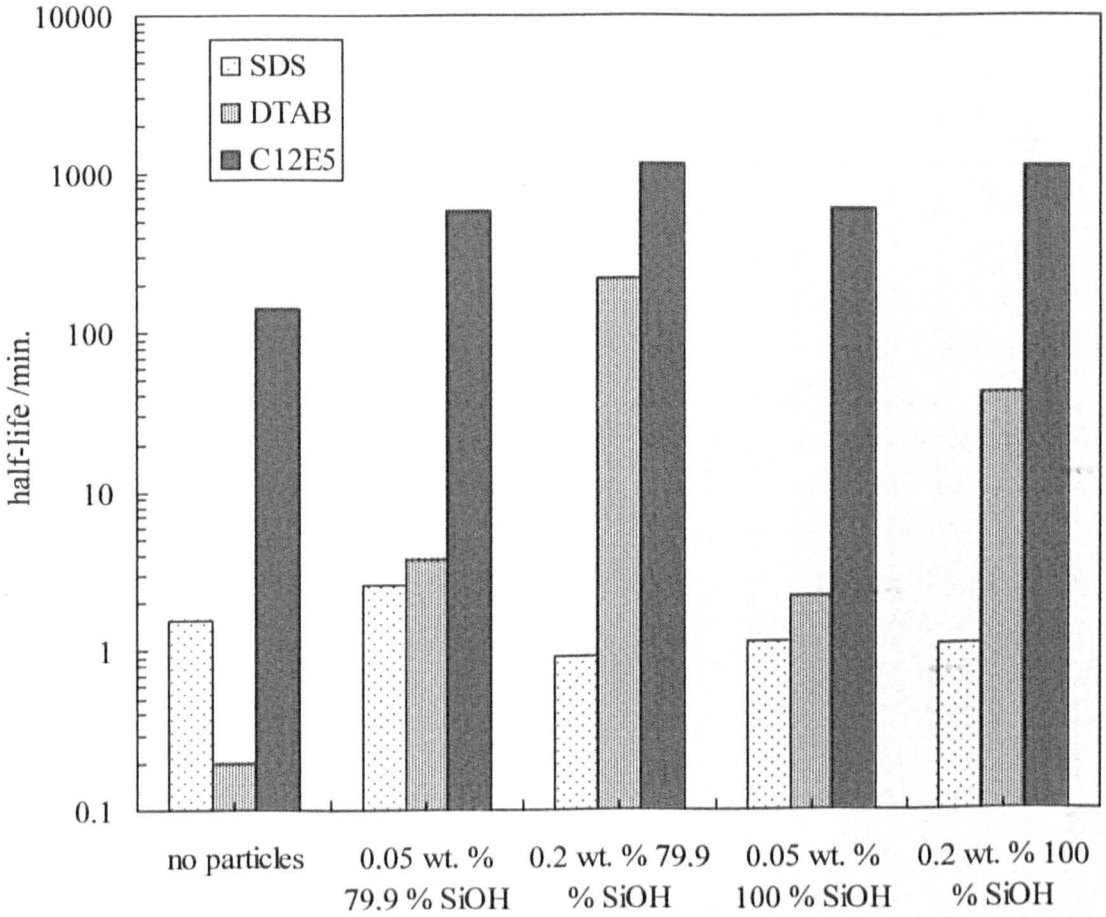

Figure 5.33 Foam half-life versus dispersion type for 1 mM of each surfactant. Foam created by shaking 20.0 cm^3 of foaming solution in a 100 cm^3 stoppered measuring cylinder. All of the measurements were made at ambient temperature.

particles. Particle concentration plays the largest role in determining foam stability and the foam with the highest stability is observed when the 79.9 % SiOH is dispersed at the highest concentration (0.2 wt. %).

From the summary above it can be concluded that hydrophilic particles are probably rendered more hydrophobic by DTAB such that they can co-adsorb with the primary surfactant and increase the foamability. They may also add rigidity to the foam structure by adsorbing in this way leading to enhanced foam stability. This effect was also observed by Johansson et al.[9] for particles of intermediate hydrophobicity. This effect is not observed in the case of $C_{12}E_5$ indicating that the particles probably remain hydrophilic by the adsorption of nonionic surfactant onto their surfaces and influence foamability by surfactant depletion and enhance foam stability by retarding liquid drainage from the foam films. For SDS the story is not as clear. Below the cmc of SDS there is no adsorption of surfactant onto the silica and so surfactant depletion is not an issue. However, foamability is increased for the 79.9 % SiOH silica indicating that there may be some co-adsorption of particles with surfactant at the interface. Above the cmc of SDS there may be some adsorption onto the particle surfaces and foamability is reduced in the presence of particles. This can possibly be attributed to surfactant depletion. Above the cmc SDS is destabilised by 0.05 wt. % particles, which may be due to a combination of surfactant depletion and film drainage not being significantly retarded because the particles are only present at relatively low concentrations. For higher concentrations of particles (0.2 wt. %) stability is increased.

$C_{12}E_5$ almost certainly renders all of the particles hydrophilic. The particles with the highest % SiOH on their contents are probably more hydrophilic than the particles with initially lower % SiOH values after surfactant adsorption has occurred. This is reflected in the foamability of $C_{12}E_5$ which does not increase in the presence of particles (indicating the absence of particles with intermediate hydrophobicities which can co-adsorb with the surfactant as they do for DTAB). Foamability is decreased because of surfactant adsorption onto the surfaces of the silica particles. In the presence of dispersed particles the enhanced stability of $C_{12}E_5$ stabilised foam arises from retardation in film drainage arising from the presence of particles within the Plateau borders. The increase in the stability of the foam with increasing % SiOH (for

a fixed particle concentration) is due to both increased surfactant concentration and the (slightly) more hydrophilic particles blocking the drainage channels more effectively. The reason that the most hydrophobic particles dispersed at the lowest concentrations destabilise the foam is due to the particles lowering the surfactant concentration and retarding the drainage the least.

5.11 Stability of $C_{12}E_5$-stabilised single soap films

In order to test the idea that silica particles increase the stability of foam by retarding film drainage, it was decided to measure the lifetimes of single films stabilised by $C_{12}E_5$ in the absence and presence of dispersed silica particles. Figure 5.34 shows the lifetimes of films stabilised by 1 mM $C_{12}E_5$ in the presence and absence of dispersed silica particles (0.2 wt. %). It was found that the experiments carried out on surfactant-silica dispersions are irreproducible and based on the errors associated with these measurements, no trend could be assigned to the data. It was therefore concluded that for the systems studied here, single film stability measurements carried out in this way were not informative and could not provide insight to bulk foam stability for these particular systems.

5.12 Foaming properties of commercially available nonionic surfactants

Studies have been carried out on Lutensol AO7 in relation to foamabilty and foam stability in the presence of silica particles. The objective of this preliminary work is to see if the same trends exist for an impure surfactant as for a chromatographically pure surfactant - the type used for the majority of the work described in this thesis.

The concentration of Lutensol AO7 was fixed at 4×10^{-2} wt. % for all of the measurements and the particles were always dispersed at 0.2 wt. %. Assuming the molecular mass is the same as $C_{12}E_7$, this equates to approximately 1 mM (as used previously in the $C_{12}E_5$ measurements in the presence of silica particles). Qualitatively, the same trends exist between Lutensol AO7 and $C_{12}E_5$ in terms of the effects of added silica (silica always reduced the foamability and always enhances

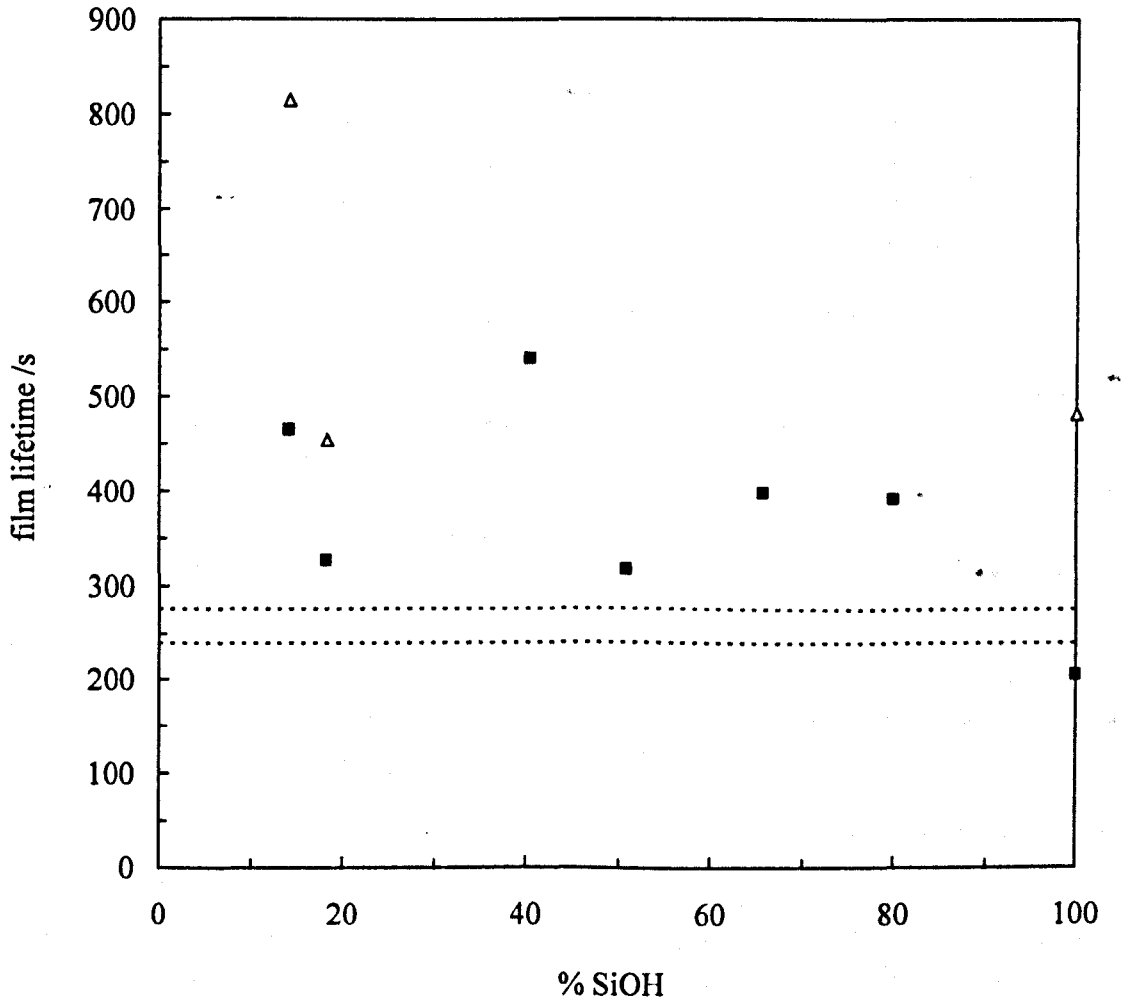

Figure 5.34 Film lifetime as a function of % SiOH on silica particles dispersed in 60.0 cm^3 of an aqueous solution of $C_{12}E_5$ (1 mM) at 0.2 wt. %. All experiments were carried out at 20.0 °C. The horizontal dashed lines show the lifetime range of films stabilised by 1 mM $C_{12}E_5$ in the absence of silica particles (2 determinations). Open triangles show repeated data in the presence of particles.

stability relative to the no particle case when dispersed at 0.2 wt. %). However, at 4 x 10^{-2} wt. %, Lutensol does not stabilise foam as effectively as $C_{12}E_5$ nor is it as foaming. Figures 5.35 and 5.36 summarise the foamability and foam stability behaviour of this commercial surfactant.

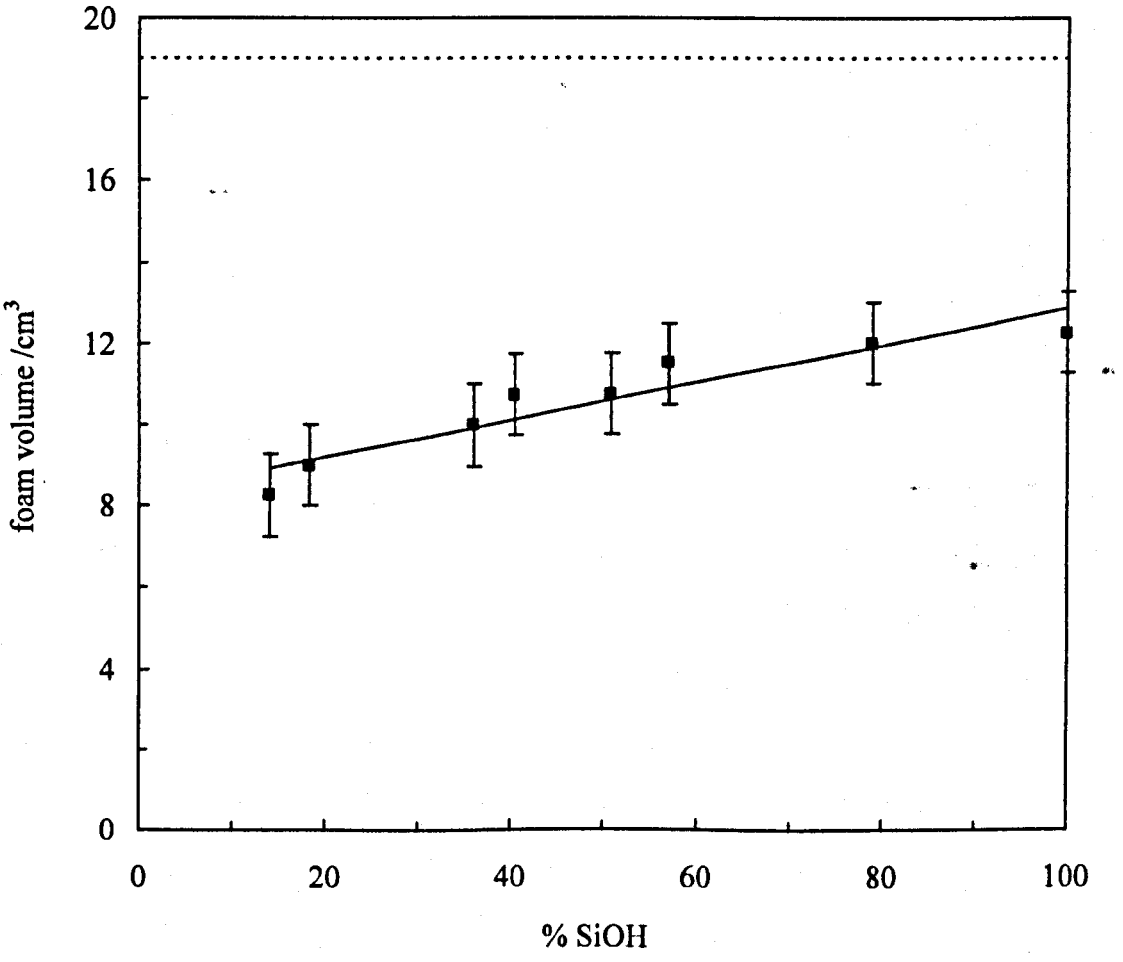

Figure 5.35 Initial foam volume as a function of % SiOH on silica particle surfaces. The particles were dispersed at 0.2 wt. % in 20.0 cm^3 aqueous Lutensol AO7 (4 x 10^{-2} wt. %) and left to equilibrate overnight. The horizontal dashed line shows the initial foam volume of the surfactant in the absence of particles. Each data point represents an average of 4 runs. All of the measurements were made at ambient temperature.

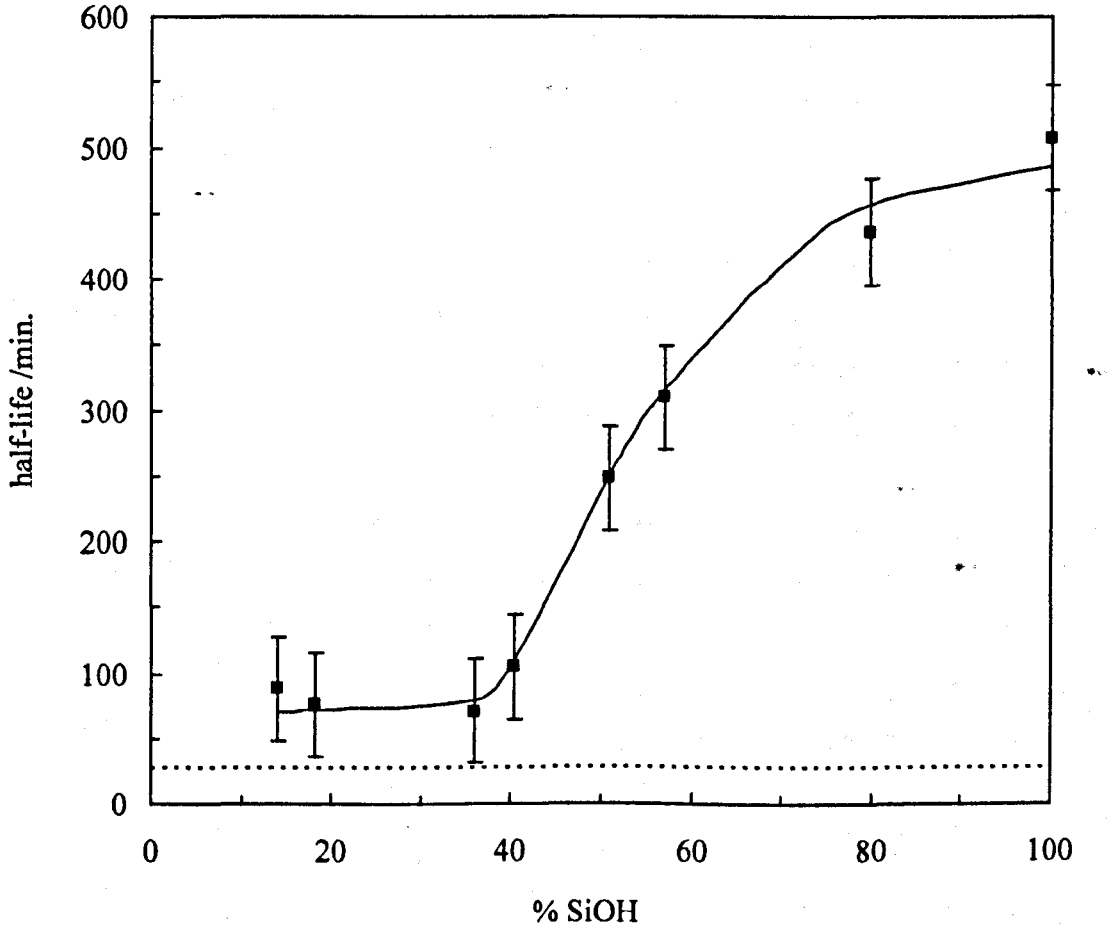

Figure 5.36 Foam half-life of 20.0 cm^3 of aqueous Lutensol AO7 (4 x 10^{-2} wt. %) containing dispersed silica particles at 0.2 wt.% as a function of % SiOH on particle surfaces. The horizontal dashed line shows the half-life of the surfactant in the absence of dispersed silica particles. All measurements were made at ambient temperature. The solid line is a guide for the eye.

5.13 Summary of experimental results

- TEM has shown that silica particles can form networks and do not necessarily exist as discrete particles when dispersed in surfactant solutions. This observation is consistent with the idea that improved foam stability is observed for $C_{12}E_5$ (except when the most hydrophobic particles are dispersed at low concentrations) due to the possible blocking of the Plateau borders and hence retardation of liquid drainage

- $C_{12}E_5$ adsorbs onto the silica with lower residual % SiOH on its surface more than silica with higher residual % SiOH. This is consistent with the idea that the foamability of $C_{12}E_5$ is reduced as a consequence of surfactant depletion. Low % SiOH silica reduces foamability more than high % SiOH silica.

- Silica may act as a surfactant reservoir and lower the time taken for a surfactant solution of $C_{12}E_5$ to reach equilibrium adsorption.

- Silica particles modify the foaming properties of SDS and DTAB but in different ways to $C_{12}E_5$. The foamability of SDS is generally lowered in the presence of particles. The most hydrophilic silica particles are capable of destabilising SDS foam when dispersed at low concentration. The most hydrophilic particles always stabilise $C_{12}E_5$ foam. For DTAB, foamability is increased by the addition of particles. This is the opposite trend to that observed for $C_{12}E_5$. DTAB is similar to $C_{12}E_5$ in terms of foam stability, as DTAB is stabilised by the most hydrophilic silicas. This stability is at its greatest when the particles are dispersed at 0.2 wt. %.

- Although the commercial equivalent of $C_{12}E_7$ (Lutensol AO7) does not stabilise foam as effectively and is not as foaming as its purer counterpart, it behaves in the same way as $C_{12}E_7$ in the presence of dispersed silica particles.

5.14 Conclusions

- nm-sized Silica particles reduce the foamability of $C_{12}E_5$ solutions by lowering the equilibrium surfactant concentration by adsorption of surfactant onto their surfaces. This surfactant depletion from solution increases with silica particle hydrophobicity (decreasing % SiOH).

- nm-sized silica particles generally increase the stability of foams stabilised by $C_{12}E_5$ because they retard liquid drainage through the Plateau borders by networking together in solution.

References

1. P. R. Garrett, *J. Colloid Interface Sci.*, (1979), **69**, 107.
2. A. Dippenaar, *Int. J. Mineral Process.*, (1982), **9**, 1.
3. M. P. Aronson, *Langmuir*, (1986), **2**, 653.
4. G. C. Frye and J. C. Berg, *J. Colloid Interface Sci.*, (1989), **127**, 222.
5. R. Aveyard, B. P. Binks, P. D. I. Fletcher and C. E. Rutherford, *J. Dispersion Science and Technology*, (1994), **15**, 251.
6. R. D. Kulkarni, E. D. Goddard and B. Kanner, *Ind. Eng. Chem. Fund.*, (1977), **16**, 472.
7. Y. Torikata, M. Kato, H. Kumagai T. Yano and H. Yoshimura, *Agric. Biol. Chem.*, (1991), **55**, 1823.
8. F. -Q. Tang, Z. Xiao, J. A. Tang and J. A. Long, *J. Colloid Interface Sci.*, (1989), **131**, 498.
9. G. Johansson and R. J. Pugh, *Int. J. Mineral Process.*, (1992), **34**, 1.
10. B. P. Binks and S. O. Lumsdon, *Phys. Chem. Chem. Phys.*, (1999), **1**, 3007.
11. B. P. Binks and S. O. Lumsdon, *Phys. Chem. Chem. Phys.*, (2000), **2**, 2959.
12. B. P. Binks and S. O. Lumsdon, *Langmuir*, (2000), **16**, 2539.
13. B. P. Binks and S. O. Lumsdon, *Langmuir*, (2000), **16**, 8622.
14. V. L. Alexeev, P. Ilekti, J. Perselle, J. Lambard, T. Gulik and B. Cabane, *Langmuir*, (1996), **12**, 2392.
15. V. L. Alexeev, *Journal of Colloid Interface Sci.*, (1998), **206**, 416.
16. F. Giorano-Palmino, R. Denoyel and J. Rouquerol, *Journal Colloid Interface Sci.*, (1994), **165**, 82.
17. P. Levitz , H. van Damme and D. Keravis, *J. Phys. Chem.*, (1984), **88**, 2228.
18. P. Levitz and H. van Damme, *J. Phys. Chem.*, (1986), **90**, 1302.
19. P. Levitz, A. El Miri, D. Keravis, H. Van Damme, *J. Colloid Interface Sci.*, (1984), **99**, 484
20. P. Levitz, *Langmuir*, (1991), **7**, 1595.
21. M. Lindheimer, E. Kehl, S. Zaini and S. Partyka, *Journal of Colloid Interface Sci.*, (1990), **138**, 83.
22. T. van den Boomgaard, T. F. Tadros and J. Lyklema, *J. Colloid Interface Sci.*, (1987), **116**, 8.

23. F. Portet, P. L. Desbène and C. Treiner, *Journal Colloid Interface Sci.*, (1998), **208**, 415.

24. M. R. Böhmer, L. K. Koopal, R. Janssen, E. M. Lee, R. K. Thomas and A. R. Rennie, *Langmuir*, (1992), **8**, 2228.

25. P. Somasundaran, E. D. Snell, E. Fu and Q. Xu, *Colloids and Surfaces*, (1992), **63**, 49.

26. E. M. Lee, R. K. Thomas, P. G. Cummins and E. Staples, *J. Chem. Phys. Lett.* (1989), **162**, 196.

27. P. J. Scales, F. Grieser, D. N. furlong and T. W. Healy, *Colloids and Surfaces*, (1986), **21**, 55.

28. L. M. Grant, F. Tiberg and W. A. Ducker, *J. Phys. Chem. B.* (1998), **102**, 4288.

29. F. Tiberg, *J. Chem. Soc. Faraday Trans.*, (1996), **92**, 531.

30. B. P. Binks, P. D. I. Fletcher, V. N. Paunov and D. Segal, *Langmuir*, (2000), **16**, 8926.

31. Value for $C(1/2)$ of $C_{12}E_5$ taken from Figure 3.7, Chapter 3.

32. V. N. Paunov, B. P. Binks and N. P. Ashby, *Langmuir*, (2002), **18**, 6946.

33. Z. P. Du, M. P. Bilbao-Montoya, B. P. Binks, E. Dickinson, R. Ettelaie and B. S. Murray, *Langmuir*, (2003), **19**, 3106.

Chapter 6

CHAPTER 6

Foam control by *n*-alkane oils and nanometre sized silica particles in combination

6.1 Introduction

This chapter is concerned with the effects that oils and particles operating in combination have on both the foamability and foam stability of aqueous nonionic surfactant-stabilised foams. The effects of nm-sized silica particles of different initial hydrophobicities and *n*-alkanes used together have on $C_{12}E_5$ stabilised foams are investigated and some preliminary results are given. It is important to emphasise here that previous studies on similar anti-foams have generally concentrated on systems containing solid particles and oils where the diameters of the solid particles fall in the micron-size range.

6.2 Mode of action of solid particles and oils in combination

In section 1.9 some mechanisms were discussed which explain the increased efficacy of oils and solid particles acting as combination anti-foam compounds compared to when the oil and solid particles are taken separately. The work described was that of Garrett[1], Kulkarni et al.[1-3], Dippenaar[4], Frye and Berg[5] and Aveyard et al.[6,7] Recently, Marinova et al.[8,9] have shown that in mixed oil/silica antifoams, the hydrophobicity of the silica particles play an important role in the overall efficacy of the antifoam compound. They noted an optimum silica hydrophobicity at which anti-foam activity was at its highest. The exact hydrophobicity of the silica particle required for this depended upon the foaming system used. They attributed this optimum hydrophobicity to two opposing requirements for the particle hydrophobicity. These both originate from the fact that the particle plays the role of assisting the antifoam globule entry by piercing the asymmetric oil-water-air films (see section 1.6).[10] The first requirement is that the particles should be sufficiently hydrophobic to be

dewetted by the oil-water and air-water interfaces. The other requirement is that the particles should protrude sufficiently deeply into the aqueous phase in order to bridge the surfaces of the asymmetric oil-water-air film. This is better satisfied by more hydrophilic particles. Therefore an optimal hydrophobicity of the particles is expected where both requirements are balanced and the antifoam is most active.

When using nm-silica particles and oil in combination, there are various possibilities for the final entity formed when they are present in surfactant solution. This entity will be a composite containing two or more of the components mentioned above. Some of the possibilities are summarised in Figure 6.1. It should also be noted that the particles could also adsorb oil onto their surfaces, resulting in an inversion of the situations (1) – (3) depicted in picture (4). Which entity forms is therefore likely to depend on the hydrophobicity of the silica particles used and whether they favour the oil phase or aqueous phase as a result of this. Surfactant adsorption is also likely to have an influence because of its ability to impart hydrophilicity to hydrophobic silica particles.[11]

6.3 Results and discussion

As discussed in Section 2.9.1, there are various ways in which silica particles and oil can be added to a surfactant solution. They can be added directly to the surfactant solution, the particles can be dispersed in the oil which can be then added to the solution, or the particles can be dispersed in the surfactant solution before the oil is homogenised into the system forming an emulsion. The way in which the anti-foam components are added to the surfactant solution may have an effect on the way they behave as anti-foam agents. The results in this section are therefore grouped together in individual sections according to the way in which the particles and oil were added to the surfactant solution.

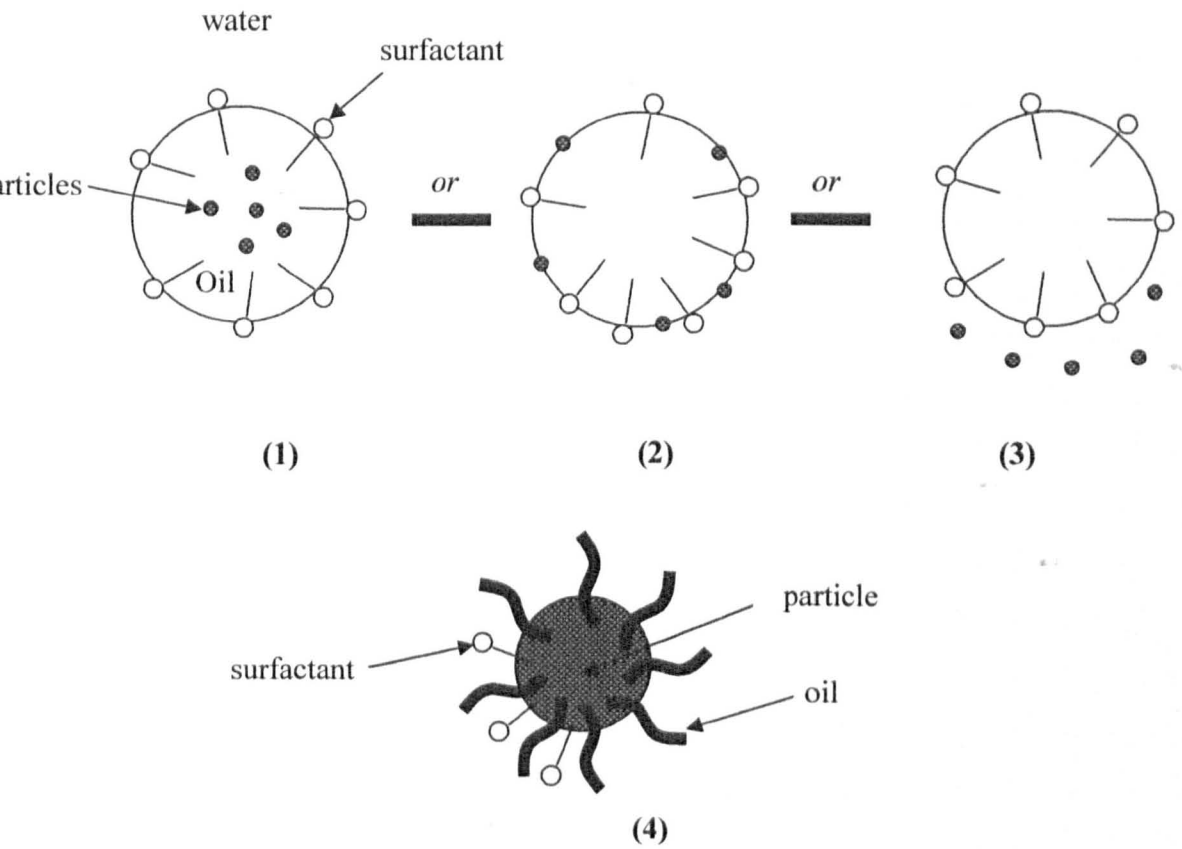

Figure 6.1 Possible entities formed from combining silica particles, oil and surfactant in aqueous medium. **(1)** Surfactant stabilised oil drop with the particles in the oil. **(2)** "Ramsden emulsion" (with or without adsorbed surfactant). **(3)** Surfactant-stabilised oil drop with particles in the aqueous phase. **(4)** Oil and surfactant adsorbed onto the surface of the silica particle.

6.3.1 *Adding silica and oil to the surfactant solution without dispersion and homogenisation*

0.2 wt. % of silica particles with a particular SiOH coverage were added to 30.0 cm^3 of aqueous $C_{12}E_5$ solution (1 mM). The particles were not dispersed using the ultrasonic probe. Oil was then added and the mixture was gently hand shaken. Figures 6.2 – 6.4 show micrographs of these systems. The micrographs show that when delivering the anti-foaming agents in this way, a system is obtained in which oil drops are stabilised in the aqueous phase, i.e. an oil-in-water emulsion is obtained. The oil drops are all poly-disperse and for the systems containing silica particles with intermediate and high values of % SiOH, the largest drops are of the order of 10 μm and the smallest drops are of the order of 1 μm. For the systems containing the most hydrophobic silica particles, the largest oil drops are of the order of 20 - 30 μm.

The mixtures were shaken in a 100 cm^3 stoppered measuring cylinder and foam volume was measured as a function of time to obtain foamability data (initial foam volume) and foam stability data (half-life derived from the foam decay curve). This process was repeated for silica particles with different % SiOH contents on their surfaces. The same foaming measurements were then repeated after the addition of a very small quantity of decane (a few drops). Upon shaking, the surfactant solution turned to a white / grey colour - indicative that an emulsion had been formed. Figure 6.5 shows the foamability of (i) pure $C_{12}E_5$, (ii) $C_{12}E_5$ + 0.2 wt. % silica particles (iii) $C_{12}E_5$ + decane and (iv) $C_{12}E_5$ + decane + 0.2 wt. % silica particles.

In the absence of silica particles, increasing the concentration of decane progressively decreases the foamability of the surfactant. In the absence of decane, the addition of silica particles reduces the foamability of the surfactant solution. Although the addition of silica particles lowers the foamability relative to the pure surfactant case, the foamability of the systems does depend on the % SiOH on the silica particles as it does when the particles are dispersed using ultrasound (see chapter 5). The differences in foamability trends observed for intermediate % SiOH contents for the systems containing 0.12 vol. % decane + 0.2 wt. % silica and 0.04 vol. % decane + 0.2 wt. % silica remain unclear at present.

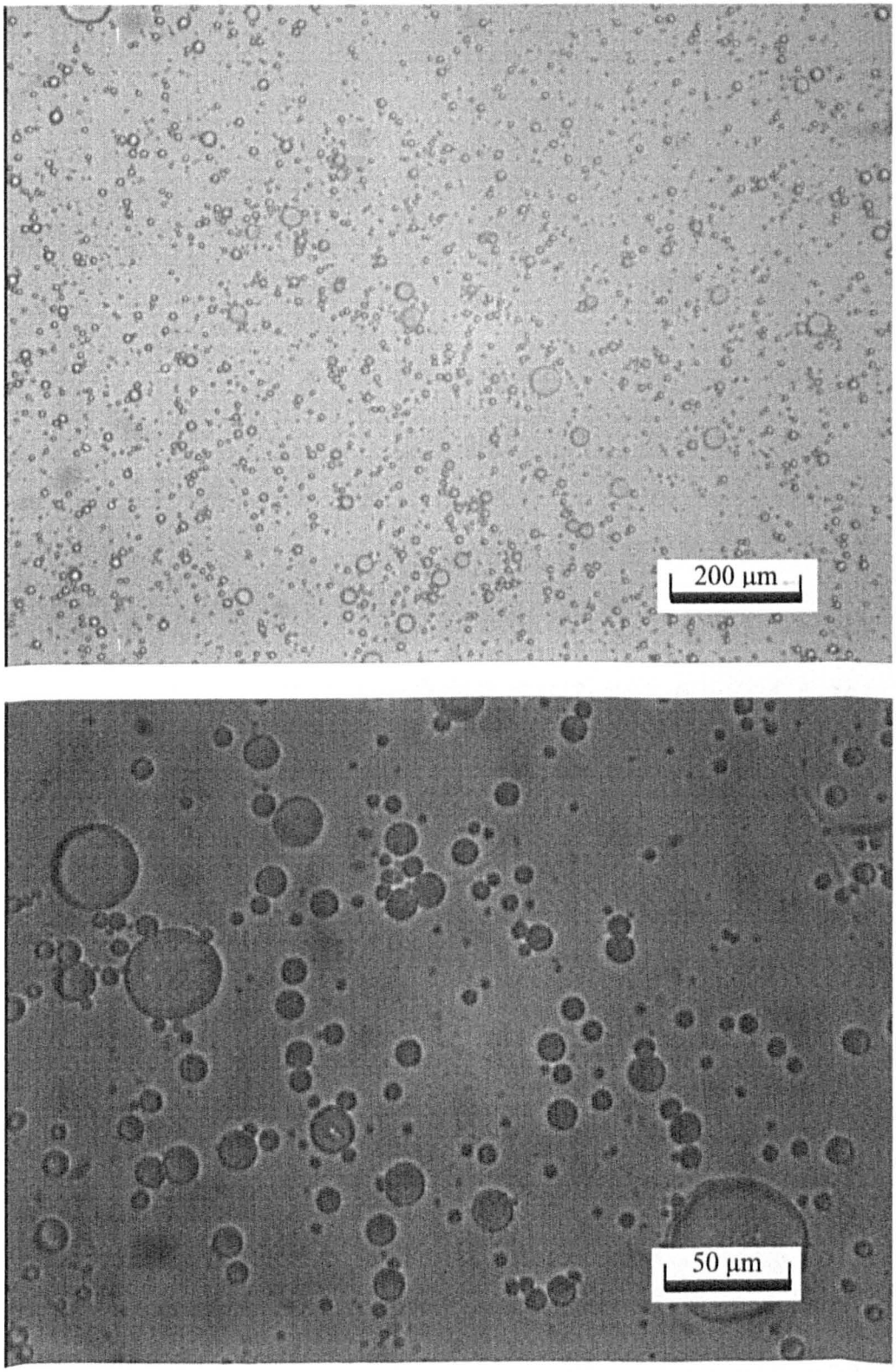

Figure 6.2 Micrographs of system containing 0.2 wt. % silica (14.1 % SiOH) and 5 vol. % decane added to 1 mM aqueous $C_{12}E_5$. No ultrasound or homogenisation treatment was used.

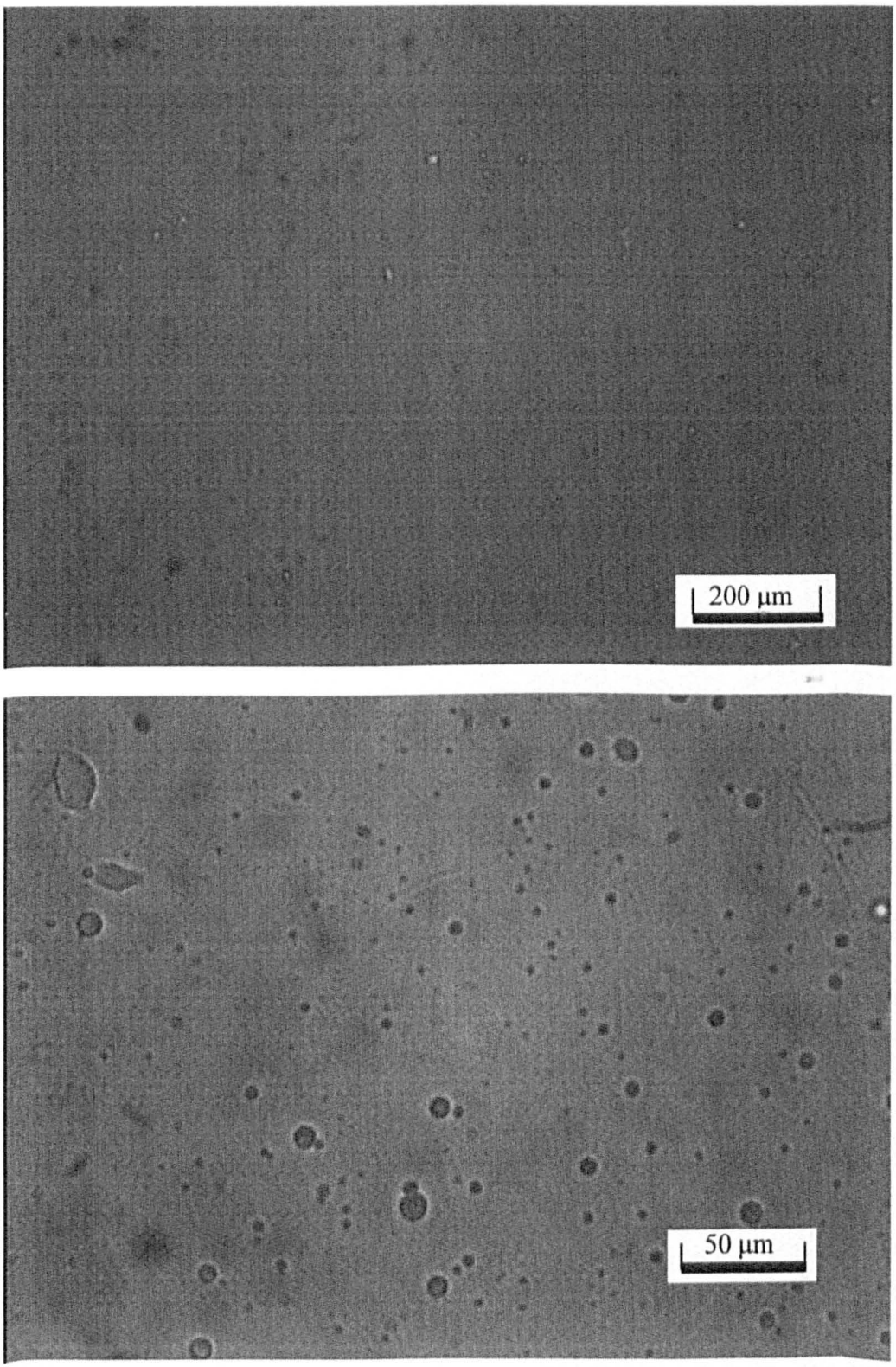

Figure 6.3 Micrographs of system containing 0.2 wt. % silica (65.7 % SiOH) and 5 vol. % decane added to 1 mM aqueous $C_{12}E_5$. No ultrasound or homogenisation treatment was used.

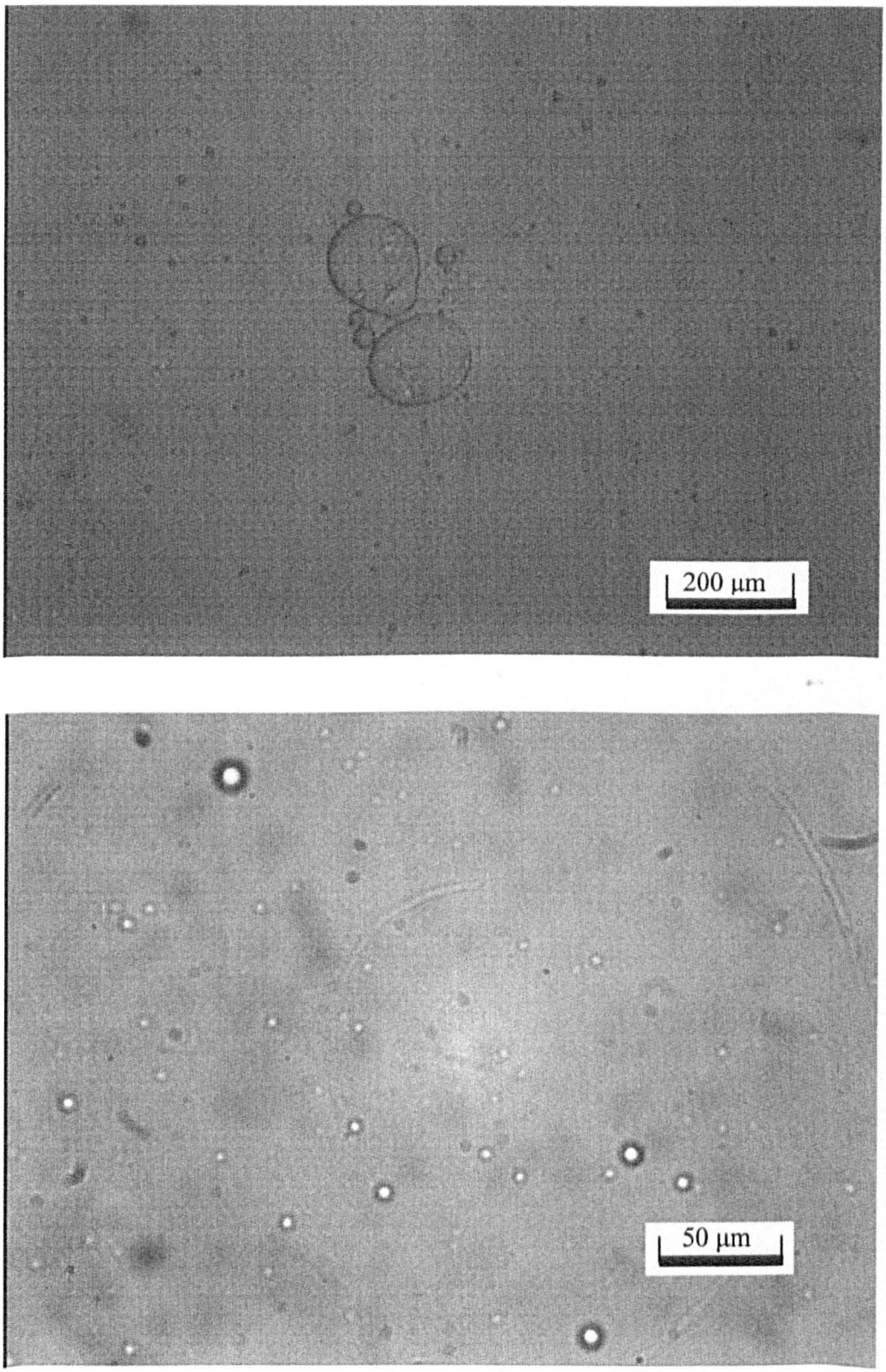

Figure 6.4 Micrographs of system containing 0.2 wt. % silica (100 % SiOH) and 5 vol. % decane added to 1 mM aqueous $C_{12}E_5$. No ultrasound or homogenisation treatment was used.

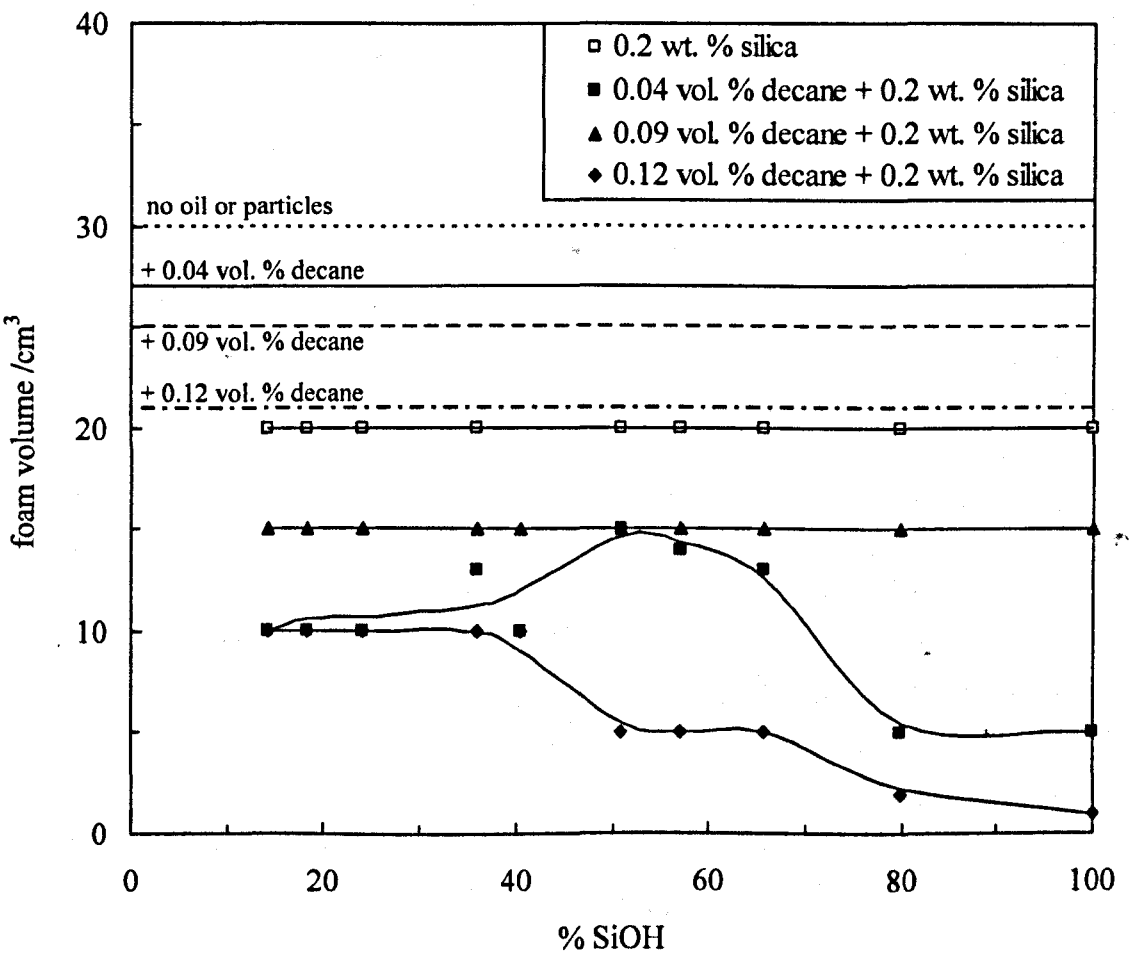

Figure 6.5 Foamability of 1 mM $C_{12}E_5$ (30.0 cm^3) as a function of % SiOH on particle surfaces for non-dispersed silica particles (0.2 wt. %) in the absence and presence of decane. The horizontal dashed line shows the foamability of $C_{12}E_5$ (1 mM) in the absence of oil or particles in the form of an initial foam volume. The horizontal solid line shows the foamability in the presence of 0.04 vol. % of decane alone, the long-dashed line shows the foamability in the presence of 0.09 vol. % of oil alone and the dot dashed line shows the foamability in the presence of 0.12 vol. % of decane alone.

The addition of decane and silica together reduces the foamability of the surfactant more than either the silica or oil alone and so it is likely that a synergistic anti-foam action between the oil and particles is occurring.

Figure 6.6 shows how the foam stability of $C_{12}E_5$, as judged by foam half-life, varies for (i) pure $C_{12}E_5$, (ii) $C_{12}E_5$ + 0.2 wt. % silica particles (iii) $C_{12}E_5$ + decane and (iv) $C_{12}E_5$ + decane + 0.2 wt. % silica particles. In the absence of silica particles, increasing the concentration of decane decreases the stability of the foam. In the absence of decane, the addition of silica particles can either stabilise or destabilise the foam (relative to the pure surfactant case) depending on the % SiOH content on the particle surfaces. The stability of the foam remains approximately constant until the % SiOH content on the particle surfaces reaches a value of approximately 60. Further increases in the % SiOH cause the stability of the foam to progressively increase. The stability finally exceeds that of the foam stabilised by $C_{12}E_5$ in the absence of particles or oil when the % SiOH on the silica particles reaches a value of approximately 80.

When the silica particles and decane are added to the surfactant solution in combination, they either increase or decrease the stability of the foam relative to the pure surfactant case. The decane and silica particles are effective foam destabilisers when the SiOH content on the silica particle surfaces is either low or high (< 50 % and > 80 %). There is evidence that the silica and decane are acting synergistically when the % SiOH is < 50 or greater than 80 because the stability of the foam is reduced more than when decane is used alone. Although the data is not shown, when 0.12 vol. % decane + 0.2 wt. % silica is added to $C_{12}E_5$, the foam breaks too quickly to ascertain a half-life but it is estimated to be of the order of a few seconds. The systems containing decane and silica exhibit interesting behaviour when the % SiOH content on the silica particle surfaces reaches a range of intermediate values. The stability of these foams are significantly higher relative to the systems containing the same concentrations of silica and decane where the % SiOH content on the particles falls above or below this middle range. This increased stability is the largest for the system containing 0.04 vol. % decane and 0.2 wt. % silica particles with intermediate % SiOH on their surfaces where the stability of foaming solution containing no additives (i.e. pure $C_{12}E_5$) is exceeded.

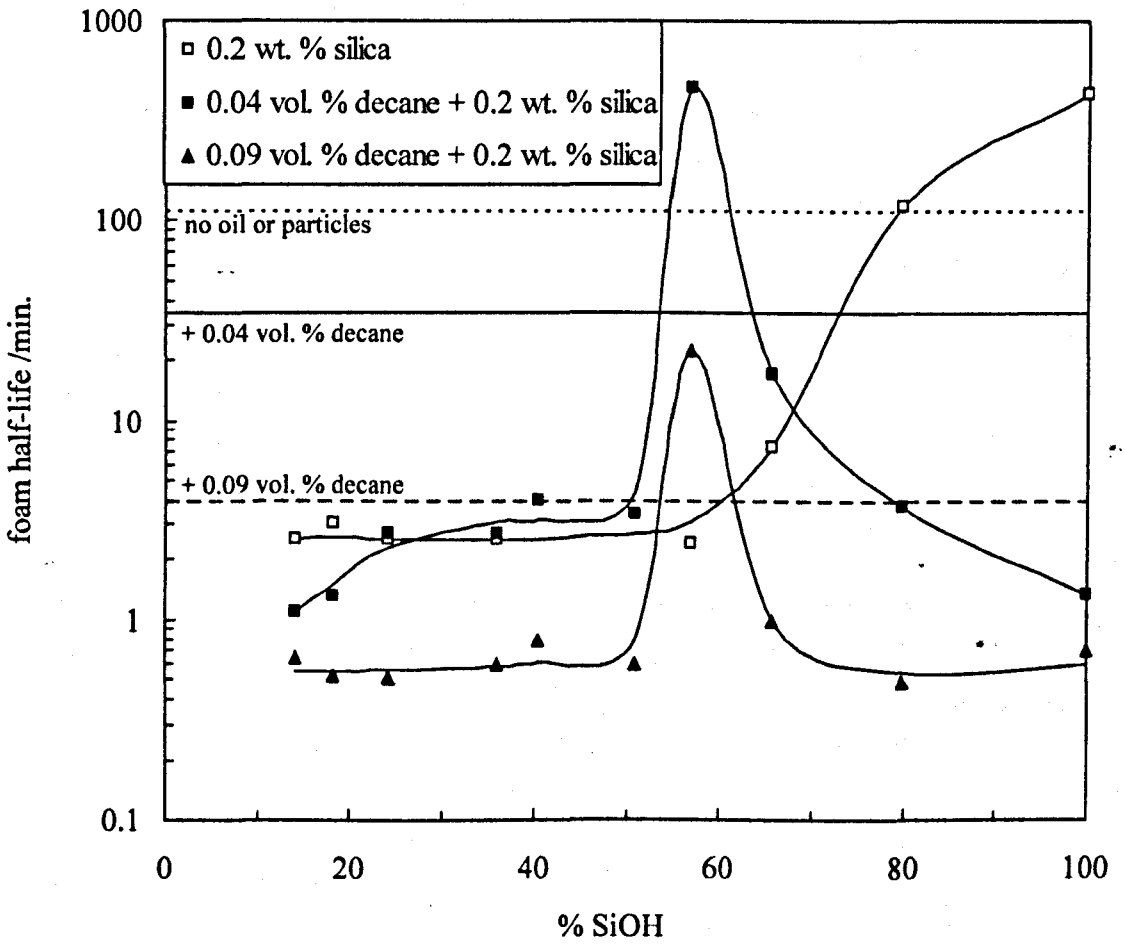

Figure 6.6 Foam half-life of 1 mM $C_{12}E_5$ solutions (30.0 cm^3) as a function of % SiOH on particle surfaces for non-dispersed silica particles (0.2 wt. %) in the absence and presence of decane. The horizontal dashed line shows the half-life of $C_{12}E_5$ (1 mM) in the absence of oil or particles. The horizontal solid line shows the half-life in the presence of 0.04 vol. % decane with no silica and the long dashed line shows the half-life of the foam in the presence of 0.09 vol. % decane in the absence of silica.

6.3.2 *Delivering oil and particles to the foaming solutions in the form of particle in oil dispersions*

0.2 g of silica particles were added to 5.0 cm^3 of decane to form a 4 wt. % mixture of particles in oil. All of the particles mixed with the oil regardless of the % SiOH on their surfaces. The particles were then fully dispersed into the oil using the ultrasonic probe and a viscous gel was formed. The most viscous gels were formed when the most hydrophilic silicas were dispersed into the oil. 1.58 cm^3 of the resulting gel was added to 30.0 cm^3 of 1 mM $C_{12}E_5$ in order to make the overall composition of the system 5 vol. % of decane and 0.2 wt. % of silica in 1 mM $C_{12}E_5$. All of the gels spread on the surface of the surfactant solution. The surfactant solutions containing the silica–decane dispersions were then shaken in order to try and produce some foam – no foam was formed. Figures 6.7 – 6.9 show micrographs of the emulsion systems prepared from the addition of particle in oil dispersions to the surfactant solution. The micrographs show that the oil is stabilised in the aqueous phase, indicative that an oil-in-water emulsion is present. All of systems exhibit poly-disperse oil droplets. The largest oil droplets are obtained when the most hydrophobic silica particle types are used (average drop diameter = 20 μm). Smaller oil droplets are observed when silica particles with 65.7 and 100 % SiOH on their surfaces are used (average oil drop diameter = 5 - 10 μm). Decane and silica particles used in combination at these relatively high concentrations are excellent foam inhibitors. In order to produce some foam, the concentration of this antifoam agent needs to be reduced. In order to fix the particle concentration at 0.2 wt. %, but reduce the decane concentration, more silica particles need to be originally dispersed in the decane. When 4 wt. % silica are dispersed in decane, a very viscous gel-like mixture is obtained. This signified the realistic limit of the concentration of silica particles that could be dispersed into decane. It follows that in order to maintain the particle concentration at a value of 0.2 wt. %, taken here as a "standard" for the majority of experiments involving particles as foam control agents, a very high concentration of particles would have to be dispersed initially in decane. This method of anti-foam delivery could therefore not be pursued any further because of this limitation.

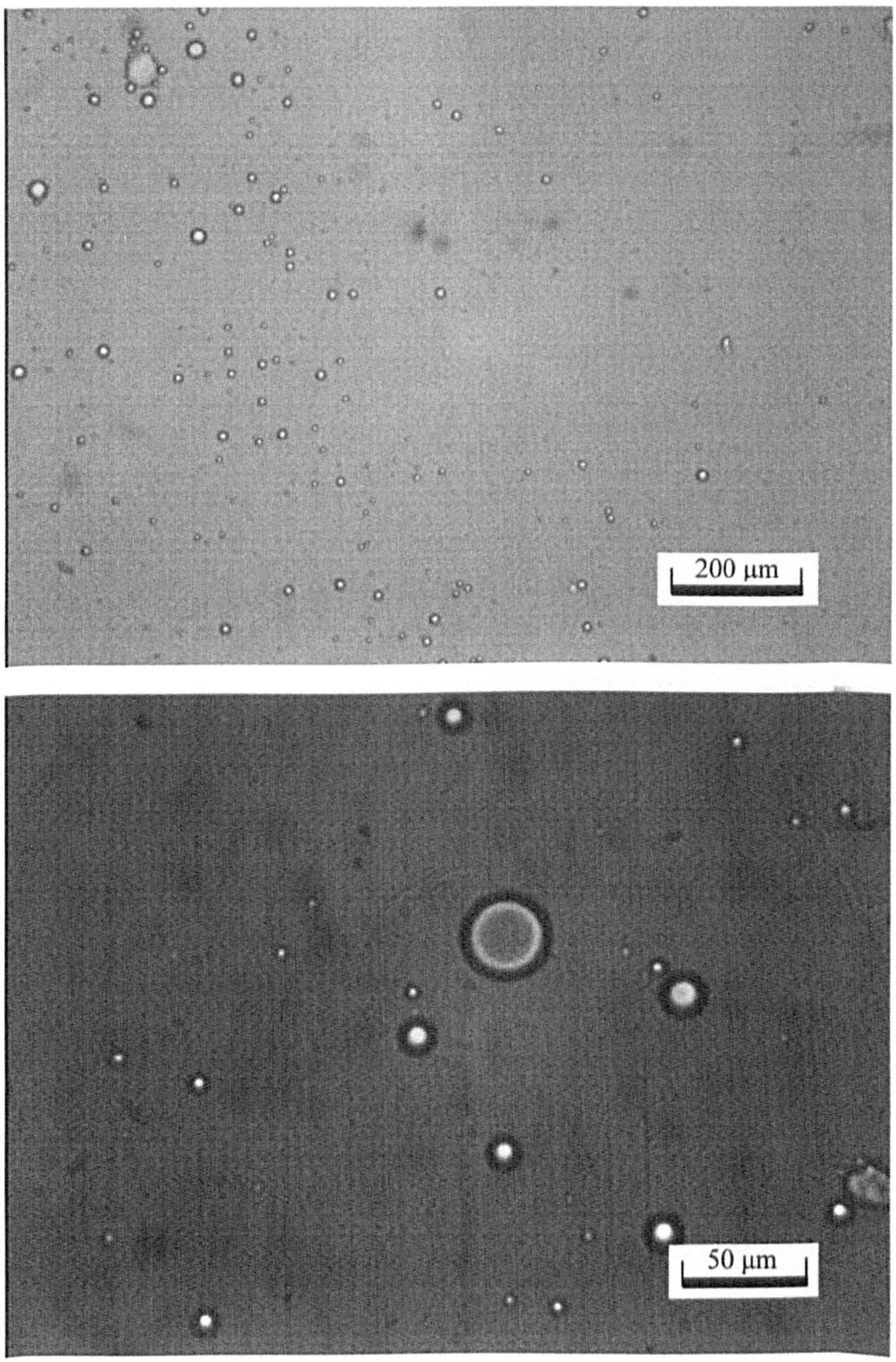

Figure 6.7 Micrographs of a particle-in-oil dispersion added to aqueous $C_{12}E_5$. 4 wt. % of silica (14.1 % SiOH) dispersed into decane, and 0.2 wt. % of this dispersion was added to aqueous $C_{12}E_5$.

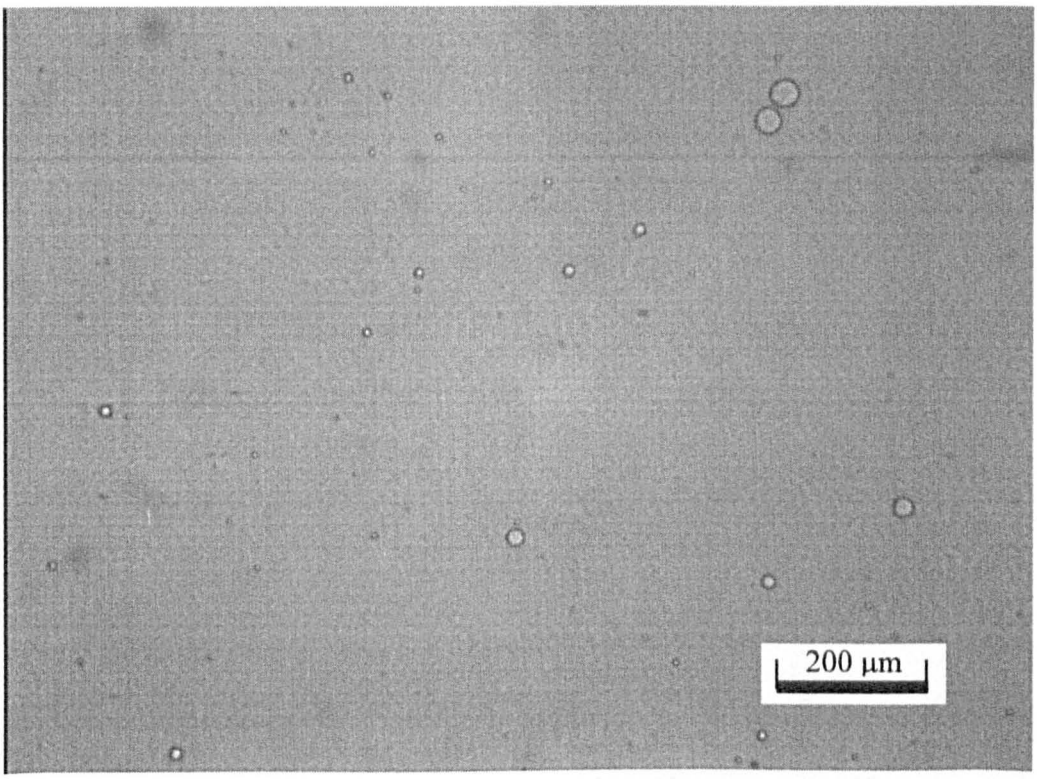

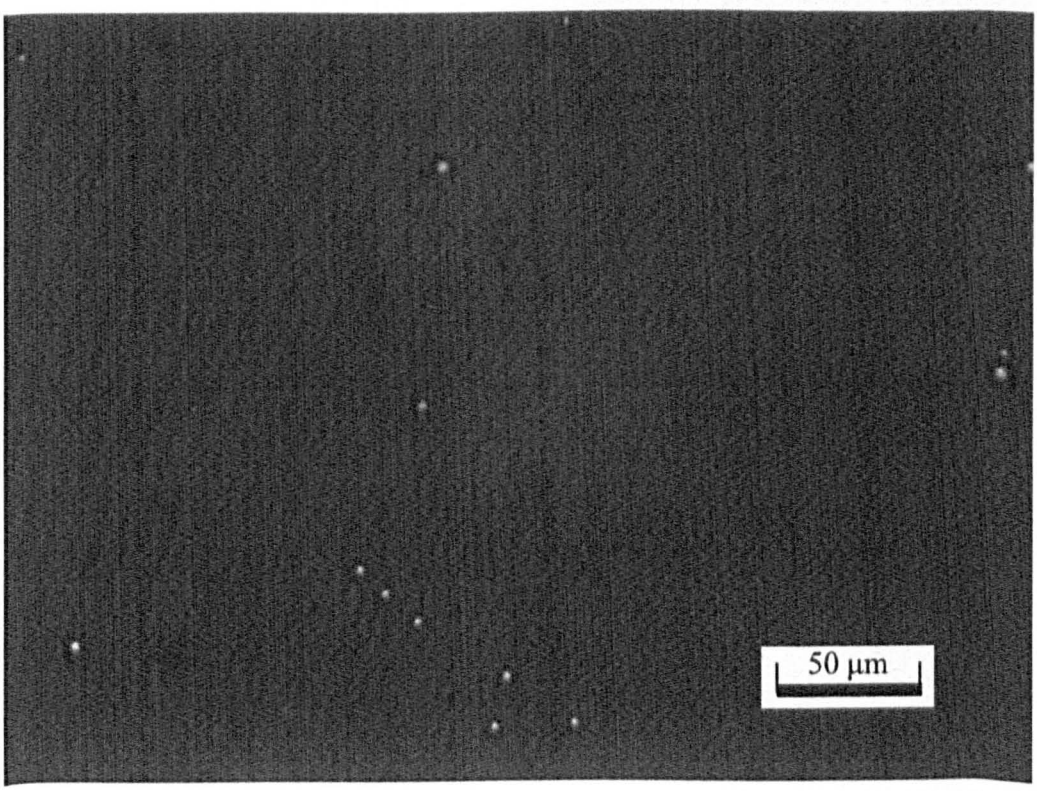

Figure 6.8 Micrographs of a particle-in-oil dispersion added to aqueous $C_{12}E_5$. 4 wt. % of silica (65.7 % SiOH) dispersed into decane, and 0.2 wt. % of this dispersion was added to aqueous $C_{12}E_5$.

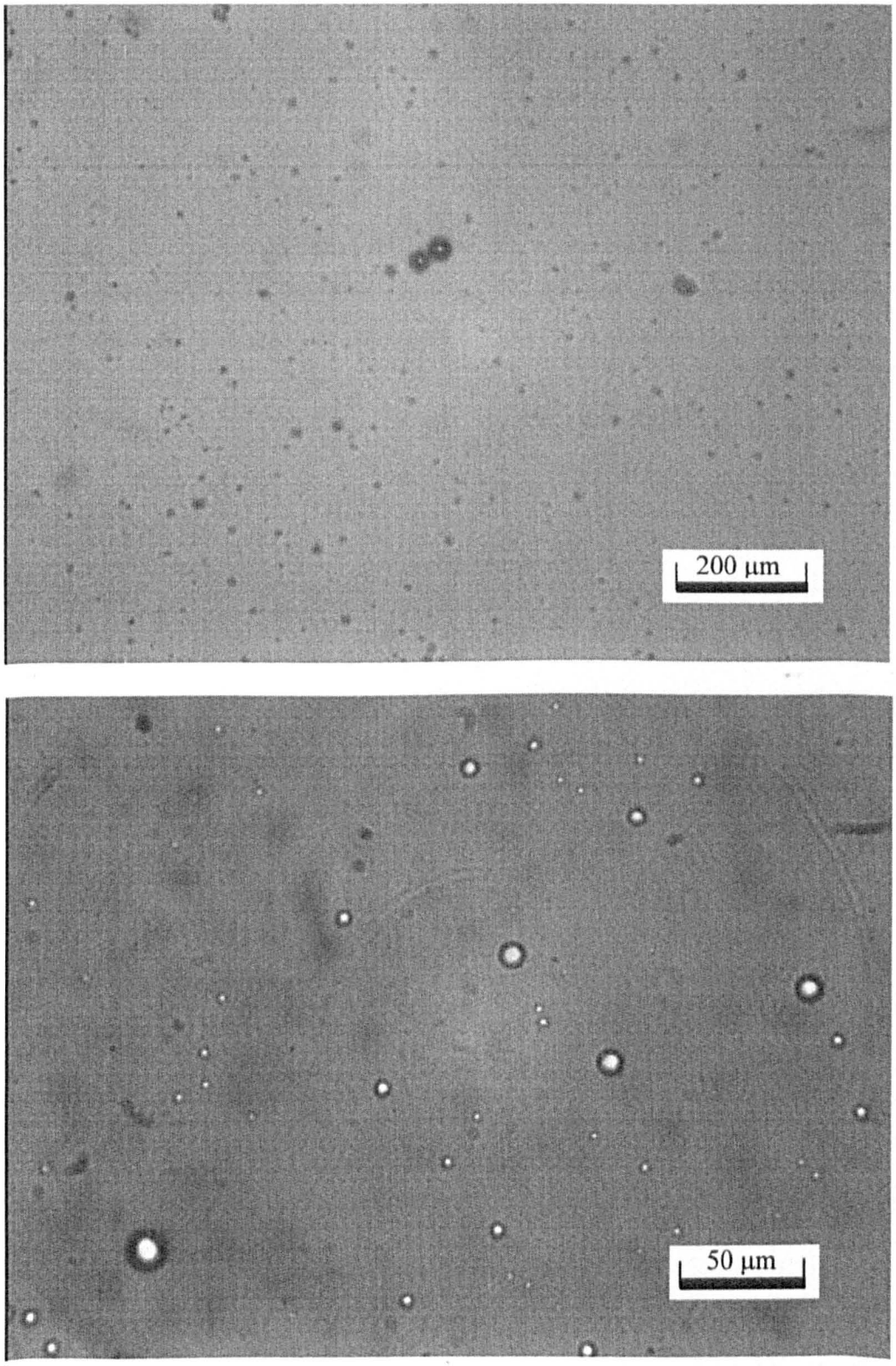

Figure 6.9 Micrographs of a particle-in-oil dispersion added to aqueous $C_{12}E_5$. 4 wt. % of silica (100 % SiOH) dispersed into decane, and 0.2 wt. % of this dispersion was added to aqueous $C_{12}E_5$.

6.3.3 Delivering oil and particles to a foaming solution in the form of an emulsion

In order to obtain a more in-depth understanding of the way in which the nm-silica particles and *n*-alkanes act in combination, the oil was homogenised into a pre-equilibrated $C_{12}E_5$-silica dispersion. This process yields an emulsion which can be characterised prior to any foaming measurements. The concentration of the oil can be reduced whilst fixing the concentration of silica particles (by diluting with a dispersion of silica in $C_{12}E_5$) or the oil and the silica particle concentrations can both be reduced by diluting the emulsion with $C_{12}E_5$ and foaming measurements can be made at each dilution. See section 2.9.2 for full details. The results obtained from the characterisation of these emulsions will be discussed first, and then the foamability and foam stability of the emulsions will be discussed in light of these results.

Characterisation of the emulsions

When an attempt was made to homogenise oil into the surfactant-silica dispersion containing silica with 65.7 % SiOH (and in certain systems 57 % SiOH) on its surface, the emulsion would not form and a hydrophobic material was formed which adhered to the head of the homogeniser. This should be noted because interestingly, it is the same % SiOH content corresponding to the system in section 6.3.1 where a maximum was obtained in foam stability.

Emulsion type and stability. A couple of drops of each emulsion comprising silica particles, $C_{12}E_5$ and decane were added to samples of water and decane. It was found that all of the emulsions favoured the water and therefore water is the continuous phase in these systems. Stability tests were carried out on the emulsions prepared as detailed in section 2.9.2. It was found that all of the emulsions creamed within a couple of hours. The fastest rate of creaming was observed for the emulsion containing silica with a % SiOH content of 100 which creamed within about 1 hr. Next fastest was the emulsion containing silica particles with a % SiOH content of 79.9 on their surfaces. Both of these emulsions were stable to coalescence however, even after a week or so. All of the other emulsions creamed and partially coalesced within a couple of hours or so, although their rate of creaming was slower than the

emulsions containing the highest % SiOH on their surfaces. Stability tests were also carried out on a decane-$C_{12}E_5$ stabilised emulsion in the absence of silica particles. This emulsion coalesced within a couple of minutes. This finding suggests that a synergy exists between silica and $C_{12}E_5$ in the stabilisation of o/w emulsions. This confirms a finding by Midmore who demonstrated that an emulsification synergy exists between silica and nonionic surfactant (depending on the particle/surfactant concentration regimes).[12]

Emulsion droplet size. Figure 6.10 shows the median oil drop diameter for the freshly formed emulsions with a composition of 1 mM $C_{12}E_5$ + 0.2 wt. % silica and 5 vol. % of decane as a function of % SiOH on the surface of the particles. The oil drop size increases with % SiOH content on the silica particles until an intermediate hydrophobicity is reached. The median oil drop size then decreases. No data is available for the emulsion system containing silica particles with 65.7 % SiOH on their surfaces because as mentioned previously, the emulsion could not be made. The oil drop sizes are then seen to increase with increasing SiOH on the particle surfaces. These results from the drop size analysis highlight some interesting behaviour in these emulsions which occurs at intermediate values of % SiOH on the particle surfaces and falls within the same % SiOH range as where the gel-like deposit is formed on the homogeniser head and where the maximum in foamability and foam stability are observed as described previously. At this point it is noteworthy to mention the work of Bergeron et al. who studied PDMS based antifoams on a range of different surfactants.[13] They found that there was a significant reduction in antifoam performance when the antifoam globule size in their system fell to below 6 μm. At this diameter antifoam entities may be too small to bridge between the two surfaces of a foam film and unable to act as effective antifoam agents. In the system studied in this work, the transition from antifoam action to foam stabilisation corresponds to a globule size in the range 4 – 8 μm which is very close to the critical size reported in the work.

Emulsion viscosity. Figure 6.11 shows the viscosity of the concentrated emulsion prior to any dilution as a function of applied shear rate. From these data it is apparent that there is a marked increase in viscosity induced by increasing the % SiOH on the silica particles from 57.0 % to 79.9 %. The systems containing silica with values of

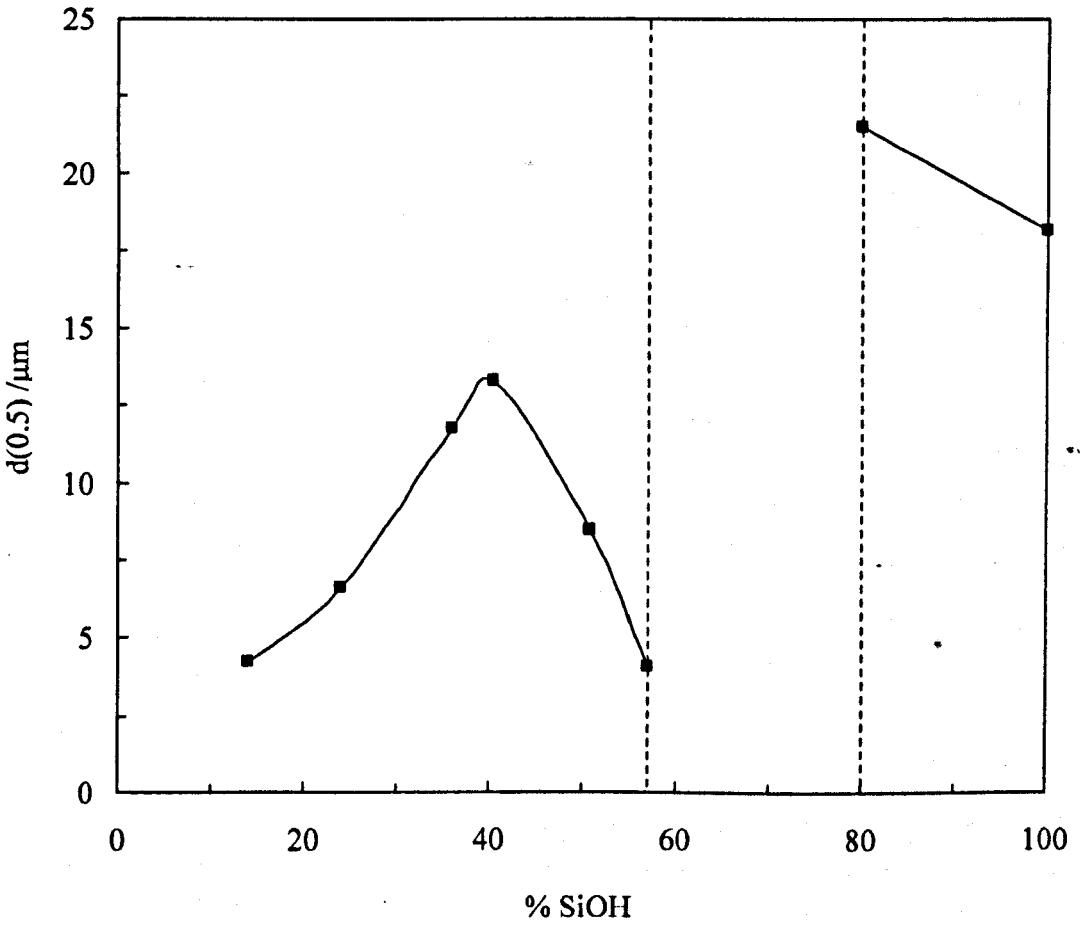

Figure 6.10 Median drop diameter as a function of SiOH content for fresh emulsions containing 0.2 wt. % silica, 1 mM $C_{12}E_5$ and 5 vol. % decane. Emulsions prepared by dispersing the silica into the $C_{12}E_5$ surfactant solution, adding the decane and then homogenising the mixture at 11000 r.p.m. for 2 minutes. The vertical dashed lines indicate the region where emulsions could not be formed.

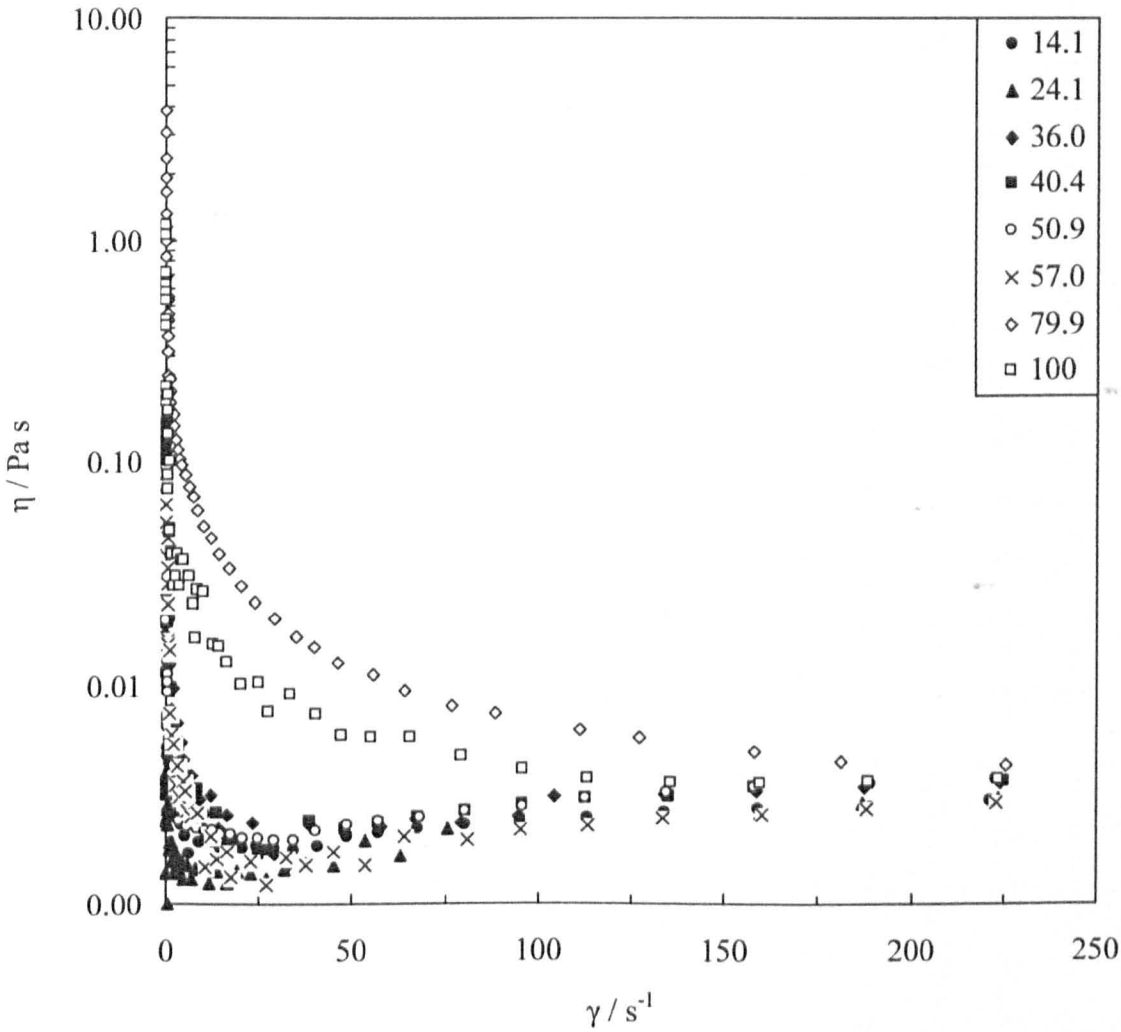

Figure 6.11 Viscosity (η) as a function of applied shear rate (γ) for oil-in-water emulsions containing 5 vol. % decane, 0.2 wt. % silica particles and 1 mM aqueous $C_{12}E_5$. The numbers in the legend show the % SiOH on the silica particle surfaces.

% SiOH on their surfaces of less than or equal to 57.0 have similar viscosities. It appears from these data that there is a significant change in the structure of the emulsion which occurs at intermediate % SiOH content on the silica particle surfaces.

Figure 6.12 is derived from figure 6.11 and shows how the viscosity of the emulsion varies as a function of % SiOH on the silica particle surfaces at a fixed applied shear rate of 25 s^{-1}. It clearly shows the significant change in the viscosity of the emulsion systems at intermediate values of % SiOH on the silica particle surfaces. These intermediate values of % SiOH coincide with the onset of a gel-like deposit observed when systems containing silica particles with intermediate values of % SiOH are homogenised. The % SiOH range at which this occurs is denoted by the vertical dashed lines in the figure. The material which adheres to the homogeniser head occurs when this critical point is reached and may arise from the fact that the emulsion cannot be effectively stabilised.

Foaming of the emulsions – variation of the silica and decane concentrations

Figure 6.13 shows the foamability of 30.0 cm^3 $C_{12}E_5$ (1 mM) in the presence of both decane and silica particles as a function of the % SiOH on the surfaces of the particles for different concentrations of silica and oil. The highest foamability corresponds to the system where the decane and silica particles are present at the lowest concentrations (0.005 vol. % decane and 0.0002 wt. % silica). Foamability is generally boosted when the oil and particles are present at these low concentrations and are used together. The boost in foamability is at its largest for intermediate % SiOH surface contents on silica. The data point corresponding to a % SiOH content of 14.1 has a higher uncertainty due to the generation of very coarse bubbles present at the top of the foam. When 0.002 wt. % of silica and 0.05 vol. % of decane are present in the foaming solution at high or low values of % SiOH, the foamability is less than the pure surfactant case. At intermediate % SiOH surface coverage however, foamability is boosted relative to the pure surfactant case at these oil / particle concentrations. When the emulsion composition is 0.02 wt. % silica and 0.5 vol. % decane, foamability is reduced below that of the pure surfactant case except for when the % SiOH coverage is 57.0 and foamability is the same as pure surfactant. No

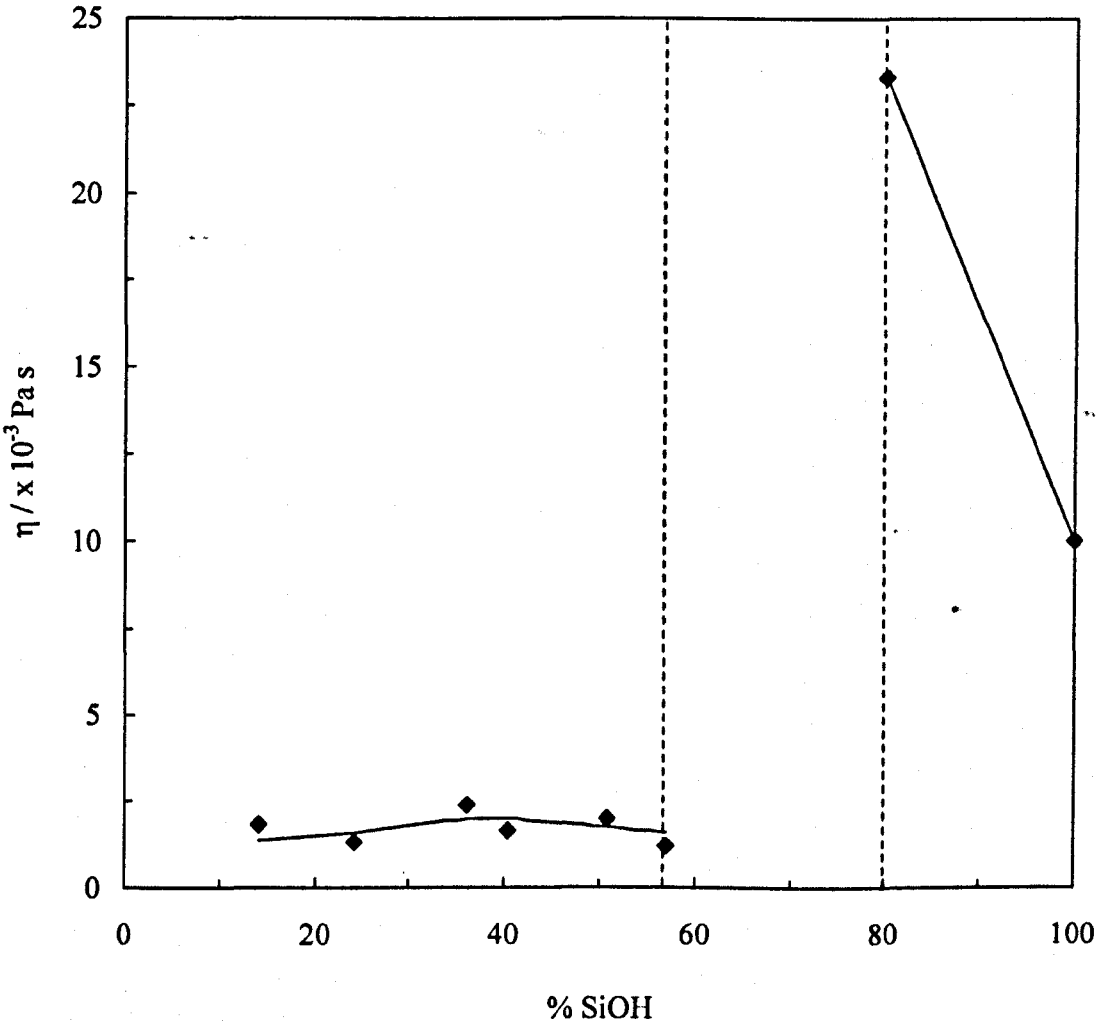

Figure 6.12 Viscosity (η) as a function of % SiOH on silica particle surfaces at a fixed applied shear rate (γ) of 25 s^{-1} for oil-in-water emulsions containing 5 vol. % decane, 0.2 wt. % silica particles and 1 mM aqueous $C_{12}E_5$. The vertical dashed lines indicate the region where a gel-like deposit was observed.

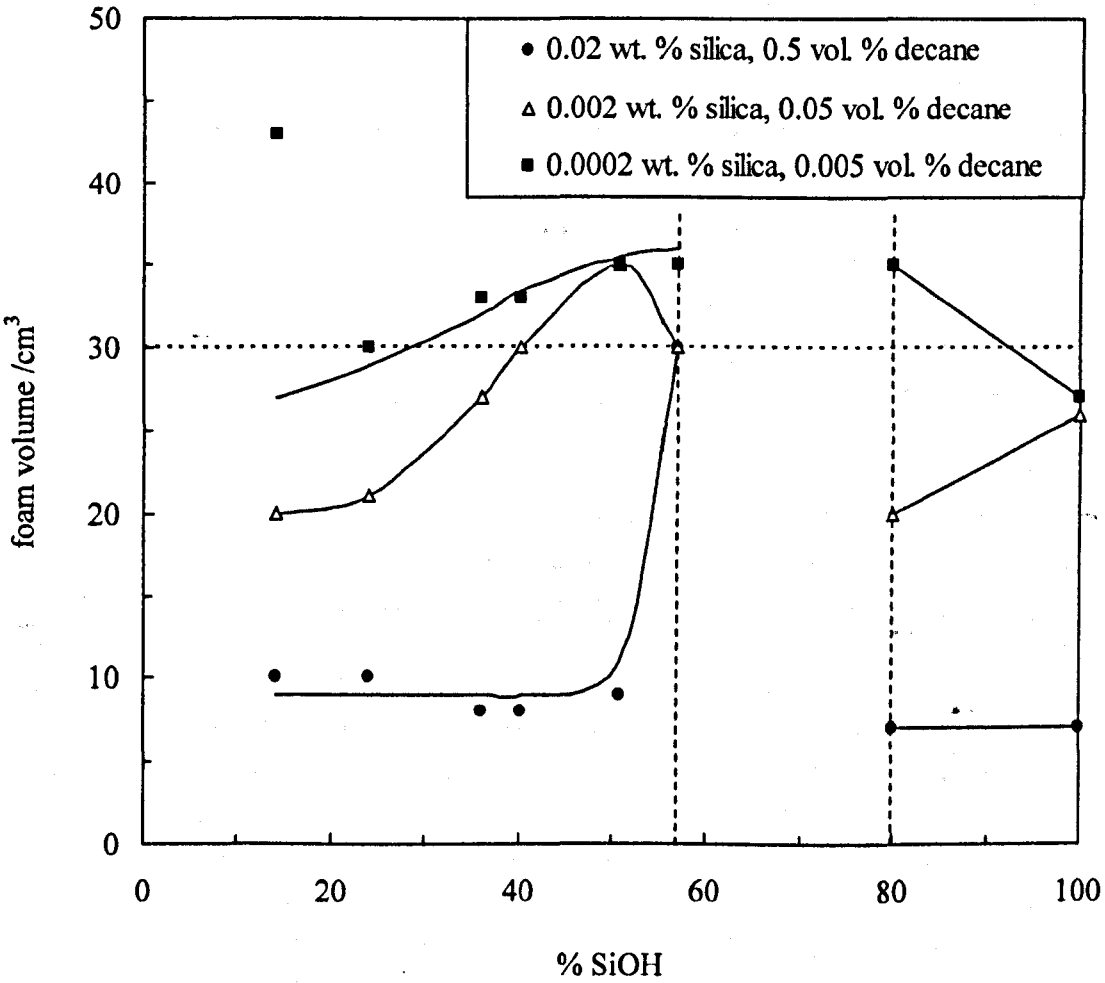

Figure 6.13 Initial foam volume as a function of % SiOH for emulsions initially containing 0.2 wt. % of silica particles, 5 vol. % of decane and 1 mM $C_{12}E_5$. Emulsion sequentially diluted using aqueous $C_{12}E_5$. Foam created by shaking 30.0 cm^3 of the emulsion in a 100 cm^3 stoppered measuring cylinder. The horizontal dashed line shows the foamability of $C_{12}E_5$ (1 mM) in the absence of oil or particles. The vertical dashed lines show the range of % SiOH values where emulsions could not be formed. Measurements made at ambient temperature.

foamability data is available for emulsions made from silica particles with a % SiOH of 65.7 because the emulsion cannot be made. All of the emulsions with compositions of 0.2 wt. % silica and 5 vol. % decane fail to foam upon shaking

Figure 6.14 shows the foam stability, as judged by half-life, of the emulsions detailed above. Systems containing 0.02 wt. % silica and 0.5 vol. % decane produce only transient foam, except for when the % SiOH on the particles is 57.0 and foam exhibiting a reasonable level of stability is formed. This foam is still less stable than the foam formed from pure surfactant however. For systems containing 0.002 wt. % silica and 0.05 vol. % decane, foam stability is generally lower than the pure surfactant case. The exception to this is at intermediate % SiOH where stability slightly exceeds that of the pure surfactant case. For the lowest concentrations of particles and oil, below % SiOH contents of approximately 50, the foam formed is less stable than foam formed from pure surfactant. There is then a dramatic increase in foam stability at intermediate SiOH surface coverage, which shifts stability in excess of the pure surfactant case. Foam stability then progressively decreases as % SiOH surface content on the particles increases and at maximum % SiOH content, the foam is less stable than for the pure surfactant case.

Foaming of the emulsions – variation of decane concentration

Figure 6.15 shows how the foamability of the nonionic surfactant solution varies as a function of the % SiOH on the silica particle surfaces for different concentrations of decane. Each data series represents a different concentration of decane but the same concentration of silica particles (0.2 wt. %). Maximum foam stability is observed for the system containing the least oil and corresponds to the situation where the % SiOH on the particle surfaces is approximately 40. All of the solutions of nonionic surfactant containing oil and silica particles have a lower foamability relative to the pure surfactant case. This is in contrast to systems containing low concentrations of both oil and silica particles, where, at intermediate SiOH surface coverages, foamability was seen to increase beyond the value of pure nonionic surfactant solution (Figure 6.13).

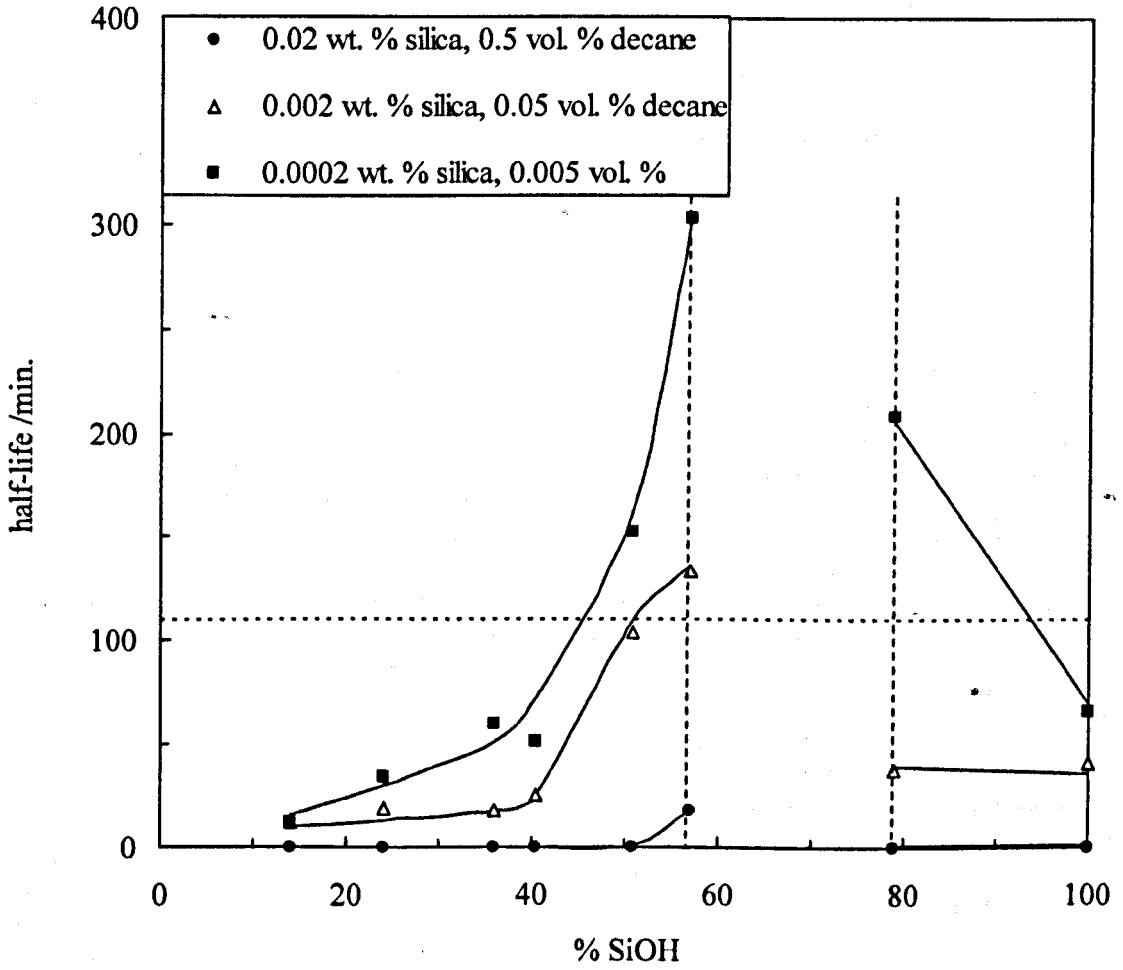

Figure 6.14 Foam half-life as a function of % SiOH for emulsions initially containing 0.2 wt. % of silica particles, 5 vol. % of decane and 1 mM $C_{12}E_5$. Emulsion sequentially diluted using $C_{12}E_5$. Foam created by shaking 30.0 cm^3 of the emulsion in a 100 cm^3 stoppered measuring cylinder. The horizontal dashed line shows the half-life of $C_{12}E_5$ foam (1 mM) in the absence of oil or particles. The vertical dashed lines show the range of % SiOH values where emulsions could not be formed. Measurements made at ambient temperature.

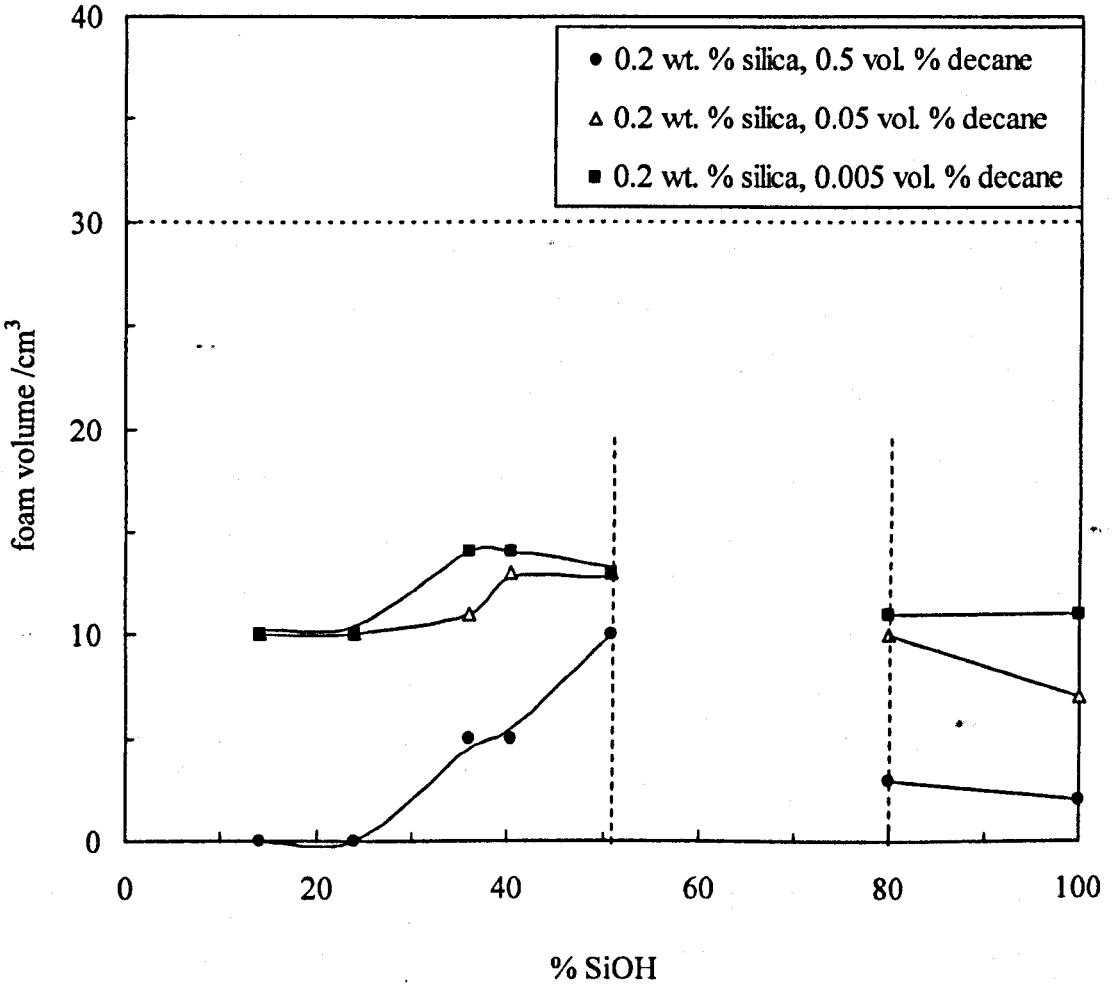

Figure 6.15 Initial foam volume as a function of % SiOH for emulsions initially containing 0.2 wt. % of silica particles, 5 vol. % of decane and 1 mM $C_{12}E_5$. Emulsion sequentially diluted using aqueous $C_{12}E_5$ (1 mM) containing dispersed silica. Foam created by shaking 30.0 cm^3 of the emulsion in a 100 cm^3 stoppered measuring cylinder. The horizontal dashed line shows the foamability of $C_{12}E_5$ (1 mM) in the absence of oil or particles. The vertical dashed lines show the range of % SiOH values where emulsions could not be formed. Measurements made at ambient temperature.

Figure 6.16 shows the stability of foam stabilised by $C_{12}E_5$ in the presence of decane and silica particles. Again, the concentration of particles is fixed throughout all of these systems, only the concentration of decane and the % SiOH on the particle surfaces are varied. All of the systems containing relatively high concentrations of decane (0.5 vol. %) have very low foam stabilities. The systems containing lower concentrations of decane, (0.05 vol. % and 0.005 vol. %) all have stabilities equal to or greater than the pure $C_{12}E_5$ case. Unlike the systems containing a lower concentration of dispersed silica particles (discussed in the previous section), increasing the % SiOH on the silica particles surfaces progressively increases the stability of the resulting foam.

6.4 Foaming behaviour at intermediate values of % SiOH on the silica particle surfaces

As observed throughout this work, at intermediate % SiOH content, foamability and foam stability are generally observed to sharply increase. For certain particle and oil concentration regimes, foam stability is boosted beyond the pure surfactant case at these intermediate hydrophobicities. When preparing the emulsions, the gel-like deposit was formed at an intermediate % SiOH content value (65.7 %) when attempting to homogenise decane into the silica-$C_{12}E_5$ dispersion. The % SiOH corresponding to the formation of this deposit also corresponds to the maximum observed in two of the stability plots (Figures 6.6 and 6.14) and the foamability plots when silica is initially dispersed in the surfactant solution (Figures 6.13 and 6.15).

It is therefore likely that this deposit is responsible for the observed increase in foamability and foam stability of several of the systems. The deposit, which is white in appearance, disperses in decane but not in water and so it can be termed hydrophobic. Figure 6.17 shows a micrograph of this material. The material was also placed under a microscope between crossed polarisers. This was to assess whether it exhibited birefringence and was therefore likely to be a liquid crystalline phase. Petrov and Naidenova demonstrated that foam films stabilised by aqueous solutions of nonionic surfactant can be stabilised by liquid crystals.[14] The liquid crystalline phase collects at the nodes of the Plateau borders and slows the flow through the

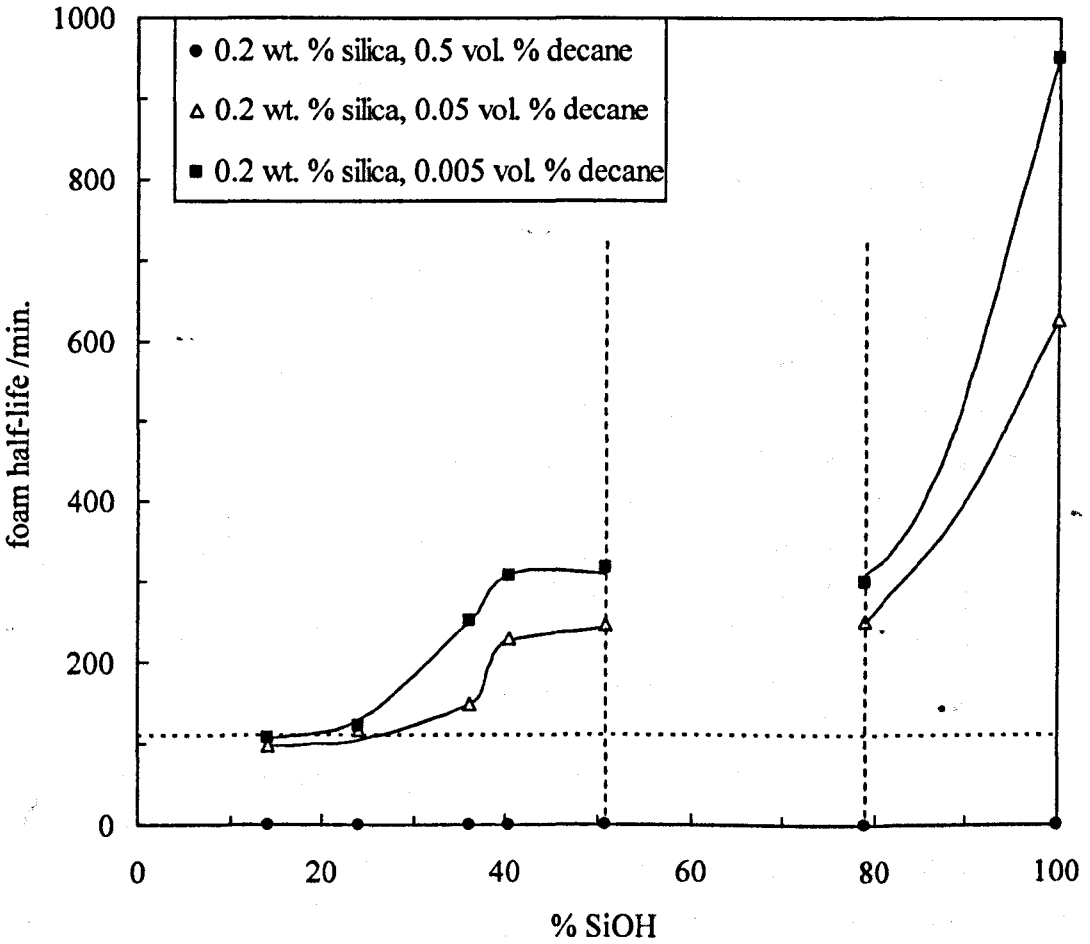

Figure 6.16 Foam half-life as a function of % SiOH for emulsions initially containing 0.2 wt. % of silica particles, 5 vol. % of decane and 1 mM $C_{12}E_5$. Emulsion sequentially diluted using aqueous $C_{12}E_5$ (1 mM) containing dispersed silica. Foam created by shaking 30.0 cm^3 of the emulsion in a 100 cm^3 stoppered measuring cylinder. The horizontal dashed line shows the half-life of $C_{12}E_5$ foam (1 mM) in the absence of oil or particles. The vertical dashed lines show the range of % SiOH values where emulsions could not be formed. Measurements made at ambient temperature.

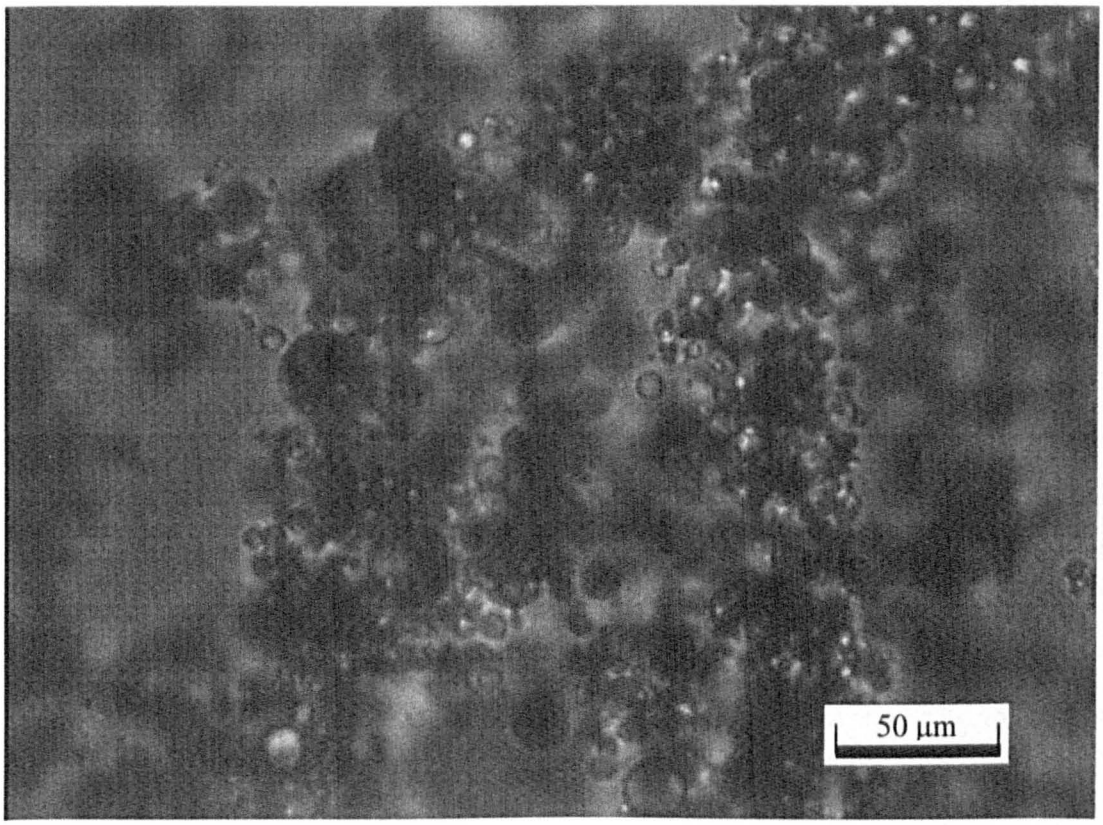

Figure 6.17 A micrograph of the gel-like deposit which is formed when decane is emulsified into 1 mM $C_{12}E_5$ containing a dispersion of 0.2 wt. % of silica with 65.7 % SiOH on their surfaces.

lamella by frictional resistance. It also acts as a non-specific reservoir for the surfactant confirming the earlier work of Friberg.[15] It was found however, that the material obtained from homogenising decane into a dispersion of 0.2 wt. % silica (57.0 % SiOH) in $C_{12}E_5$ did not exhibit birefringence.

6.5 Postulated mode of action of nm-silica particles and decane

For systems containing silica, decane and $C_{12}E_5$, a maximum in foam stability is observed at intermediate % SiOH coverage on the silica particles although for % SiOH values above and below this, good anti-foam action is observed. The fact that a deposit is formed at intermediate % SiOH coverage when attempting to prepare emulsions using the homogeniser, suggests that it is this material which is responsible for the observed increases in foam stability.

As noted in section 6.2, it is possible that different entities are formed depending upon the % SiOH surface content on the silica particles used. At low % SiOH coverages, the particles remain largely, dispersed in the oil (Figure 6.1, picture 1). This oil drop will act as an anti-foam by a bridging-type mechanism. An intermediate % SiOH on the silica particle surfaces results in them no longer remaining completely dispersed in the oil. The silica particles may now prefer to co-adsorb with surfactant at the oil-water interface (Figure 6.1, picture 2). The entity is predicted to be partially hydrophobic (due to the presence of the relatively hydrophobic particles at the interface) and will favour the air-water interface as opposed to the aqueous phase within the foam. The system containing the partially hydrophobic gel-like deposit which is formed when particles of intermediate hydrophobicites are used in combination with decane and $C_{12}E_5$ is expected to be in this configuration. This configuration of particles and oil may increase the stability of the foam in a similar was to that observed by Johansson et al.[16] They noted that particles of intermediate hydrophobicity concentrated along the edges of Plateau borders and provided rigidity to the foam structure.

When the most hydrophilic silica particles (high % SiOH) are used, the particles favour the aqueous phase and so the oil drop is stabilised solely by the surfactant.

(Figure 6.1, picture 3). Again, the oil drop can reduce foam stability by acting in a bridging mechanism. This explanation is viable because of the increase in viscosity noted for the two emulsion systems containing surfactant, decane and the two most hydrophilic silica particle types. This increase in viscosity could be attributed to the particles being present in the aqueous solution and networking together. In Figure 6.16, it can be seen that increasing the % SiOH on the silica particle surfaces results in a progressive increase in the resulting stability of the foam. This could be due to the higher concentration of particles in the system retarding film drainage by (blocking the Plateau borders) and opposing the bridging effect by the oil/particle entity.

The data relating to the foamability of $C_{12}E_5$ in the presence of particles and oil is now considered. When the oil and silica are added to an aqueous solution of $C_{12}E_5$ (without particle dispersion or homogenisation), the foamability is decreased relative to the pure surfactant case. There is not a substantial boost in foamability at intermediate % SiOH on the particles - in fact the only increase is when 0.04 vol. % decane is used in combination with 0.2 wt. % silica. The reasons for this boost in foamability remain unclear at present. For the foaming systems created by dispersing the silica particles into solutions of $C_{12}E_5$ using ultrasound and then homogenising decane into the resulting dispersion, there is an increase in foamability as the value of % SiOH on the silica particle surfaces approaches intermediate values. This boost in foamability is the greatest for the lowest silica particle concentrations. The reason for this is probably due to the enhanced surfactant depletion associated with the higher concentration of dispersed particles. Depleting the surfactant would oppose the foamability boosting effect (presumably caused by the gel-like deposit) by lowering the equilibrium surfactant concentration (see chapter 5).

6.6 Conclusions

- Silica particles not initially dispersed in surfactant solution can be used in conjunction with decane to reduce the foamability of a $C_{12}E_5$ surfactant solution. This reduction in foamability is greater than for the reduction induced by either decane or particles alone. The hydrophobicity of the silica particles has no effect on this foamability reduction.

- The foam stability of $C_{12}E_5$ is reduced by the presence of decane and silica particles (not initially dispersed) when they are used in combination for either high or low % SiOH on the particle surfaces. This decrease is greater than for when either decane or silica particles are used alone. However, an increase in foam stability is observed at intermediate % SiOH coverage.

- Foamability of a $C_{12}E_5$ solution can be controlled using silica particles and decane in combination when particles are initially dispersed in aqueous solution and decane is homogenised into the dispersion to form an emulsion. Depending upon the concentration of decane and silica particles, the foam can be made more or less stable relative to the pure surfactant case. At intermediate % SiOH, a maximum in foamability (for a fixed concentration of particles and oil) is observed.

- The foam stability of $C_{12}E_5$ can be controlled by emulsifying decane into an aqueous $C_{12}E_5$-silica dispersion. Depending upon the concentration of decane or particles used, the foam can be made to be more or less stable relative to the no particle case. At intermediate values of % SiOH on the particles surfaces, there is a dramatic increase in the stability observed.

- The increases in foamability and foam stability can be attributed to the onset of the formation of a gel-like deposit which is formed when systems containing an aqueous solution of $C_{12}E_5$, decane and nm-silica particles with intermediate % SiOH contents on their surfaces are emulsified.

References

1. R. D. Kulkarni, E. D. Goddard and B. Kanner, *Ind. Eng. Chem. Fundam.*, (1977), **16**, 472.
2. R. D. Kulkarni, E. D. Goddard and B. Kanner, *J. Colloid Interface Sci.*, (1977), **59**, 468.
3. R. D. Kulkarni, E. D. Goddard and B. Kanner, *Croat. Chem. Acta*, (1977), **50**, 163.
4. A. Dippenaar, *Int. J. Miner. Process*, (1982), **9**, 1.
5. G. C. Frye and J. C. Berg, *J. Colloid Interface Sci.*, (1989), **127**, 222.
6. R. Aveyard, B. P. Binks, P. D. I. Fletcher, T. G. Peck and C. E. Rutherford, *Adv. Colloid Interface Sci.*, (1994), **48**, 93.
7. R. Aveyard, P. Cooper, P. D. I. Fletcher and C. E. Rutherford, *Langmuir*, (1993), **9**, 604.
8. K. G. Marinova, N. D. Denkov, P. Branlard, Y. Giraud and M. Deruelle, *Langmuir*, (2002), **18**, 3399.
9. K. G. Marinova, N. D. Denkov, S. Tcholakova and M. Deruelle, *Langmuir*, (2002), **18**, 8761.
10. P. R. Garrett in *Defoaming: Theory and Industrial Applications*; P. R. Garrett, Ed., Marcel Dekker, New York, 1993, Chapter 1.
11. See Chapter 5 of this thesis for details of the adsorption of nonionic surfactant onto the nm-silica particles.
12. B. R. Midmore, *Colloids and Surfaces A*, (1998), **145**, 133.
13. V. Bergeron, P. Cooper, C. Fischer, J. Giermanska-Kahn, D. Langevin and A. Pouchelon, *Colloids and Surfaces A*, (1997), **122**, 103.
14. A. G. Petrov and S. Naidenova, *J. Dispers. Sci. Technol.* (1980), **1**, 283.
15. S. Friberg, *Mol. Cryst. Liq. Cryst.* (1977), **40**, 49.
16. G. Johansson and R. J. Pugh, *Int. J. Mineral Process.*, (1992), **34**, 1.

Chapter 7

CHAPTER 7

Conclusions and future work

This chapter is separated into two sections. In the first section (7.1), the overall conclusions from the various studies in this thesis are summarised. In the second section (7.2), some suggestions for future work are given.

7.1 Conclusions

7.1.1 Foaming of nonionic surfactants in the absence of additives

The foamability of the aqueous solutions of C_nE_m series of surfactants depends on the hydrophobic tail length. Increasing the tail length of the surfactant increases the surfactant's foamability. The foamability of the C_nE_m series of surfactants does not depend on the hydrophilic chain length. Additionally, for the C_nE_m series of surfactants, $C(1/2)$ (the concentration corresponding to the transition from non-foaming to foaming behaviour) is below the cmc for short chain surfactants (suggesting equilibrium control of the foamability) and above the cmc for long chain surfactants, suggesting dynamic adsorption control and/or surfactant depletion.

At a fixed surfactant concentration in excess of the cmc, increasing either the hydrophobic tail length or the size of the hydrophilic head group of a surfactant increases the resulting foam's stability.

7.1.2 Foaming of nonionic surfactants in the presence of n-alkane oil vapours

The main effect of incorporating oil vapours during foam generation with nonionic surfactant is that the surfactant concentration required to achieve the transition from non-foaming to foaming behaviour $C(1/2)$ is increased. In the presence of oil vapour,

$C(1/2)$ is higher than the cmc for the range of oil + surfactant systems studied in this work. Following foam generation, its decay is accelerated by the presence of oil vapour. Increasing the oil vapour concentration causes a progressive decrease in both the foamability and stability of foam stabilised by $C_{12}E_5$ and decreasing the molar volume of oil results in increased foam inhibition effects for foam stabilised by $C_{10}E_5$.

7.1.3 Foaming of $C_{12}E_5$ in the presence of nm-silica particles

In the presence of dispersed silica particles, the foamability of $C_{12}E_5$ is reduced relative to the pure surfactant case. For a fixed dispersed particle concentration, this reduction in foamability is the greatest for the most hydrophobic silica particles (low % SiOH). For a fixed value of % SiOH on the particle surfaces, the reduction in foamability is the greatest for higher concentrations of dispersed particles. These findings are consistent with the fact that $C_{12}E_5$ adsorbs onto the surfaces of the more hydrophobic silica particles more than the more hydrophilic particles. This adsorption reduces the equilibrium surfactant concentration. Lower equilibrium surfactant concentrations correspond to lower foamabilities.

TEM has shown that silica particles form networks and do not exist as discrete particles when dispersed in surfactant solutions. This observation is consistent with the idea that improved foam stability is observed for $C_{12}E_5$ (except when the most hydrophobic particles are dispersed at low concentrations) due to the possible blocking of the Plateau borders and hence retardation of liquid drainage from the foam films.

Although the commercial equivalent of $C_{12}E_7$ (Lutensol AO7) does not stabilise foam as effectively and is not as foaming as its purer counterpart, it behaves in a similar way to $C_{12}E_7$ in the presence of dispersed silica particles.

7.1.4 Foaming of $C_{12}E_5$ in the presence of n-alkanes and nm-silica particles

Foamability of a $C_{12}E_5$ solution can be controlled using silica particles and decane in combination when particles are initially dispersed in aqueous solution and decane is homogenised into the dispersion to form an emulsion. Depending upon the concentration of decane and silica particles, the foam can be made more or less stable relative to the pure surfactant case. At intermediate % SiOH, a maximum in foamability (for a fixed concentration of particles and oil) is observed.

The increase in foamability and foam stability observed for certain systems can be attributed to the onset of the formation of a deposit of unknown structure which is formed when emulsifying (either by shaking or homogenisation) systems containing an aqueous solution of $C_{12}E_5$, decane and nm-silica particles with intermediate % SiOH contents on their surfaces.

7.2 Future work

7.2.1 Developing the understanding of foaming limits as a function of surfactant tail length

Figure 7.1 shows a way in which the crossover in foamability as a function of surfactant tail length described in section 3.3.1 and 3.3.3 could be investigated further. As stated in section 3.3.3, surfactant depletion may play an important role in limiting foamability when surfactants with longer tails are used. This is due to the low values of $C(1/2)$ associated with longer-tailed surfactants required to induce foaming. By having a larger surfactant reservoir as depicted in Figure 7.1, this potential complication is completely avoided. The bubble rise time could not be varied in the experiments described in chapter 3. The apparatus in Figure 7.1 does however allow this to be changed by varying the immersion depth. This allows the factors limiting foamability to be more fully examined. For example, if the foamability for a particular surfactant is limited by adsorption dynamics (suspected for long-tailed surfactants), increasing the time the bubble travels through the surfactant solution for (by raising the immersion depth) should allow the critical level of adsorption, required

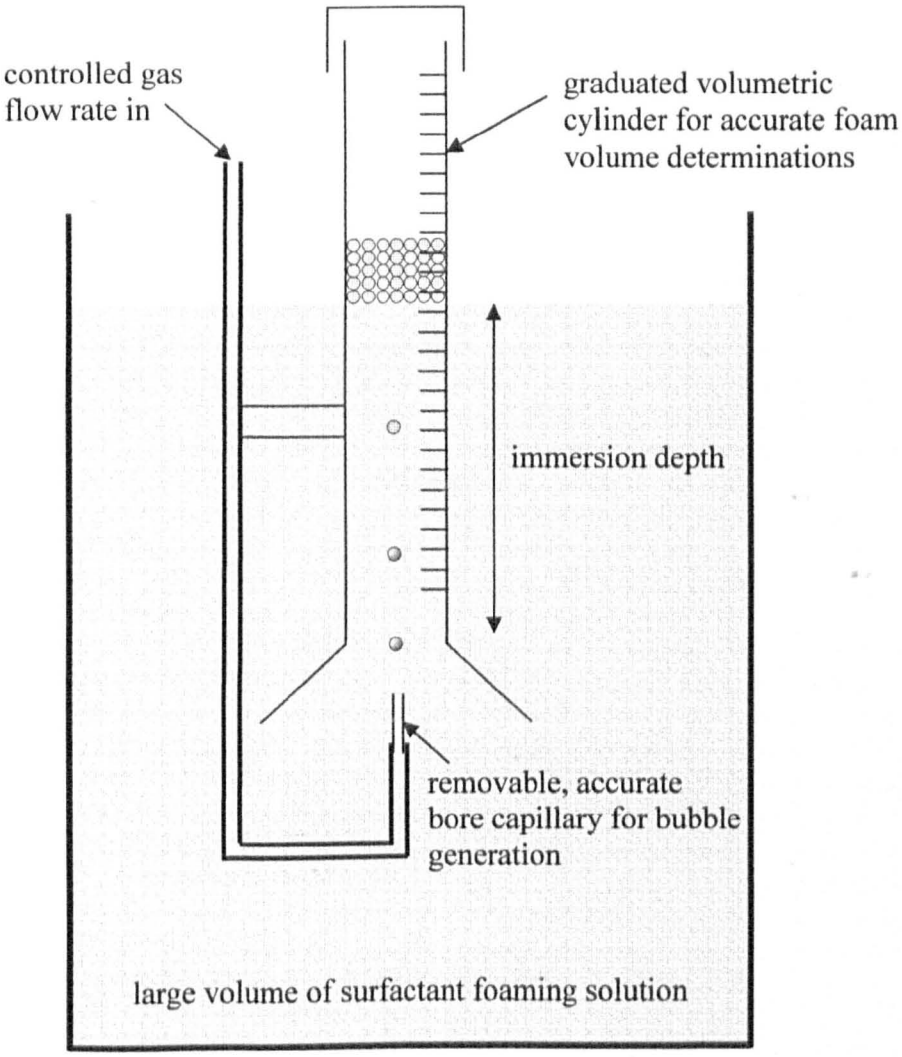

Figure 7.1 A refined foam generation system which permits the rise time of the bubble to be controlled and avoids the complications arising from surfactant depletion.

to stabilise the bubble to occur at a lower surfactant concentration because although the surfactant adsorption dynamics will be slower, the gas bubble is in contact with the surfactant solution for longer. This would be reflected experimentally by a decrease in the value of $C(1/2)$ obtained for this surfactant as a function of increasing bubble rise time. As discussed above, surfactant depletion would not complicate the measurements.

7.2.2 Foams stabilised in the absence of surfactant

As part of ongoing exploratory work, an attempt was made to stabilise foam in the absence of any surfactant using only silica particles.

Just as surfactants can be described by using their hydrophile-lipophile balance number depending on whether they are mostly oil-liking or water-liking, solid spherical particles can be described by their wettabilities as judged by their contact angle.[1] By dispersing hydrophilic silica particles in water and bubbling through a volatile compound which is capable of reacting with the surface silanols (Si-OH) groups and making the surface of the silica more hydrophobic, one would expect the particles to be gradually promoted to the air/water surface. At a critical hydrophobicity, the particles may sit in the interface and be capable of forming a shell around a gas bubble thus stabilising foam. To test this idea, N_2 gas was bubbled through HMDS, and through a solution of hydrophilic silica dispersed in water.

HMDS can react with silica surfaces in the following way:

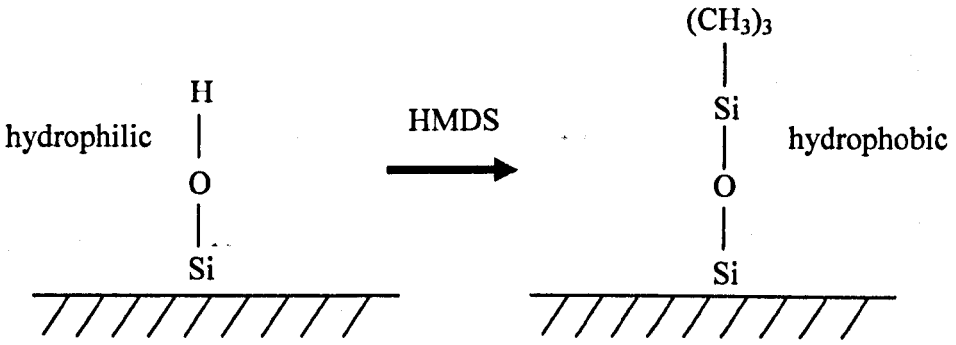

This process will make hydrophilic silica more hydrophobic.

2 wt. % of silica (79.9 % SiOH) was dispersed in 25.0 cm^3 of water. HMDS was bubbled through this dispersion for 305 min. Towards the end of this time, the bubbles became more persistent at the surface. The dispersion was transferred to a glass bottle and was shaken. There was evidence of foam being formed, and the time it took to collapse fully was around 3 min. When 0.1 M salt was added, the time taken for the bubbles to fully collapse increased slightly to 4 min.

4 wt. % of silica (79.9 % SiOH) was dispersed in 25.0 cm^3 of water using the ultrasonic probe. HMDS was bubbled through the dispersion for 5 hrs. The resulting solution was reminiscent of an emulsion. This was centrifuged for 1 hr at 5000 rpm. A white precipitate collected at the bottom of the tube. There was also evidence of particles at the top of the solution and around the edges of the tube. The supernatant was not clean and there was evidence of silica which remained suspended. Slight agitation resulted in the supernatant becoming cloudy. The supernatant did not appear to be oily in nature and there was no evidence of an oily film. The solution still foamed slightly upon shaking.

HMDS was bubbled through pure water for 300 min. The surface tension of the water before bubbling was 72.0 mN m^{-1} and after bubbling it dropped to 58.1 mN m^{-1}. This

indicates that the reaction of HMDS and water yields a substance which appears to be surface active. However, the water-HMDS system did not foam upon shaking. The fact that foam is formed when bubbling HMDS through water containing dispersed particles but not formed when HMDS is bubbled through pure water, suggests that the particles give rise to a certain level of foam stability when they reach a critical hydrophobicity. More work is required to test these preliminary ideas further.

References

1. B. P. Binks, *Curr. Opin. Colloid Interface Sci.*, (2002), **7**, 21.

Appendix A

APPENDIX A

Code for the Visual BASIC modules used within Excel to calculate values of $C(1/2)$.

Module used to calculate C_{eq}

```
Function ceq(Gcrit, Gfactor, Gcmc, y, cmc, cmcfactor)
a = Application.Ln(-Gcrit / (Gcrit - Gfactor * Gcmc))
b = Application.Ln(cmc / cmcfactor)
c = Exp((a + b * y) / y)
If c <= cmc Then ceq = c Else ceq = "error"
End Function
```

Module used to calculate C_{dyn}

```
Function cdyn(Gcrit, Gfactor, Gcmc, y, cmc, cmcfactor, t, x, c1, c0, ceqm)
cmax = 1
c = ceqm
10 If c <= cmc Then Geq = Gfactor * Gcmc * (c ^ y / (c ^ y + (cmc / cmcfactor) ^ y))
Else Geq = Gcmc
thalf = 10 ^ (c1 * 0.4342944 * Application.Ln(c) + c0)
rhs = Geq * (t ^ x / (t ^ x + (thalf) ^ x))
If rhs > Gcrit Then GoTo 100
c = c * 1.01
If c >= cmax Then GoTo 100
GoTo 10

100 If c < cmax And (rhs / Gcrit) < 1.02 Then cdyn = c Else cdyn = "error"
End Function
```

Appendix B

Figure 3.1

upper plot

x	y
5	33.5
7	66.0
8	81.4
9	89.5

lower plot

x	y
14	25.5
12	33.5
10	47.0
8	65.0

Figure 3.2

$n = 8$		$n = 10$		$n = 12$		$n = 14$	
x	y	x	y	x	y	x	y
0.00001	0.0	0.00001	0.0	0.00001	0.0	0.000001	0.0
0.00004	22.5	0.00004	0.0	0.00004	50.0	0.00001	60.0
0.0001	47.5	0.0001	0.0	0.0001	200.0	0.00002	115.0
0.0005	100.0	0.0002	72.5	0.0005	387.5	0.00004	170.0
0.001	122.5	0.0003	163.0	0.001	457.5	0.0001	275.0
0.005	200.0	0.0005	230.0	0.005	457.5	0.0002	400.0
0.01	280.0	0.001	305.0	0.01	452.5	0.0005	400.0
0.04	280.0	0.003	352.5	0.04	455.0	0.001	415.0
		0.005	375.0			0.005	410.0
		0.01	375.0			0.01	415.0
		0.04	388.0			0.04	420.0

Figure 3.3

x	y
8	284.0
10	385.0
12	456.0
14	400.0

Figure 3.4

x	log(cmc /M)	log(C(1/2) /M)
8	-2.17	-2.89
10	-3.09	-3.46
12	-4.22	-3.91
14	-5.00	-4.24

Figure 3.5

$m = 5$		$m = 7$		$m = 8$		$m = 9$	
x	y	x	y	x	y	x	y
0.00001	0.0	0.000001	0.0	0.000001	0.0	0.000001	0.0
0.00004	50.0	0.00001	0.0	0.00001	10.0	0.00001	0.0
0.0001	200.0	0.00004	57.5	0.00004	52.5	0.00004	47.5
0.0002	300.0	0.0001	110.0	0.0001	100.0	0.0001	200.0
0.0005	387.5	0.0002	350.0	0.0002	320.0	0.0002	400.0
0.001	457.5	0.0005	447.5	0.0005	400.0	0.0005	445.0
0.005	457.5	0.001	470.0	0.001	445.0	0.001	467.5
0.01	452.5	0.005	480.0	0.005	460.0	0.005	480.0
0.04	455.0	0.01	477.5	0.01	457.5	0.01	480.0
		0.04	480.0	0.04	460.0	0.04	480.0

Figure 3.6

x	y
5	456.0
7	481.0
8	456.6
9	479.0

Figure 3.7

x	log(cmc/ M)	log(*C*(1/2) /M)
5	-4.19	-3.91
7	-4.10	-3.71
8	-4.04	-3.71
9	-4.00	-3.89

Figure 3.8

x	log(cmc/M)	log(*C*(1/2) /M) exp	log(*C*(1/2) /M) calc
6	-1.05	-	-1.62
8	-2.17	-2.89	-2.88
10	-3.09	-3.46	-3.46
12	-4.22	-3.91	-3.68
14	-5.00	-4.24	-3.75
16	-6.00	-3.70	-3.83

Figure 3.9

x	y
0.000024	0.0
0.00024	1.0
0.0024	2.0
0.024	10.0
0.10697	17.0

Figure 3.10

x	y
0	480.0
1	470.0
2	465.0
3	460.0
4	460.0
6	450.0
9	430.0
15	310.0
19	230.0
22	200.0
23	180.0
24	150.0
25	140.0
26	120.0
31	70.0
36	40.0
40	25.0
51	10.0
120	0.0

Figure 3.11

x	y
8	3.8
10	9.4
12	18.0
14	23.4

Figure 3.12

x	y
5	18.0
7	21.2
8	23.0
9	22.3

Figure 3.13

20.0 °C		25.0 °C	
x	y	x	y
0.000001	0.0	0.00001	0.0
0.00001	0.0	0.00004	50.0
0.0001	85.0	0.0001	200.0
0.001	480.0	0.0005	387.5
0.01	485.0	0.001	457.5
0.1	475.0	0.005	457.5
		0.01	452.5
		0.04	455.0

Appendix C

Figure 4.1

hexane		octane		decane		dodecane	
x	y	x	y	x	y	x	y
0	0.21	0	0.2	0	0.2	0	0.2
15	0.13	15	0.19	15	0.2	15	0.2
30	0.09	30	0.18	30	0.2	30	0.2
45	0.06	45	0.18	45	0.2	45	0.2
60	0.03	60	0.17	60	0.2	60	0.2
75	0.02	75	0.17	75	0.2	75	0.2
90	0.004	90	0.16	90	0.19	90	0.2

Figure 4.2

x	y
6	65.19
8	96.69
10	98.3
12	99.68

Figure 4.3

x	theory	1 bubbler	2 bubblers	3 bubblers
0	0.0000	0.0000	0.0000	0.0000
15	0.0300	0.0130	0.0260	0.0290
30	0.0600	0.0246	0.0490	0.0590
45	0.0900	0.0365	0.0700	0.0900
60	0.1300	0.0456	0.0950	0.1200
75	0.1600	0.0567	0.1160	0.1520
90	0.1900	0.0667	0.1400	0.1850

Figure 4.4

no oil		+ decane	
x	y	x	y
0.00001	0.0	0.00001	0.0
0.00004	22.5	0.00004	25.0
0.0001	47.5	0.0001	40.0
0.0005	100.0	0.0005	40.0
0.001	122.5	0.001	45.0
0.005	200.0	0.005	50.0
0.01	280.0	0.01	80.0
0.04	280.0	0.02	150.0
		0.04	240.0
		0.07	330.0
		0.1	345.0
		0.3	345.0

Figure 4.5

no oil		+ decane	
x	y	x	y
0.00001	0.0	0.00001	0.0
0.00004	0.0	0.00004	40.0
0.0001	0.0	0.0001	50.0
0.0002	72.5	0.0005	90.0
0.0003	163.0	0.001	110.0
0.0005	230.0	0.003	170.0
0.001	305.0	0.005	270.0
0.003	352.5	0.01	350.0
0.005	375.0	0.04	440.0
0.01	375.0	0.1	440.0
0.04	388.0		

Figure 4.6

no oil		+ decane	
x	y	x	y
0.00001	0.0	0.00001	0.0
0.00004	50.0	0.00004	60.0
0.0001	200.0	0.0001	80.0
0.0005	387.5	0.0005	100.0
0.001	457.5	0.001	300.0
0.005	457.5	0.005	400.0
0.01	452.5	0.01	420.0
0.04	455.0	0.04	450.0
		0.2	455.0

Figure 4.7

no oil		+ decane	
x	y	x	y
0.000001	0.0	0.00001	0.0
0.00001	60.0	0.00004	35.0
0.00002	115.0	0.0001	80.0
0.00004	170.0	0.0002	155.0
0.0001	275.0	0.0003	220.0
0.0002	400.0	0.0005	330.0
0.0005	400.0	0.001	390.0
0.001	415.0	0.005	405.0
0.005	410.0	0.01	410.0
0.01	415.0	0.04	410.0
0.04	420.0		

Figure 4.8

x	log(cmc /M)	log(*C*(1/2) /M) no oil	log(*C*(1/2) /M) decane
8	-2.17	-2.89	-1.65
10	-3.09	-3.46	-2.49
12	-4.22	-3.91	-3.13
14	-5.00	-4.24	-3.56

Figure 4.9

x	no oil	+ decane
8	284.0	345.0
10	385.0	445.0
12	456.0	456.0
14	400.0	400.0

Figure 4.10

no oil		+ decane	
x	y	x	y
0	480.0	0	460.0
1	470.0	1	400.0
2	465.0	2	350.0
3	460.0	3	300.0
4	460.0	4	280.0
6	450.0	5	260.0
9	430.0	6	240.0
15	310.0	7	200.0
19	230.0	8	180.0
22	200.0	9	150.0
23	180.0	10	130.0
24	150.0	11	110.0
25	140.0	12	90.0
26	120.0	13	70.0
31	70.0	14	60.0
36	30.0	15	50.0
40	20.0	22	25.0
51	10.0	50	10.0
120	0.0	116	0.0

Figure 4.11

x	no oil	+ decane
8	3.84	1.46
10	9.39	3.60
12	18.00	6.50
14	23.40	14.00

Figure 4.12

	no oil				+ decane			
x	$n=5$	$n=7$	$n=8$	$n=9$	$n=5$	$n=7$	$n=8$	$n=9$
0.000001	0.0	0.0	0.0	0.0	0.0	0.0	0.0	0.0
0.00001	0.0	0.0	10.0	0.0	0.0	0.0	0.0	0.0
0.00004	50.0	57.5	52.5	47.5	60.0	0.0	0.0	0.0
0.0001	200.0	110.0	100.0	200.0	80.0	50.0	60.0	50.0
0.0005	387.5	447.5	400.0	445.0	100.0	140.0	100.0	85.0
0.001	457.5	470.0	445.0	467.5	300.0	300.0	260.0	150.0
0.005	457.5	480.0	460.0	480.0	400.0	450.0	455.0	300.0
0.01	452.5	477.5	457.5	480.0	420.0	450.0	450.0	400.0
0.04	455.0	480.0	460.0	480.0	450.0	440.0	455.0	450.0
0.1								450.0
0.2					455.0			

Figure 4.13

x	log(cmc/M)	log(C(1/2) /M) no oil	log(C(1/2) /M) decane
5	-4.19	-3.91	-3.13
7	-4.10	-3.71	-3.16
8	-4.04	-3.71	-3.08
9	-4.00	-3.89	-2.65

Figure 4.14

x	no oil	+ decane
5	456.0	456.0
7	481.0	446.0
8	456.6	456.6
9	479.0	446.0

Figure 4.15

x	no oil	+ decane
5	18.0	6.5
7	21.2	3.9
8	23.0	3.9
9	22.3	3.9

Figure 4.16

x	Γ_{os}	$R_{foamability}$	$R_{foam\ stability}$
8	1.22	17.36	0.070
10	1.28	9.34	0.137
12	1.42	6.13	0.232
14	1.63	4.78	0.341

Figure 4.17

x	Γ_{os}	$R_{foamability}$ /cmc	$R_{foam\ stability}$ /cmc
8	1.22	2591.69	392.56
10	1.28	11527.38	3220.16
12	1.42	102185.79	46153.85
14	1.63	478260.87	167142.86

Figure 4.18

x	Γ_{os}	$R_{foamability}$	$R_{foam\ stability}$
5	1.42	6.13	2.771
7	2.02	3.55	5.44
8	2.31	4.27	5.90
9	2.59	17.36	5.72

Figure 4.19

no oil		octane		decane		dodecane	
x	y	x	y	x	y	x	y
0.00001	0.0	0.00001	0.0	0.00001	0.0	0.00001	0.0
0.00004	0.0	0.00004	0.0	0.00004	40.0	0.00004	15.0
0.0001	0.0	0.0001	25.0	0.0001	50.0	0.0001	45.0
0.0002	72.5	0.0005	50.0	0.0005	90.0	0.0005	55.0
0.0003	163.0	0.001	70.0	0.001	110.0	0.001	195.0
0.0005	230.0	0.005	80.0	0.003	170.0	0.005	365.0
0.001	305.0	0.01	160.0	0.005	270.0	0.01	405.0
0.003	352.5	0.04	350.0	0.01	350.0	0.063	405.0
0.005	375.0	0.1	470.0	0.04	440.0		
0.01	375.0			0.1	440.0		
0.04	388.0						

Figure 4.20

decane		dodecane	
x	y	x	y
0.00	395.0	0.00	385.0
0.09	395.0	0.20	395.0
0.20	345.0	0.40	345.0
0.39	305.0	0.60	325.0
0.61	285.0	0.79	285.0
0.78	185.0	1.00	285.0
1.00	100.0		

Figure 4.21

0.00		0.09		0.14		0.20		0.39		0.61		0.78		1.00	
x	y	x	y	x	y	x	y	x	y	x	y	x	y	x	y
0	385.0	0	395.0	0	425.0	0	345.0	0	305.0	0	285.0	0	185.0	0	100.0
1	385.0	1	395.0	1	355.0	1	285.0	1	285.0	1	285.0	1	135.0	1	80.0
5	365.0	2	385.0	2	265.0	2	235.0	2	245.0	2	135.0	2	85.0	2	60.0
12	255.0	3	365.0	3	215.0	3	185.0	3	215.0	3	85.0	3	35.0	3	45.0
15	195.0	5	355.0	6	105.0	4	135.0	5	85.0	6	35.0	15	0.0	5	20.0
20	135.0	6	205.0	11	65.0	5	105.0	7	35.0	17	0.0			6	15.0
28	75.0	7	135.0	14	35.0	6	85.0	19	0.0					10	0.0
32	50.0	8	85.0	19	0.0	18	35.0								
36	25.0	15	0.0			22	0.0								
43	10.0														
50	0.0														

Appendix D

Figure 5.6

1.03E-07		3.73E-06		1.17E-05		2.14E-05		6.01E-05	
x	y	x	y	x	y	x	y	x	y
1	71.05	0	63.19	0	53.44	0	43.8	0	39.61
6	70.94	1	62.88	1	51.92	1	43.83	1	39.92
14	71.08	3	62.77	2	52.29	3	43.92	5	40.66
23	71.12	5	62.75	20	54.57	8	44.17	19	41.54
38	71.17	9	62.62	54	54.80	15	43.99	31	41.62
52	71.09	18	62.11	120	54.76	21	44.00	42	41.54
85	70.98	28	61.86	200	54.76	41	43.67	50	41.65
100	70.91	39	61.58			54	43.64		
110	70.91	47	61.48			65	43.46		
140	70.94	55	61.40			110	43.24		
160	71.01	68	61.13			130	43.12		
252	70.63	85	61.08			222	43.11		
308	70.78	103	60.67						
337	70.94	113	60.90						
		331	59.86						

2.03E-04		5.53E-04		1.17E-03		5.49E-03	
x	y	x	y	x	y	x	y
0	37.43	0	34.77	0	39.68	0	30.42
1	37.34	1	34.74	1	32.69	1	30.40
4	37.39	2	34.74	2	32.69	2	30.38
10	37.37	5	34.74	4	32.62		
15	37.39			5	32.62		
24	37.57						
30	37.57						

Figure 5.7

1.12E-07		6.80E-07		4.93E-06		1.30E-05		2.47E-05	
x	y	x	y	x	y	x	y	x	y
0	70.00	0	69.00	0	63.54	0	53.02	0	53.68
1	70.00	1	69.00	1	63.32	1	53.20	1	54.74
18	69.90	3	68.90	6	63.15	2	53.61	2	53.62
31	69.84	7	68.90	12	62.90	5	53.82	4	53.40
42	69.86	15	68.90	25	62.60	15	53.91	10	53.22
69	69.60	25	68.88	30	62.13	30	54.06	16	53.26
97	69.62	41	68.30	60	61.90	48	54.21	25	53.10
125	69.54	75	68.25	80	61.85	65	54.56	46	52.60
140	69.50	100	68.12	130	61.68	120	54.79	82	52.46
172	69.47	130	67.98	200	61.60	190	55.26	98	52.31
194	69.49	150	68.00	255	61.25	223	55.59	150	52.28
300	69.45	200	67.90	290	61.00	250	55.88	191	52.12
310	69.45	212	67.85	300	61.00	260	55.88	215	52.07
		280	67.83					226	52.00
								233	51.82
								240	51.82

3.36E-05		5.55E-05		1.50E-04		3.19E-04		1.73E-03	
x	y	x	y	x	y	x	y	x	y
0	41.52	0	39.96	0	40.01	0	39.50	0	36.02
1	41.68	1	39.99	1	40.12	1	39.20	1	35.20
2	41.75	5	40.20	2	40.25	2	39.01	4	33.92
7	41.82	12	40.56	8	40.39	4	38.69	5	32.88
12	41.99	25	40.79	25	40.49	5	38.63	6	32.88
25	42.30	38	41.38	30	40.49	6	38.63		
38	42.53	41	42.80						
40	42.61	47	42.80						
46	42.69								
50	42.69								

5.40E-03	
x	y
0	31.40
1	31.38
2	31.40
3	31.40

Figure 5.8

8.31E-07		6.14E-06		2.14E-05		6.01E-05		8.96E-05	
x	y	x	y	x	y	x	y	x	y
0	68.96	0	64.93	0	51.42	0	50.98	0	46.33
1	69.32	1	65.56	1	53.84	1	51.32	1	46.89
2	69.57	5	66.15	4	54.84	2	51.21	2	47.17
41	71.55	15	66.96	13	55.04	5	51.18	33	47.78
109	72.05	72	67.71	43	55.63	7	50.92	58	47.81
114	72.04	116	67.77	64	56.08	46	50.03	76	47.74
166	72.03	120	67.73	151	56.39	60	49.80	90	47.72
		155	67.83	199	56.35	86	49.23	107	47.64
		186	67.89	230	56.35	91	49.18	160	47.68
		189	67.82			110	48.92		
		196	67.84			138	48.77		
						168	48.76		

1.23E-04		3.35E-04		9.10E-04		2.47E-03	
x	y	x	y	x	y	x	y
0	45.35	0	38.96	0	35.04	0	30.45
1	46.31	1	39.27	1	35.12	1	30.43
6	46.84	3	39.58	2	35.02	3	30.43
10	46.90	7	39.64	12	34.35	6	30.44
13	47.20	14	39.73	20	34.34	19	30.40
18	47.24	22	39.93				
22	47.29	40	39.93				
28	47.34						
48	47.40						
62	47.47						
69	47.47						
78	47.44						

Figure 5.9

4.50E-05		6.01E-05		8.96E-05		9.75E-05		1.23E-04	
x	y	x	y	x	y	x	y	x	y
0	57.90	0	57.71	0	53.01	0	53.00	0	50.83
1	57.86	1	58.03	1	52.94	1	52.97	1	50.50
2	57.68	2	58.08	8	52.95	5	53.00	2	50.52
8	57.91	6	58.38	21	52.92	8	53.04	37	50.00
27	58.38	9	58.71	32	52.90	11	52.94	60	50.00
73	58.30	14	59.03	45	52.98	31	52.86	71	50.00
87	58.17	20	59.33	51	52.90	41	52.78		
125	58.10	49	59.61	75	52.70	60	52.78		
135	57.90	58	59.63	95	52.70				
151	57.89	75	59.66						
165	57.85	86	59.65						
217	57.02	97	59.65						
240	57.02								

2.00E-04		3.35E-04		9.10E-04		2.47E-03	
x	y	x	y	x	y	x	y
0	45.43	0	39.85	0	32.73	0	30.01
1	45.43	1	40.30	1	33.20	1	30.01
4	45.78	2	40.47	2	33.54	4	30.06
40	45.79	6	40.62	10	34.16	20	30.26
60	45.79	23	41.03	20	34.43	55	30.18
		59	40.81	61	34.93		
		84	40.80	102	35.00		
		120	40.68	125	35.02		
		180	40.61	180	35.02		
		223	40.49				
		300	40.50				

Figure 5.10

5.80E-06		3.07E-06	
x	y	x	y
0	53.68	1	70.08
1	54.74	3	68.77
2	53.62	6	64.02
4	53.40	11	58.59
10	53.22	17	54.93
16	53.26	25	53.34
25	53.10	39	53.19
46	52.60	53	53.38
82	52.46	135	52.52
98	52.31		
150	52.28		
191	52.12		
215	52.07		
226	52.00		
233	51.82		
240	51.82		

Figure 5.11

no particles		0.2 wt. % 100 %		0.4 wt. % 100 %		0.2 wt. % 79.9 %		0.2 wt. % 65.7 %	
x	y	x	y	x	y	x	y	x	y
-7.51	30.06	-5.20	30.38	-5.22	31.40	-6.01	30.40	-6.01	30.18
-9.25	30.34	-6.01	30.38	-6.36	32.88	-7.00	34.34	-7.00	35.02
-9.72	31.33	-6.75	32.62	-8.05	38.63	-8.00	39.93	-8.00	40.50
-10.01	33.37	-7.50	34.74	-8.80	40.49	-9.00	47.44	-8.52	45.79
-10.42	37.63	-8.50	37.57	-9.80	42.80	-9.32	47.68	-9.00	50.00
-11.00	42.72	-9.25	40.04	-10.30	42.69	-9.72	48.76	-9.24	52.78
-11.50	47.32	-9.72	41.65	-10.35	45.00	-10.05	50.97	-9.32	52.70
-11.75	49.25	-10.01	42.59	-10.42	47.42	-10.38	54.54	-9.72	59.65
-12.20	52.59	-10.38	42.48	-10.61	51.82	-10.75	56.35		
-13.20	58.79	-10.50	43.38	-11.25	55.88	-11.43	61.83		
-14.00	63.27	-10.75	43.11	-12.22	61.00	-12.00	67.84		
-15.00	67.52	-10.80	46.46	-14.20	67.83	-14.00	72.03		
-16.02	71.12	-11.08	45.41	-16.00	69.45				
		-11.36	54.76						
		-12.50	59.86						
		-14.00	65.90						
		-16.09	70.81						

Figure 5.12

100, 0.2 wt. %		79.9, 0.2 wt. %		65.7, 0.2 wt. %	
x	y	x	y	x	y
0.11	0.00	0.11	0.72	1.80	28.54
0.31	0.10	0.31	2.98	4.98	43.22
0.84	0.39	1.91	9.25	7.58	57.30
2.07	1.41	7.89	22.17	10.13	70.30
5.40	3.74	10.23	31.57	16.70	118.42
10.65	5.29	17.91	102.36	29.83	256.15
16.70	5.01	31.05	227.31	44.06	575.24
18.46	4.54	45.86	501.53	58.88	1185.39
18.46	13.93	61.28	1148.29		
30.43	80.59				
46.32	361.50				
54.35	673.72				
63.15	1035.17				
65.07	1146.39				

Figure 5.13

100, 0.2 wt. %		100, 0.4 wt. %	
x	y	x	y
0.11	0.00	0.26	0.14
0.31	0.10	0.81	0.77
0.84	0.39	1.78	1.69
2.07	1.41	4.98	4.50
5.40	3.74	10.33	5.26
10.65	5.29	17.38	4.23
16.70	5.01	27.26	63.23
18.46	4.54	45.40	395.81
18.46	13.93	58.88	1006.97
30.43	80.59		
46.32	361.50		
54.35	673.72		
63.15	1035.17		
65.07	1146.39		

Figure 5.14

0.05 wt. %		0.1 wt. %		0.2 wt. %	
x	y	x	y	x	y
14.1	0.64	14.1	0.52	14.1	0.22
18.3	0.70	18.3	0.52	18.3	0.26
24.1	0.70	24.1	0.57	24.1	0.30
36.0	0.70	36.0	0.61	36.0	0.30
40.4	0.74	40.4	0.61	40.4	0.35
50.9	0.78	50.9	0.65	50.9	0.39
57.0	0.74	57.0	0.74	57.0	0.43
65.7	0.78	65.7	0.74	65.7	0.39
79.9	0.87	79.9	0.78	79.9	0.43
100	0.91	100	0.78	100	0.48

Figure 5.15

0.05 wt. %		0.1 wt. %		0.2 wt. %	
x	y	x	y	x	y
14.1	130.0	14.1	180.0	14.1	0.0
18.3	400.0	18.3	412.5	18.3	15.0
24.1	425.0	24.1	425.0	24.1	35.0
40.4	450.0	40.4	435.0	40.4	185.0
57.0	460.0	57.0	450.0	57.0	435.0
100	470.0	100	475.0	100	460.0

Figure 5.16

0.05 wt. %		0.1 wt. %		0.2 wt. %	
x	y	x	y	x	y
0	1.00	0	1.00	0	1.00
31	1.00	210	0.82	8	1.00
70	0.10	300	0.53	167	0.90
124	0.05	350	0.29	300	0.80
1298	0.00	500	0.12	1422	0.40
		700	0.06	1566	0.30
		1200	0.00	2901	0.05
				5000	0.00

Figure 5.17

0.05 wt. %		0.1 wt. %		0.2 wt. %	
x	y	x	y	x	y
14.1	46	14.1	52	14.1	357
18.3	42	18.3	99	18.3	338
24.1	156	24.1	184	24.1	341
36.0	144	36.0	167	36.0	366
40.4	242	40.4	248	40.4	376
50.9	253	50.9	279	50.9	507
57.0	158	57.0	308	57.0	780
65.7	344	65.7	314	65.7	950
79.9	580	79.9	698	79.9	1142
100	599	100	549	100	1106

Figure 5.19

no particles		0.2 wt. % 100 % SiOH	
x	y	x	y
0	9.0	0	10.0
2	8.0	2	10.0
4	8.0	4	10.0
8	8.0	8	10.0
19	7.5	19	10.0
33	7.0	33	10.0
48	7.0	48	10.0
81	6.5	81	10.0
150	5.0	150	10.0
285	4.0	285	10.0
360	3.0	360	10.0
544	2.5	544	10.0
679	2.0	679	10.0
1337	0.25	1337	4.0
1500	0.25	1500	2.5
2750	0.0	2750	1.25
		3170	1.0
		4190	1.0
		4610	0.0

Figure 5.20

0.2 wt. % 100 % SiOH		0.2 wt. % 79.9 % SiOH		0.2 wt. % 65.7 % SiOH	
x	y	x	y	x	y
0	7.0	0	7.0	0	7.0
2	6.0	2	7.0	2	6.0
4	5.0	4	7.0	4	5.0
8	5.0	8	7.0	8	5.0
19	5.0	19	7.0	19	4.5
33	5.0	33	6.5	33	4.0
48	4.5	48	6.5	48	3.5
81	4.0	81	6.0	81	3.0
150	4.0	150	5.0	150	2.5
285	3.5	285	4.5	285	2.0
360	2.5	360	4.0	360	1.0
544	2.0	544	2.0	544	1.0
679	1.0	679	1.0	679	0.5
1337	0.5	1337	0.5	2350	0.0
1500	0.25	1500	0.5		
2750	0.0	2750	0.5		
		3170	0.0		

Figure 5.21

no particles		0.2 wt. % 100 % SiOH		[C12E5]eq	
x	y	x	y	x	y
0.000001	0.0	0.000001	0.0	0.000003	0.0
0.00001	0.0	0.00001	0.0	0.000021	135.0
0.0001	84.0	0.0001	135.0	0.00005	464.0
0.001	481.0	0.001	464.0		
0.01	485.0	0.01	485.0		
0.1	477.0	0.1	489.0		

Figure 5.22

no particles		0.2 wt. % 100 % SiOH		[C12E5]eq	
x	y	x	y	x	y
0.0001	0.4	0.0001	6.6	0.000021	6.6
0.001	16.0	0.001	210.0	0.00005	210.0
0.01	22.0	0.01	270.0		
0.1	30.0	0.1	370.0		

Figure 5.23

no added salt		+ 0.1 M NaCl	
x	y	x	y
14.1	0.22	14.1	0.29
18.3	0.26	18.3	0.29
24.1	0.30	24.1	0.33
36.0	0.30	36	0.38
40.4	0.35	40.4	0.42
50.9	0.39	50.9	0.42
57.0	0.43	57	0.42
65.7	0.39	65.7	0.42
79.9	0.43	79.9	0.42
100	0.48	100	0.46

Figure 5.28

	0.004	0.016
no particles	40.0	100.0
0.05 wt.% 79.9 % SiOH	20.0	90.0
0.2 wt.% 79.9 % SiOH	30.0	90.0
0.05 wt.% 100 % SiOH	50.0	90.0
0.2 wt.% 100 % SiOH	25.0	70.0

Figure 5.29

	0.004	0.016
no particles	100.0	374.9
0.05 wt.% 100 % SiOH	27.3	131.4
0.2 wt.% 100 % SiOH	155.3	427.6
0.05 wt.% 79.9 % SiOH	50.0	226.8
0.2 wt.% 79.9 % SiOH	234.4	434.8

Figure 5.30

run 1		run 2	
x	y	x	y
0	23.0	0	63.0
1	22.0	3	62.0
3	22.0	13	53.0
5	22.0	18	53.0
12	22.0	30	49.0
27	21.0	34	48.0
40	18.0	56	43.0
58	13.0	77	38.0
75	13.0	102	34.0
90	12.0	120	32.0
100	11.0	122	31.0
180	6.0	234	22.0
210	5.5	360	11.0
371	5.0	1020	3.0
679	4.0	1560	0.0
1390	1.0		
1741	0.0		

Figure 5.31

run 1		run 2	
x	y	x	y
0	58.0	0	43.0
3	56.0	1	43.0
13	53.0	3	43.0
18	48.0	5	28.0
30	45.0	12	22.0
34	43.0	27	13.0
56	35.0	40	7.0
77	26.0	58	5.0
102	14.0	75	5.0
120	8.0	90	4.5
122	7.0	100	4.0
234	1.0	180	0.5
360	0.0	210	0.0

Figure 5.32

	SDS	DTAB	C12E5
no particles	15.0	15.0	23.0
0.05 wt. % 79.9 % SiOH	20.0	40.0	20.0
0.2 wt. % 79.9 % SiOH	20.0	40.0	10.0
0.05 wt. % 100 % SiOH	15.0	30.0	21.0
0.2 wt. % 100 % SiOH	15.0	30.0	11.0

Figure 5.33

	SDS	DTAB	C12E5
no particles	1.5	0.2	141
0.05 wt. % 79.9 % SiOH	2.6	3.7	580
0.2 wt. % 79.9 % SiOH	0.9	214.5	1142
0.05 wt. % 100 % SiOH	1.2	2.2	599
0.2 wt. % 100 % SiOH	1.1	40.9	1106

Figure 5.34

filled squares		open trianges		dashed line 1		dashed line 2	
x	y	x	y	x	y	x	y
14.1	463.94	14.1	813.40	0	239.17	0	273.44
18.3	325.71	18.3	454.55	100	239.17	100	273.44
40.4	540.95	100	482.00				
50.9	315.70						
65.7	396.66						
79.9	392.38						
100	204.17						

Figure 5.35

0.2 wt. % silica		no particles	
x	y	x	y
14.1	8.3	0	19.0
18.3	9.0	100	19.0
36.0	10.0		
40.4	10.8		
50.9	10.8		
57.0	11.5		
79.0	12.0		
100	12.3		

Figure 5.36

0.2 wt. % silica		no particles	
x	y	x	y
14.1	88.0	0	26.7
18.3	76.2	100	26.7
36.0	71.4		
40.4	104.8		
50.9	247.7		
57.0	309.5		
79.9	436.0		
100	507.0		

Appendix E

Figure 6.5

0.2 wt. % silica		0.04 vol. % decane + 0.2 wt. % silica		0.09 vol. % decane + 0.2 wt. % silica		0.12 vol. % decane + 0.2 wt. % silica	
x	y	x	y	x	y	x	y
14.1	20.0	14.1	10.0	14.1	15.0	14.1	10.0
18.3	20.0	18.3	10.0	18.3	15.0	18.3	10.0
24.1	20.0	24.1	10.0	24.1	15.0	24.1	10.0
36.0	20.0	36.0	13.0	36.0	15.0	36	10.0
50.9	20.0	40.4	10.0	40.4	15.0	40.4	10.0
57.0	20.0	50.9	15.0	50.9	15.0	50.9	5.0
65.7	20.0	57.0	14.0	57.0	15.0	57	5.0
79.9	20.0	65.7	13.0	65.7	15.0	65.7	5.0
100	20.0	79.9	5.0	79.9	15.0	79.9	2.0
		100	5.0	100	15.0	100	1.0

no oil or particles		0.04 vol. % decane		0.09 vol. % decane		0.12 vol. % decane	
x	y	x	y	x	y	x	y
0	30.0	0	27.0	1	25.0	1	21.0
100	30.0	100	27.0	100	25.0	100	21.0

Figure 6.6

0.2 wt. % silica		0.04 vol. % decane + 0.2 wt. % silica		0.09 vol % decane + 0.2 wt. % silica	
x	y	x	y	x	y
14.1	2.5	14.1	1.1	14.1	0.65
18.3	3.0	18.3	1.3	18.3	0.53
24.1	2.5	24.1	2.7	24.1	0.52
36.0	2.5	36.0	2.7	36.0	0.6
50.9	3.4	40.4	4.0	40.4	0.8
57.0	2.4	50.9	3.4	50.9	0.6
65.7	7.4	57.0	464.5	57.0	22.4
79.9	116.6	65.7	16.9	65.7	1.0
100	430.0	79.9	3.7	79.9	0.49
		100	1.35	100	0.7

no oil or particles		0.04 vol. % decane		0.09 vol. % decane	
x	y	x	y	x	y
0	109.0	0	34.4	0	3.9
100	109.0	100	34.4	100	3.9

Figure 6.10

x	y
14.1	4.266
24.1	6.619
36.0	11.753
40.4	13.287
50.9	8.444
57.0	4.057
79.9	21.516
100	18.130

Figure 6.12

x	y
14.1	1.83
24.1	1.32
36.0	2.38
40.4	1.70
50.9	2.00
57.0	1.22
79.9	23.30
100	10.00

Figure 6.13

x	0.02 wt. % silica, 0.5 vol. % decane	0.002 wt. % silica, 0.05 vol. % decane	0.0002 wt. % silica, 0.005 vol. % decane
14.1	10.0	20.0	43.0
24.1	10.0	21.0	30.0
36.0	8.0	27.0	33.0
40.4	8.0	30.0	33.0
50.9	9.0	35.0	35.0
57.0	30.0	30.0	35.0
79.9	7.0	20.0	35.0
100	7.0	26.0	27.0

Figure 6.14

x	0.02 wt. % silica, 0.5 vol. % decane	0.002 wt. % silica, 0.05 vol. % decane	0.0002 wt. % silica, 0.005 vol. % decane
14.1	0.0	12.0	12.0
24.1	0.0	19.0	34.0
36.0	0.0	18.3	60.0
40.4	0.0	26.0	51.0
50.9	0.0	104.0	152.0
57.0	18.0	133.0	303.0
79.9	0.0	38.0	208.0
100	0.0	40.8	66.0

Figure 6.15

x	0.2 wt. % silica, 0.5 vol. % decane	0.2 wt. % silica, 0.05 vol % decane	0.2 wt. % silica, 0.005 vol. % decane
14.1	0.0	10.0	10.0
24.1	0.0	10.0	10.0
36.0	5.0	11.0	14.0
40.4	5.0	13.0	14.0
50.9	10.0	13.0	13.0
79.9	3.0	10.0	11.0
100	2.0	7.0	11.0

Figure 6.16

x	0.2 wt. % silica, 0.5 vol. % decane	0.2 wt. % silica, 0.05 vol % decane	0.2 wt. % silica, 0.005 vol. % decane
14.1	0.0	98.0	107.0
24.1	0.0	117.0	123.0
36.0	0.0	149.0	252.0
40.4	0.0	230.0	309.0
50.9	1.0	248.0	318.0
79.0	0.6	252.0	300.0
100	0.0	626.0	951.0